Séparation et détection des trajets dans un guide d'onde en eau peu profonde

Long Yu Jiang

▶ **To cite this version:**

Long Yu Jiang. Séparation et détection des trajets dans un guide d'onde en eau peu profonde. Autre. Université de Grenoble, 2012. Français. NNT : 2012GRENT050 . tel-00765238v2

HAL Id: tel-00765238

https://theses.hal.science/tel-00765238v2

Submitted on 17 Jul 2013

HAL is a multi-disciplinary open access archive for the deposit and dissemination of scientific research documents, whether they are published or not. The documents may come from teaching and research institutions in France or abroad, or from public or private research centers.

L'archive ouverte pluridisciplinaire **HAL**, est destinée au dépôt et à la diffusion de documents scientifiques de niveau recherche, publiés ou non, émanant des établissements d'enseignement et de recherche français ou étrangers, des laboratoires publics ou privés.

UNIVERSITÉ DE GRENOBLE

THÈSE

POUR OBTENIR LE GRADE DE

DOCTEUR DE L'UNIVERSITÉ DE GRENOBLE

Spécialité: Signal, Image, Parole et Télécom

Arrêté ministériel : 7 août 2006

PRÉSENTÉE PAR

Longyu JIANG

THÈSE DIRIGÉE PAR **Jérôme I. Mars**

PRÉPARÉE AU SEIN DU **Laboratoire Gipsa**
DANS L'**École Doctorale**:
Electronique Electrotechnique Automatique Traitement du Signal

Séparation et détection de trajets dans un guide d'onde en eau peu profonde

THÈSE SOUTENUE PUBLIQUEMENT EN **22. Nov. 2012**,
DEVANT LE JURY COMPOSÉ DE:

Monsieur Philippe Roux
DR, ISTERRE, CNRS Grenoble, Président

Monsieur Salah Bourennane
PR, Institut Fresnel, Ecole Centrale de Marseille, Rapporteur

Monsieur Jean Pierre Sessarego
DR, LMA, CNRS Marseille, Rapporteur

Monsieur Gang Feng
PR, Gipsa-lab, Grenoble-INP, Examinateur

Monsieur Hervé Liebgott
MCF, CREATIS, Université Lyon 1, Examinateur

Monsieur Jérôme I Mars
PR, Gipsa-lab, Grenoble-INP, Directeur de Thèse

To my parents.

Where there is a will, there is a way.

—-*Thomas Alva Edison*

Acknowledgments

I owe my deepest gratitude to Mr. Feng Gang. Without his helps, I would not have obtained the chance of beginning my doctorate study in Gipsa-lab.

I would like to thank the president of my oral defense committee —- Mr. Philippe Roux. He is a world-class scientist and give me useful advices for the future studies.

I wish to thank the two reviewers of my thesis —- Mr. Salah Bourennane and Mr. Jean Pierre Sessarego. They are the distingushed experts in both signal processing and in underwater acoustics. My thesis is well reviewed by them. These very good comments are encouragements of my research life, even ones of my life.

I am indebted to the members of my oral defense committee —- Mr. Hervé Liebgott and Mr. Feng Gang. They suggest that I should continue this study in several other applications; for instance, medical application.

It is with immense gratitude that I acknowledge the support and help of my supervisor —- Mr. Jérôme I. Mars. Without his guidance and patience this dissertation would not have gone on smoothly.

I am indebted to my many colleagues who supported me a lot, especially Silvia and François. Our discussions about research, cultures, food and daily life made the research life more colorful. Besides, they also give me a lot of encouragements when I faced difficulties in research. These encouragements gave me greater confidence in overcoming difficulties.

I cannot find words to express my gratitude to my friends, especially Shenghong and her husband. They are warm-hearted, sincere and easy-going. They always put themselves in my place, and help me a lot to the best of their abilities.

Finally, I wish to thank my parents, my sister, my brother in law and my new nephew. Their love is a driving force for my advance forever. My dissertation is dedicated to them.

Abstract

As the studies on shallow-water acoustics became an active field again, this dissertation focuses on studying the separation and detection of raypaths in the context of shallow-water ocean acoustic tomography. As a first step of our work, we have given a brief review on the existing array processing techniques in underwater acoustics so as to find the difficulties still faced by these methods. Consequently, we made a conclusion that it is still necessary to improve the separation resolution in order to provide more useful information for the inverse step of ocean acoustic tomography. Thus, a survey on high-resolution method is provided to discover the technique which can be extended to separate the raypaths in our application background. Finally, we proposed a high-resolution method called smoothing-MUSICAL (MUSIC Actif Large band), which combines the spatial-frequency smoothing with MUSICAL algorithm, for efficient separation of coherent or fully correlated raypaths. However, this method is based on the prior knowledge of the number of raypaths. Thus, we introduce an exponential fitting test (EFT) using short-length samples to determine the number of raypaths. These two methods are both applied to synthetic data and real data acquired in a tank at small scale. Their performances are compared with the relevant conventional methods respectively.

Keywords: array processing, shallow water, source separation, ocean acoustic tomography, smoothing-MUSICAL, exponential fitting test.

Contents

Acknowledgments **5**

Abstract **7**

Contents **9**

List of Figures **15**

List of Tables **19**

1 Introduction **1**
1.1 Objectives 4
1.2 Outline 5

2 Background knowledge on Ocean Acoustic Tomography **7**
2.1 Fundamentals of Ocean Acoustics 10
2.2 Characteristic Sound Paths 12
2.3 Sound Propagation Models 14
2.3.1 Ray Theory 15
2.3.2 Parabolic Equation (PE) Model 16
2.4 General Technique Steps of OAT 18
2.5 OAT in Shallow Water Waveguide 19
2.5.1 Shallow Water 19
2.5.2 Recent Studies on Shallow water 20
2.5.3 Multiple RayPaths Propagation 22

3 Array Processing in Underwater Acoustics **25**
3.1 Sampling and Digitization Techniques 27
3.1.1 Plane-Wave Beamforming 27
3.1.2 Adaptive Beamformers (Maximum-likelihood method (MLM)) . . 28
3.1.3 Double Beamforming 29
3.1.4 A Gibbs sampling localization-deconvolution approach 31
3.1.4.1 Signal model in time domain 33

3.1.4.2 Gibbs sampler . . . 33
3.2 Directly from the received signals . . . 37
3.2.1 Matched Field Processing . . . 37
3.2.1.1 Green's functions . . . 37
3.2.1.2 Signal Models . . . 38
3.2.1.3 Noise Models . . . 38
3.2.1.4 Sample covariance estimation . . . 39
3.2.1.5 The Conventional (Barlett) Beamformer . . . 41
3.2.1.6 Maximum-likelihood method MFP . . . 41
3.2.2 The Time Reversal Mirror . . . 42
3.2.3 Discussion on matched-field processing and phase conjugation of time reversal mirror . . . 48
3.3 Discussion and comparison . . . 49

4 Survey on High Resolution Methods **51**
4.1 Subspace-based Methods . . . 53
4.1.1 MUSIC Algorithm . . . 53
4.1.2 Coherent Signals . . . 54
4.2 Parametric Methods . . . 55
4.2.1 Deterministic Maximum Likelihood . . . 55
4.2.2 Stochastic Maximum Likelihood . . . 57
4.2.3 A Bayesian Approach to Auto-Calibration for Parametric Array Signal Processing . . . 58
4.2.3.1 Data model . . . 58
4.3 Uniform Linear Arrays . . . 61
4.3.1 Root-MUSIC . . . 61
4.3.2 ESPRIT . . . 62
4.4 Multi-dimensional high resolution method . . . 63
4.5 Higher order method . . . 65
4.5.1 MUSIC-4 . . . 65
4.6 Polarization sensitivity and Quaternion-MUSIC for vector- sensor array processing . . . 67
4.6.1 Background knowledge on quaternions . . . 68
4.6.2 Polarization model . . . 69
4.6.3 Quaternion spectral matrix . . . 71
4.6.4 Quaternion eigenvalue decomposition . . . 71
4.6.5 Quaternion-MUSIC estimator . . . 72
4.7 Number of Signals Estimation . . . 72
4.8 Discussion and comparison . . . 73

5 Raypaths Separation with High Resolution Processing in a Shallow-Water Waveguide **77**
5.1 Introduction . . . 79

5.2 Smoothing-MUSICAL . . . 82
5.2.1 Signal model . . . 83
5.2.2 Principle of the algorithm . . . 84
5.2.2.1 Estimation of interspectral matrix . . . 84
5.2.2.2 Projection onto the noise subspace . . . 89
5.3 Simulations . . . 90
5.3.1 Configuration . . . 90
5.3.2 Large time-window data . . . 90
5.3.3 Small time-window experiments . . . 95
5.3.4 Robustness against noise . . . 95
5.4 Application on real data . . . 99
5.4.1 Configuration . . . 99
5.4.2 Results . . . 99
5.5 Conclusion . . . 99

6 Automatic Detection of the Number of Raypaths in a Shallow-Water Waveguide 103
6.1 Introduction . . . 105
6.2 Demonstration on Importance of Detection of the Number of Raypaths . 107
6.3 Problem of Detection of Number of Raypaths . . . 109
6.4 Techniques for detection of the number of Raypaths . . . 110
6.4.1 Information Theoretic Criteria . . . 110
6.4.1.1 AIC . . . 110
6.4.1.2 MDL . . . 111
6.4.2 EFT . . . 111
6.4.2.1 Eigenvalue Profile Under Noise Only Assumption . . . 111
6.4.2.2 Principle of the Recursive EFT . . . 115
6.5 Simulations . . . 116
6.5.1 Performance in various SNR . . . 117
6.5.2 Performance for close raypaths . . . 120
6.6 Small-Scale Experiment . . . 120
6.6.1 Noise-whitening process . . . 120
6.6.2 Small-Scale Experiment . . . 123
6.7 Conclusion . . . 124

7 Conclusion 127
7.1 Summary of Contributions . . . 129
7.2 Perspectives . . . 132

A Résumé en Français 135

Résumé en Français 135
A.1 Introduction . . . 135
A.1.1 Objectifs . . . 136

A.1.2 Organisation du résumé 136
A.2 Connaissances de base sur la TAO 137
A.2.1 Fondamentaux de l'acoustique océanique 137
A.2.2 Modèles de propagation du son 138
A.2.3 Étapes Techniques générales de la TAO 138
A.3 La TAO en eaux peu profondes 139
A.3.1 Eau peu profonde 139
A.3.2 Études récentes sur la TAO en zone cotière 140
A.3.3 Propagation Multiple Targets 140
A.4 Traitement vectoriel en acoustique sous-marine 141
A.5 Les méthodes à haute résolution 142
A.6 Séparation des trajets par méthodes haute résolution dans un guide d'onde en eau peu profonde 145
A.6.1 Introduction 145
A.6.2 Smoothing-MUSICAL 146
A.6.2.1 Modéle de signal 146
A.6.2.2 Estimation de la matrice interspectrale 148
A.6.2.3 Projection sur le sous-espace bruit 151
A.6.3 Simulations 152
A.6.3.1 Configuration 152
A.6.3.2 Grandes fenêtres temporelles de données 153
A.6.3.3 Robustesse en fonction du bruit 153
A.6.4 Application sur des données réelles 156
A.6.4.1 Configuration 156
A.6.4.2 Résultats 156
A.7 Détection automatique du nombre de trajets dans un guide d'onde en eau peu profonde 156
A.7.1 Déetection du n ombre de rayons 159
A.7.2 Exponentiel Fitting Test 160
A.7.2.1 Profil des valeurs propres 161
A.7.2.2 Principe de l'EFT récursif 164
A.7.3 Simulations 165
A.7.4 Performances pour divers RSB 165
A.7.4.1 Performance pour trajets proches 167
A.7.4.2 Expérience à petite échelle 167
A.8 Conclusion 168
A.8.1 Sommaire des contributions 169
A.8.2 Perspectives 170

Bibliography **171**

Author's Publications **187**

Abstract **189**

Résumé **189**

List of Figures

2.1 Generic Sound Speed Profiles [SRD*07] 12

2.2 schematic representation of basic types of sound propagation in the ocean [SRD*07] 13

2.3 Two Main Steps of OAT 19

2.4 Multiple Ray Paths Propagation 22

3.1 Signal model of plane-wave beamforming 27

3.2 The schematic presentation of the double beamforming (a) The pressure field $p(t, z_r, z_s)$ recorded on the received array is transformed into $p(t, \theta_r, z_s)$ space (b) In second step, $p(t, \theta_r, z_s)$ is transformed into $p(t, \theta_r, \theta_s)$ space, where θ_r denotes the emitted angle. 30

3.3 The separation results of beamforming vs double beamforming (Crosses indicate the theoretical prediction values.) from [IRN*09]: (a) two ray-paths are extracted from the FAF03 data set [RKH*04] at depth $z_s = 87.3m$ and $z_r = 39.3m$; (b) the separation results of the two raypaths in (a) using beamforming; (c) the separation results of the two raypaths in (a) using double beamforming. 32

3.4 The expected source location is at 2 km in range and 34 m in depth. The Gibbs sampling approach produces a clear ambiguity surface with the main mode at the correct source location [Mico0].(a) Bartlett and (b) Gibbs sampling ambiguity surfaces for source location. 36

3.5 Array narrow model, sample matrix estimation, and data preconditioning for MFP 40

3.6 Matched field processing (MFP) [KL04]. If you want to know where a singing whale locates at, first, the sound of the wave is recorded as an data vector; and then based on your sufficient accurate model of waveguide propagation, compare the recorded data from the singing wave, one frequency at a time, with the replica data. The location of highest correlation (the red peak in the fig. 3.6) denotes the estimated where the whale locates at. The feedback loop suggests a way to optimize the model. Matched field processing can then be used in the context of ocean acoustic tomogtraphy [TDF91]. The data is from [KL04] [BBR*96] 43
3.7 the configuration of a TRM experiment 44
3.8 (a) a signal is launched by a probe source and it excites a series of normal modes that propagate to theTRM (b) a probe signal received by TRM. [KKH*03] 47
3.9 (a) time reversal signals propagate backward to the probe source (b) a focused signal observed by VRA. [KKH*03] 47

4.1 An example demonstrating the separation capability of beamforming and MUSIC, where each peak represents a detected position of one signal. (Red line denotes the MUSIC separation and the blue line of dashes shows the separation result of beamforming) 55
4.2 (a) LV estimation result [MLBM05] (b) Q-MUSIC estimation result [MLBM06] 72

5.1 Subantenna structure of spatial smoothing 86
5.2 Subband structure of frequential smoothing 87
5.3 The point-array configuration explored to obtain the synthetic data 90
5.4 An experimental example of Recorded Signal (large time-window and without noise) 91
5.5 The separation result of an experimental example of Recorded Signal (large time-window and without noise). (a) Separation results with Smoothing-MUSICAL. (b) Separation results with Beamforming. 92
5.6 The separation result of an experimental example of Recorded Signal (Large time-window and without noise) (Mesh).(a) Separation results (mesh) with Smoothing-MUSICAL. (b) Separation results (mesh)with Beamforming. 93
5.7 Part of recorded signal which includes the first two arrival raypaths (Large time-window and without noise) 93
5.8 The separation result of part of recorded signal (Large time-window and without noise) (a) Separation results with Smoothing-MUSICAL. (b) Separation results with Beamforming. (c) Separation results (mesh) with Smoothing-MUSICAL. 94
5.9 An experimental example of Recorded Signal (Small time-window and without noise) (a) Recorded Signal (without noise). (b) Separation results with Beamforming. (c) Separation results with Smoothing-MUSICAL. . . 96

5.10 An experimental example of Recorded Signal (SNR=0dB) (a) Recorded Signal (SNR=0dB). (b) Separation results with Beamforming (SNR=0dB). (c) Separation results with Smoothing MUSICAL (SNR=0dB). 97
5.11 An experimental example of Recorded Signal (SNR=-15dB) (a) Recorded Signal (SNR=-15dB). (b) Separation results with Beamforming (SNR=-15dB). (c) Separation results with Smoothing MUSICAL (SNR=-15dB). . 98
5.12 An experimental example of Recorded Signal for real data obtained at small scale (a) Recorded Signal for real data obtained at small scale. (b) Separation results with Beamforming for real data obtained at small scale. (c) Separation results with Smoothing MUSICAL for real data obtained at small scale. 100

6.1 An experimental example of which the real number of raypaths equals 7 (a) Separation results using smoothing-MUSICAL with $P = 3$. (b) Separation results using smoothing-MUSICAL with $P = 5$. (c) Separation results using smoothing-MUSICAL with $P = 7$. 108
6.2 Profile of ordered noise eigenvalues for eight realizations (a) Profile of ordered noise eigenvalues estimated by 15 samples. (b) Profile of ordered noise eigenvalues estimated by 1025 samples. 116
6.3 Profiles of eigenvalue with two eigenvalues corresponding to raypaths. When the eigenvalue corresponding to raypath appears, a break exists between the profile of EFT and the profile of recorded eigenvalues. . . . 117
6.4 Profile of ordered eigenvalues in the first group of experiments when SNR = 20dB (a) the received signals on 15 sensors. (b) Profile of ordered eigenvalues estimated by 1025 samples. (c) Profile of ordered eigenvalues estimated by 15 samples. 118
6.5 Profile of ordered eigenvalues in the first group of experiments when SNR = 5 dB (a) the received signals on 15 sensors. (b) Profile of ordered eigenvalues estimated by 1025 samples. (c) Profile of ordered eigenvalues estimated by 15 samples. 119
6.6 Profile of ordered eigenvalues in the second group of experiments when SNR = 20dB (a) the received signals on 15 sensors. (b) Profile of ordered eigenvalues estimated by 1025 samples. (c) Profile of ordered eigenvalues estimated by 15 samples. 121
6.7 Experimental Setup of Small-scale Experiment in ISTerre 124
6.8 (a) The received signals on 64 sensors for 5000 samples. (b) Separation result of beamforming with theoretical location for 64 samples. It provides a reference value for checking the separation result of the proposed method. (c) Profile of ordered eigenvalues of 64 samples. 125

A.1 Deux principales étapes d'OAT 139
A.2 Propagation Multiple Targets 141
A.3 Structure d'antenne sous lissage spatial 149

A.4 Structure de sous-bande pour le lissage fréquentiel 150
A.5 Configuration Point-Antenne permettant d'obtenir les données synthètiques 153
A.6 Résultat de séparation sur un signal enregistré (grande fenêtre de temps et sans bruit). (a) Avec smoothing-MUSICAL. (b) Avec Formation de voie. (c) Résultats de la séparation d'une partie du signal enregistré avec smoothing-MUSICAL. (d) Résultats de la séparation d'une partie du signal enregistré avec Formation de voies. 154
A.7 Un exemple expérimental de signal enregistré (RSB = 0 dB) (a) les résultats de séparation avec Formation de voie (RSB = 0 dB). (b)Les résultats de séparation avec smoothing-MUSICAL (RSB = 0 dB). (c) les résultats de séparation avec Formation de voie (RSB = -15 dB). (d)Les r'esultats de séparation avec smoothing-MUSICAL (RSB = -15dB). 155
A.8 Un exemple expérimental de signal enregistré pour les données réelles obtenues à petite échelle (a) Signal enregistré pour les données réelles obtenues à petite échelle. (b) Résultats de séparation avec formation de voies pour les données réelles obtenues à petite échelle. (c) Résultats de séparation avec smoothing-MUSICAL pour les données réelles obtenues à petite échelle. 157
A.9 Profil des valeurs propres ordonnées de bruit sur huit réalisations (a) Profil des valeurs propres ordonnées de bruit estimés par 15 échantillons. (b) Profil des valeurs propres ordonnées de bruit estimée par 1025 échantillons. 166
A.10 Profils des valeurs propres avec deux valeurs propres correspondant aux rayons. Lorsque la valeur propre correspond au rayons apparaît, une rupture existe entre le profil de l'EFT et le profil des valeurs propres enregistrées. 166
A.11 (a) Résultat de la formation de voies avec emplacement théorique de 64 échantillons. Il fournit une valeur de référence pour vérifier le résultat de séparation de la méthode proposée. (b) Profil des valeurs propres ordonnées de 64 échantillons. 168

List of Tables

3.1 Comparison on the existing array-processing methods in underwater acoustics based on different criteria (Plane-wave and Experiment configuration)-I 50
3.2 Comparison on the existing array-processing methods in underwater acoustics based on different criteria (Statistical order and Computations)-II . . 50

4.1 Comparison of the existing high-resolution methods based on different criterions (Consistency, Coherent Signals and Statistical Order)-I 74
4.2 Comparison of the existing high-resolution methods based on different criterions (Computation, Dimensional and Sensor Type)-II 74
4.3 Comparison of the existing high-resolution methods based on different criterions (Statistical Performance and Polarization Sensitivity)-IIII 74
4.4 Comparison of the existing high-resolution methods based on different criterions (Prior knowledge of model order, Assumption of Signal Type and Array Geometries)-III 75

6.1 Number of raypaths detected by AIC, MDL and EFT in the first group of experiments (the real number of raypaths $P = 5$) 120
6.2 Number of raypaths detected by AIC, MDL and EFT in the second group of experiments (the real number of raypaths $P = 5$) 120

A.1 Comparaison des différentes méthodes de traitement d'antenne basée sur plusieurs crités (Onde place and configuration de l'expérimentation)-I . 142
A.2 Comparaison des différentes méthodes de traitement d'antenne basée sur plusieurs crités (Statistique et temsp de calcul)-II 143
A.3 Comparaison des méthodes à haute résolution à partir de different critéres (Consistance, Cohérence, Statistique)-I 144
A.4 Comparaison des méthodes à haute résolution à partir de different critéres (Calcul, imension, Type de capteurs)-II 144
A.5 Comparaison des méthodes à haute résolution à partir de different critéres (Performance statistique, Polarisation)-III 145

A.6 Comparaison des méthodes à haute résolution à partir de different critéres (Connaissance de l'ordre, Hypothéses signal, Géométrie de l'antenne)-IIII 145
A.7 Nombre de raypaths détectés par l'AIC, MDL et l'EFT dans le premier groupe d'expériences (le nombre réel de trajets $P = 5$) 167
A.8 Nombre de raypaths détectés par l'AIC, MDL et l'EFT dans le deuxième groupe d'expériences (le nombre réel de raypaths $P = 5$) 167

Chapter 1

Introduction

Contents

1.1 Objectives 4

1.2 Outline 5

Ocean acoustic tomography is a technique which uses the time variation of sound propagation in the ocean to estimate the property variation of ocean, such as temperature, salinity ..... etc. This technique is first explored as a remote sensing method for large-scale ocean. After the cold war, the shallow water studies become very attractive. In fact, the ocean acoustic tomography in a shallow-water wave guide at small scale has the same technique process as the one in deep water. That means it is also composed of the forward problem and the inverse problem. What is called the forward problem? The sound propagates in the ocean through multiple paths. This property can provide more informations by that each raypath covers the different part of the ocean. However, when two raypaths arrive closely, the parameters, like travel time and direction of arrival, which contain these informations, can not be extracted directly and easily from the received signals. Because of this, some signal processing techniques are explored to separate the close raypaths and also to extract more raypaths. This is a process solving the forward problem. At the same time, the performance of inverse problem is based on the efficient solution of the forward problem. Thus, improving the performance of forward problem has great significance to finally obtain an efficient inversion results for ocean acoustic tomography.

Specifically, the analysis is begun from the recorded signal in a specific experiment configuration. At beginning and in the first experiment conducted by Munk, the signal is emitted by a point source and recorded by a single sensor (point to point configuration). The raypaths are separated by arrival time of each raypath. When these two raypaths arrive very closely, methods in this point to point configuration generally fail in correctly separating the raypaths. Consequently, beamforming has been applied to a configuration which is composed of one point source and a vertical array (point to array configuration) [MWW95] to obtain more information on raypaths. It can separate more close raypaths due to the added discrimination parameter—-the direction of arrival corresponding to each raypath on the vertical array. In order to further improve the performance of beamforming, more recently, a double-beamforming method was presented to solve the forward problem in an array to array configuration, which is composed of one source array and a received array. Inheriting the sprit of beamforming in the point to array configuration, this novel configuration can provide a new parameter—the emitted angle as a discrimination variation. This method was first performed in a shallow-water wave guide [RCKH08] and then is applied to a shallow-water tomography problem [IRNM08] for getting correct simulation results. Finally, this shallow-water tomography based on double-beamforming was demonstrated by the experiment at an ultrasonic scale [RIN*11]. Although double-beamforming has largely improved the res-

olution compared the beamforming, it still has the main drawback of beamforming: the low resolution ability.

Besides, there exist numerous approaches in underwater acoustic to source localization or geoacoustic inversion which also depend on the acurate raypaths extraction.

Thus, it is still quite necessary to present high resolution method for extracting more raypaths. Although our work in this dissertation is mainly focused on the forward problem of shallow-water acoustic tomography, it is possible to extend these methods similarly to solve the raypaths extraction problem to source localization or geoacoustic inversion or some other similar applications in underwater acoustics.

1.1 Objectives

Based on the discussion above, we want to achieve three major objectives in this dissertation. Because these common forward problems of source localization, geoacoustic and ocean acoustic tomograghy, we will first give a comprehensive survey on corresponding signal processing methods which are already applied to these applications in underwater acoustics, especially in shallow water. Advantages and limitations of each technique will be analyzed and compared. Then, a group of high resolution methods, which has been presented to overcome the resolution limitation of spectral-based algorithms, will be reviewed comprehensively. Through the study results of reviewing literatures, we further make the problems which we will solve in the context of shallow-water acoustic tomography specific and obvious. Finally, we propose a subspace-based high resolution method for separating the coherent raypaths in a shallow-water waveguide. (Two coherent signals (or raypaths in our context) means: if one signal is a scaled and delayed version of the other.) The corresponding state of art on coherent sources separation will be also reviewed. Subsequently, we pay attention to one of technique limitations of subspace-based methods. That is, they are all under the assumption of prior knowledge of model order. In our application context, it is the number of raypaths. Model order selection is an important problem in applications of model-based methods. There are few methods which are not based on the accurate estimation of covariance matrix and the assumption of spatially white noise. However, these two assumption are not easy to be satisfied in a practical perspective. Accordingly, we propose an exponential fitting test using short-length samples to automatically detect the number of raypaths. In addition, a noise whitening processing step is added to try to solve this problem in a practical shallow-water environment. This detection problem and our initial effort to try to find a solution will be analyzed and presented in Chapter 6.

1.2 Outline

The remainder of this manuscript is organized as follows.

Chapter 2 first introduces some background knowledges on ocean acoustic tomography (OAT). These knowledges are the theoretical basis of our simulation experiment and real experiment at small scale. Then, the shallow-water environment is defined and we present the major characteristics of a general ocean acoustic tomography process in a shallow-water wave-guide. Moreover, the state of art on recent studies of shallow-water OAT is provided.

Because of the essential relationship between the existing signal processing methods in under water acoustics and the forward problem of shallow-water OAT, a survey on these methods is provided in Chapter 3.

From the conclusions of reviewing literatures on both shallow-water studies and signal processing techniques, the resolution of signal processing method attract our attentions. Consequently, a comprehensive review of high resolution method is described in Chapter 4. It is supposed that we can find or extend some high resolution methods to adapt to giving satisfied solutions in the context of shallow-water wave guide.

Chapter 5 presents a high resolution processing called smoothing-MUSICAL for coherent raypaths, which is a combination of spatial-frequency smoothing and MUSICAL algorithm.

In Chapter 6, we propose a noise-whitening exponential fitting test to correctly detect the number of raypaths in a shallow-water waveguide.

Chapter 7 summarizes the contribution of the proposed algorithms and draws conclusions of this manuscript. Some further works on the proposed algorithms are stated. In addition, several future study directions concerning on signal processing techniques in underwater acoustics are described.

Chapter 2

Background knowledge on Ocean Acoustic Tomography

Contents

2.1 Fundamentals of Ocean Acoustics 10

2.2 Characteristic Sound Paths 12

2.3 Sound Propagation Models 14

2.3.1 Ray Theory 15

2.3.2 Parabolic Equation (PE) Model 16

2.4 General Technique Steps of OAT 18

2.5 OAT in Shallow Water Waveguide 19

2.5.1 Shallow Water 19

2.5.2 Recent Studies on Shallow water 20

2.5.3 Multiple RayPaths Propagation 22

A body of saline water is defined as an ocean or a sea. Approximately 71% of the planet's surface ($3.6 \times 10^8 km^2$) is covered by several principal oceans and smaller seas. Humans begin to acquire knowledge of the waves and currents of the seas and oceans in pre-historic times. Early modern exploration of the oceans was primarily for cartography and mainly limited to its surfaces and of the creatures that fishermen brought up in nets, though depth soundings by lead line were taken. With the development of further study of oceans, oceanography also called oceanology or marine science is formed, which covers a wide range of topics referring to multiple disciplines, such as biology, chemistry, geology, meteorology, and physics as well as geography. As a key branch of oceanography, physical oceanography study the physical conditions and physical processes within the ocean, especially the motions and physical properties of ocean waters.

The motivation of studying the physics of the ocean depends on three major factors. The first one is that oceans are the main supply source for the fishing industry. For example, some of the more important ones are shrimp, fish, crabs and lobster. In addition, the oceanic weather, such as temperature changes and currents, fertilizes the sea. Hence we are interested in the processes which influence the sea just as farmers are interested in the weather and climate. Secondly, the oceans are essential and crucial to transportation: most of the world's goods move by ship between the world's seaports. These activities are influenced by the physics process of the oceans, especially waves, winds, currents, and temperature. The last and important one is that the study of the oceans is linked to understanding global climate changes, potential global warming and related biosphere concerns. Specifically, the interaction of ocean circulation, which serves as a type of heat pump, and biological effects such as the concentration of carbon dioxide can result in global climate changes on a time scale of decades. Known climate oscillations resulting from these interactions include the Pacific decadal oscillation, North Atlantic oscillation, and Arctic oscillation. The oceanic process of thermohaline circulation is a significant component of heat redistribution across the globe, and changes in this circulation can have major impacts upon the climate.

For analysis and studies of physical properties of the ocean, oceanography has essentially two types of techniques. On the one hand, direct measurement of physical properties such as conductivity, temperature or density of the sedimentary layers are available. These instruments allow to have relevant information on backgrounds, but they present significant cuts to use and provide a very limited spatial sampling with respect to size of physical phenomena to be studied.

On the other hand, less investigative techniques exist. They consist in a wave propagating in the ocean environment, for approximating physical properties from the in-

teraction between the medium and the wave that is propagated. These techniques can have a better sampling space, but their reliability is often more unreliable than direct measurements.

Practically, there are two types of waves which have been utilized in the indirect measurements of the physical properties of ocean. Concretely, in order to study the ocean surface (the sea state, surface waves, ...), many methods using electromagnetic waves have been developed. Unfortunately, these waves can not be exploited to analyze the internal structures (outside surface) due to their high attenuation in the water. In this case, sound waves, much less attenuated, are the only medium that allows us to image the submerged part of the oceans.

As discussed above, the oceans are opaque to most electromagnetic radiation, but there is a strong acoustic waveguide and sound can propagate for 10 Mm with distinct multiply-refracted raypaths. Consequently, ocean acoustic tomography (OAT) was proposed in 1979 by Walter Munk and Carl Wunsch [MW79][MWW95] as one of important indirect techniques on studying physical properties of oceans. It is an analogue to X-ray computed axial tomography for the oceans. A quick briefing of this technique process is given as: the acoustic signal is first emitted by a point source; then, transmitting broadband pulses (particularly sound at low frequencies, i.e., less than a few hundred hertz.) in the ocean leads to a set of impulsive arrivals at the receiver which characterize the impulse response of the sound channel. The peaks observed at the receiver are assumed to represent the arrival of energy traveling along geometric ray paths. These raypaths can be distinguished by several parameters, such as arrival time and arrival angle, etc, depending on the experiment configuration. Variations in these parameters can be used to infer changes in ocean structure. This will be explained in detail in Section 2.4.

In this chapter, we first introduce the fundamental knowledge of ocean acoustics. In Section 2.2, the characteristic of sound propagation is studied in both deep water and shallow-water. Section 2.3 presents two basic sound propagation models. Section 2.4 illustrates the general technic steps of OAT. Finally, we introduce recent research works in shallow water and the specific problem is encountered by OAT in shallow water in Section 2.5.

2.1 Fundamentals of Ocean Acoustics

It has been pointed out that the ocean can be considered as an acoustic waveguide. It is a waveguide limited above by the sea surface and below by the seafloor. The speed of sound in the waveguide plays the same role as the index of refraction does in optics.

The sound speed in the ocean increases with the increasing of pressure, temperature and salinity. As the pressure is a function of depth, the dependence of sound speed and three independent variables [Bae81] is expressed as Equation A.1:

$$c = 1449.2 + 4.6T - 0.055T^2 + 0.00029T^3 + (1.34 - 0.01T)(S - 35) + 0.016z \qquad (2.1)$$

where

- c is sound speed.
- T represents temperature in degrees centigrade.
- S expresses the salinity in parts per thousand.
- z is depth in meters.

The sensitivity of sound speed to salinity is generally much smaller than that of either temperature or pressure. In non-polar regions, the oceanographic properties of the water near the surface result essentially from mixing due to wind and wave activity at the air-sea interface and this near-surface mixed layer has a constant temperature. Hence, in this isothermal mixed layer we have a sound-speed profile which increases with depth because of the pressure gradient effect. This is the surface duct region, and its existence depends on the near-surface oceanographic conditions. Note that the more agitated the upper layer is, the deeper the mixed layer and the less likely will there be any departure from the mixed-layer part of the profile depicted in Figure. 2.1. Thus, an atmospheric storm passing over a region mixes the near-surface waters so that a surface duct is created or an existing one deepened or enhanced.

The midlatitude ocean is warmest near the surface and the temperature drops off rapidly in the upper 200 to 700 m, forming the ocean main thermocline and greatly decreasing the sound speed. Below the main thermocline, the ocean temperature decreases very slowly with depth and the increasing pressure with depth dominates the sound speed, creating a minimum in sound speed at the bottom of the main thermocline. However, in polar regions, the water is coldest near the surface and hence the minimum sound-speed is at the ocean-air interface as indicated in Figure. 2.1. In shallow water (continental shelf regions) with water depth in the order of a few hundred meters, only the upper part of the sound-speed profile in Figure. 2.1 is relevant. This upper region is dependent on season and time of day, which, in turn, affects sound propagation in the water column. Specifically, in a warmer season (or warmer part

of the day), the temperature increases near the surface and hence the sound speed increases toward the sea surface. This near surface heating (and subsequent cooling) has a profound effect on surface-ship application. For instance, for surface-ship sonars, the diurnal heating causes poorer sonar performance in the afternoon–a phenomenon known as the afternoon effect. The seasonal variability, however, is much greater and therefore more important factor with respect to underwater acoustic.

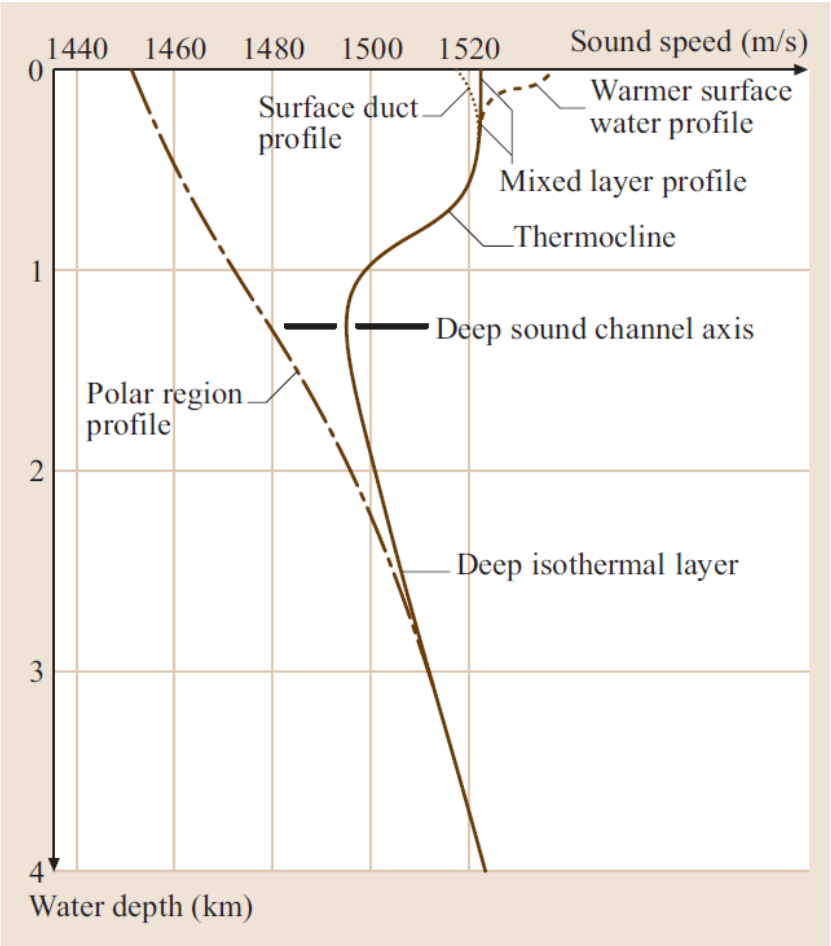

Figure 2.1: Generic Sound Speed Profiles [SRD*07]

2.2 Characteristic Sound Paths

The schematic of the basic types of propagation in the ocean is shown by Figure. 2.2, which results from the sound-speed profiles (indicated by the dashed lines) discussed in Figure. 2.1. Mathematically, these sound paths can be understood from Snell's law,

$$\frac{cos\theta_z}{c_l} = const \tag{2.2}$$

where θ_z indicates the propagation angle of ray at depth z with respect to the horizontal and c_l is the local sound speed. This law implicates that sound bends locally toward region of low sound speed.

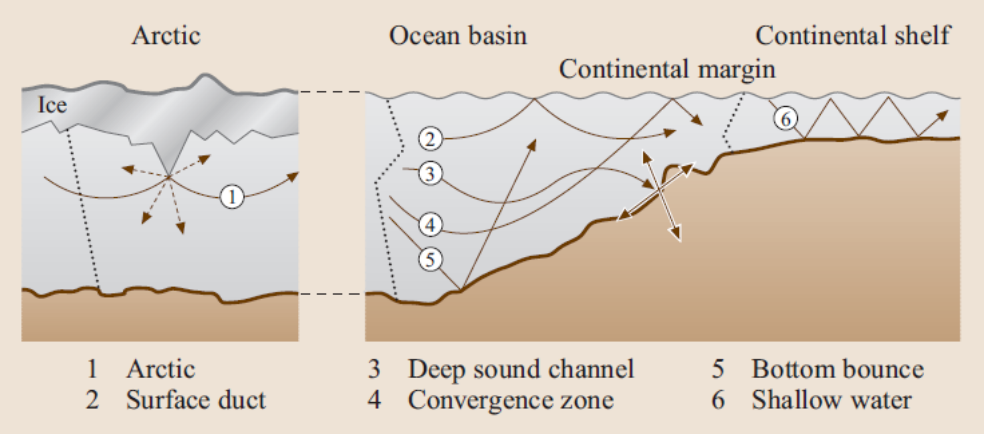

Figure 2.2: schematic representation of basic types of sound propagation in the ocean [SRD*07]

The simplest cases to explain are the paths about local sound speed minima: path1, path 2, and path 3. Among these three types of paths, paths 1 and 2 correspond to surface duct propagation where the minimum sound speed is beneath the ice cover for the Arctic case or at the ocean surface. The ray leaving a deeper source at a shallow horizontal angle depicts path 3, which propagates in the deep sound channel whose axis is at the shown sound speed minimum. As shown in Figure 2.2, this local minimum converging to the Arctic surface minimum (path 1) tends to become more shallow toward polar latitudes. Moreover, because sound in the deep channel for mid-latitudes has few interactions with lossy boundaries, it can propagate over long distances. In particular, many ocean exploration technique in deep water, such as ocean acoustic tomography of large scales, are based on this property of low-frequency propagation via this path, which has been observed to distances of thousands of kilometers. Also, it can be expected that the shallow sources combined with the water column at polar latitudes will tend to propagate more horizontally around an axis based on both the geographical variation of the acoustic environment and Snell's law. There exists a type of convergence zone propagation —- path 4 with slightly steeper angles than those of path 3. These convergence zones of high intensity near the surface, which is caused by the upward refracting nature of the deep sound-speed profile, is produced by a spatially periodic (35-70km) refocusing phenomenon.

Another periodic phenomenon exists as path 5. It is reflected by the ocean bottom, so the sound path with energy losses propagates in a shorter cycle distance and a shorter

total propagation distance. Finally, in a shallow-water region such as a continental shelf, the sound (depicted in the right-hand-side of Figure 2.2) is channeled in a waveguide reflected by the ocean both surface and bottom. Because of the reflection of the bottom, negative critical depth environments exhibit much of the sound propagation physics descriptive of shallow-water environments. It is also the path propagation based on which the work of my thesis is discussed.

There exists an alternative classification of raypaths in the ocean, which classifies raypaths into four types:

1. *Refracted Refracted (RR) rays (path 3):* rays propagating via refracted path only.

2. *Refracted Surface Reflected (RSR) rays (paths 1, 2, and 4):* refracted rays bouncing off the sea surface.

3. *Refracted Bottom-Reflected (RBR) rays (path 5) :* rays bouncing off the seafloor.

4. *Surface-Reflected Bottom-Reflected (SRBR) rays: (path 6)* rays reflected off both the sea surface and the seafloor.

The RR paths have no boundary losses because they are only affected by attenuation and scattering within the water column. At the same time, it is obvious that the SRBR paths are the most lossy since they are subjected to all of the loss mechanisms present in the ocean waveguide.

2.3 Sound Propagation Models

The wave equation is derived to describe sound propagation. Concretely, it is obtained from the equations of hydrodynamics and its coefficients and boundary conditions. The computer solutions to the wave equation [JKP*95] are called sound propagation models. They are developed so as to perform and describe sound propagation in the sea by computer simulation. Normally, there are four types of sound propagation models: ray theory, the spectral method or fast field program (FFP), normal mode (NM) and parabolic equation (PE). These models consider not only the ocean variation with depth but also those in horizontal direction (range-dependent). The appropriate choice of sound propagation models differs from the value of frequencies. If the frequencies are a few kilohertz or above, ray theory is mainly used. While the other three model types are more applicable and useable in the cases that the frequencies are below 1 kHz. If the frequency is between these frequencies, we can choose either of them.

A solution of wave equation with the cylindrical coordinates in frequency domain for a frequency bin ν is called the Helmholtz equation ($K \equiv 2\pi\nu/c$). It is given by:

$$\bigtriangledown^2 p_C(\mathbf{r}_C, z) + K_H^2 p_C(\mathbf{r}_C, z) = 0 \tag{2.3}$$

where the pressure p_C in cylindrical coordinates with the range coordinates denoted by $\mathbf{r}_C = (x, y)$ and the depth coordinate denoted by z (taken positive downward) for a source-free region.
with

$$K_H^2(\mathbf{r}_C, z) = \frac{(2\pi\nu)^2}{c^2(\mathbf{r}_C, z)}. \tag{2.4}$$

describing the variation of propagation environment in horizontal direction.

For an acoustic field obtained from a point source, the Helmholtz equation is described as:

$$\bigtriangledown^2 \mathbf{G}(\mathbf{r}_C, z) + K_H^2(\mathbf{r}_C, z)\mathbf{G}(\mathbf{r}_C, z) = -\delta^2(\mathbf{r}_C - \mathbf{r}_s)\delta(z - z_s) \tag{2.5}$$

where the subscript C_s denotes the source coordinates. As we mentioned at the beginning of this section, there are four types of propagation models. Actually, here, they are divided into four types depending on the method of acquiring the solution of Green's function $\mathbf{G}$. Spectral method or normal modes is obtained by solving the boundary-value problem of Equation 2.5 while ray theory model and parabolic equation model are obtained by using an initial value to approximate Equation 2.5. As two representatives, we will briefly introduce ray theory and Parabolic Equation (PE) Model, which will be used in following chapters to generate the synthetic data sets of our experiments.

2.3.1 Ray Theory

Ray theory approximate the Equation 2.5 geometrically in high-frequency. It is mostly utilized in the deep-water environment and also applied to shallow water for some specific purposes. Mathematically, it is described by:

$$\mathbf{G}(\mathbf{r}_C, z) = A_e(\mathbf{r}_C, z)e^{[iP_h(\mathbf{r}_C, z)]} \tag{2.6}$$

where $A_e(r_C, z)$ is the amplitude envelope, and P_h is the phase (eikonal). Curves orthogonal to the iso-phase surfaces are called rays. Both the amplitude and eikonal are functions of the spatial coordinates $(\mathbf{r}_C, z)$. Moreover, $A(\mathbf{r}_C, z)$ varies with the spatial coordinates $(\mathbf{r}_C, z)$ slowly compared with the exponential term including the phase S.

Since the amplitude varies slowly with the spatial coordinates (i.e.,$(1/A) \bigtriangledown^2 A \ll K^2$), the corresponding eikonal equation (geometrical approximation) yielded from 2.3 has the well-known form:

$$(\bigtriangledown P_h(\mathbf{r}_C, z))^2 = K_H^2 \tag{2.7}$$

and the ray trajectory can be given mathematically by:

$$\frac{d}{d(l_a)}(K_H \frac{d\mathbf{R}}{d(l_a)}) = \bigtriangledown K_H \tag{2.8}$$

where l_a is the length of the curve along the direction of the ray $d(l_a) = \sqrt{d\mathbf{r}_C^2 + dz^2}$ and $\mathbf{v}_d = (\mathbf{r}_C, z)$ is the displacement vector to a point on the ray. The density of rays is utilized to compute the direction of average flux (energy) at any point according to that of the trajectories and the amplitude of the field. The ray theory is applicable to both depth-dependence and range dependence environments. The advantages of ray theory are the rapid computation velocity and making the acoustic propagation visible not only in shallow and deep water but also in mid-latiutde to polar regions. That is, the ray traces provide a physical view of the acoustic paths, which is useful to describe the acoustic propagation paths, especially over long distance. On the other hand, the classical ray theory has limitations as without considering the diffraction and the effects describing the low-frequency dependence.

2.3.2 Parabolic Equation (PE) Model

The Parabolic Equation (PE) method, which is based on the geometrical configurations that naturally arise in the sound channel mode of propagation, is unarguably one of the most useful approximations for solving the problem of wave propagation in inhomogeneous media. PE in underwater acoustics is an extension of a method first invented by Leontovich and Fock (1946) [also see Fock (1965)] in the propagation of radio wave [LF46] [Foc65], in which waves propagation in certain preferred directions were studied. The extension to acoustic waves was first done by Tappert (1977) [Tap77] and since has been extended by many other authors attempting to improving the applicability and accuracy. If the angle with respect to horizontal is small, for instance:

$$|\theta_z| \approx |z - z_s| << 1 \tag{2.9}$$

where z_s is the source depth. then we may use the approximation:

$$p(r_C, z) = \psi(r_C, z)\frac{1}{\sqrt{r_C}}e^{iK_H^0 r_C} \tag{2.10}$$

Where K_H^0 is the number of horizontal wavenumber.

and we define $K_H^2(r_C, z) \equiv K_0^2(n(r_C, z))^2$, $n(r_C, z)$ therefore being an index of refraction c_0/c, where c_0 is a reference sound speed. Substituting equation 2.10 into equation 2.3 and invoking the paraxial (narrow-angle) approximation,

$$\frac{\partial^2\psi}{\partial {r_C}^2} \ll 2K_0\frac{\partial\psi}{\partial r_C} \tag{2.11}$$

we obtain the parabolic equation (in r_C),

$$\frac{\partial\psi^2}{\partial z^2} + 2iK_H^0\frac{\partial\psi}{\partial r_C} + K_H^0(n^2 - 1)\psi = 0 \tag{2.12}$$

As we known, the standard numerical method to solve the above equation is to utilize the split-step range-marching algorithm. It is first introduced in [Tap77]. Then, there are some modifications and extensions to higher-angle propagation [Col93a], elastic media [Col93b] and so on. In addition, the solution for $\psi(r_C, z)$ based on this split-step range-marching algorithm, actually which exploys the fast Fourier transform to calculate the second-order spatial derivatives of the pressure field, is shown as follows:

$$\psi(r_C + \Delta r_C, z) = exp[\frac{iK_H^0}{2}(n^2 - 1)\Delta r_C]F_{tr}^{-1} \times \{[exp(-\frac{i\Delta r_C}{2K_H^0}{K_H^z}^2)]F_{tr}[\psi(r_C, z)]\} \tag{2.13}$$

In Equation 2.13, the Fourier transforms F_{tr} are performed using FFTs. However, there are errors introduced by this split-step range-marching algorithm. For example, in this method, one marching step of the solution is completed by splitting it into two sub-steps sequentially, not simultaneously, and solving for free space propagation and phase anomaly. Because of the sequential splitting, errors can arise from the neglected cross terms. Recently, several attempts have been done on the proposals to reduce such errors and accomplished the extension to a three-dimensional Cartesian parabolic-equation model with a higher-order approximation to the square-root Helmholtz operator [Dud06] [LD12] .

2.4 General Technique Steps of OAT

Over the past decade, it has been increasingly aware of that " the ocean weather " is superimposed on "the ocean climate" by the oceanographers. Generally, the ocean weather is defined as an intense and compact ocean 'mesoscale' eddy structure and sluggish large scale circulation is called ocean climate. Unfortunately, traditional ship-based observing systems are not adequate for monitoring the ocean at mesoscale resolution (for example: a 300km $\times$ 300km) [BBB*82]. Thus, to fully represent atmospheric weather, ocean acoustic tomography was introduced by Munk and Wunsch [MW79][MWW95] as a remote-sensing technique for large-scale monitoring of the ocean interior using low-frequecy sound.

In the original conception of the method, measuring the travel times of sound pulses is the first step. Classically, the sound is emitted by a source and recorded by a receiver or a vertical array composed by several receivers. We call these two configurations respectively point-point and point-array. The sound pulse corresponding to each ray needs to be separated. This is the process of extraction of observation from the recorded data. (shown in the left-hand-side of the Fig. A.1). In the point to point configuration, the sound pulses are usually separated by time of arrival while in the point to array configuration, the reception angle are also provided as a discrimination parameter. Simultaneously, the pulse arrival corresponding to each ray can be calculated from the known physical parameters of a fixed physical propagation model (shown in the right-hand-side of the Fig.A.1) or from ray-tracing programs.

Then, the identification is performed by matching these two types of rays arrivals. In the ray approximation, the observed arrival time change can be ascribed to sound speed changes along the ray path corresponding to the arrival. Although the intensity of the arrival peaks can vary strongly due to the influence of internal wave variability, the arrival times are stable and many can be tracked over a year-long experiment. Sound speed is related to ocean temperature (and weakly to salinity), so the ocean temperature field can be estimated from arrival time measurements over multiple paths. This is some analogy with computerized tomography (CT): multiple sectional X-rays from a source and receiver which are rotated around the patient, and are processed by computer to yield two dimensional displays of the interior structure.

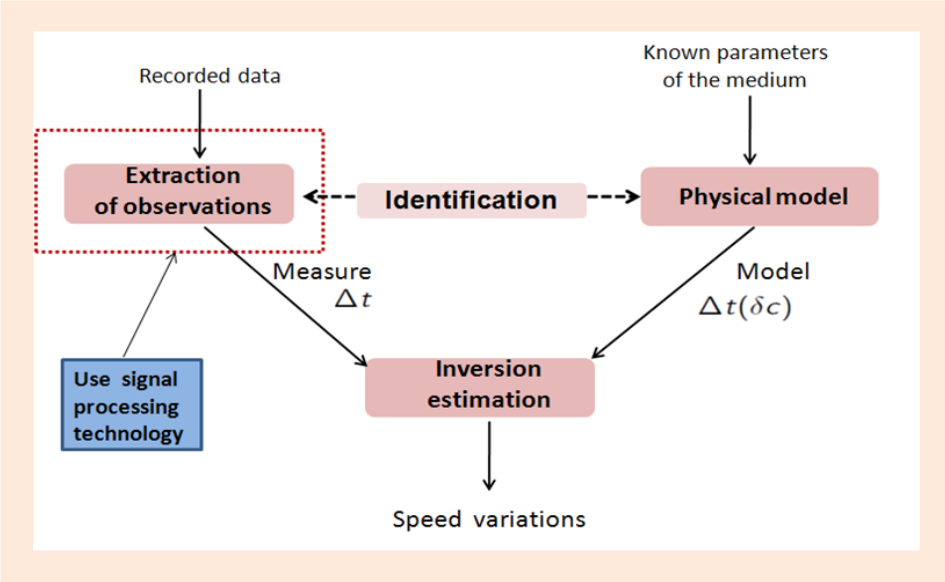

Figure 2.3: Two Main Steps of OAT

2.5 OAT in Shallow Water Waveguide

2.5.1 Shallow Water

The definition of shallow water is that the region from the end of the surf zone out to the continental shelf break. Practically, the typical shallow-water environments are found on the continental shelf for water depths down to 200m. The important motivation of research on shallow water acoustics is that it has great contributions to naval defense issues (for instance, Anti-submarine warfare (ASW) and mine warfare (MWF)). However, at the present, shallow water acoustic techniques are widely used in biology (marine mammals and fish), geology (seabed properties and mapping), and physical oceanography (temperature and current measurements). Besides, the underwater sound in shallow water are also used in commercial and industrial applications (shipping and oil exploration).

Indeed, shallow water is a different environment from deep water. Firstly, it is a far more complicated acoustic medium than deep water, because in shallow water, all the important factors, such as the surface, column, and bottom properties, are spatially varying. At the same time, the oceanographic parameters are also temporally varying.

Furthermore, the principal characteristic of shallow water propagation is that the sound wave is refracted or reflected by the surface and or the bottom. These interactions change the physical properties of sound and in particular cause the lossy of energy. For example, in the summer, there is a warm surface layer causing downward refraction

and hence repeated bottom interaction for all ray paths. Since the seafloor is a lossy boundary, propagation in shallow water is dominated by bottom reflection loss at low and intermediate frequencies ($< 1kHz$) and scattering losses at high frequencies.

Another different aspect of shallow water acoustic is caused by the physical phenomena existing in the coastal ocean. Coastal fronts, eddies, internal waves (linear and nonlinear), create structure on a variety of scales to affect significantly acoustics in the frequency range we are interested in.

Fish and marine mammals, most of which live in shallow water environment, not only make more noise but also could absorb and scatter sound. It also makes shallow water be a different medium from deep water for acoustic propagation.

The last main difference that should be noted is the stronger 3D effects in shallow water (both random and deterministic ones). In shallow water, the slope of the shelf, the shelf break and the canyons can have significant 3D acoustic effects. Moreover, horizontal refraction by the water column itself can also be appreciable, as has been seen recently by both theory and experiment. In deep water, only the bathymetry of seamounts and islands is a serious 3D acoustic concern, a very limited bit of the ocean's area.

2.5.2 Recent Studies on Shallow water

Based on the practical importance and theoretical difference discussed above, oceanographers shifted the study focus again to shallow water after the cold war. The efforts of researchers are paid to both theoretical and experiments study.

Theoretically, the four popular theories introduced in Section 2.3 (normal modes, rays, parabolic equation, wavenumber integration) have been improved and refined in the context of shallow water [Pie65][Mil69][TW80][MW83]. For example, as an extension of Normal mode theory, coupled normal mode theory [Pie65][Mil69] is introduced to deal with the range dependence of the medium in a slice between source and receiver, and even fully 3D effects in theory.

On the other hand, experimental efforts in shallow water have been made by researchers on several aspects. Let us begin with the oceanography. Several experiments (the 1992 Barents Sea Polar Front experiment [LJP*96], the 1996-1997 Shelf break PRIMER experiments, and the recent (2006) SW06 experiment [TML*07]) on the study of coastal fronts are performed, because the drastic change in the acoustic field strength going across a front.

The researchers have also examined the strong mode coupling by internal waves, par-

ticularly nonlinear coastal internal waves in numerous recent experiments. A sampling of those experiments includes the 1995 Shallow Water Acoustic Random Medium experiment (SWARM) [ABC*97], the 1995-1996 PRIMER experiments [GPL*97] [GBB*04], the 2000-2001 Asian Seas Acoustics Experiment (ASIAEX) [DZM*04], and the recent Shallow Water 2006 (SW06) experiment [TML*07].

Thirdly, experiments as the 1985 GEMINI cruises off Corpus Christi, Texas, [CKS92] and the above-cited PRIMER [GPL*97] [GBB*04] and ASIAEX [DZM*04] demonstrated new methods to obtain bottom properties based on acoustic data.

To avoid the technical limitations of large scale experiments, a series of small scale experiments using broadband acoustic signal [RCKH08] [RKH*04] [RJF*01] [KEK*01] [KKH*03] [EAH*02] [KHS*98] [HSK*99] has been performed. The typical range of these experiments are from 1 to 8 km in a 50-120 m deep waveguide.

Besides, as an recent active area of signal processing technology, time-reversed acoustics [Fin97] [Fin99] [FCD*00] are studied a lot.The time reversal technique is based upon a feature of the wave equation known as reciprocity: given a solution to the wave equation, then the time reversal (using a negative time) of that solution is also a solution. This occurs because the standard wave equation only contains even order derivatives. The media are not (e.g. very lossy or noisy media), acoustic waves in water or air are approximately reciprocal and linear. Another way to think of a time reversal experiment is that the time reversal mirror (TRM) is a "channel sampler". The TRM measures the channel during the recording phase, and uses that information in the transmission phase to optimally focus the wave back to the source. This property is first used in underwater communications of shallow water [EAH*02].The experimental results obtained between two source/ receive arrays [EAH*02].

Inspired by the two dimensional configuration, time-delay beamforming is performed simultaneously on both the source and receive arrays to separate the ray paths in the context of shallow water tomography [RCKH08]. Then, the shallow water acoustic tomography performed from double-beamforming algorithm is demonstrated by both simulation results [IRNM08] [IRN*09] and experiment results [RIN*11].

In [IRNM08], they extract efficiently source and receive angles as well as travel times of ray paths by applying the double-beamforming algorithm on two arrays. From these information of ray paths, a uniform coverage of the waveguide by the ray paths is obtained, from which sound-speed fluctuations are reconstructed using a ray-based direct tomography model.

In [RIN*11], a feasibile OAT in a shallow ultrasonic waveguide is demonstrated at the laboratory scale between two source-receiver arrays. At a 1/1000 scale, the waveg-

uide represents a 1.1 km long, 52-m deep ocean acoustic channel in the kilohertz frequency range. Two coplanar arrays record the transfer matrix in the time domain of the waveguide between each pair of source-receiver transducers. A time-domain, double-beamforming algorithm is simultaneously performed on the source and receiver arrays that projects the multi-reflected acoustic echoes into an equivalent set of eigenrays, which are characterized by their travel times and their launch and arrival angles. Travel-time differences are measured for each eigenray every 0.1 s when a thermal plume is generated at a given location in the waveguide.

Using DBF is a clear advantage because the tomography inversion benefits from the identification of a large number of acoustic eigenrays, which cover the whole acoustic waveguide. Travel-time tomography inversion is then performed using two forward models based either on ray theory or on the diffraction-based sensitivity kernel. The travel-time sensitivity kernel (TSK) applied to travel-time fluctuations after DBF takes advantage of the limited bandwidth of the acoustic signals. Compared to tomography data based on ray theory that are no longer relevant at low frequencies, this provides diffraction-limited spatial accuracy in range and depth. The spatially resolved range and depth inversion data confirm the feasibility of acoustic tomography in shallow water.

2.5.3 Multiple RayPaths Propagation

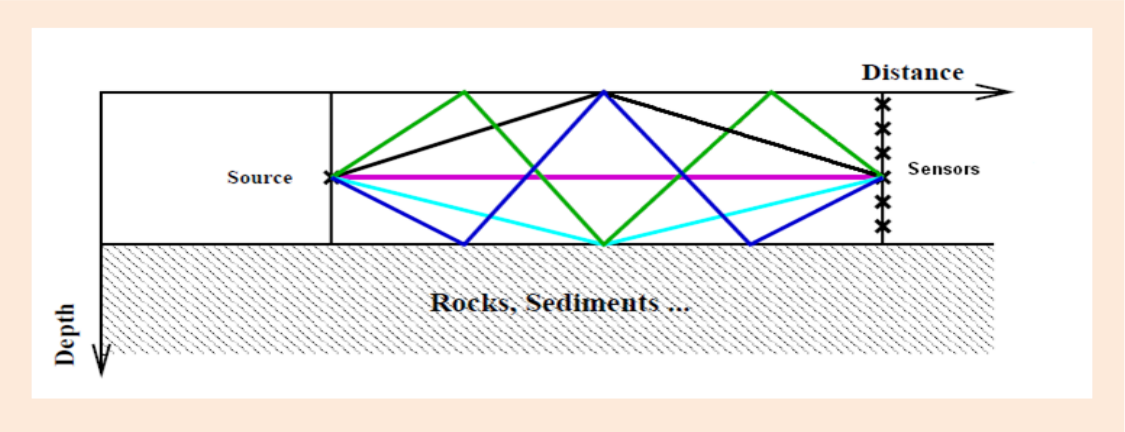

Figure 2.4: Multiple Ray Paths Propagation

In Fig. A.2, an example on raypaths propagation is shown in the configuration of one source and one vertical array. As discussed in Section 2.5.2, in shallow water a beam of rays launched by a source will be refracted or reflected above by the surface and / or down by the continental shelf or refracted in the water. Thus, each ray will follow a different path and provide the information to the OAT. More ray paths can

provide more information by covering the different range of the propagation medium. However, multiple propagation also produces interferences between them. That is why we need the signal processing technology in the OAT, at the same time, the separation and further identification of ray paths becomes an important step of OAT(shown in Fig. A.1). depending on the complexity of the sound-speed structure, distinct wave front arrivals may seem to share the same arrival angle and time on the receive array due to the resolution limits imposed by the pulse bandwidth and the array size.

Chapter 3

Array Processing in Underwater Acoustics

Contents

3.1 Sampling and Digitization Techniques 27

3.1.1 Plane-Wave Beamforming 27

3.1.2 Adaptive Beamformers (Maximum-likelihood method (MLM)) . 28

3.1.3 Double Beamforming 29

3.1.4 A Gibbs sampling localization-deconvolution approach 31

3.1.4.1 Signal model in time domain 33

3.1.4.2 Gibbs sampler 33

3.2 Directly from the received signals 37

3.2.1 Matched Field Processing 37

3.2.1.1 Green's functions 37

3.2.1.2 Signal Models 38

3.2.1.3 Noise Models 38

3.2.1.4 Sample covariance estimation 39

3.2.1.5 The Conventional (Barlett) Beamformer 41

3.2.1.6 Maximum-likelihood method MFP 41

3.2.2 The Time Reversal Mirror 42

3.2.3 Discussion on matched-field processing and phase conjugation of time reversal mirror 48

3.3 Discussion and comparison 49

From the investigation of the Chapter 2, we can conclude that the shallow-water OAT is a vey active research topic in recent studies on oceans. In addition, the separation resolution of the forward problem of OAT is still needed to be improved. This also belongs to source localization or separation problems using a vertical array in underwater acoustics. In this chapter, we will give a brief investigation on these techniques so as to analyze our problem in a more wider persperctive. At the same time, we may get some inspirations for solving our problem through this investigation. Basically, array processing is signal processing utilizing the outputs of an array of sensors. It has been widely used and become a huge technical area in underwater acoustics. In the following part, they will be discussed specifically. Generally, they are usually divided into two categories depending on whether the received signals recorded at the array are directly used to process or will be first sampled by specific sampling and digitization techniques. In addition, we will overview not only some well-known and typical techniques, like beamforming, matched-field processing, but also some important techniques presented more recently, such as double-beamforming and the Gibber sampling technique.

3.1 Sampling and Digitization Techniques

3.1.1 Plane-Wave Beamforming

Plane-wave Beamforming is one of the simplest algorithms for array processing. It can be performed using phase shading in the frequency and time delay in time domain. As an example to introduce the plane-beamforming, a signal model of linear array shown in Figure. 3.1 is considered.

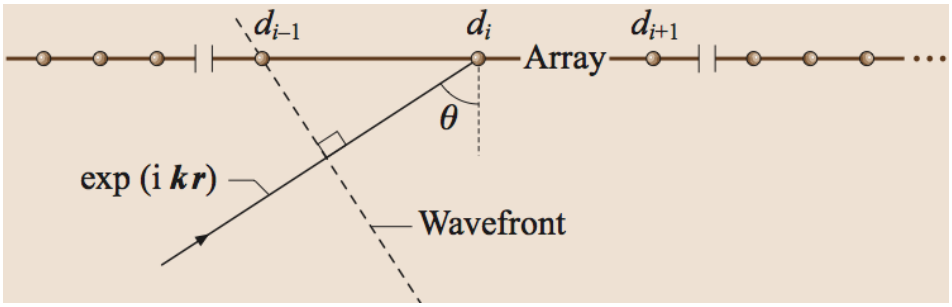

Figure 3.1: Signal model of plane-wave beamforming

Based on the signal model in Figure. 3.1, a plane-wave can be represented as:

$$s(\theta) = a\ exp(i\mathbf{kr}) = a\ exp(i\frac{2\pi\nu Dsin\theta}{c}) \tag{3.1}$$

where θ denotes the arrival angle. D is the distance between two adjacent sensors of the vertical array [VVB88].

$$\boldsymbol{B}(\theta_{sc}) = |\sum_{i=1}^{M} d_i^*(\theta_{sc})[s_i(\theta)+n_i]|^2 = (\sum_{i=1}^{M} d_i^*[s_i+n_i])(\sum_{j=1}^{M}(s_j^*+n_j^*)d_j) = \sum_{i,j=1}^{M} d_i^*(\theta_{sc})(s_{ij}+n_{ij})d_j(\theta_{sc}) \tag{3.2}$$

where

$$d_i^* = exp(-i\frac{2\pi\nu D_i sin\theta_{sc}}{c}) \tag{3.3}$$

and θ_{sc} denotes the scanning angle in the steering directional vector $\mathbf{d}(\theta_{sc})$. D_i is the distance of the ith sensor referring to the reference sensor. The above equation can be rewritten in matrix notation:

$$\boldsymbol{B}(\theta_{sc}) = \mathbf{d}^{\dagger}(\theta_{sc})\mathbf{R}(\theta)\mathbf{d}(\theta_{sc}) \tag{3.4}$$

with the $\mathbf{R}(\theta)$ denoting the covariance matrix of received data which contains the information of true arrival angles. Specifically, $R_{ij} = s_{ij} + n_{ij}$. Assume that the signal and noise are uncorrelated, $\mathbf{R}$ can be expressed as the sum of the covariance of noise $\mathbf{R}_n$ and the signal covariance matrix $\mathbf{R}_s$:

$$\mathbf{R} = \mathbf{R}_s + \mathbf{R}_n \tag{3.5}$$

The main process of plane-beamforming is to find the maximum value of Equation. 3.4 since this maximum value exists only when the scanning angle equals the true arrival angle of the signal.

3.1.2 Adaptive Beamformers (Maximum-likelihood method (MLM))

Differing from the conventional beamforming, the adaptive beamformer depends on a weight steering vector, which is constructed according to some rule of optimization based on the theoretical directional vector $\mathbf{d}$. Specifically, the weight directional vector (denoted as $\mathbf{d}_{MLM}$) is constructed using the Lagrange multiplier method based on the expression [GJ82] [CZO87] [JD92]:

$$F_{lag} = \mathbf{d}_{MLM}^*\mathbf{R}\mathbf{d}_{MLM} + \lambda_L(\mathbf{d}_{MLM}^*\mathbf{d} - 1) \;\text{ with }\; \mathbf{d}_{MLM}^*\mathbf{d} = \mathbf{\Lambda} \tag{3.6}$$

$$2\mathbf{R}\mathbf{d}_{MLM} - \lambda_L\mathbf{d} = 0 \tag{3.7}$$

$$\mathbf{d}_{MLM} = \frac{\lambda_L}{2}\mathbf{R}^{-1}\mathbf{d} \tag{3.8}$$

Using $\mathbf{d}^*_{MLM}\mathbf{d} = \mathbf{\Lambda}$, we obtain:

$$\lambda_L = \frac{2}{\mathbf{d}^*\mathbf{R}^{-1}\mathbf{d}} \tag{3.9}$$

Thus, the connection between the weighting directional vector $\mathbf{d}_{MLM}$ and the theoretical steering directional vector $\mathbf{d}$ is expressed as:

$$\mathbf{d}_{MLM} = \frac{\mathbf{R}^{-1}\mathbf{d}}{\mathbf{d}^*\mathbf{R}^{-1}\mathbf{d}} \tag{3.10}$$

Substituting the above equation to Equation. 3.4, the estimator of MLM is expressed as:

$$\boldsymbol{B}_{MLM}(\theta_s) = \frac{1}{\mathbf{d}^*(\theta_{sc})\mathbf{R}^{-1}(\theta)\mathbf{d}(\theta_{sc})} \tag{3.11}$$

3.1.3 Double Beamforming

Invoking by a series of broadband shallow water acoustic experiments, which employs both source and receive arrays and focus on time reversal, an experiment of illustrating the structure of ray like arrivals in a shallow water waveguide is presented in [RCKH08]. Specifically, it uses a source array to provide an additional parameter (emitted angle) of selecting raypaths. Then, it is used in a shallow water acoustic tomography simulation experiment [IRN*09]. This method will be introduced in detail.

Equation 3.12 and Figure 3.2 demonstrate the process of double beamforming mathematically or with graphic expression. That is, first, the beamforming is performed on the receive array for each source. The pressure field $p(t, z_r, z_s)$ recorded on the received array is transformed into $p(t, \theta_r, z_s)$. Similarly, based on the reciprocity property [MF53], the beamforming is used the second time on the emission array. In this step, $p(t, \theta_r, z_s)$ is transformed into $p(t, \theta_r, \theta_s)$, where θ_r denotes the emitted angle.

$$p(t, \theta_r, \theta_s) = \frac{1}{M_r\ M_s} \times \sum_{i=1}^{M_r}\sum_{j=1}^{M_s} a_{ij}p(t + \tau(\theta_r, z_{ri}) + \tau(\theta_s, z_{sj}), z_{ri}, z_{sj}) \tag{3.12}$$

In equation 3.12, z_{ri} and z_{sj} are the receiver and source depth respectively. $\tau(\theta, z)$ denotes the delay produced by both the angle and distance intervals between the depth of reference sensor z_0 and the specific depth z where one of sensors is at either the received array or the emitted array. If we consider the case of plane wave, the velocity

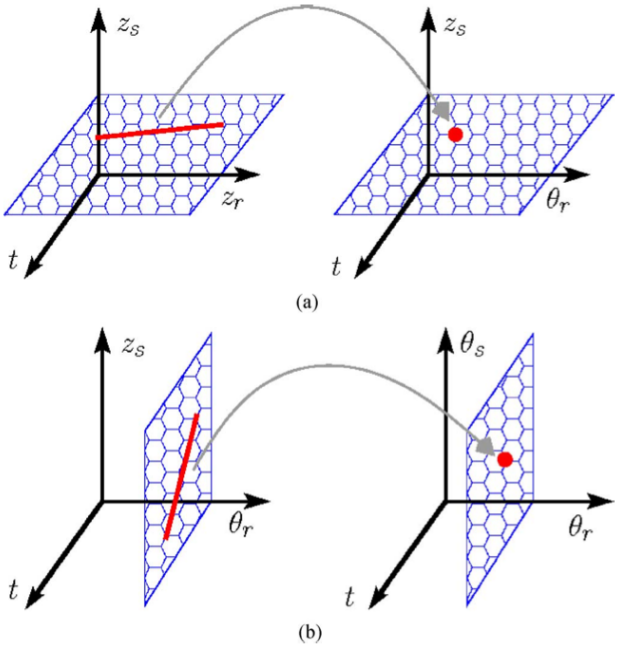

Figure 3.2: The schematic presentation of the double beamforming (a) The pressure field $p(t, z_r, z_s)$ recorded on the received array is transformed into $p(t, \theta_r, z_s)$ space (b) In second step, $p(t, \theta_r, z_s)$ is transformed into $p(t, \theta_r, \theta_s)$ space, where θ_r denotes the emitted angle.

$c(z) = c$ at which the acoustic wave propagates is uniform along the array. Therefore, the delay $\tau(\theta, z)$ can be obtained by equation 3.13:

$$\tau(\theta, z) = (z - z_0)\frac{sin\theta}{c} \tag{3.13}$$

Otherwise, if the sound velocity $c(z)$ changes over depth along the array, the time delay $\tau(\theta, z)$ can be computed by turning point filter [DWM01]:

$$\tau(\theta, z) = \int_{z_0}^{z} \sqrt{\frac{1}{c^2(z)} - \frac{cos^2\theta}{c_{min}^2}}dz \tag{3.14}$$

where c_{min} is the minimum sound speed along the array.

An analytic formulation of single beamforming pattern (SB) [LL93] [ST98] is given by:

$$SB(\theta_{obs}, \theta, \nu) = S(\nu)\frac{sin(\frac{\Pi M d\nu}{c}(sin\theta_{obs} - sin\theta))}{sin(\frac{\Pi d\nu}{c}(sin\theta_{obs} - sin\theta))} \times exp(i\phi_e(\theta_{obs}, \theta, \nu, z_0)) \tag{3.15}$$

It is composed by the spectrum of signal $S(\nu)$, the amplitude gain of beamforming filter $\frac{sin(\frac{\Pi M d\nu}{c}(sin\theta_{obs} - sin\theta))}{sin(\frac{\Pi d\nu}{c}(sin\theta_{obs} - sin\theta))}$ and the phase $exp(i\phi_e(\theta_{obs}, \theta, \nu, z_0))$. Where θ and θ_{obs} denotes the

actual arrival angle and the estimated one. From equation 3.15, we obtain the angular resolution as:

$$\triangle\theta \approx \frac{\lambda}{Md} \tag{3.16}$$

The phase term at frequency ν in equation 3.15 can be specifically written as:

$$\phi_e(\theta_{obs}, \theta, \nu, z_0) = 2\Pi\nu\frac{1}{c}(sin\theta - sin\theta_{obs})(d\frac{M-1}{2} + z_1 - z_0) \tag{3.17}$$

with z_1 is the depth of the first receiver. Its time delay is $t_e = \phi_e/2\Pi M\nu$. In order to make the estimation angle θ_{bs} exactly equal to the real angle θ, the subarray must be centered on the reference point z_0.

If we define $a_r = sin\theta_r$ and $a_s = sin\theta_s$, equations 3.18, 3.19 and 3.20 give the conditions in which two raypaths can be separated in the array to array configuration, point to array configuration and point to point configuration respectively.

$$(\frac{t_2 - t_1}{\triangle t})^2 + (\frac{a_{r2} - a_{r1}}{\triangle a_r})^2 + (\frac{a_{s2} - a_{s1}}{\triangle a_s})^2 > 1 \tag{3.18}$$

$$(\frac{t_2 - t_1}{\triangle t})^2 + (\frac{a_{r2} - a_{r1}}{\triangle a_r})^2 > 1 \tag{3.19}$$

$$(\frac{t_2 - t_1}{\triangle t})^2 > 1 \tag{3.20}$$

Through observing from these three equations, we can get the conclusion that an additional parameter can provide a positive term, such as $(\frac{a_{r2}-a_{r1}}{\triangle a_r}^2)$ in equation 3.19, $(\frac{a_{s2}-a_{s1}}{\triangle a_s})^2$ in equation 3.18, to more easily satisfy the condition of separating two raypaths. Therefore, the double beamforming shows a better separation ability. The improved separation resolution is also helpful to identify more raypaths. The improved resolution becomes particularly important when the two raypaths have very close receive angles and different emitted angles. Figure 3.3 shows an example obtained from FAF03 (the Focused Acoustic Field) data set presented in [RKH*04]. The two raypaths in Fig. 3.3 (a) cannot be separated by beamformng while double beamforming successes in separation using the emitted angles.

3.1.4 A Gibbs sampling localization-deconvolution approach

Using maximization a posteriori (MAP) estimation of the time delay and amplitude has been presented in [EEM78] [TCL87]. Recently, a MAP approach is implemented using Gibber sampler for the derivation of the joint posterior probability distribution of time

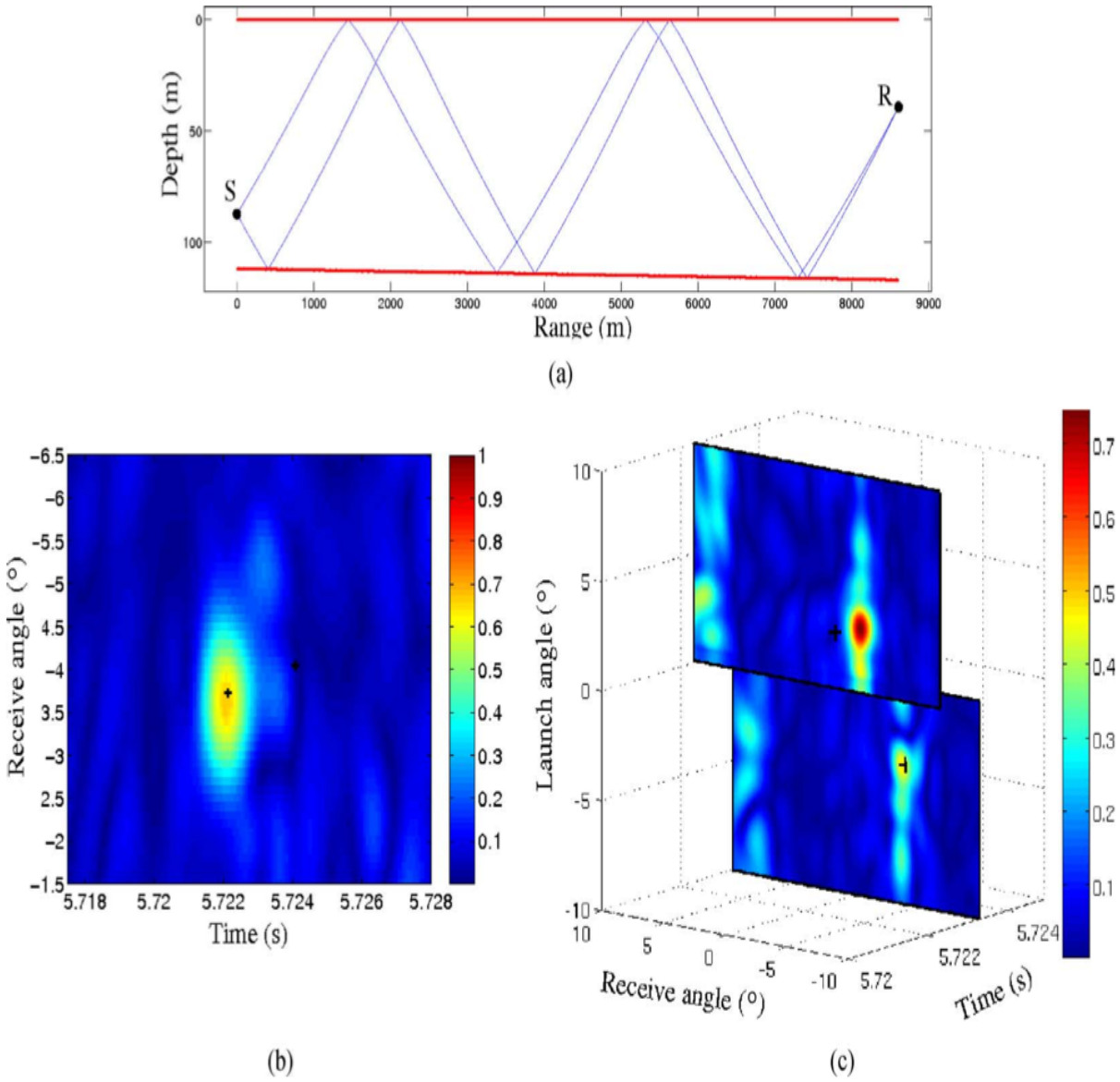

Figure 3.3: The separation results of beamforming vs double beamforming (Crosses indicate the theoretical prediction values.) from [IRN*09]: (a) two raypaths are extracted from the FAF03 data set [RKH*04] at depth $z_s = 87.3m$ and $z_r = 39.3m$; (b) the separation results of the two raypaths in (a) using beamforming; (c) the separation results of the two raypaths in (a) using double beamforming.

delay and amplitude, and what is entailed in its maximization [MP05]. We will begin to introduce it from the signal model.

3.1.4.1 Signal model in time domain

$$x(t) = \sum_{i=1}^{P} a_i s(t - t_i) + n(t) \tag{3.21}$$

where $t = 1, \ldots, N$ (N is the time duration of the received signal), P is the number of paths (assuming that it is known in the following discussion). a_i is the amplitude of the ith path, and t_i is the arrival time of the ith path. $n(t)$ is the additive noise, which is assumed white noise with zero mean and variance ${\sigma_n}^2$. The variance ${\sigma_n}^2$ is assumed as a known parameter here. Then, the extended case for it is unknown will be analyzed. First, the amplitudes distribution is assigned as the uniform, improper prior distributions under the assumptions of no prior information.

$$P_{ro}(a_i) = 1 \quad -\infty < a_i < \infty, \quad i = 1, \ldots, P. \tag{3.22}$$

And, the uniform priors for the delays is set as:

$$P_{ro}(t_i) = \frac{1}{N} \quad 1 \ll t_i \ll N, \quad i = 1, \ldots, P. \tag{3.23}$$

The posterior probability distribution function of all the a_i and t_i $i = 1, \ldots, P$ is given by:

$$P_{ro}(t_1, t_2, \ldots, t_P, a_1, a_2, \ldots, a_P | x(t)) = C(exp(-\frac{1}{2{\sigma_n}^2}) \sum_{t=1}^{N} (x(t) - \sum_{i=1}^{P} a_i s(t - t_i))^2) \tag{3.24}$$

where C is a constant and equal to $K\ (1/N^P)[1/(\sqrt{2\pi})^N {\sigma_n}^N]$

The above equation is the joint posterior distribution. If this is obtained, on the basis of it, the maximization a posteriori estimation in [EEM78] [TCL87] is performed by searching a maximum value of this function in a $2 \times P$ dimensional space. If P is large, this algorithm has the problem of the big computation price.

3.1.4.2 Gibbs sampler

On the basis of the above discussion, the case when the noise variance is unknown will be discussed specifically in this part. At the same time, the technique details of Gibbs sampler will be presented.

A non informative prior distribution [Ber85] is considered for the variance as:

$$P_{ro}({\sigma_n}^2) \propto \frac{1}{{\sigma_n}^2} \tag{3.25}$$

If the prior information of the unknown variance and consolidating constants are considered, we can obtain the joint posterior distribution as:

$$P_{ro}(t_1, t_2, \ldots, t_P, a_1, a_2, \ldots, a_P, {\sigma_n}^2 | x(t)) = C\frac{1}{{\sigma_n}^{N+2}} exp(-\frac{1}{2{\sigma_n}^2}\sum_{t=1}^{N}(x(t) - \sum_{i=1}^{P} a_i s(t-t_i))^2) \tag{3.26}$$

And the conditional posterior distribution for the variance, which satisfies an inverse χ^2 distribution, is:

$$P_{ro}({\sigma_n}^2 |\ t_1, t_2, \ldots, t_P, a_1, a_2, \ldots, a_P, x(t)) \propto \frac{1}{{\sigma_n}^{N+2}} exp(-\frac{1}{2{\sigma_n}^2}\sum_{t=1}^{N}(x(t) - \sum_{i=1}^{P} a_i s(t-t_i))^2) \tag{3.27}$$

Based on the joint posterior function shown by Equation. 3.26 and the assumption of all the other parameters like amplitudes $a_j, j = 1, \ldots, P$ *and* $j \neq i$ and delays $t_i, i = 1, \ldots, P$ are known, the conditional distribution for amplitude a_i can be derived as:

$$\begin{aligned} &P_{ro}(a_i |\ t_1, t_2, \ldots, t_P, a_1, a_2, \ldots, a_P, {\sigma_n}^2, x(t)) \\ &= C\frac{1}{{\sigma_n}^{N+2}} exp(-\frac{1}{2{\sigma_n}^2}(a_i - (\sum_{t=1}^{N} x(t)s(t-t_i) - \sum_{j=1(j\neq i)}^{P} a_j s(t-t_i)s(t-t_j)))^2) \end{aligned} \tag{3.28}$$

Actually, it is a normal distribution whose variance equal to ${\sigma_n}^2$ and it has the mean:

$$(\sum_{t=1}^{N} x(t)s(t-t_i) - \sum_{j=1(j\neq i)}^{P} a_j s(t-t_i)s(t-t_j)) \tag{3.29}$$

Similarly, the conditional posterior distribution of t_i for known $a_j, j = 1, \ldots, P$, t_k, $k = 1, \ldots, P, k \neq i$, and ${\sigma_n}^2$ is:

$$P_{ro}(t_i |\ t_1, t_2, \ldots, t_P, a_1, a_2, \ldots, a_P, {\sigma_n}^2, x(t)) = C\ exp(-\frac{1}{2{\sigma_n}^2}\sum_{t=1}^{N}(x(t) - \sum_{i=1}^{P} a_i s(t-t_i))^2) \tag{3.30}$$

Essentially, the Gibbs sampling is an iteration process beginning from drawing a sample from the inverse σ_n^2 distribution of Equation. 3.27. After that, we obtained the first updated value of the variance σ_n^2. Subsequently, this value is used to compute the updated value of a_1 from the normal marginal conditional posterior of a_1 obtained with Eq. 3.28. With the new value of σ_n^2, a_1 and all the initial values of parameters, that is, $a_3, \ldots, a_P$ and $t_1, t_2, \ldots, t_P$, the updated value of a_2 can be gotten through the same process of

obtaining a_1. This procedure is continued until all unknown parameters are updated. These updated values consist of the Gibbs sample sequences. The larger number of iterations is useful to make the obtained sample sequences more converge to the true joint posterior distribution of all the parameters. [GRS96][GG84][GS90]

In [MP05], the performance of this Gibbs sampling is evaluated and is compared with expectation-maximization. To give an intuitive understanding of performance for Gibbs sampling, here, we will give an example to illustrate the performance of conventional narrowband Bartlett processor and the Gibbs sampling approach in the context of source location. To avoid the intensive computation cost of searching the estimated values of the unknown parameters in a multi-dimensional space, a Gibbs sampling to source localization and deconvolution is developed as an efficient search methods for the fast exploration of the parameter space. The following figure shows the source location estimates obtained using (a) the conventional narrowband Bartlett processor and (b) a Gibbs sampling localization-deconvolution approach developed by Michalopoulou [Mic00]. The expected source location is at 2 km in range and 34 m in depth. The Bartlett processor produces a range-depth surface with the peak away from the true source location. The Gibbs sampling approach, on the other hand, produces a clear ambiguity surface with the main mode at the correct source location.

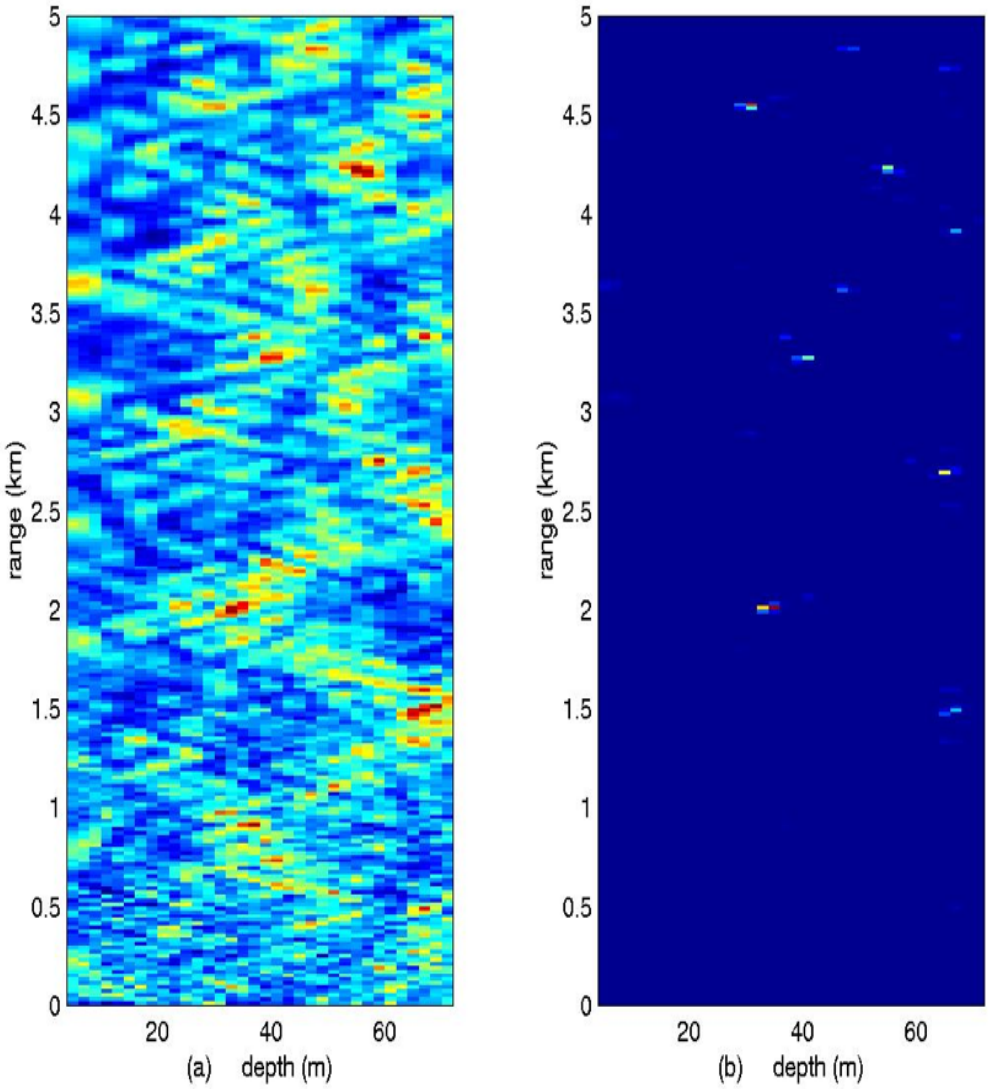

Figure 3.4: The expected source location is at 2 km in range and 34 m in depth. The Gibbs sampling approach produces a clear ambiguity surface with the main mode at the correct source location [Micoo].(a) Bartlett and (b) Gibbs sampling ambiguity surfaces for source location.

3.2 Directly from the received signals

3.2.1 Matched Field Processing

Matched Field Processing (MFP) is a method of optimal signal processing using and exploiting the realistic structure of the sound field and can be taken as an extension of plane-wave beamforming in situation of the ocean environment where can not be taken as a homogeneous space. The process of MFP involves examining the resolution consistent of the actual acoustic pressure field measured at the receiver array with a predicted field through calculating their correlation. The predicted field is evaluated from the ocean model and a postulated source position. The location of highest correlation indicates where the source locates. At the same time, ocean model can be readjusted by resolution of location as a feedback. However, the difficulty faced by MFP is how to specify the coefficients and boundary conditions of the acoustic wave equation for the shallow water.

A specific MFP method is usually composed by three principal steps: first, signal models is built from computing the Green's Function; then, data samples are used to estimate the covariance matrix $\hat{\mathbf{R}}$ or the ambient field $\mathbf{R}$; finally, estimators, which are functions of steering vector containing the environment or location parameter and the sample covariance matrix $\hat{\mathbf{R}}$, are exploited to estimate the field distribution. In the following part, they will be introduced orderly.

3.2.1.1 Green's functions

We have introduced Green's functions in Chapter 2. In equation 2.5, $\mathbf{G}$ represents the velocity potential (or scaled pressure) for a unit normalized source which satisfies the frequency ($\omega = 2\pi\nu$) domain wave equation. The source coordinates and the parameters associated with the ocean environment determine wave equation as coefficients and boundary of the wave field. Those parameters are denoted as $\mathbf{A}_{in}$. Moreover, the field at any point $(\mathbf{r}, z)$ can be represented as $\mathbf{G}(\nu, \mathbf{A}_{in})$ as it is a function of frequency, source coordinates and the parameters associated with the ocean environment. We assume that the ocean field is only horizontal stratification, thus, $\mathbf{G}$ can be decomposed into a depth dependent Green's $g(\mathbf{k}, z, z_s)$ and set of plane waves $e^{i\mathbf{kr}}$. (k is the horizontal wavenumber of plane waves)

$$\mathbf{G}(\mathbf{r}, z) = \frac{1}{4\pi^2} \int_{-\infty}^{\infty} d^2\mathbf{k} g(\mathbf{k}, z, z_s) e^{i\mathbf{k}(\mathbf{r}-\mathbf{r}_s)} \tag{3.31}$$

where $g(\mathbf{k}, z, z_s)$ satisfies:

$$\frac{d^2g}{dz^2} + (K_H^2(z) - k_H^2)g = -\delta(z - z_s) \tag{3.32}$$

3.2.1.2 Signal Models

We discuss signal models exploited in MFP in the context of point source in this part and the Green' s function is used as a basis to form signal model. Specifically, $\mathbf{G}(\mathbf{r}_i, (\mathbf{z}_i)$ at the array positions are incorporated into a signal vector $\mathbf{G}(\boldsymbol{\nu}, \mathbf{A}_{in})$ to express the spatial structure of signal as:

$$\mathbf{G}(\boldsymbol{\nu}, \mathbf{A}_{in}) = \begin{bmatrix} G(\mathbf{r}_1, z_1, \mathbf{A}_{in}) \\ G(\mathbf{r}_2, z_2, \mathbf{A}_{in}) \\ \vdots \\ G(\mathbf{r}_M, z_M, \mathbf{A}_{in}) \end{bmatrix} \tag{3.33}$$

In addition, the covariance is given by:

$$\mathbf{R}_s = \sigma_a^2 \mathbf{G}(\boldsymbol{\nu}, \mathbf{A}_{in}) \mathbf{G}^H(\boldsymbol{\nu}, \mathbf{A}_{in}) \tag{3.34}$$

with σ_a^2 denoting the variance of the amplitude value of source which varies in a complex Gaussian random process.

3.2.1.3 Noise Models

Considering a real ocean environment, the ocean noise is divided into three categories [KI80]: sensor noise, distributed noise and discrete noise sources. We denote the relevant noise covariance as $\mathbf{R}_W$, $\mathbf{R}_C$ and $\mathbf{R}_D$. $\mathbf{R}_n$ denotes cross spectral density matrix or the covariance of ocean noise. Thus, it is

$$\mathbf{R}_n = \mathbf{R}_W + \mathbf{R}_C + \mathbf{R}_D \tag{3.35}$$

Since sensor noise is spatially uncorrelated, its covariance matrix is expressed by:

$$\mathbf{R}_w = \sigma_n^2 \mathbf{I} \tag{3.36}$$

with $\mathbf{I}$ is the identity matrix. $\mathbf{R}_C$ is structured according to the ocean environment in

which the signal propagates.

$$\mathbf{R}_C(\mathbf{r}_{ij}, z_i, z_j) = q^2 \int d^2\mathbf{k}\mathbf{P}(\mathbf{k})g(\mathbf{k}, z_i, z^{'})g^*(\mathbf{k}, z_j, z^{'})e^{i\mathbf{k}\mathbf{r}_{ij}} \tag{3.37}$$

with

q is the surface noise spectrum amplitude;

$P(k)$ the spatial spectral distribution of homogeneous noise sources;

g the solutions of 3.40 with the same ocean environment as the signal and replica fields;

$\mathbf{r}_{ij}$ the horizontal vector between the i th and j th sensor.

z_i and z_j the corresponding depths and $z^{'}$ is the noise sourced layer depth.

$\mathbf{R}_D$ is the covariance from discrete noise sources which can be treated as point source signals.

3.2.1.4 Sample covariance estimation

If we assume that signal and noise are uncorrelated, the covariance $\mathbf{R}$ is given by:

$$\mathbf{R} = \mathbf{R}_s + \mathbf{R}_n \tag{3.38}$$

However, it must be estimated from the data or predicted using some propagation model. To estimate the covariance matrix $\mathbf{R}$, the received signal is segmented into " snapshots " using a specific window:

$$R_i^l(\nu) = \int_{T_l}^{T_l+T_w} r_i(t)W(t-T_l)e^{-i2\pi\nu t}dt \tag{3.39}$$

where

$r_i(t)$ the signal from the *ith* channel;

$W(t)$ a taper, sampling window, function applied to the data to control sidelobes;

T_l the start time point of the l th segment of data;

T_w the duration of the taper function.

Then, these snapshots form a data vector $\mathbf{R}^l(\nu)$. We assume that we have an array with M sensors located at z_i, $i = 1, \ldots, M$ and a narrowband model as shown in Fig.

3.5·

$$\mathbf{R}^l(\nu) = \begin{bmatrix} R_1^l(\nu) \\ R_2^l(\nu) \\ \vdots \\ R_M^l(\nu) \end{bmatrix} \tag{3.40}$$

Generally, the covariance matrix is estimated by averaging L data vectors:

$$\hat{\mathbf{R}}(\nu) = \frac{1}{L}\sum_{l=1}^{L} \mathbf{R}^l(\nu)\mathbf{R}^l(\nu)^* \tag{3.41}$$

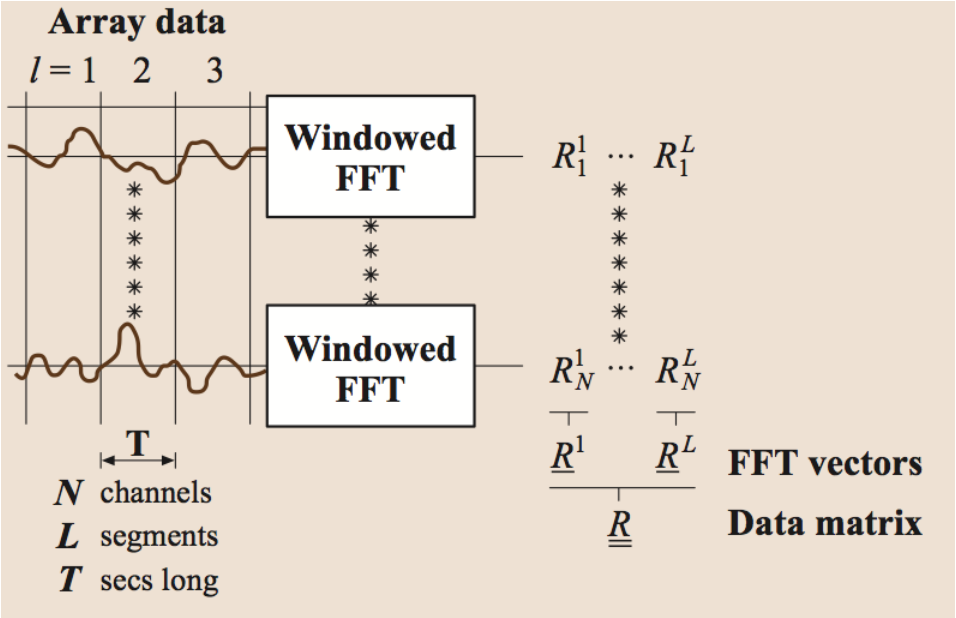

Figure 3.5: Array narrow model, sample matrix estimation, and data preconditioning for MFP

The singular value decomposition (SVD) of the covariance matrix $\mathbf{R}$ is used in several of the MFP algorithms and given by:

$$\mathbf{R} = \mathbf{E}\Lambda\mathbf{E}^* \tag{3.42}$$

with the columns of $\mathbf{E}$ are the eigenvectors $\mathbf{e}_i$ $(i = 1, \ldots, M)$ of $\mathbf{R}$ and Λ is a diagonal matrix. The values in the diagonal of $\mathbf{R}$ are eigenvalues σ_i^2 $(i = 1, \ldots, M)$. That is:

$$\mathbf{R}\mathbf{e}_i = \sigma_i^2\mathbf{e}_i \tag{3.43}$$

In practice, it is convenient to express the SVD decomposition of $\mathbf{R}$ directly using its

eigenvalues and eigenvectors.

$$\mathbf{R} = \sum_{i=1}^{M} \sigma_i^2 \mathbf{e}_i \mathbf{e}_i^* \tag{3.44}$$

In subsection 3.2.1.5 and 3.2.1.6, we will present two representative estimators as examples: The Conventional (Barlett) Beamformer and Maximum-likelihood method MFP. The rest of estimators can be exploited in MFP, like power law MFP's [BK79] [DL90], controlled sensor noise MVDF [Cox73] [CZO87] [Yan87], multiple constraint processors [EC83], [Ste83], [Vur79], please refer to the related references.

3.2.1.5 The Conventional (Barlett) Beamformer

The conventional beamformer is an estimator which is largely used in MFP. Essentially, the data vectors $\mathbf{R}^l$ are projected on the normalized replica vectors $\mathbf{w}_c(\hat{\mathbf{A}}_{in})$ and L projection are formed an average. Specifically, this process is given by:

$$\mathbf{B}_c(\hat{\mathbf{A}}_{in}) = \frac{1}{L} \sum_{i=1}^{L} |\mathbf{w}_c^*(\hat{\mathbf{A}}_{in}) \mathbf{R}^l|^2 \tag{3.45}$$

where

$$\mathbf{w}_c(\hat{\mathbf{A}}_{in}) = \frac{\mathbf{G}(\hat{\mathbf{A}}_{in})}{|\mathbf{G}(\hat{\mathbf{A}}_{in})|} \tag{3.46}$$

In the matrix form, we have the conventional beam former as:

$$\mathbf{B}_c(\hat{\mathbf{A}}_{in}) = \mathbf{w}_c^*(\hat{\mathbf{A}}_{in}) \hat{\mathbf{R}} \mathbf{w}_c(\hat{\mathbf{A}}_{in}) \tag{3.47}$$

3.2.1.6 Maximum-likelihood method MFP

Another variety of Beamformer estimator is connected with the maximum likelihood method (MLM) of parameter estimation. It is originally proposed and used in Ref. [Cap69] and also called the minimum variance or distortionless filter (MVDF). The main idea of MFP is to minimize the variance at the output of a linear weighting, $\mathbf{w}_{MLM}(\hat{\mathbf{A}}_{in})$ of the sensors subject to the distortionless constraint that signals in the " look direction" have unity gain.

Specifically, the formulation required to minimize the variance is expressed as:

$$B(\hat{\mathbf{A}}_{in}) = \mathbf{w}^*(\hat{\mathbf{A}}_{in}) \mathbf{R} \mathbf{w}(\hat{\mathbf{A}}_{in}) \tag{3.48}$$

The distortionless constraint is described mathematically as follow:

$$\mathbf{w}^*(\hat{\mathbf{A}}_{in})\mathbf{w}_c(\hat{\mathbf{A}}_{in}) = 1 \tag{3.49}$$

Substituting the Eq. 3.49 to Eq. 3.48, we can obtain:

$$\mathbf{w}^*_{MLM}(\hat{\mathbf{A}}_{in}) = \mathbf{B}_{MLM}(\hat{\mathbf{A}}_{in})\mathbf{R}^{-1}\mathbf{w}_c(\hat{\mathbf{A}}_{in}) \tag{3.50}$$

Thus, the MLM estimator function in MFP $\boldsymbol{B}_{MLM}$ is obtained as:

$$\boldsymbol{B}_{MLM}(\hat{\mathbf{A}}_{in}) = \frac{1}{\mathbf{w}^*_c(\hat{\mathbf{A}}_{in})\mathbf{R}^{-1}\mathbf{w}_c(\hat{\mathbf{A}}_{in})} \tag{3.51}$$

If the sample covariance $\hat{\mathbf{R}}$ is used instead of the covariance $\mathbf{R}$ in above equation, $\boldsymbol{B}_{MLM}$ can be computed by:

$$\boldsymbol{B}_{MLM}(\hat{\mathbf{A}}_{in}) = \frac{1}{\mathbf{w}^*_c(\hat{\mathbf{A}}_{in})\hat{\mathbf{R}}^{-1}\mathbf{w}_c(\hat{\mathbf{A}}_{in})} \tag{3.52}$$

To show how the matched field processing (MFP) is carried out in a real source localization problem, we give an example of localizing a singing whale in the ocean from [TDF91].

3.2.2 The Time Reversal Mirror

The Fourier conjugate of phase conjugation implemented over a finite spatial aperture is called "time-reversal mirror" [FPWC89][Fin93]. Phase conjugation is a physical transformation of a wave field where the resulting field has a reversed propagation direction but keeps are amplitudes and phases. Phase conjugation [ZPS85] has been first demonstrated in nonlinear optics, then in ultrasonic acoustic experiments [FPWC89][Fin93] and recently in underwater acoustics [JD91] [DJ92] [Dow93] [Dow94].

The time reversal technique is based upon a feature of the wave equation known as reciprocity: given a solution to the wave equation, then the time reversal (using a negative time) of that solution is also a solution. This occurs because the standard wave equation only contains even order derivatives. Wave propagation has the property of reciprocity when the acoustic wave propagates in a static medium. Although some media are not reciprocal (e.g. very lossy or noisy media), sound waves in water is approximately reciprocal. As an specific example, if the source is passive, i.e. some type of isolated reflector, an iterative technique can be used to focus energy on it. The TRM transmits a plane wave which travels toward the target and is reflected off it. The reflected wave returns to the TRM, where it looks as if the target has emitted a (weak)

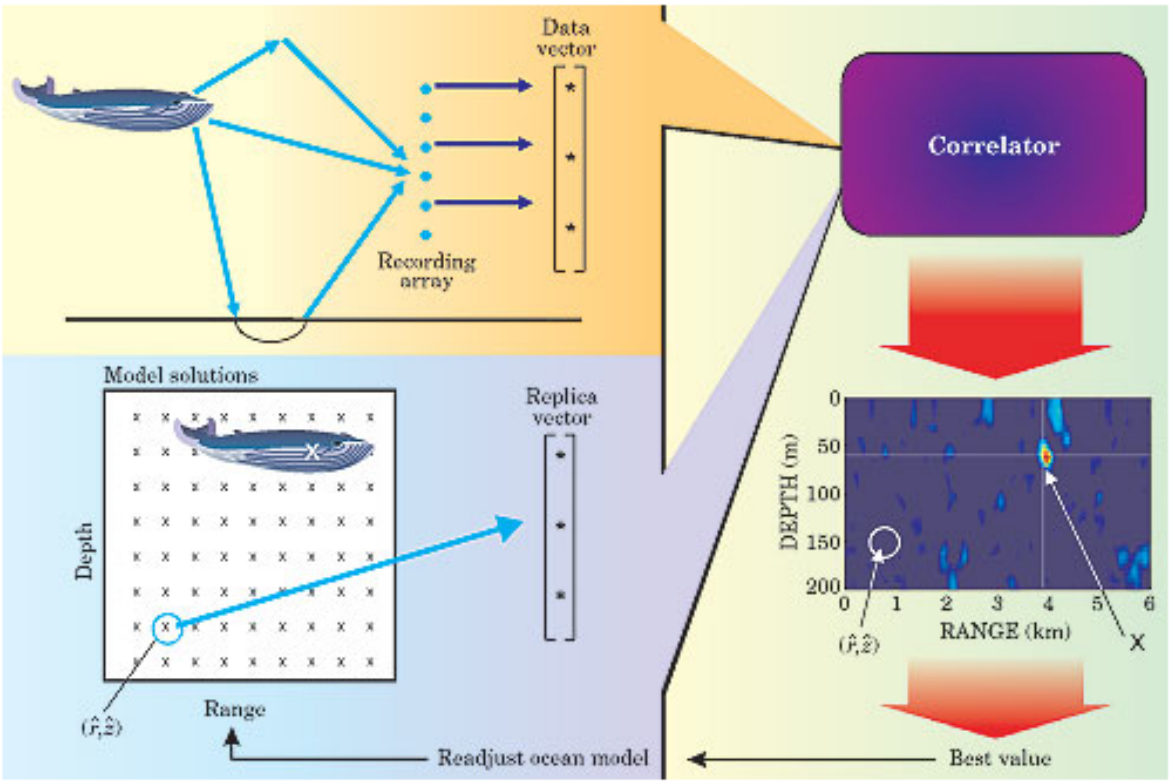

Figure 3.6: Matched field processing (MFP) [KL04]. If you want to know where a singing whale locates at, first, the sound of the wave is recorded as an data vector; and then based on your sufficient accurate model of waveguide propagation, compare the recorded data from the singing wave, one frequency at a time, with the replica data. The location of highest correlation (the red peak in the fig. 3.6) denotes the estimated where the whale locates at. The feedback loop suggests a way to optimize the model. Matched field processing can then be used in the context of ocean acoustic tomogtraphy [TDF91]. The data is from [KL04] [BBR*96]

signal. The TRM reverses and retransmits the signal as usual, and a more focused wave travels toward the target. As the process is repeated, the waves become more and more focused on the target.

The general configuration of the time reversal technique is implemented by a source-receiver array (SRA) and a probe source (PS). The SRA is composed of several hydrophones with a nominal resonance frequency. It carries out the main operations of the time reversal technique: first, each hydrophone receives the emitted signal from the PS; then, the received signal is done the time reversal operation by the calculation of the complex-conjugate spectrum; and, finally, the time reversal signal is emitted. The schematic in Fig. 3.7 illustrates the components of a TRM experiment. A probe source (PS), indicated by one of the rectangles on the vertical receiver array (VRA), sends out a pulse that is received at the source-receiver array (SRA). The dispersed signal with all its multipath structure is time reversed and retransmitted by the SRA. The resulting signal multipath structure collapses to a spatial and temporal focus (original PS pulse length) at the original PS position that is co-located in range with the VRA.

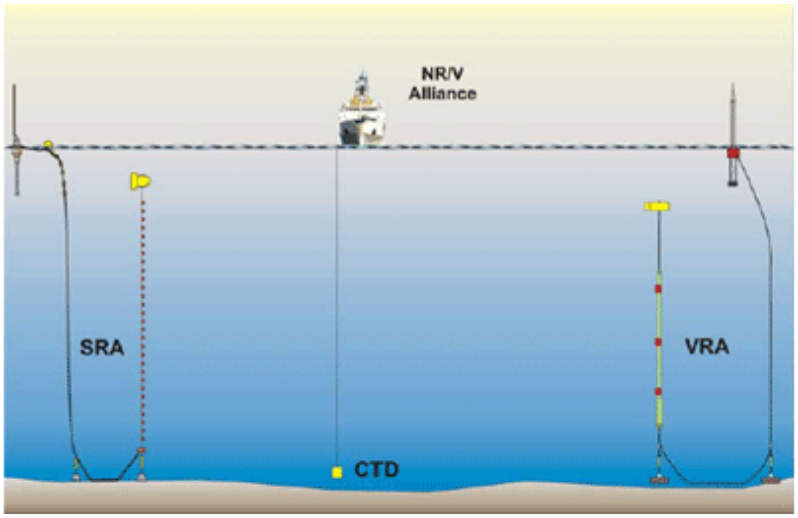

Figure 3.7: the configuration of a TRM experiment

In the following part, the theory of the time reversal mirror will be reviewed assuming that is in a range-independent waveguide. More completed discussion on this can be found in [KHS*98].

We assume that the a probe source (PS) emits a simple harmonic sound signal with frequency $\omega = 2\pi\nu$, so the received acoustic field at the j th receiver element of the SRA from the point source satisfies the Helmholtz equation as equation 2.5 :

Thus, the symmetric normal mode solution of equation 2.3 for pressure is given by :

$$G_\omega(r;z,z_s) = \frac{i}{\rho(z_s)(8\pi r)^{\frac{1}{2}}} exp(-i\pi/4) \times \sum_n \frac{u_n(z_s)u_n(z)}{k_n^{1/2}} exp(ik_n r) \tag{3.53}$$

where u_n, k_n are the normal mode eigenfunctions and modal wave numbers. They can be obtained from the well-known boundary conditions:

$$\frac{d^2u_n}{dz^2} + [K_H^2(z) - k_n^2]u_n(z) = 0 \tag{3.54}$$

The mode eigenfunctions satisfy the orthonormality condition:

$$\int_0^\infty \frac{u_m(z)u_n(z)}{\rho(z)} dz = \delta_{nm} \tag{3.55}$$

with θ_{nm} is the Kronecker delta symbol, and all modes form a complete set:

$$\sum_{all\ modes} \frac{u_n(z)u_n(z_s)}{\rho(z_s)} = \delta(z - z_s) \tag{3.56}$$

We denote the received field at the source/receiver array (SRA) at range r' from PS with source/receive elements at depths z_j as $G_\omega(r', z_j, z_s)$, and the wave equation is built from the J sources:

$$\nabla^2 p_C(r,z) + K_H^2(z)p_C(r,z) = \sum_{j=1}^{J} \delta(z - z_j)G_\omega^*(r';z_j,z_s) \tag{3.57}$$

where the range r is with respective to the SRA. The solution of Equation. 3.57 can be obtained by the calculation of the product of the source term in Eq. 3.57 and the Green function determed in Eq. 2.3. For the vertical SRA array, the result can be calculated using a sum:

$$p_C(r,z,\omega) = \sum_{j=1}^{J} G_\omega(r;z,z_j)G_\omega^*(r';z_j,z_s) \tag{3.58}$$

where r' is the horizontal distance of the SRA from PS and r is the horizontal distance from the SRA to a field point.

Sum over all the modes and array sources by substituting 2.4 to 3.58 and we obtained:

$$p_C(r,z,\omega) \approx \sum_m \sum_n \sum_j \frac{u_m(z)u_m(z_j)u_n(z_j)u_n(z_s)}{\rho(z_j)\rho(z_s)\sqrt{k_m k_n rr'}} \times expi(k_m r - k_n r') \tag{3.59}$$

The expression of the solution of Equation 2.3 in time domain is shown by:

$$p(r', z_j, t) = \int G_\omega(r', z_j, z_s) S(\omega) e^{-i\omega t} d\omega \tag{3.60}$$

That is, the received signal in time domain on j th hydrophone of the SRA is computed by the inverse Fourier transform from the one in frequency domain. Where $S(\omega)$ is the Fourier transform of the probe source pulse. In order to excite the j th transmitting element of the SRA, we assume the time origin such that $p(r', z_j, t) = 0$ outside the time interval$(0, \tau)$. Then, the time reversed signal $P(r', z_j, T - t)$ (such that $T > 2\tau$ this condition is imposed by causality) is:

$$p(r', z_j, t) = \int G_\omega(r', z_j, z_s) S(\omega) e^{-i\omega(T-t)} d\omega = \int [G^*_\omega(r', z_j, z_s) e^{i\omega T} S^*(\omega)] e^{-i\omega t} d\omega \tag{3.61}$$

where considering the multipath propagation property and the resulted time delay, the quantity in brackets in Equation 3.61 is the Fourier transform of the signal received by the j th SRA receiver after time reversal and time delay.That is the signal retransmitted by the j receiver of the SRA. On the basis of this, the representation in time domain of the produced acoustic field by the j receiver of the SRA is obtained by substituting Eq. 3.58 to Eq. 3.61:

$$p_C(r, z, t) = \sum_{j=1}^{J} \int G_\omega(r, z, z_j) G^*_\omega(r', z_j, z_{C_s}) e^{i\omega T} \times S^*(\omega) e^{-i\omega t} d\omega \tag{3.62}$$

and time-reversal process

$$p_{trm}(r, z, t) = \frac{1}{(2\pi)^2} \sum_{j=1}^{J} \int \int G(r, z, t''; 0, z_j, t') \times G(r', z_j, t'; 0, z_{C_s}, 0) \times S(t'' - t + T) dt dt'' \tag{3.63}$$

where S is the source function, $G(r', z_j, t'; 0, z_s, 0)$ is the time-domain Green's function (TDGF) from the probe source at depth z_s to each element of the SRA at range r' and depth z_j. $G(r, z, t''; 0, z_j, t')$ is the TDGF from each element of the SRA back to range r and depth z. The focused field at the probe source position is $p_{trm}(r, z, t)$. The summation is performed on the J elements of the TRM. The signal $S(t'' - t + T)$ of duration τ is the time reversed version of the original probe source signal.

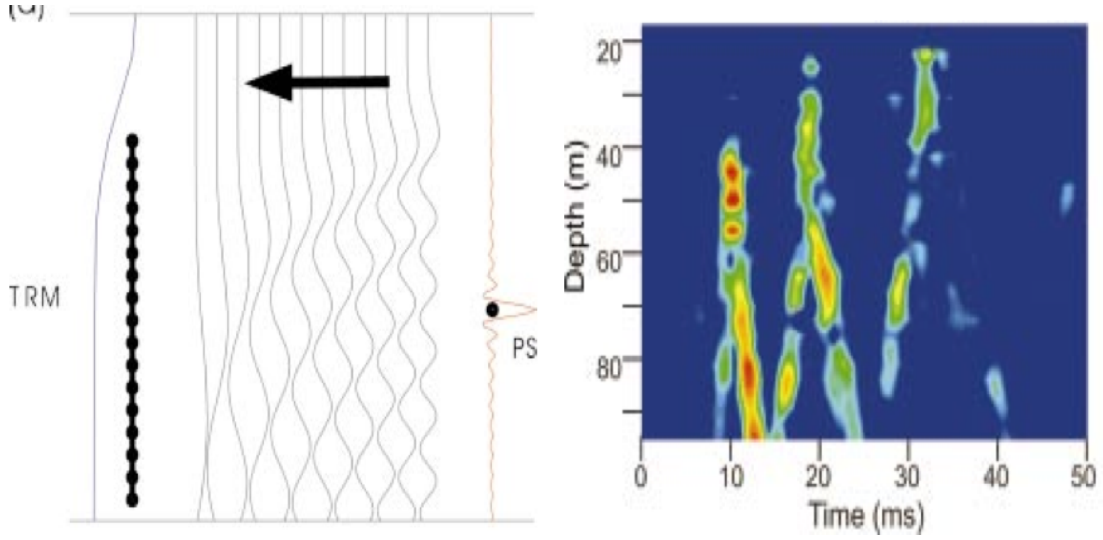

(a) (b)

Figure 3.8: (a) a signal is launched by a probe source and it excites a series of normal modes that propagate to theTRM (b) a probe signal received by TRM. [KKH*03]

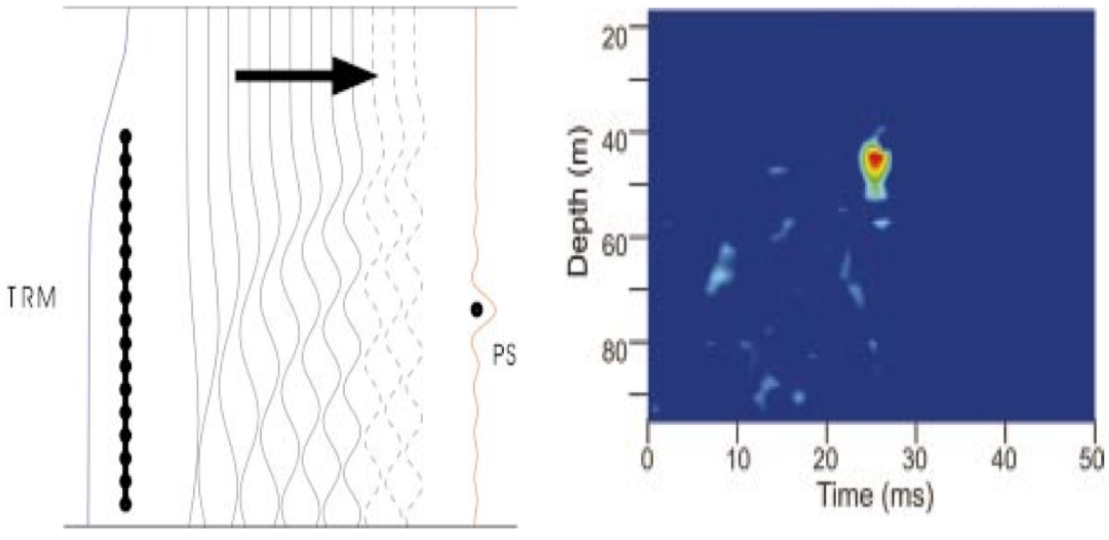

(a) (b)

Figure 3.9: (a) time reversal signals propagate backward to the probe source (b) a focused signal observed by VRA. [KKH*03]

3.2.3 Discussion on matched-field processing and phase conjugation of time reversal mirror

If the matched-field processing is performed with the conventional (Barlett) beamformer estimator in subsection 3.2.1.5, Eq. 3.45 will be used to estimate the spatial and time distribution of the acoustic field. If we take the $G_\omega(r; z, z_j)$ and $G^*_\omega(r'; z_j, z_{C_s})$ as the data and the replica field respectively, the magnitude squared of the right side of Eq. 3.58 is a specific example of the conventional (Barlett) beamformer estimator shown in Eq. 3.45. Theoretically, on the one hand, if the ocean itself is used to construct the replica field, the process of phase conjugation is an implementation of matched-field processing; on the other hand, the matched field processing demonstrates the experiment of phase conjugation in a special case of the configuration which is composed of a source and a receive array.

3.3 Discussion and comparison

Before beginning to discuss and compare the above algorithms, we would like first to address several significant concepts as follows:

- *Plane wave* — In the physics of wave propagation, a plane wave (also spelled planewave) is a constant-frequency wave whose wavefronts (surfaces of constant phase) are infinite parallel planes of constant peak-to-peak amplitude normal to the phase velocity vector. These waves are solutions for a scalar wave equation in a homogeneous medium.

- *Homogeneous medium* — A transmission medium (plural transmission media) is a material substance (solid, liquid, gas, or plasma) that can propagate energy waves. Uniform medium or homogeneous medium is one type of transmission medium and its physical properties are unchanged at different points;

- *Reciprocity property (Acoustic propagates in ocean)* — Because the standard wave equation only contains even order derivatives, if given a solution to the wave equation, then using a negative time of that solution can also get a solution.

On the basis of briefly reviewing the well-known source separation (or localization) techniques in underwater acoustics, such as beamforming, matched-field processing, the time reversal mirror, etc, but also the novel and most interesting methods in recent publications, such as double-beamforming, a Gibbs sampler approach, etc, we divide these methods into two categories depending on whether they are under the assumption of the sound propagates in a homogenous space. Excepting the Gibbs sampler source-localization method, they are all beamforming-like methods and are connected by several key words: plane-wave, non-plane wave, point to array configuration, array to array configuration and reciprocity property. For instance, the essential of matched-field processing is that plane-wave beamforming was extended to be adaptable to the case where the acoustic propagates in a inhomogenous medium. To improve the resolution of plane-wave beamforming, double-beamforming is developed by using beamforming in a array to array configuration, which is in accord with the same theoretical basis – reciprocity property as time reversal mirror; if the ocean itself is used to construct the reciprocal field, the process of phase conjugation is an implementation of matched-field processing while the matched-field processing is a special case of time reversal mirror in the configuration of point to array. Mathematically, they all use the 2-order statistic moments of the recorded signals. These comparisons are also illustrated in Table 3.1 and

Table 3.2. Resolution limitation still exists in these algorithms and the improvement of resolution is still a promising perspective for these methods. We hope that our attempt of global analysis on these methods can provide a brief guide for a first time exposure to an interested reader.

Method	Plane-wave	Experiment configuration
Beamforming	Yes	Point to array
Adaptive-beamformer	Yes	Point to array
MFP	No	Point to array
Time reversal mirror	No	Array to array
Double-beamforming	Yes	Array to array
Gibbs sampling approach	Yes	Point to array

Table 3.1: Comparison on the existing array-processing methods in underwater acoustics based on different criteria (Plane-wave and Experiment configuration)-I

Method	Statistical order	Computations
Beamforming	2-order	1-D Search
Adaptive-beamformer	2-order	1-D Search
MFP	2-order	1-D Search
Time reversal mirror	2-order	—
Double-beamforming	2-order	2-D Search
Gibbs sampling approach	–	Iteration process

Table 3.2: Comparison on the existing array-processing methods in underwater acoustics based on different criteria (Statistical order and Computations)-II

Chapter 4

Survey on High Resolution Methods

Contents

4.1 Subspace-based Methods 53

4.1.1 MUSIC Algorithm 53

4.1.2 Coherent Signals 54

4.2 Parametric Methods 55

4.2.1 Deterministic Maximum Likelihood 55

4.2.2 Stochastic Maximum Likelihood 57

4.2.3 A Bayesian Approach to Auto-Calibration for Parametric Array Signal Processing 58

4.2.3.1 Data model 58

4.3 Uniform Linear Arrays 61

4.3.1 Root-MUSIC 61

4.3.2 ESPRIT 62

4.4 Multi-dimensional high resolution method 63

4.5 Higher order method 65

4.5.1 MUSIC-4 65

4.6 Polarization sensitivity and Quaternion-MUSIC for vector- sensor array processing 67

4.6.1 Background knowledge on quaternions 68

4.6.2 Polarization model 69

4.6.3 Quaternion spectral matrix 71

4.6.4 Quaternion eigenvalue decomposition 71

4.6.5 Quaternion-MUSIC estimator 72

4.7 Number of Signals Estimation 72

4.8 Discussion and comparison 73

From the brief review of the existing methods for solving the forward problem, we found that improving the resolution of algorithms still is of great interest given their importance in various applications of underwater acoustics. Simultaneously, several categories of high-resolution methods are proposed in order to improve the limited resolution of classical methods (beamforming..... etc). The word "resolution" in the research topics of this manuscript is defined as the ability of distinguishing closely spaced signal sources. Although sonar is one of classical application domains of high-resolution methods [Ows85][Lig73][Böh95], high-resolution methods still have great potentials for other applications in under-water acoustic, such as OAT, source localization and ocean geoacoustic etc. Consequently, in this chapter, we selected several representative methods among them to first give an initially global understanding of high-resolution methods and then emphasize the relatively more recent sub-spaced-based methods in relation to beamforming. At the same time, we specify the problems concerning on shallow-water acoustic tomography which we want to solve in this manuscript.

4.1 Subspace-based Methods

The subspace-based approaches are first introduced in Ref. [Hot33] [Koo37]. This category of method became more attractive until the MUSIC (Multiple Signal Classification) algorithm was introduced in [BK80], [Sch86]. Compared with beamforming, MUSIC algorithm achieve a significant improvement of the performance. We will briefly describe its technique process in this section. It is theoretically a method which can not be limited by the array aperture.

4.1.1 MUSIC Algorithm

The estimation of parameters in MUSIC is from the measurements made on the signal received at the elements of a vertical array. The same signal model as the one described in Section 3.1.1 of Chapter 3 is considered. Based on this model, if the signals between themselves are not correlated and the signal are not correlated with noise, the covariance of received signal can be computed and decomposed as follows:

$$\mathbf{R} = \mathbf{APA}^* + \sigma_n^2\mathbf{I} = \mathbf{E}_s\mathbf{\Lambda}_s\mathbf{E}_s^* + \sigma_n^2\mathbf{E}_n\mathbf{E}_n^* \tag{4.1}$$

where $\mathbf{\Lambda}_s$ contains P largest eigenvalues corresponding to signals. $\mathbf{E}_n$ are composed of the noise eigenvectors. $\mathbf{E}_s$ are composed of the signal eigenvectors. If here taking the first sensor of the vertical array as a reference, the classical steering vector can be defined

as:

$$\mathbf{d}(\theta) = [1, e^{-2i\pi\nu\tau_{1,2}(\theta)}, \ldots, e^{-2i\pi\nu\tau_{1,M-1}(\theta)}]^{+} \tag{4.2}$$

In the above equation, the $\tau_{1,M-1}(\theta)$ denotes the delay between the $M-1$ th sensor and the first sensor, which is taken as a reference sensor. We can mathematically describe the orthogonal relationship between the noise eigenvector and the steering vector defined by the real DOA ($\theta \subseteq \{\theta_1, \ldots, \theta_P\}$) of each signal in Equation 4.3:

$$\mathbf{E}_n^{*}\mathbf{d}(\theta) = 0, \qquad \theta \in \{\theta_1, \ldots, \theta_P\} \tag{4.3}$$

In practice, the covariance matrix is always estimated from a specific length of signal samples and is noted by$\hat{\mathbf{R}}$. Sequentially, the corresponding sample noise subspace is given by:

$$\hat{\mathbf{\Pi}}^{\perp} = \hat{\mathbf{E}}_{\mathbf{n}}\hat{\mathbf{E}}_{\mathbf{n}}^{*} \tag{4.4}$$

Finally, the correct estimations of DOA are achieved by minimizing the distance from the steering vector $\mathbf{d}(\theta)$ to the signal subspace. That is, it is needed to maximize the following function consisted of noise subspace $\hat{\Pi}^{\perp}$ and steering vector $\mathbf{d}^{*}(\theta)$:

$$F_{MUSIC}(\theta) = \frac{1}{\mathbf{d}^{*}(\theta)\hat{\mathbf{\Pi}}^{\perp}\mathbf{d}(\theta)} \tag{4.5}$$

Fig. 4.1 gives an example on results comparison between the beamforming and MUSIC separation for five signals . Practically, MUSIC algorithm gives a more accurate separation than beamforming. However, there are some limitations of MUSIC, for instance, it fails in separating closely signals in short samples and at low SNR scenarios. The researchers made attempts to overcome these shortcomings resulting in the extensional algorithms of MUSIC [KFP92] [BX90] [XB93] [KB90] [HFB*10] [BHF09][BB02][BBS02].

4.1.2 Coherent Signals

As we noted before, two coherent signals refer to the case that one signal is a scaled and delayed version of the other. In fact, it is a result of multi-path propagation. For the coherent signals, generally, MUSIC-type methods fail in giving an accurate separation results due to the insufficient rank of covariance matrix. It is a significant question in practical perspective. Thus, it is one of major questions with which we will deal in this manuscript. The comprehensive statement of the state of art will be described in chapter 5. At the same time, we will present a high resolution processing for coherent signals in

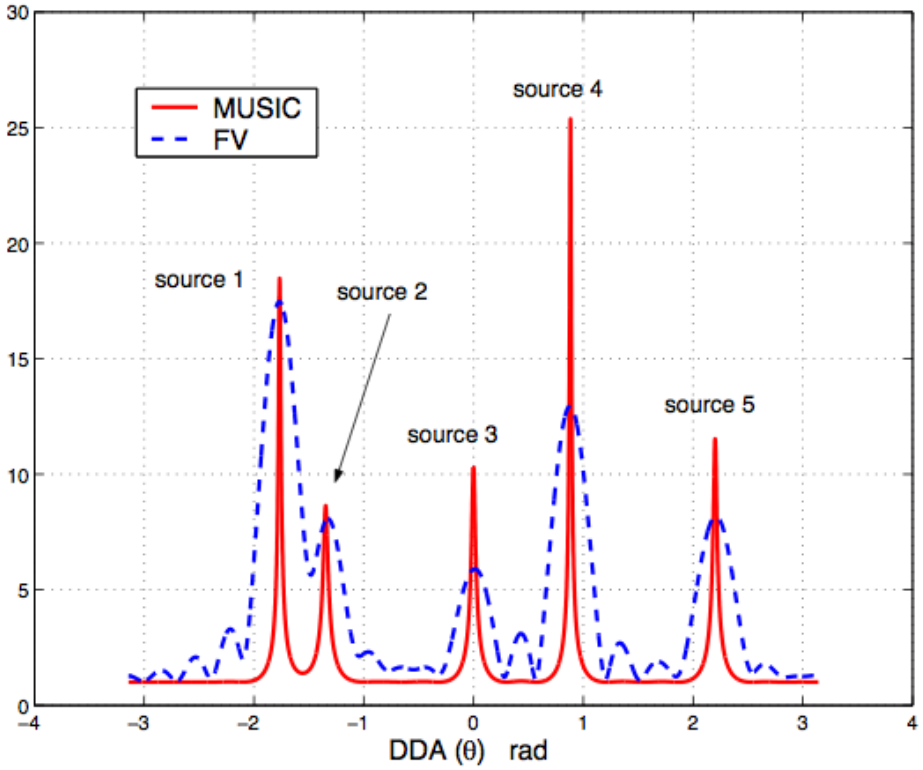

Figure 4.1: An example demonstrating the separation capability of beamforming and MUSIC, where each peak represents a detected position of one signal. (Red line denotes the MUSIC separation and the blue line of dashes shows the separation result of beamforming)

the context of shallow- water acoustic tomography.

4.2 Parametric Methods

To improve the performance of covariance matrix (spectral matrix)-based methods (such as beamforming, MUSIC etc.) and get sufficient accuracy, parametric array processing methods are proposed. This type of methods can provide more efficient and robust estimates even in the case of coherent signals at the price of requiring a multidimensional search.

4.2.1 Deterministic Maximum Likelihood

If assume that the received noise on the array as signals from a large number of independent noise sources, the noise can be modeled as a stationary Gaussian white random process. The second-order moments of noise under the assumption of spatially white

and circularly symmetric and identically distributed imaginary parts is given by:

$$\mathbb{E}\{\mathbf{n}(t)\mathbf{n}^*(s)\} = \sigma_n^2 \mathbf{I}\delta_{t,s} \tag{4.6}$$

$$\mathbb{E}\{\mathbf{n}(t)\mathbf{n}^T(s)\} = 0 \tag{4.7}$$

Thus, the received signal $\mathbf{x}(t) = \mathbf{A}s(t) + n(t)$ can also be assumed as a circularly symmetric and Gaussian white random process. Its mean and covariance are $\mathbf{As}(t)$ and $\sigma_n^2\mathbf{I}$ respectively. Based on the above assumption, the probability density function (PDF) of an observation of $\mathbf{x}(t)$ is described:

$$\frac{1}{(\pi\sigma_n^2)^M} e^{-\|\mathbf{x}(t)-\mathbf{As}(t)\|^2/{\sigma_n}^2} \tag{4.8}$$

with $\|\|$ denotes the Euclidean norm. In addition, for all the observations, the likelihood function for all unknown parameters (the DOA θ, $\mathbf{s}(t)$ and the noise variance σ_n^2) is obtained as

$$L_{DML}(\theta, s(t), \sigma_n^2) = \prod_{t=1}^{N} \frac{1}{(\pi\sigma_n^2)^M} e^{-\|\mathbf{x}(t)-\mathbf{As}(t)\|^2/{\sigma_n}^2} \tag{4.9}$$

The log-likelihood function is drawn by normalizing by N and by ignoring the parameter independent $Mlog\pi$ term:

$$L_{DML}(\theta, s(t), \sigma_n^2) = M\ log\sigma_n^2 + \frac{1}{\sigma_n^2 N}\sum_{t=1}^{N}\|\mathbf{x}(t) - \mathbf{As}(t)\|^2 \tag{4.10}$$

furthermore, $\hat{\sigma_n}^2$ and $\hat{s}(t)$ in Equation 4.10 can be computed by [Boh84] [Boh85][Wax92]:

$$\hat{\sigma_n}^2 = \frac{1}{L}\mathrm{Tr}\{\Pi_{\mathbf{A}}^{\perp}\hat{\mathbf{R}}\} \tag{4.11}$$

$$\hat{s}(t) = \mathbf{A}^{\dagger}\mathbf{x}(t) \tag{4.12}$$

in addition, the estimation of sample covariance matrix is given by:

$$\hat{\mathbf{R}} = \frac{1}{N}\sum_{t=1}^{N}\mathbf{x}(t)\mathbf{x}^*(t) \tag{4.13}$$

at the same time, the Moore-Penrose pseudo-inverse of $\mathbf{A}$ is obtained by:

$$\mathbf{A}^{\dagger} = (\mathbf{A}^*\mathbf{A})^{-1}\mathbf{A}^* \tag{4.14}$$

$$\mathbf{\Pi_A} = \mathbf{A}\mathbf{A}^{\dagger} \tag{4.15}$$

besides, the orthogonal projector onto the null space of $\mathbf{A}^*$: $\Pi_{\mathbf{A}}^{\perp}$ refers to

$$\mathbf{\Pi}_{\mathbf{A}}^{\perp} = \mathbf{I} - \mathbf{\Pi_A} \tag{4.16}$$

Substituting the equations 4.11 and 4.12 into equation 4.10, the DML method finally estimates signal parameters by the following equation:

$$\hat{\theta}_{DML} = \arg\{\min_{\theta} \mathrm{Tr}\{\mathbf{\Pi}_{\mathbf{A}}^{\perp}\hat{\mathbf{R}}\}\} \tag{4.17}$$

This process consists of projecting the received signal $\mathbf{x}(t)$ onto the subspace $\mathbf{\Pi}_{\mathbf{A}}^{\perp}$, which is orthogonal to the anticipated signal subspace, and finding a minimum power value when the projector indeed removes all the true signal components [Boh84] [Wax92].

4.2.2 Stochastic Maximum Likelihood

Differing from the deterministic maximum likelihood method presented above, the stochastic maximum likelihood is built from modeling the signal waveforms as a Gaussian random processes. Assume the signals are zero-mean with second-order properties:

$$\mathbb{E}\{s(t)s^*(t)\} = \mathbf{P}\delta_{t,s} \tag{4.18}$$

$$\mathbb{E}\{s(t)s^T(t)\} = 0 \tag{4.19}$$

Thus, the observation vector $\mathbf{x}(t)$ is a white, zero-mean and circularly symmetric Gaussian random vector. Moreover, its covariance matrix is given by:

$$\mathbf{R} = \mathbf{A}(\theta)\mathbf{P}\mathbf{A}^*(\theta) + \sigma_n^2\mathbf{I} \tag{4.20}$$

In the case of stochastic maximum likelihood, the likelihood function depends on θ, $\mathbf{P}$ and σ^2 and the negative log-likelihood function is proportional to

$$\frac{1}{N}\sum_{t=1}^{N} \|\Pi_{\mathbf{A}}^{\perp}\mathbf{x}(t)\|^2 = \mathrm{Tr}\{\Pi_{\mathbf{A}}^{\perp}\hat{\mathbf{R}}\} \tag{4.21}$$

From the studies results in [Boh86] [Jaf88], for fixed θ, σ_n^2 and $\mathbf{P}$ are given by:

$$\sigma^2_{SML} = \frac{1}{M-P}\mathrm{Tr}\{\Pi^{\perp}_{\mathbf{A}}\} \tag{4.22}$$

$$\hat{\mathbf{P}}_{SML}(\theta) = \mathbf{A}^{\dagger}(\hat{\mathbf{R}} - \hat{\sigma^2}_{SML}(\theta)\mathbf{I})\mathbf{A}^{\dagger *} \tag{4.23}$$

Thus, substituting the estimates of parameters (σ^2 and $\mathbf{P}$) in Equation 4.22 and Equation 4.23 to the log-likelihood function shown by 4.21, the SML method estimates are achieved by finding the minimum value of the following equation:

$$\hat{\theta}_{SML} = \arg\{\min_{\theta} log|\mathbf{A}\hat{P}_{SML}(\theta)\mathbf{A}^{*} + \hat{\sigma}^2_{SML}(\theta)\mathbf{I}|\} \tag{4.24}$$

4.2.3 A Bayesian Approach to Auto-Calibration for Parametric Array Signal Processing

In [VS94], an extension of deterministic maximum likelihood method, called Bayesian approach to auto-calibration, is proposed to overcome the limitations on prior knowledge of the array. Specifically, most of high resolution array methods are limited by the knowledge of characterization of the array, such as the sensor positions, sensor gain or phase response, mutual coupling, and receiver equipment effects. To get these information, the process called calibration is often implemented by special experiments. However, all such information is inevitably subject to errors. The methods considering alleviating the inherent sensitivity of parametric methods to such modeling errors are called auto-calibration methods. In [VS94], the Bayesian approach to auto-calibration is described in detail, which is a combination of the maximum a posteriori (MAP) method in [WOV91] and the noise subspace fitting (NSF) approach of [SS90], and hence is referred to as the MAP-NSF algorithm. It is not only computationally much simpler than the MAP estimator but also asymptotically equivalent in performance.

4.2.3.1 Data model

In this part, we will address the data model again. In fact, it is essentially a signal model built on the assumption of plane-wave, and same as the one in Section 3.1.1 of Chapter

3. Considering

$$\mathbf{x}(t) = [d(\theta_1, \mathbf{a}), \ldots, d(\theta_P, \mathbf{a})] \begin{bmatrix} s_1(t) \\ \vdots \\ s_P(t) \end{bmatrix} + \mathbf{n}(t) = \mathbf{A}(\boldsymbol{\theta}, \mathbf{a})\mathbf{s}(t) + \mathbf{n}(t) \tag{4.25}$$

where the signal $s(t)$ is an arbitrary deterministic sequence assumed to satisfy the following limit:

$$\mathbf{P} = \lim_{n\to\infty} \sum_{t=1}^{N} s(t)s^*(t) > 0 \tag{4.26}$$

In addition, the noise term $\mathbf{n}(t)$ is assumed as a stationary, complex Gaussian random process, uncorrelated with the signals. where $\mathbf{A}$ is consisted of M steering vector $\mathbf{d}(\theta_i, \mathbf{a})$, $i = 1, \ldots, M$. M denotes the number of sensors. θ_i is the arrival angle at the ith sensor of array. In [WOV91], they assume θ_i is a real scalar and define $\boldsymbol{\theta}_0$ as the true values. Considering the case of the array response parameters in $\mathbf{d}$ has small deviations from their known nominal values in $\mathbf{d}_0$. Thus, the a prior covariance matrix of perturbation is also assumed known, denoted by $\boldsymbol{\Omega}$. In [VS94], they consider both the modeling errors and the errors produced by finite sample. The errors produced by finite sample are proportional to $1/N$ in the finite-sample only case whereas the modeling errors are proportional to $\boldsymbol{\Omega}$. If these two factors are taken into account, the covariance matrix of the perturbations is described as:

$$E[(\mathbf{d} - \mathbf{d}_0)(\mathbf{d} - \mathbf{d}_0)^T] = \boldsymbol{\Omega} = \overline{\boldsymbol{\Omega}}/N \tag{4.27}$$

where $\overline{\boldsymbol{\Omega}}$ represents a parameter independenting of N. Compute the eigendecomposition of sample covariance $\hat{\mathbf{R}}$:

$$\hat{\mathbf{R}} = \hat{\mathbf{E}}_s \hat{\boldsymbol{\Lambda}}_s \hat{\mathbf{E}}_s^* + \hat{\mathbf{E}}_n \hat{\boldsymbol{\Lambda}}_n \hat{\mathbf{E}}_n^* \tag{4.28}$$

To avoid the nonlinear minimization of criterion function of MAP or NSF, the vectorized steering matrix is approximated locally around $\mathbf{d}_0$ as:

$$\mathbf{a} = \mathbf{a}(\theta, \mathbf{d}) \approx \mathbf{a}_0 + \mathbf{D}_d \tilde{d} \tag{4.29}$$

where

$$\mathbf{a}_0 = \mathbf{a}(\boldsymbol{\theta}, \mathbf{d}_0) \tag{4.30}$$

$$\mathbf{D}_d = \{\frac{\partial \mathbf{a}(\theta, \mathbf{d})}{\partial d_1}, \ldots, \frac{\partial \mathbf{a}(\theta, \mathbf{d})}{\partial d_n}\}|_{\theta, d_0} \tag{4.31}$$

$$\tilde{\mathbf{d}} = \mathbf{d} - \mathbf{d}_0 \tag{4.32}$$

Consequently, the MAP-NSF criterion with respect to $\boldsymbol{\theta}$ and $\mathbf{d}$ is approximated as follows:

$$(\mathbf{a}_0 + \mathbf{D}_d\tilde{\mathbf{d}})^*\hat{\mathbf{M}}(\mathbf{a}_0 + \mathbf{D}_d\tilde{\mathbf{d}}) + \frac{1}{2}\tilde{\mathbf{d}}^T\overline{\boldsymbol{\Omega}}^{-1}\tilde{\mathbf{d}} \tag{4.33}$$

The estimates of $\boldsymbol{\theta}$ and $\mathbf{d}$ are obtained by minimizing the MAP-NSF criterion.

Compute an initial estimate $\hat{\theta}$ of the DOA

$$\hat{\mathbf{M}} = \hat{\sigma}^{-2}(\hat{\mathbf{A}}^{\dagger}\hat{\mathbf{E}}_s(\hat{\boldsymbol{\Lambda}}_s - \hat{\sigma}^2\mathbf{I})^2\hat{\boldsymbol{\Lambda}}_s^{-1}\hat{\mathbf{E}}_s^*\hat{\mathbf{A}}^{\dagger *})^T \otimes (\hat{\mathbf{E}}_n\hat{\mathbf{E}}_n^*) \tag{4.34}$$

Given the sample covariance matrix and the initial estimate $\hat{\boldsymbol{\theta}}$ of the DOA, the MAP-NSF criterion is written as follows:

$$\hat{\boldsymbol{\theta}}_{MAP-NSF} = arg\min_{\theta} V(\boldsymbol{\theta}) \tag{4.35}$$

With

$$V(\boldsymbol{\theta}) = \mathbf{a}_0^*\hat{\mathbf{M}}\mathbf{a}_0 - \mathbf{f}^T\hat{\boldsymbol{\Gamma}}^{-1}\mathbf{f} \tag{4.36}$$

And the variations $\hat{\sigma}^2$, $\hat{\boldsymbol{\Gamma}}$ and $\hat{f}$ can be computed from Equation 4.37, Equation 4.38 and Eq. 4.39 respectively:

$$\hat{\sigma}^2 = \frac{1}{M-P}Tr\{(\mathbf{I} - \hat{\mathbf{A}}\hat{\mathbf{A}}^{\dagger})\hat{\mathbf{R}}\} \tag{4.37}$$

$$\hat{\boldsymbol{\Gamma}} = Re\{\hat{\mathbf{D}}_d^*\hat{\mathbf{M}}\hat{\mathbf{D}}_d + \frac{1}{2}\overline{\Omega}^{-1}\} \tag{4.38}$$

$$\hat{f} = Re\{\hat{\mathbf{D}}_d^*\hat{M}\mathbf{a}_0\} \tag{4.39}$$

4.3 Uniform Linear Arrays

4.3.1 Root-MUSIC

The Root-MUSIC method [Bar83] is a polynomial-root version of MUSIC algorithm. The estimator of MUSIC algorithm shown by Eq. 4.5 can be written as:

$$F_{MUSIC}(\theta)^{-1} = \sum_{m=1}^{P}\sum_{n=1}^{P} e^{-i2\pi m(d/\lambda)sin\theta} A_{mn} e^{-i2\pi n(d/\lambda)sin\theta} = \sum_{l=-P+1}^{P+1} a_l e^{-i2\pi l(d/\lambda)sin(\theta)} \quad (4.40)$$

with

$$a_l = \sum_{m-n=l} A_{mn} \quad \text{and wavelength:} \quad \lambda = \frac{c}{f} \quad (4.41)$$

a_l is the sum of entries of A along the l^{th} diagonal, thus, the polynomial is defined as:

$$z_l = \sum_{m-n=l} A_{mn} \quad (4.42)$$

$$p_l(z) = \sum_{-P+1}^{P+1} a_l z^{-l} \quad (4.43)$$

That is,

$$p_l(z) = \mathbf{e}_l^* \mathbf{p}(z), l = P+1, P+2, \ldots, M \quad (4.44)$$

where $\mathbf{e}_l$ is the l^{th} eigenvector of covariance matrix $\mathbf{R}$

$$\mathbf{p}^*(z) = [1, z, \ldots, z^{M-1}]^T \quad (4.45)$$

The zeros of the following MUSIC-like function is needed to find for using the information from all noise eigenvectors simultaneously:

$$\mathbf{p}^*(z)\hat{\mathbf{E}}_n\hat{\mathbf{E}}_n^*\mathbf{p}(z) \quad (4.46)$$

If $\mathbf{p}^T(z^{-1})$ is instead of $\mathbf{p}^*(z)$, the Root-MUSIC polynomial is rewritten as:

$$p_l(z) = z^{M-1}\mathbf{p}^T(z^{-1})\hat{\mathbf{E}}_n\hat{\mathbf{E}}_n^*\mathbf{p}(z) \quad (4.47)$$

Based on the discussion above, the roots of polynomial $p(z)$ which has the largest magnitude yield the estimate of the corresponding DOA and the phase of these roots are

used to estimate the DOA:

$$(\theta_m) = arccos(\frac{\lambda}{2\pi d} arg\hat{z}_m), m = 1, 2, \ldots, P \tag{4.48}$$

4.3.2 ESPRIT

For the ESPRIT algorithm [PRK86] [RPK86] [RK89], the steering vectors of the uniform linear array (ULA) can be expressed in a matrix form:

$$\mathbf{A}(\theta) = \begin{pmatrix} 1 & 1 & \cdots & 1 \\ e^{j\Phi_1} & e^{j\Phi_2} & \ldots & e^{j\Phi_P} \\ \vdots & \vdots & \ddots & \vdots \\ e^{j(M-1)\Phi_1} & e^{j(M-1)\Phi_2} & \ldots & e^{j(M-1)\Phi_P} \end{pmatrix} \tag{4.49}$$

A *shift structure* is developed for the steering vector of ESPRIT algorithm:

$$\mathbf{A}(\theta) = \begin{pmatrix} \mathbf{A}_1(\theta) \\ \text{first row} \end{pmatrix} = \begin{pmatrix} \text{last row} \\ \mathbf{A}_2(\theta) \end{pmatrix} \tag{4.50}$$

It is easy to get the following relation between $\mathbf{A}_1$ and $\mathbf{A}_2$:

$$\mathbf{A}_2 = \mathbf{A}_1\Phi = \mathbf{A}_1 \begin{pmatrix} e^{j\Phi} & 0 & \cdots & 0 \\ 0 & e^{j2\Phi} & \cdots & 0 \\ \vdots & \vdots & \ddots & \vdots \\ 0 & 0 & \cdots & e^{j(M-1)\Phi} \end{pmatrix} \tag{4.51}$$

Use the properties of covariance $\mathbf{R}$:

$$\mathbf{R} = \mathbf{APA}^* + \sigma_n^2\mathbf{I} = \mathbf{E}_s\Lambda_s\mathbf{E_s}^* + \sigma_n^2\mathbf{E}_n\mathbf{E}_n^* \tag{4.52}$$

Substitute $\mathbf{I}$ in Eq. 4.52 for $\mathbf{I} = \mathbf{E}_s\mathbf{E}_s^* + \mathbf{E}_n\mathbf{E}_n^*$:

$$\mathbf{APA}^* + \sigma_n^2\mathbf{E}_s\mathbf{E}_s^* + \sigma_n^2\mathbf{E}_n\mathbf{E}_n^* = \mathbf{E}_s\Lambda_s\mathbf{E_s}^* + \sigma_n^2\mathbf{E}_n\mathbf{E}_n^* \tag{4.53}$$

That is:

$$\mathbf{APA}^* + \sigma_n^2\mathbf{E}_s\mathbf{E}_s^* = \mathbf{E}_s\Lambda_s\mathbf{E_s}^* \tag{4.54}$$

Post-multiplying on the right by $\mathbf{E}_s$, the following relation is given:

$$\mathbf{E}_s = \mathbf{AT} \tag{4.55}$$

where

$$\mathbf{T} = \mathbf{P}\mathbf{A}^{*}\mathbf{E}_s(\Lambda_s - \sigma^2\mathbf{I})^{-1} \tag{4.56}$$

Apply the property in 4.55 to $\mathbf{A}_1$ and $\mathbf{A}_2$ respectively:

$$\mathbf{E}_1 = \mathbf{A}_1\mathbf{T}, \qquad \mathbf{E}_2 = \mathbf{A}_2\mathbf{T} \tag{4.57}$$

By combining the Eq. 4.51 and Eq. 4.56

$$\mathbf{E}_1 = \mathbf{A}_1\mathbf{\Phi}\mathbf{T}, \qquad \mathbf{E}_2 = \mathbf{T}^{-1}\mathbf{\Phi}\mathbf{T}, \tag{4.58}$$

That is :

$$\mathbf{E}_2 = \mathbf{E}_1\mathbf{T}^{-1}\mathbf{\Phi}\mathbf{T} = \mathbf{E}_2\mathbf{\Psi} \tag{4.59}$$

Then, we can use a Least Squares sense (LS-ESPRIT) or a Total-Least-Squares [GVL80] [VHV91] [GVL96] to solve 4.59 approximately. In addition, the DOA estimates are obtained by applying the inversion formula Eq. 4.48 to the eigenvalues of $\hat{\mathbf{\Psi}}$.

4.4 Multi-dimensional high resolution method

As we presented in Chapter 2, Refs. [IRNM08] and [IRN*09] introduced a novel shallow-water tomography algorithm which exploits the double-beamforming to improve the resolution of raypath separation and identification. Actually, we can take the improvement as a result of using a multidimensional received-data in a two-dimensional implementing configuration. Probably, we can infer that the processing based on this two-dimensional configuration on shallow-water OAT will become an interesting research topic in future. Although this is a new and engaging topic in shallow-water OAT, the operation of multidimensional spectral analysis arises in many fields of application [McC82]. That is to say, situations in which the signals are inherently multidimensional can be found in geophysics, radio astronomy, sonar, and radar. However, these algorithms in other related fields are inspirations for the studies on shallow-water OAT. Thus, we will briefly review the representative algorithms. In fact, these multidimensional problems present a challenging set of theoretical and computational difficulties that must be tackled. We present here a two-dimensional processing using MUSIC for superresolution radar imaging [OBP94] to demonstrate how this two-dimensional method is implemented and deals with the difficulties existing in multidimensional data structure.

The measured radar signal model is defined as [WJ90]:

$$x(m,l) = \sum_{i=1}^{P} a_i e^{j4\pi\nu_m/c(x_k cos\theta_l - y_k sin\theta_l)} + n(m,l) \tag{4.60}$$

where P is the number of scattering centers. $m = 0, 1, \ldots, M_1 - 1$. M_1 means there are M_1 sampled frequency points ν_m. L_1 different look angles θ_l ($l = 0, 1, \ldots, L_1 - 1$). A focused image [Men91] can be obtained by interpolating the frequency angular domain data to Cartesian coordinates (rectangular grid) with $\nu_m^x = \nu cos\theta$ and $\nu_l^y = \nu sin\theta$. Then, Eq. 4.60 can be given by:

$$x(m,l) = \sum_{i=1}^{P} a_i e^{j4\pi/c(\nu_m^x x_k - \nu_l^y y_k)} + n(m,l) \tag{4.61}$$

Further, Eq. 4.61 is written in a matrix form:

$$\mathbf{x} = \mathbf{A}\mathbf{s} + \mathbf{n} \tag{4.62}$$

and the column-vectors of each matrix respectively are:

$$\mathbf{x} = [x_{00}x_{10}, \ldots x_{M-10}x_{01} \ldots x_{M_1-1L_1-1}]^T \tag{4.63}$$

$$\mathbf{s} = [s_1 s_2 \ldots s_P]^T \tag{4.64}$$

$$\mathbf{n} = [n_{00}u_{10} \ldots n_{M-10}n_{01} \ldots n_{M_1-1L_1-1}]^T \tag{4.65}$$

$$\mathbf{A} = [\mathbf{a}(x_1, y_1)\mathbf{a}(x_2, y_2) \ldots \mathbf{a}(x_P, y_P)] \tag{4.66}$$

$\mathbf{A}$ is an $ML \times P$ matrix, which is composed of the delay parameters. And the steering vector $\mathbf{a}(x_k, y_k)$ is:

$$\begin{aligned} \mathbf{a}(x_k, y_k) \quad &= \quad [e^j \frac{4\pi}{c}(\nu_0^x x_k - \nu_0^y y_k) e^j \frac{4\pi}{c}(\nu_1^x x_k - \nu_0^y y_k) \\ &\ldots \quad e^j \frac{4\pi}{c}(\nu_{M_1-1}^x x_k - \nu_0^y y_k) \ldots e^j \frac{4\pi}{c}(\nu_{M_1-1}^x x_k - \nu_{L_1-1}^y y_k)]^T \end{aligned} \tag{4.67}$$

Sequently, it is necessary to estimate the sample covariance matrix from the measured signals, which is similar to MUSIC algorithm [Sch86]. This sample covariance

matrix can be taken as full rank with the assumption of uncorrelated scattering centers.

$$\Gamma = \mathbb{E}[\mathbf{x}\mathbf{x}^*] \tag{4.68}$$

where Γ denotes the sample covariance matrix. $\mathbb{E}$ represents the mathematical expectation and $*$ is the complex conjugate transpose. Following by an eigen-decomposition process, Γ is decomposed into two orthogonal space: noise subspace and signal subspace. In Eq. 4.69, $\mathbf{E}_n$ is the $M_1 \times L_1$ noise eigenvector. Finally, the position of each scattering center is denoted by the peak of the following function through searching in corresponding variation spaces.

$$F_{2D-MUSIC}(\theta) = \frac{\mathbf{a}^*(x,y)\mathbf{a}(x,y)}{\mathbf{a}^*(x,y)\mathbf{E}_n\mathbf{E}_n^*\mathbf{a}(x,y)} \tag{4.69}$$

Where $\mathbf{a}(x,y)$ is defined in Eq. 4.67.

4.5 Higher order method

4.5.1 MUSIC-4

The higher order methods refer to using order over 2 *order* cumulants to estimate the random process in this subsection. $MUSIC-4$ [PF91] is one of higher order methods [PF91] [CN89] is developed to separate sources for non Gaussian signals. Higher order moments contain valuable statistical information of non-Gaussian process. We recall the standard linear model in the context of narrow band array processing as:

$$\mathbf{x}(t) = \mathbf{A}\mathbf{s}(t) + \mathbf{n}(t) = \mathbf{y}(t) + \mathbf{n}(t) \tag{4.70}$$

where $\mathbf{A}(\theta) = [\mathbf{d}(\theta_1), \ldots, \mathbf{d}(\theta_P)]$ and $\mathbf{n}(t)$ is a complex white Gaussian noise with zero mean and arbitrary covariance matrix $E(\mathbf{n}(t)\mathbf{n}^*(t))$ From the standard linear model, we can write the entries of covariance and quadricovariance of the recorded signals respectively as:

$$q_r(i_1, j_1) = Cum\{x_{i_1}(t), x_{j_1}^*(t)\} \qquad i_1, j_1 = 1, \ldots, M. \tag{4.71}$$

$$q(i_1, i_2, j_1, j_2) = Cum\{x_{i_1}(t), x_{i_2}^*(t)x_{j_1}(t)x_{j_2}^*(t)\} \qquad i_1, i_2, j_1, j_2 = 1, \ldots, M. \tag{4.72}$$

Based on the Fisher information theory demonstrated in [CM94], the sample covariance and sample quadricovariance are asymptotically normal and unbiased estimates of the true cumulants. We further note the covariance and sample covariance by:

$$q_r(i_1, j_1) = E\{x_{i_1}(t)x^*_{j_1}(t)\} \qquad i_1, j_1 = 1, \ldots, M. \tag{4.73}$$

$$\hat{q}_r(i_1, j_1) = \frac{1}{N}\sum_{t=1}^{N} x_{i_1}(t)x^*_{j_1}(t) \qquad i_1, j_1 = 1, \ldots, M. \tag{4.74}$$

Similarly, the fourth order moments and its sample estimate are denoted by:

$$q(i_1, i_2, j_1, j_2) = E\{x_{i_1}(t)x_{i_2}(t)x^*_{j_1}(t)x^*_{j_2}(t))\} \qquad i_1, j_1, i_2, j_2 = 1, \ldots, M. \tag{4.75}$$

$$\hat{q}(i_1, i_2, j_1, j_2) = \frac{1}{N}\sum_{t=1}^{N} x_{i_1}(t), x^*_{j_1}(t)x_{i_2}(t)x^*_{j_2}(t) \qquad i_1, j_1, i_2, j_2 = 1, \ldots, M. \tag{4.76}$$

Because for most quadrature amplitude modulation signals the symbols process sufficient symmetry, $E\{x_{i_1}x_{j_1}\}$ is identically zero. Thus, the fourth-order cumulants and its estimate are obtained by second-order and fourth-ordermoments as:

$$q_k(i_1, i_2, j_1, j_2) = q(i_1, i_2, j_1, j_2) - q_r(i_1, j_1)q_r(i_2, j_2) - q_r(i_1, j_2)q_r(i_2, j_1) \qquad i_1, j_1, i_2, j_2 = 1, \ldots, M. \tag{4.77}$$

$$\hat{q}_k(i_1, i_2, j_1, j_2) = \hat{q}(i_1, i_2, j_1, j_2) - \hat{q}_r(i_1, j_1)\hat{q}_r(i_2, j_2) - \hat{q}_r(i_1, j_2)\hat{q}_r(i_2, j_1) \qquad i_1, j_1, i_2, j_2 = 1, \ldots, M. \tag{4.78}$$

In the following discussion, a fourth-order MUSIC algorithm will be discussed using this definition of fourth-order cumulants. First, the P signals are divided into G statistically dependent group with P_g signals in each group and $\sum_{g=1}^{G} P_g = P$. Thus,

$$\mathbf{y}_g(t) = \mathbf{A}_g\mathbf{s}_g(t), \qquad 1 \leq g \leq G \tag{4.79}$$

Define the vector $z_g(t)$ as:

$$z_g(t) = \mathbf{y}_g(t) \otimes \mathbf{y}_g(t)^* = [\mathbf{A}_g\mathbf{s}_g(t)] \otimes [\mathbf{A}_g\mathbf{s}_g(t)]^*, \tag{4.80}$$

where $\otimes$ denotes the Kronecker product.

$$\mathbf{C}_g = (\mathbf{A}_g \otimes \mathbf{A}_g^*)\mathbf{S}_g(\mathbf{A}_g \otimes \mathbf{A}_g^*)^T \tag{4.81}$$

where

$$\begin{aligned} \mathbf{S}_g &= E\{(s_g(t) \otimes s_g^*(t))(s_g(t) \otimes s_g^*(t))^T\} \\ &- E\{(s_g(t) \otimes s_g^*(t))\} \times E\{(s_g(t) \otimes s_g^*(t))^T\} \\ &- E\{s_g(t)s_g^T(t)\} \otimes E\{s_g(t)s_g^T(t)\} \end{aligned} \tag{4.82}$$

$$\mathbf{C} = \sum_{g=1}^{G} \mathbf{C}_g = \sum_{g=1}^{G} (\mathbf{A}_g \otimes \mathbf{A}_g^*)\mathbf{S}_g(\mathbf{A}_g \otimes \mathbf{A}_g^*)^T \tag{4.83}$$

Singular value decomposition:

$$\mathbf{C} = [\mathbf{U}_1 \;\; \mathbf{U}_2] \begin{pmatrix} \mathbf{\Lambda} & 0 \\ 0 & 0 \end{pmatrix} \begin{pmatrix} \mathbf{V}_1^T \\ \mathbf{V}_2^T \end{pmatrix} \tag{4.84}$$

That is:

$$\mathbf{C} = [(\mathbf{A}_1 \otimes \mathbf{A}_1^*), \ldots, (\mathbf{A}_G \otimes \mathbf{A}_G^*)] \begin{pmatrix} \mathbf{S}_1 & & 0 \\ & \ddots & \\ 0 & & \mathbf{S}_G \end{pmatrix} \begin{pmatrix} (\mathbf{A}_1 \otimes \mathbf{A}_1^*)^T \\ \vdots \\ (\mathbf{A}_G \otimes \mathbf{A}_G^*)^T \end{pmatrix} \tag{4.85}$$

where $\otimes$ denotes konector multiplication. In addition, the estimation is given by the 4-order MUSIC function:

$$F_{MUSIC-4}(\theta) = \frac{1}{\|[\mathbf{d}(\theta) \otimes \mathbf{d}^*(\theta)]^T \mathbf{U}_2\|^2} \tag{4.86}$$

4.6 Polarization sensitivity and Quaternion-MUSIC for vector-sensor array processing

During the last two decades, the source signals location or separation using the vector sensor array was studied [HN03][HN99][NP94a] [NP94b] [MLBM05], especially for both electric magnetic signals [NP94b] and acoustic signals [NP94a]. Vector sensor refers the sensor whose output is a *vector*. Recently, a Quaternion-MUSIC is proposed for vector-sensor array in the case of multicomponent observations [MLBM06]. It considers the problem of estimating the direction of arrival (DOA) and polarization parameters

based on a Quaternion models. Consequently, a reduction of memory requirements is achieved. As an important representative method for vector-sensor array, it will be reviewed in the following section.

4.6.1 Background knowledge on quaternions

In this section, quaternions is basically introduced. Quaternions are a four dimensional hypercomplex numbers system which is an extension of complex numbers. Its Cartesian form is defined as:

$$q = a + ib + jc + kd \tag{4.87}$$

where:

$$\begin{aligned} i^2 &= j^2 = k^2 = ijk = -1 \\ ij &= k\ ji = -k \\ ki &= j\ ik = -j \\ ik &= i\ kj = -i \end{aligned} \tag{4.88}$$

Some properties of quaternion which can be extended from complex numbers are listed below:

- The conjugate of q, is given by : $\bar{q} = a - ib - jc - kd$;
- A *pure* quarternion is a quaternion which real part is null: $q = ib + jc + kd$;
- The modulus if a quaternion q is given by $\|q\| = \sqrt{q\bar{q}} = \sqrt{\bar{q}q} = \sqrt{a^2 + b^2 + c^2 + d^2}$ and its inverse is given by: $q^{-1} = \bar{q}/|q|^2$;
- A quaternions is said to be null if $a = b = c = d = 0$;
- The set of quaternions, denoted by $\mathbb{H}$ is a non-commutative normed division algebra, that is $q_1 q_2 \neq q_2 q_1$;
- Conjugation over $\mathbb{H}$ is an anti-involution: $q_1 \bar{q}_2 = q_2 \bar{q}_1$.

Any quaternion q can be written in a Carley-Dickson form:

$$q = q^{'} + iq^{''}, \quad \text{where } q^{'} = a + jc \quad \text{and} \quad q^{''} = b + jd \tag{4.89}$$

4.6.2 Polarization model

The polarization model is built with a scenario of one polarized source and a two-component noise free sensor. A signal, which is assumed to be a centered, stationary random process, is emitted by the polarization source and propagated in an isotropic, homogeneous medium. It is recorded on each component of the sensor, denoting by $s_1[t_n]$ and $s_2[t_n]$. Their Fourier transforms are written as:

$$x_1[\nu_m] = \beta_1[\nu_m]e^{j\alpha_1[\nu_m]} \quad \text{and } x_2[\nu_m] = \beta_2[\nu_m]e^{j\alpha_2[\nu_m]} \tag{4.90}$$

Where x_1 and x_2 are two complex vectors, ν_m is the frequency, β_1 , β_2, α_1, and α_2 are the amplitudes and phases of the recorded signals at the given frequency ν_m. Using the Carley-Dickson form noted by Eq. 4.89, the recorded signal on the two-components sensor is described as a quaternion signal x:

$$x = \beta_1 e^{j\alpha_1} + i\beta_2 e^{j\alpha_2} \tag{4.91}$$

where:

$$\begin{aligned} e^{j\alpha_1} &= cos\alpha_1 + jsin\alpha_1 \\ e^{j\alpha_2} &= cos\alpha_2 + jsin\alpha_2 \end{aligned} \tag{4.92}$$

In addition, it can be also written as follows:

$$x = \beta_1 cos\alpha_1 + i\beta_2 cos\alpha_2 + j\beta_1 cos\alpha_1 + k\beta_2 cos\alpha_2 \tag{4.93}$$

To rewrite the signal model in Eq. 4.91 with the polarized relation between the two components, the β_2 and α_2 is replaced by:

$$\begin{aligned} \beta_2 &= \rho\beta_1 \\ \alpha_2 &= \phi + \alpha_1 \end{aligned} \tag{4.94}$$

That is, substituting equation 4.94 to equation 4.91, we obtained:

$$x = p(\rho, \phi)\beta_1 e^{j\alpha_1} \tag{4.95}$$

where

$$p(\rho, \phi) = 1 + i\rho e^{j\phi} \tag{4.96}$$

And ρ is the amplitude ratio and ϕ is the phase-shift between two components. For one of the two components array, the source direction of arrival (DOA) can be computed as:

$$\theta = 2\pi\nu\frac{Dsin\alpha}{c} \tag{4.97}$$

And the transfer function for one component of the vector array described by complex vector where we take the first sensor as the reference one is obtained by:

$$\mathbf{a}_k(\theta_k) = [1, e^{-j\theta_k}, \ldots, e^{-j(M-1)\theta_k}]^T \tag{4.98}$$

Using the similar polarized relation of recorded signals between two components and the first component described in Eq. 4.95 and Eq. 4.96, the transfer function described by a quaternion steering vector $\mathbf{d}_k(\theta_k, \rho_k, \phi_k)$ is given by:

$$\mathbf{d}_k(\theta_k, \rho_k, \phi_k) = p_k(\rho_k, \phi_k)\mathbf{a}_k(\theta_k) \tag{4.99}$$

and

$$p(\rho_k, \phi_k) = 1 + i\rho_k e^{j\phi_k} \tag{4.100}$$

That is:

$$\mathbf{d}_k(\theta_k, \rho_k, \phi_k) = [1 + i\rho_k\, e^{j\phi_k}, e^{-j\theta_k} + i\rho_k e^{j(\phi_k-\theta_k)}, \ldots, e^{-j(N-1)\theta_k} + i\rho_k e^{j(\phi_k-(N-1)\theta_k)}]^T \tag{4.101}$$

And the unitary vector $\mathbf{c}_k$ is given by:

$$\mathbf{c}_k = \frac{\mathbf{d}_k}{\|\mathbf{d}_k\|} \tag{4.102}$$

where $\|\mathbf{d}_k\| = \sqrt{N(1+\rho_k^2)}$

From all the discussion above in Section 4.6.2, the recorded signal of the vector-sensor array with noise can be modeled as a quaternion vector $\mathbf{x}_Q$:

$$\mathbf{x}_Q = \sum_{k=1}^{P} \mathbf{d}_k \beta_{1k} e^{j\alpha_{1k}} + \mathbf{n}_Q \tag{4.103}$$

Where $\mathbf{n}_Q$ represents all the noise added on the vector-sensor array. β_{1k} and α_{1k} are given by Eq. 4.91.

4.6.3 Quaternion spectral matrix

The second order moment for a vector sensor array using quaternion formalism, referred to quaternion spectral matrix (QSM) $\Omega \in \mathbb{H}^{N\times N}$ is obtained from the observation on the vector-sensor array (Eq. 4.103):

$$\mathbf{\Omega} = \mathbb{E}\{\mathbf{x}_Q \mathbf{x}_Q^{\triangleleft}\} \tag{4.104}$$

With the assumption of the noise and the sources are not correlated and the source signals are not correlated, the quaternion spectral matrix can be further written as:

$$\mathbf{\Omega} = \mathbb{E}\{(\sum_{k=1}^{K} c_k \|\mathbf{d}_k\|)\beta_{1k} exp(j\alpha_{ik} + \mathbf{n})\}(\mathbb{E}\{(\sum_{k=1}^{K} c_k \|\mathbf{d}_k\|)\beta_{1k} exp(j\alpha_{ik} + \mathbf{n})\})^{\triangleleft} = \mathbf{\Omega}_S + \mathbf{\Omega}_N \tag{4.105}$$

where

$$\mathbf{\Omega}_S = \sum_{k=1}^{K} \sigma_k^2 \mathbf{c}_k \mathbf{c}_k^{\triangleleft} \tag{4.106}$$

the norm of a quaternion vector is defined as $\|q\| = \sqrt{qq^{\triangleleft}}$ represents the quaternionic transposition-conjugation operator. Using the Carley-Dickson form given by equation 4.89, the quaternion spectral matrix can be computed from the two-order moments with two complex vectors $\mathbf{x}_1$ and $\mathbf{x}_2$:

$$\mathbf{\Omega} = \mathbb{E}\{\mathbf{x}_1 \mathbf{x}_1{}^*\} - \mathbb{E}\{\mathbf{x}_1 \mathbf{x}_2{}^*\} + i\mathbb{E}\{\mathbf{x}_2 \mathbf{x}_1{}^*\} - i\mathbb{E}\{\mathbf{x}_2 \mathbf{x}_2{}^*\} \tag{4.107}$$

4.6.4 Quaternion eigenvalue decomposition

From averaging of several samples of recorded signals, the quaternion spectral matrix is estimated as $\hat{\Omega}$ and is further decomposed, which is based on eigenvalue decomposition theory and right quaternion eigenvalue theory [Lee48] [Woo85], as follows:

$$\hat{\mathbf{\Omega}} = \sum_{k=1}^{N} \lambda_k \mathbf{u}_k \mathbf{u}_k{}^{\triangleleft} \tag{4.108}$$

where λ_k are the real eigenvalues and $\mathbf{u}_k$ are the N orthonormal quaternion valued eigenvectors. In addition, in [MLBM06], the orthogonality for quaternion-valued vectors is defined and the approximation error for the long vector [MLBM05] and quaternionic decompositions are discussed. Theoretically, it turns out that compared with the long vector method, the use of quaternion vector orthogonality give a more accurate estimation.

4.6.5 Quaternion-MUSIC estimator

Eventually, a MUSIC-like estimator (Quaternion-MUSIC estimator) is proposed by the projection of quaternion steering vector $\mathbf{q}(\theta, \rho, \phi)$ on the noise subspace in order to correctly estimate the parameters θ, ρ, and ϕ:

$$F_{Q-MUSIC}(\theta, \rho, \phi) = \frac{1}{\mathbf{q}^{\triangleleft}(\theta, \rho, \phi)\Pi_N \mathbf{q}(\theta, \rho, \phi)} \tag{4.109}$$

And the quaternion steering vector $\mathbf{q}(\theta, \rho, \phi)$ is noted by:

$$\mathbf{q}(\theta, \rho, \phi) = \sqrt{M(1+\rho^2)}[1 + i\rho e^{j\phi}, e^{-j\theta} + i\rho e^{j(\phi-\theta)}, \ldots, e^{-j(M-1)\theta} + i\rho e^{j(\phi-(M-1)\theta)}] \tag{4.110}$$

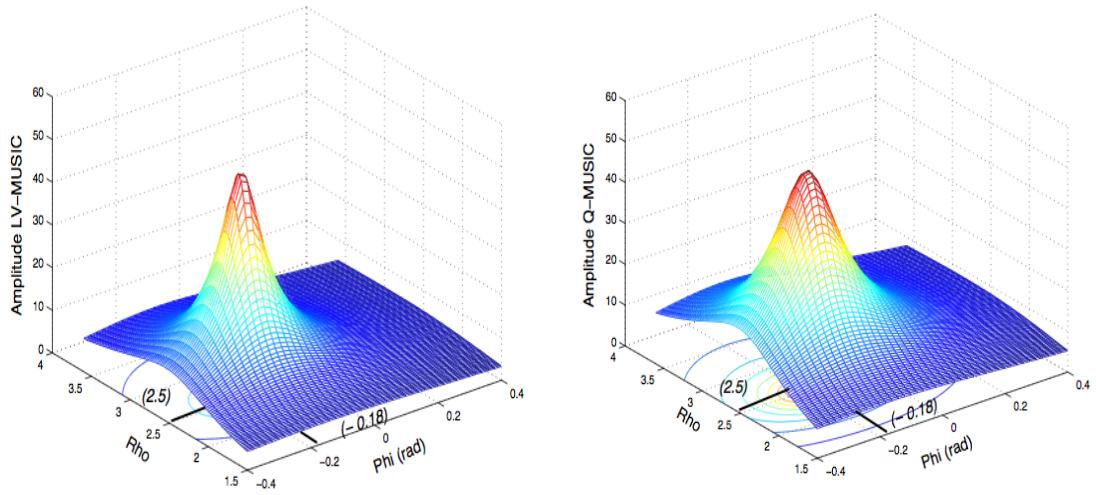

(a) (b)

Figure 4.2: (a) LV estimation result [MLBM05] (b) Q-MUSIC estimation result [MLBM06]

4.7 Number of Signals Estimation

Efficient detection the number of signals is necessary for most of models-based high-resolution methods. If this prior knowledge is not correctly determined, the separation or localization performance will be hampered. In charpter 6, we will pay attention to this topic again and proposed a more efficient method in practical perspective for the forward problem of shallow-water acoustic tomography.

4.8 Discussion and comparison

In this Section, we will discuss and compare these representative algorithms after defining and address several important concepts.

- *Consistency* — In this discussion, consistency refers to the property of an estimator, which is considered as a random variable indexed by the number of items in the data-set, converges to the value that the estimation procedure is designed to estimate.

- *Statistical Performance* — We use the concept of good statistical performance to denote that an estimator asymptotically attains the Cramer-Rao Bound, which is a lower bound on the covariance matrix of any unbiased estimator.

- *Polarization (also polarisation)* — It is a property of certain types of waves that describes the orientation of their oscillations, such as electromagnetic waves. However, acoustic waves in ocean do not have polarization due to the same direction of vibration and direction of propagation.

According with these concepts and the essential difference between these high-resolution methods, the introduced techniques are compared in the following four tables. First, they almost all have a good statistical performance. Most of subspace methods are based on the 2-order statistical moments of the received signals except MUSIC-4 algorithm under the assumption of Gaussian random process. The main disadvantages of subspace-based methods are the sensibility to coherent signals and their correct detection needs the prior knowledge of the number of signals compared with DML, SML, and MAP-NSF. Nevertheless, DML, SML and MAP-NSF can avoid these two problems at the cost of relatively low resolution and large computation cost. In our opinion, applying multiple-dimensional, high-order statistical moments, or multiple-dimensional with high-order moments to specific applications will probably an study trend in future. At the end of this section, we expect that the brief survey on high-resolution method in Chapter 4 will be useful for interested readers to select and extend suitable algorithm to their application backgrounds.

Method	Consistency	Coherent Signals	Statistical Order
Beamforming	L=1	-	2-order
MUSIC	Yes	No	2-order
DML	Yes	Yes	2-order
SML	Yes	Yes	2-order
MAP-NSF	Yes	Yes	2-order
Esprit	Yes	No	2-order
Root-MUSIC	Yes	No	2-order
MUSIC-4	Yes	No	4-order
Q-MUSIC	Yes	No	2-order
2D-MUSIC	Yes	No	2-order

Table 4.1: Comparison of the existing high-resolution methods based on different criterions (Consistency, Coherent Signals and Statistical Order)-I

Method	Computation	Dimensional	Sensor Type
Beamforming	1-D search	1-D	Scalar
MUSIC	EVD, 1-D search	1-D	Scalar
DML	M-D search	1-D	Scalar
SML	M-D search	1-D	Scalar
MAP-NSF	M-D search	1-D	Scalar
Esprit	EVD	1-D	Scalar
Root-MUSIC	EVD, polynomial	1-D	Scalar
MUSIC-4	EVD, 1-D search	1-D	Scalar
Q-MUSIC	EVD, 1-D search	M-D	Vector
2D-MUSIC	EVD, 1-D search	M-D	Scalar

Table 4.2: Comparison of the existing high-resolution methods based on different criterions (Computation, Dimensional and Sensor Type)-II

Method	Statistical Performance	Polarization Sensitivity
Beamforming	-	Yes
MUSIC	Good	Yes
DML	Good	Yes
SML	Good	Yes
MAP-NSF	Good	Yes
Esprit	Good	–
Root-MUSIC	Good	–
MUSIC-4	Good	Yes
Q-MUSIC	Good	No
2D-MUSIC	Good	Yes

Table 4.3: Comparison of the existing high-resolution methods based on different criterions (Statistical Performance and Polarization Sensitivity)-IIII

Method	Prior knowledge of order	Assumption of Signal Type	Array Geometries
Beamforming	No	Gaussian	Arbitrary
MUSIC	Yes	Gaussian	Arbitrary
DML	No	-	Arbitrary
SML	No	-	Arbitrary
MAP-NSF	No	-	Arbitrary
Esprit	Yes	Gaussian	ULA
Root-MUSIC	Yes	Gaussian	ULA
MUSIC-4	Yes	No	Arbitrary
Q-MUSIC	Yes	Gaussian	Arbitrary
2D-MUSIC	Yes	Gaussian	Arbitrary

Table 4.4: Comparison of the existing high-resolution methods based on different criterions (Prior knowledge of model order, Assumption of Signal Type and Array Geometries)-III

Chapter 5

Raypaths Separation with High Resolution Processing in a Shallow-Water Waveguide

Contents

5.1 Introduction 79
5.2 Smoothing-MUSICAL 82
5.2.1 Signal model 83
5.2.2 Principle of the algorithm 84
5.2.2.1 Estimation of interspectral matrix 84
5.2.2.2 Projection onto the noise subspace 89
5.3 Simulations 90
5.3.1 Configuration 90
5.3.2 Large time-window data 90
5.3.3 Small time-window experiments 95
5.3.4 Robustness against noise 95
5.4 Application on real data 99
5.4.1 Configuration 99
5.4.2 Results 99
5.5 Conclusion 99

5.1 Introduction

As the background knowledge we has introduced in Chapter 2, ocean Acoustic Tomography (OAT) is a technique of measurement to acquire information of temperatures and currents of oceans —- travel time and other measurable acoustic parameters are function of temperature and water velocity, so they are interpreted to provide information about the intervening ocean using inverse methods. Due to not only the practical importance we mentioned in Chapter 2 but also some experimental benefits, the shallow-water OAT at small scale has been paid more attention in recent years [IRN*09], [RKH*04], [RIN*11]. Furthermore, these experimental merits are summarized as: firstly, at the smaller scale the measurement of the environment parameters such as bathymetry and the sound-speed fluctuations are easier; secondly, array deployments are also simpler in shallow water since array lengths can be shorter. In a shallow-water oceanic medium modeled by waveguide, shallow-water OAT technique also takes advantage of the multi-path properties of the wave field: using as many raypaths as possible allows to estimate the sound speed distribution over a larger part of the waveguide. Unfortunately, the shallow-water OAT still need to face the difficulty produced by the multi-path properties of the wavefield —- interfering fields in both time and frequency domain. Therefore, ray identification and arrival time estimation cannot be realized without using a specific signal processing technology in a suitable configuration in the background of shallow-water OAT. Although we have introduced the beamforming, double beamforming algorithms and their configurations in Chapter 2 and Chapter 3, in the following part, these methods and their limitations will be addressed again in terms of their separation performance and robustness to SNR.

The initial configuration which OAT relies on is to make sound signals travel between an acoustic source and a receiver, but the separation and identification of raypaths is rarely possible from the received signal in this kind of configurations particularly because of the mixture of raypaths (several raypaths arrive at the same time) and / or a low signal to noise (SNR). On the other hand, as a classical method, beamforming is frequently used to separate raypaths, typically applied on a vertical receiver array at the reception, which record the signal emitted by a single emitter. Compared with the configuration of a single hydrophone receiver, a vertical receiver array will provide two significant benefits at the cost of somewhat increased receiver complexity [MWW95]: vertical receiving arrays can improve the SNR as well as enabling the separation of some raypaths that are not resolved in the time domain using the arrival angles.

Although advantages of using beamforming on a received array have been presented

above, its major drawback is the limited resolving ability. It is necessary to provide more separated raypaths to improve the possibilities to get satisfying tomography results. Recently, a tomography method has been developed using double beamforming to separate the different paths and extract more observations. Based on the principle of reciprocity, beamforming is applied twice to a configuration of array-array. Once is in the vertical array of emission and the other in the one of reception. Thanks to exploiting the emitted angles of raypaths, the method has improved the conventional beamforming performances [IRN*09]. However, double beamforming is still confronted to the main beamforming drawback: the low resolution performance.

Another important characteristic of multi-path propagation in the case of OAT is that multiple raypaths are always correlated due to producing by the reflections of the emitted signal. In particular, if the delay between two raypaths is small enough, raypaths are coherent. That is the problem of coherent signals separation, which we have briefly presented in Chapter 4. In addition, in practical environments, it is difficult to obtain multiple realizations for a certain random process. Based on the discussion above, it is crucial to present a high resolution processing adapting to the coherent or highly correlated ray paths in view of practical importance.

It is known that high resolution methods built from MUSIC algorithm have been developed to separate spatially close sources. They are based on a multi-path propagation model and take advantage of the statistical properties of the received signal. Then certain parameters, for example, the angle of reception or arrival time, are estimated by maximizing or minimizing a function [Sch86], [WK85a], [BG88], [GB95]. In the context of OAT, as the emitted signal is known, a MUSIC Actif large band (MUSICAL) [GB95] is introduced to separate close raypaths by using the spectrum and module information of the emitted signal. Although MUSICAL performs better than matched filtering beamforming, it is restricted on the assumption of decorrelated raypaths. MUSICAL performance with respect to its separation or the noise level drops sharply when the correlation of raypaths is high.

To still use the localization methods in the presence of highly correlated sources, effective spatial smoothing has been developed for narrowband sources, which is first extensively studied by [EJS81] and [ESJ82]. A more complete analysis of spatial smoothing is demonstrated with simulation results in conjunction with the eigenstructure technique by [SWK85]. Then, it is extended to forward-backward spatial-smoothing approach by [RH93]. Furthermore, the performance of the weighted eigen-based state space methods / ESPRIT and weighted MUSIC based on the spatially smoothed forward-backward covariance estimator is analyzed. It is shown that combing spatial smoothing with the

forward-backward approach is more effective than using forward spatial smoothing alone. In [Red87] they propose an alternative proof for the number of subarrays required of the spatial smoothing technique to ensure a nonsingular covariance matrix is $m+1$ where m is the nullity of the source covariance matrix. Since the conventional spatial smoothing is obtained at the cost of a reduction of array aperture leading to poorer DOA estimation, an enhanced spatial smoothing method is presented by [SWK85] and [Cho02], which improves significantly the resolution of the conventional method. Besides, the computational cost of spatial smoothing is large, owing to eigen-decomposition of the array covariance matrix. To reduce the computational cost, [AASAM04] proposes a iterative spatial smoothing algorithm. By resolving uncorrelated and correlated signals separately, it performs in two stages. In the first stage, it needs to form the uncorrelated signals covariance matrix, which is difficult in realization. Due to using only the forward spatial smoothing instead of the forward-backward spatial smoothing in the construction of the smoothed data matrix, the effective aperture of the array is largely reduced. Excepting the methods lied in the assumption of white Gaussian noise, a group of spatial smoothing methods are proposed for DOA estimation in the presence of correlated noise fields, such as: a matrix decomposition method introduced by [RR93], a weighted spatial smoothing algorithm proposed by [TO97] and a spatial difference smoothing method presented by [QWZH05]. Coherent signal-subspace processing for wideband signals in view of frequency domain is shown by [WK85a]. The problem of detecting multiple wide-band sources and estimating DOA due to the signals received by a vertical array is addressed, in particular, when the sources are completely correlated. Specifically, the coherently constructed signal space results in an appropriately frequency-averaged estimate of the spatial covariance matrix that is statistically more accurate and that is, to a large extent, immune to the degree of correlation between the sources. The performance of the signal-subspace processing for estimations of the DOA and detection multiple wide-band sources is studied analytically by [WK87]. Despite it has the convenience of locating multiple coherent sources without any preprocessing technique, it is still not exactly suitable to the context of OAT. Recently, [PM06] present a new wavefield filter for multicomponent seismic data. Smoothing methods considering respectively in spatial, frequency and spatial-frequency domain are introduced to correctly estimate multicomponent wideband spectral matrix.

Besides, using cumulants is to estimate the direction of arrival (DOA) in a coherent environment is first studied by [GDM94]. Correspondingly, adding a step of blind estimation of the steering vector with fourth-order cumulants, [YF97] present a SV-DOA algorithm to perform the estimation of DOA in the presence of multipath propagation

of communication systems operating in a mobile communications environment. It also could not be applied directly in the context of OAT for both estimating DOA and arrival time.

In this Chapter, inspired by [PM06], spatial, frequency and spatial-frequency domain smoothing preprocessing are presented to adapt to the active wideband spatial-temporal localization; in addition, in order to separate close raypaths of OAT in coherent environment, we propose a high resolution processing [JALT*11] [JM12] named by Smoothing-MUSICAL in the point-array configuration, which combines MUSICAL algorithm [GB95] and spatial-frequency smoothing. Its resolution performances are compared to those of conventional beamforming processing.

The Chapter is structured as follows: in Section 5.2, the signal model and principle of smoothing-MUSICAL are introduced; in Section A.6.3, firstly, the performance of Smoothing-MUSICAL is illustrated by synthetic data; then, the results with low SNR simulation are shown to test the robustness of Smoothing-MUSICAL. In Section 5.4, Smoothing-MUSICAL is applied to real data obtained from a small-scale experiment.

5.2 Smoothing-MUSICAL

Generally, high resolution methods require an accurate modeling of the received signals on the antenna (plane waves, uncorrelated sources, ...). First, these methods were designed for passive antennas with the assumption that there is no information on the temporal shape of the received signal. The signal is assumed to be random and stationary. For instance, one of the easiest case is to analyze narrowband signals. By taking into account spectral range of the signal, the narrow band methods have been extended to wideband signals. But either by a frequency analysis [WK85a] or temporal [BG88]of the signal, these methods still consider signals as wideband random ones and therefore do not provide information on frequency characteristics (amplitude and phase spectrum) or time (waveform) signal. By taking advantage of the frequency characteristics, [GB95] propose an active wideband MUSIC algorithm using multiple realizations and it lies in the assumption of decorrelated sources. However, these assumption are difficult to be achieved in practical OAT environment. Thus, we propose a Smoothing-MUSICAL, which is based on a single realization and enable to separate the fully correlated or coherent raypaths. The algorithm is described in the following sections:

5.2.1 Signal model

The signal model is built on an acoustic field composed of P raypaths arriving on an active vertical antenna of M sensors. The temporal signal received on the m^{th} sensor is modeled as:

$$x_m(t) = \sum_{p=1}^{P} a_p s(t - \tau_{m,p}) + n_m(t) \tag{5.1}$$

With:

- $x_m(t)$: received signal on the m^{th} sensor.
- $s(t)$: signal transmitted by the source.
- a_p: amplitude of the p^{th} raypath on the m^{th} sensor.
- $n_m(t)$: additive noise received at the m^{th} sensor.
- $\tau_{m,p}$: the arrival time.

In frequency domain, equation 5.1 is written as:

$$x_m(\nu) = \sum_{p=1}^{P} a_p s(\nu) \exp(-j2\pi\nu\tau_{m,p}) + n_m(\nu) \tag{5.2}$$

The arrival time $\tau_{m,p}$ can be expressed as follows:

$$\tau_{m,p} = t_p^{'} + t_m(\theta_p) \tag{5.3}$$

Where $t_p^{'}$ represents the arrival time of the p^{th} raypath on the reference sensor, $t_m(\theta_p)$ is the delay between the reference sensor and the m^{th} sensor. $t_m(\theta_p)$ is a function of θ_p, which is the arrival direction of raypath on the antenna.

Equation 5.2 can be rewritten with equation 5.3 as follows:

$$x_m(\nu) = \sum_{p=1}^{P} a_p s(\nu) \exp(-j\nu(\Psi_p + (m-1)\Phi_p)) + n_m(\nu) \tag{5.4}$$

With: $\Psi_p = 2\pi t_p^{'}$, $\Phi_p = 2\pi t_m(\theta_p)$.

In Equation 5.2, the term $s(\nu)$ is the deterministic amplitude of the emitted signal at the frequency ν. The amplitudes of each raypath, a_p, are considered random and uncorrelated. To separate the deterministic terms from the random ones, equation 5.2 can be written as a matrix form by using F frequency bins of the signal:

$$\mathbf{x}_g = \mathbf{H}.\mathbf{c} + \mathbf{n}_g \tag{5.5}$$

With:

- $\mathbf{x}_g = [\mathbf{x}^T(\nu_1), \mathbf{x}^T(\nu_2), \ldots, \mathbf{x}^T(\nu_F)]^T$ is a vector of dimension $M \times F$ obtained by concatenation of the observation vectors at each frequency.
- $\mathbf{x}(\nu_i) = [x_1(\nu_i), x_2(\nu_i), \ldots, x_M(\nu_i)]^T$
- F: the number of frequency bins of the signal.
- $\mathbf{n}_g = [\mathbf{n}^T(\nu_1), \mathbf{n}^T(\nu_2), \ldots, \mathbf{n}^T(\nu_F)]^T$ is a vector of dimension $M \times F$ obtained by concatenation of the observation of noise vectors at each frequency.
- $\mathbf{n}(\nu_i) = [n_1(\nu_i), n_2(\nu_i), \ldots, n_M(\nu_i)]^T$
- $\mathbf{c} = [a_1, a_2, \ldots, a_P]^T$ is a vector of dimension P.
- $\mathbf{H} = [\mathbf{h}_1, \mathbf{h}_2, \ldots, \mathbf{h}_P]^T$ puts together the terms $e^{-2i\pi\nu_1\tau_{mp}}$ characterizing the transfer functions between the sources and the sensors.
- $\mathbf{h}_p = [s(\nu_1)e^{-2i\pi\nu_1\tau_{1p}}, \ldots, s(\nu_F)e^{-2i\pi\nu_F\tau_{Mp}}]^T$ the term $s(\nu_i)$ characterizing the emitted signal.
- T meaning transposed

5.2.2 Principle of the algorithm

After the modelization step, we will present the principle of the algorithm to detect and separate raypaths starting from estimating interspectral matrix.

5.2.2.1 Estimation of interspectral matrix

Based on the Equation 5.5, the interspectral matrix of the received data is obtained as:

$$\mathbf{\Gamma} = E\{\mathbf{x}_g \mathbf{x}_g^*\} = \mathbf{H}\,\mathbf{\Gamma_C}\,\mathbf{H}^* + \mathbf{\Gamma_N} = \mathbf{\Gamma_Y} + \mathbf{\Gamma_N} \tag{5.6}$$

Where $*$ means transpose-conjugated. $\mathbf{\Gamma_C}$ is the correlation matrix of sources in $P \times P$ dimension. $\mathbf{\Gamma_Y}$ is the wideband interspectral matrix of non-noisy observation. $\mathbf{\Gamma_N}$ is the interspectral matrix of wideband noise.

The assumption of multi-realizations or uncorrelated raypaths implies that $\mathbf{\Gamma_Y}$ is diagonal and its rank must be at least equal to the number of raypaths P. MUSICAL could get effective separation with this assumption. However, in practical experiment,

a single realization and correlated raypaths lead to rank deficiency. When the raypaths are fully correlated (or coherent), the rank of interspectral matrix is 1 (singular matrix) and the separation is impossible. To increase this rank and enable to obtain all the eigenvalues corresponding to raypaths, spatial and frequency smoothing techniques can be used. Although there exists spatial and frequency smoothing techniques, extending the narrowband methods to the active wideband case is not directly as the nature and structure of interspectral matrices are indeed different.

Wideband spatial smoothing

The basic idea of the spatial smoothing method in wideband is the same as that used in narrowband. This is to divide the principal antenna composed of M sensors into $2K_s + 1$ partially overlapping antennas and each sub-antenna with $M - 2K_s$ successive sensors. The sub-antenna of index k_s includes the sensors $[k_s, k_s + 1, \ldots, k_s + M - 2K_s]$. All these $2K_s + 1$ sub-antennas used to estimate $2K_s + 1$ broadband spectral matrices $\mathbf{\Gamma}^{k_s} = E\{\underline{\mathbf{x}}_{l,k_s}\underline{\mathbf{x}}^*_{l,k_s}\}$. The smoothing spectral matrix is then defined as the arithmetic mean of spectral matrices corresponding to the $2K_s + 1$ sub-antennas, which is shown in Equation 5.7.

$$\hat{\mathbf{\Gamma}} = (2K_s + 1)^{-1} \sum_{k_s=1}^{2K_s+1} \underline{\mathbf{x}}_{g,k_s}\underline{\mathbf{x}}^*_{g,k_s} \tag{5.7}$$

These subarrays are supposed to be linear and uniform. With the assumption, which is that the ray does not vary rapidly over the number of sensors used in the average, especially, without amplitude fluctuations. It has proven that if the number of subarrays is greater than or equal to the number of sources, then the spectral matrix is nonsingular. As an example, in Fig. 5.1 a uniform linear array with $M = 7$ identical sensors (1, ...,7) be divided into overlapping subarrays of size $M - 2K_s = 5$, with sensors (1, ..., 5) forming the first subarray, senors (2, ..., 6) forming the second subarray, etc.

Given the particular structure of broadband spectral matrix, two essential problems still need to be solved. The first one is whether the undergone structural changes during the smoothing of broadband spectral matrices are compatible with the broadband modeling methods used by high-resolution localization. The second one concerns the rank that is affected by the correlation matrices of source is also treated.

Actually, for each source p, the transition from the sensor m to the sensor $m + 1$ results in an additional phase shift. The linear antenna being equidistant sensors, the transition from the first sub-antenna to the k sub-antenna can be modeled by introducing $\mathbf{B}^k$ a matrix which includes the phase shifts of sources observed at F frequencies. The

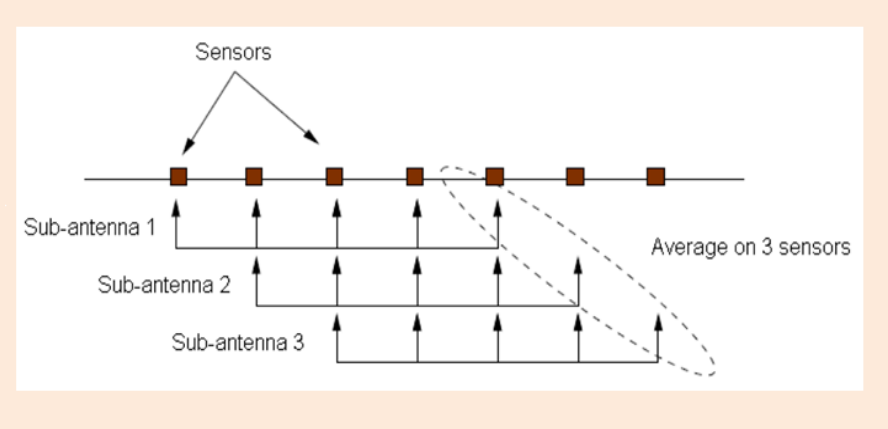

Figure 5.1: Subantenna structure of spatial smoothing

matrix is of dimension $M.F \times P$ and Eq. 5.8 describes its generic term:

$$B_f^k = exp[-j\nu(k-1)\Phi_p] \tag{5.8}$$

With these notations, the vector of the broadband observation of the sub-antenna of index k is written as:

$$\underline{\mathbf{x}}_g^k = \mathbf{H}\mathbf{B}^k\mathbf{c} + \mathbf{N}^k \tag{5.9}$$

From this expression, the algebraic characterization of the transformations caused by broadband spectral matrices in the spatial smoothing can show that:

1. The changes of spectral matrices due to smoothing are reduced essentially to a change in the correlation matrix sources $\mathbf{\Gamma}_C$;

2. The augmentation of rank of $\mathbf{\Gamma_C}$ depends on the number of sub-antennas $2K_s + 1$ and the number of groups of coherent sources Q, the value of the rank follows $(2K_s + 1) \times Q$;

3. The new ranks of $\mathbf{\Gamma_C}$ and $\mathbf{\Gamma_Y}$ are greater than or equal to P when the condition $2K_s + 1 \geq \frac{P}{Q}$ is satisfied;

4. The rank of the smoothing spectral matrix is increased by the value of $F \times P$.

These four items are sufficient to ensure that the smoothing spectral matrices are similar to those that could have been obtained with partially uncorrelated sources. They therefore express the decorrelation alone actually made by the processing. However, it should give special attention to the last two points and emphasize that it is not desirable

to have a processed rank of matrices, which is too high compared to P. In some situations it may indeed lead to dysfunctions that is similar to those matrices encountered with non-smoothed during excessive overestimation of the number of sources.

Frequency smoothing

Smoothing process being similar to that used in the previous paragraph can be applied in the frequency domain. This is largely due to the particular structure of the broadband observation vectors used by MUSICAL. Then, it is possible to introduce a frequency smoothing if the following two assumptions are met:

1. Prior whitening of received signals;

2. Frequency channels equally spaced on the analysis band.

For this, frequency smoothing is performed by dividing the band composed of F frequency channels into $2K_f + 1$ partially overlapping subbands of $F - 2K_f$ channels. Thus, the sub-band of index k_f is composed of channels $[k_f, k_f + 1, \ldots, k_f + F - 2K_f]$. The broadband smoothed spectral matrix of the observation is then defined as the average of the $2K_f + 1$ matrix corresponding to the $2K_f + 1$ subbands seen in Eq. 5.10.

$$\hat{\mathbf{\Gamma}} = (2K_f + 1)^{-1} \sum_{k_f=1}^{2K_f+1} \underline{\mathbf{x}}_{g,k_f} \underline{\mathbf{x}}_{g,k_f}^{*} \tag{5.10}$$

$$B_m^k = exp[-j\Delta(k-1)(\Psi_p + (m-1)\Phi_p)] \tag{5.11}$$

Fig. 5.2 shows an example of subbands division for $F = 10$ and $K_f = 2$.

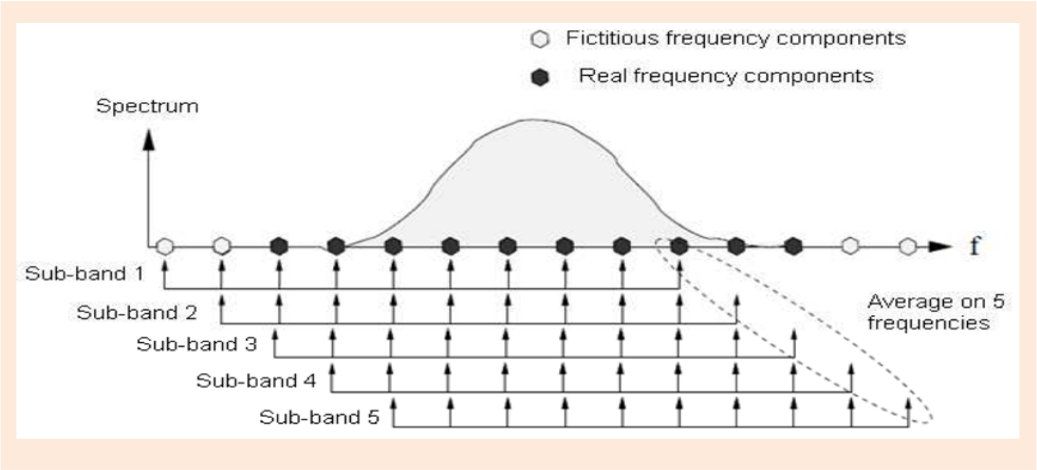

Figure 5.2: Subband structure of frequential smoothing

The expression giving the shape of the observation vector corresponding to the broadband sub-band index k is analogous to that given in Equation 5.9. As a result, in an analytical point of view, the M^2 blocks of the broadband smoothed spectral matrix in frequency domain have properties and structure quite similar to those of F^2 blocks of spatially smoothing matrix. The characteristics of the frequency smoothing can be deduced from this fact in all of those obtained in the study of broadband spatial smoothing. It shows in particular that $2K_f + 1$ subbands are enough for that the ranks of $\mathbf{\Gamma_C}$ and $\mathbf{\Gamma_Y}$ are equal to $(2K_f + 1) \times Q$.

Spatial-frequency smoothing

The two methods discussed above may well obviously be used together and making a strong smoothing either in distance or in frequency may introduce significant bias in the estimation of the matrix. To solve this problem, the combination of the two types of smoothing provides more flexibility in processing, particularly for the antenna which are composed of a limited number of sensors and for which the spatial smoothing methods are not applicable [PM06]. (K_s, K_f respectively denotes the spatial and frequency smoothing factor). From the single available observation $\underline{\mathbf{x}}$, by jointly using the two forms of smoothing, it is possible to generate a set of $(2K_s + 1)$ spatially recurrences $\underline{\mathbf{x}}_{g,k_s}$. These $2K_s + 1$ recurrences are then shifted frequentially to obtain $K = (2K_s + 1)(2K_f + 1)$ recurrences $\underline{\mathbf{x}}_{g,k_s,k_f}$. Finally, we can estimate the wideband interspectral matrix by the following formula:

$$\hat{\mathbf{\Gamma}} = (2K_s + 1)(2K_f + 1)^{-1} \sum_{k_s=1}^{2K_s+1} \sum_{k_f=1}^{2K_f+1} \underline{\mathbf{x}}_{g,k_s,k_f} \underline{\mathbf{x}}_{g,k_s,k_f}^{*} \tag{5.12}$$

The rank of the interspectral matrix thus estimated is equal to K. To achieve effective separation of raypaths and noise, it is necessary to select K greater than P.

Estimation of signal subspace

Using the above spatial-frequency smoothing, the wideband interspectral matrix is estimated as $\hat{\mathbf{\Gamma}}$. Due to the assumptions that the sources and the noise are uncorrelated, $\hat{\mathbf{\Gamma}}$ is decomposed as:

$$\hat{\mathbf{\Gamma}} = \hat{\mathbf{\Gamma}}_s + \hat{\mathbf{\Gamma}}_n \tag{5.13}$$

Because the spectral matrix has a Hermitian symmetry:

$$\hat{\mathbf{\Gamma}} = \hat{\mathbf{\Gamma}}^{*} \tag{5.14}$$

It can be decomposed in a single way using EVD as

$$\hat{\mathbf{\Gamma}} = \mathbf{U}\mathbf{\Lambda}\mathbf{U}^* = \sum_{k=1}^{MF} \lambda_k \mathbf{u_k}\mathbf{u_k}^* = \sum_{k=1}^{P} \lambda_k \mathbf{u_k}\mathbf{u_k}^* + \sum_{k=P+1}^{MF} \lambda_k \mathbf{u_k}\mathbf{u_k}^* \tag{5.15}$$

where $\mathbf{\Lambda} = diag(\lambda_1, \ldots, \lambda_M)$ are the eigenvalues and $\mathbf{U}$ is a unitary $(M \times F)$ by $(M \times F)$ matrix whose columns are the orthonormal eigenvectors $\mathbf{u}_1, \ldots, \mathbf{u}_M$ of $\hat{\mathbf{\Gamma}}$. The eigenvalues λ_i correspond to the energy of the data associated with the eigenvalue $\mathbf{u}_i$. They are arranged in a descending order as follows: $\lambda_1 \geq \lambda_2 \geq \cdots \geq \lambda_M \geq 0$.

5.2.2.2 Projection onto the noise subspace

Based on the above eigendecomposition, the signal subspace is spanned by the first P eigenvectors of $\hat{\mathbf{\Gamma}}$, and its complementary, the noise subspace is spanned by the orthogonal $MF - P$ last eigenvectors. The orthogonal projection onto the noise subspace is estimated as:

$$\hat{\mathbf{\Gamma}}_n = \sum_{k=P+1}^{MF} \mathbf{u_k}\mathbf{u_k}^* \tag{5.16}$$

Finally, the high resolution algorithm consists in maximizing the following function:

$$F_{s_{MUSIC}}(\theta, t^{'}) = \frac{1}{\mathbf{a}(\theta, t^{'})^* \, \hat{\mathbf{\Gamma}}_n \, \mathbf{a}(\theta, t^{'})} \tag{5.17}$$

With: The wideband steering vector $\mathbf{a}(\theta, t^{'})$ is the concatenation of the vectors $\mathbf{d}(\nu_i, \theta)$, which is the classical steering vector used in narrowband analysis. It is written as follows:

$$\mathbf{a}(\theta, t_p^{'}) = \begin{bmatrix} s(\nu_1) e^{-2j\pi\nu_1 t^{'}} \mathbf{d}^T(\nu_1, \theta) \\ s(\nu_2) e^{-2j\pi\nu_2 t^{'}} \mathbf{d}^T(\nu_2, \theta) \\ \vdots \\ s(\nu_F) e^{-2j\pi\nu_F t^{'}} \mathbf{d}^T(\nu_F, \theta) \end{bmatrix} \tag{5.18}$$

where $\mathbf{d}(\nu_i, \theta) = [1, e^{-2j\pi\nu_i t_{1,2}(\theta)}, \ldots, e^{-2j\pi\nu_i t_{1,M-1}(\theta)}]^T$. $\mathbf{d}(\nu_i, \theta)$ contains the informations concerning the phase shifts between sensors at a given frequency and for a raypath with arrival angle θ.

5.3 Simulations

5.3.1 Configuration

We illustrate the method presented previously on two sets of synthetic data obtained with a parabolic equation algorithm. We will use these two sets of synthetic data to implement several experiments depending on different property tests. In these experiments, we use one source and a vertical antenna of 61 receivers. In the first group of synthetic experiment, the source is fixed at 40 m under the ocean and the 61 receivers are regularly spaced in the water column between 25 m and 55 m. We choose the 31th sensors as the reference one. The distance between the source and the reference sensor is 2 km. The configuration is shown by Fig. 5.3. The source position of the experiment configuration which is explored to obtain the second group of synthetic data is fixed at 40.5 m.

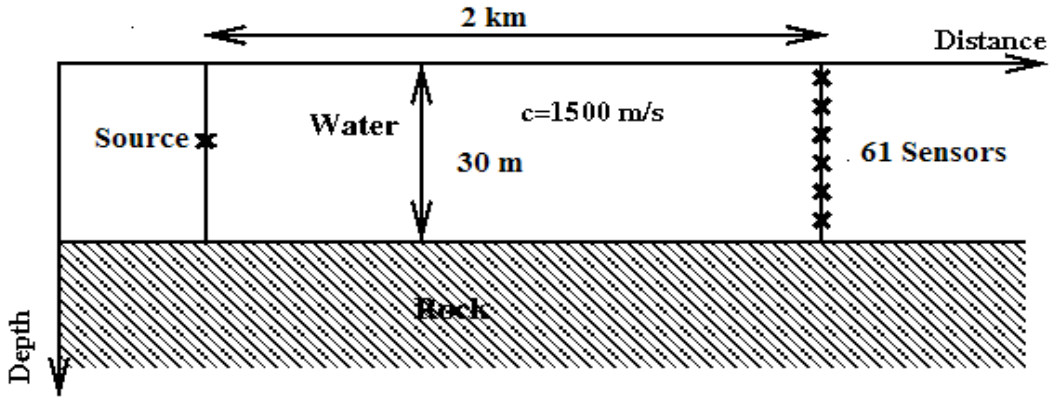

Figure 5.3: The point-array configuration explored to obtain the synthetic data

The sampling frequency and central frequency of the emitted signal are respectively 10400 Hz and 1000 Hz. Raypaths propagate between the source and a receiver of the receiving antenna. All raypaths are recorded on the receiving antenna for the given source.

5.3.2 Large time-window data

In the first group of synthetic data, we choose a relative large time-window (1560 samples in time domain) to test the separation performance of the proposed algorithm. Figure 5.4 shows the recorded signals on the vertical array. To illustrate the performance of the improvement of smoothing-MUSICAL, we take conventionnal beamforming [DWM01] as a comparative method. The separation results for recorded signal

are illustrated by Figure 5.5 and Figure 5.6 in the form of mesh. Each spot in these figures denotes a raypath with arrival time and arrival direction. In general, smoothing-MUSICAL gives a more accurate separation with the smaller spot corresponding to each raypath than beamforming method. For giving more sufficient demonstration of this benefit, we enlarge the figure 5.4 to show part of recorded signal which includes the first two arrival raypaths (Fig. 5.7). In addition, Figure 5.8 (a), (b) and (c) show the separation results with smoothing-MUSICAL and beamforming. When facing to close raypaths, iIt is obvious that smoothing-MUSICAL (Fig. 5.8 (a), and (c)) enables to separate the two raypaths.

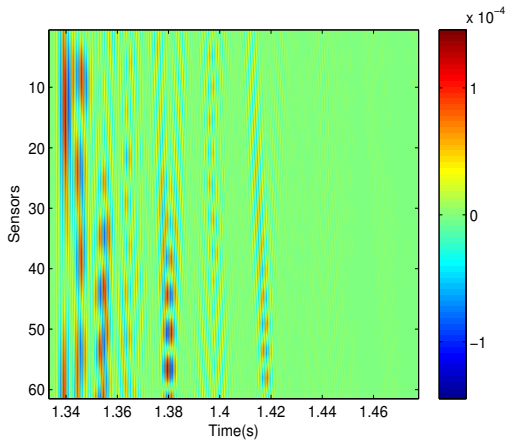

Figure 5.4: An experimental example of Recorded Signal (large time-window and without noise)

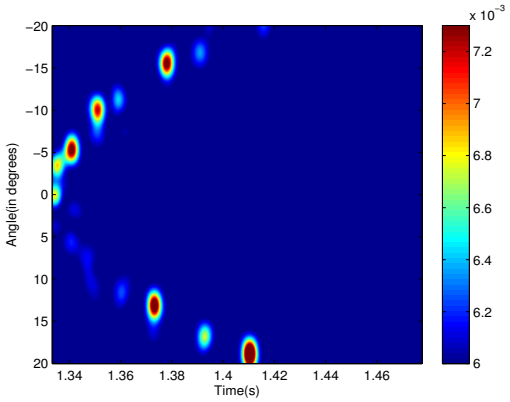

(a)

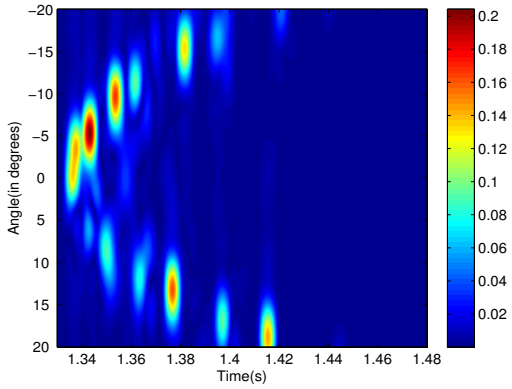

(b)

Figure 5.5: The separation result of an experimental example of Recorded Signal (large time-window and without noise). (a) Separation results with Smoothing-MUSICAL. (b) Separation results with Beamforming.

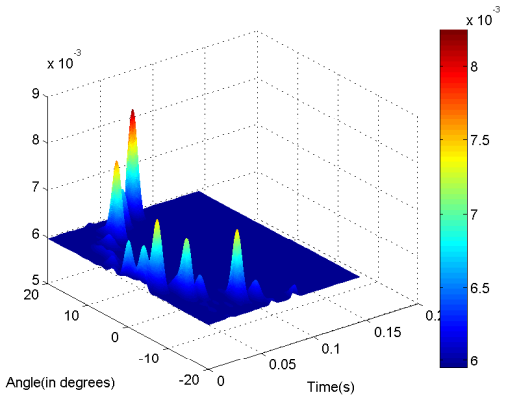

(a)

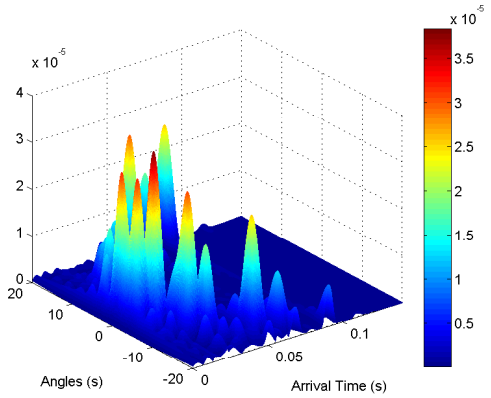

(b)

Figure 5.6: The separation result of an experimental example of Recorded Signal (Large time-window and without noise) (Mesh).(a) Separation results (mesh) with Smoothing-MUSICAL. (b) Separation results (mesh)with Beamforming.

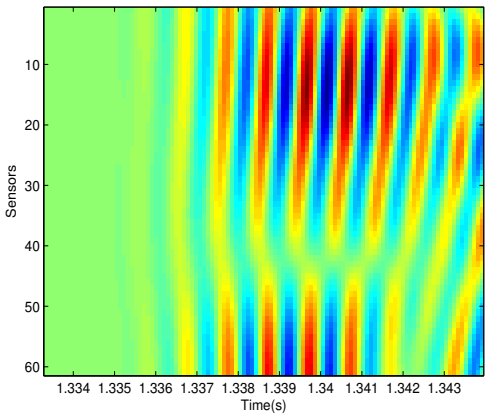

Figure 5.7: Part of recorded signal which includes the first two arrival raypaths (Large time-window and without noise)

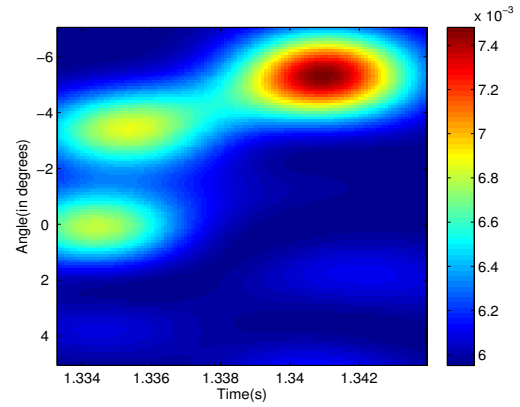

(a)

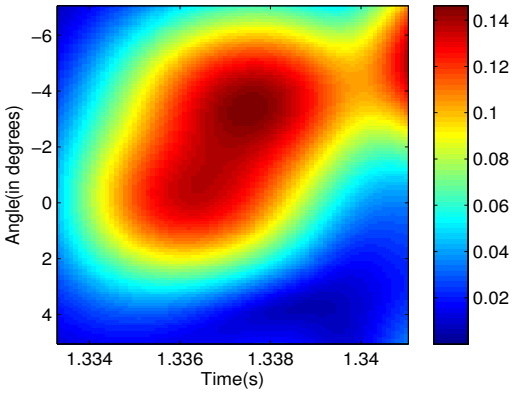

(b)

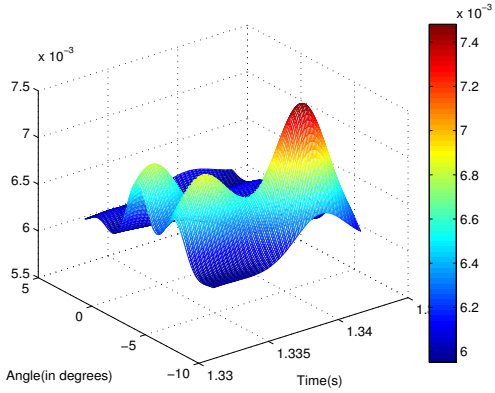

(c)

Figure 5.8: The separation result of part of recorded signal (Large time-window and without noise) (a) Separation results with Smoothing-MUSICAL. (b) Separation results with Beamforming. (c) Separation results (mesh) with Smoothing-MUSICAL.

5.3.3 Small time-window experiments

In this section, the further discussion on the resolution of the proposed method will be performed on a small time-window data (312 time samples). In order to illustrate the performance of our method, we also take conventionnal beamforming [DWM01] as a comparative method. Thus, both methods are applied to synthetic data. Both methods identify the raypaths in a plan of reception angle and propagation time. Separation results are presented using conventionnal beamforming (Figure. 5.9 (b)) and the proposed processing (Figure. 5.9 (a)). Besides, the theoretical position value is utilized to verify the separation results of both smoothing-MUSICAL and beamforming.

As we presented before, each of the visible spots in (Figure. 5.9 (b)) and (Figure. 5.9 (c)) corresponds to the arrival of a raypath, with its travel time and the angle of reception. Liking the common advantage of high resolution methods [SA89], [SN90], the proposed algorithm performes a stronger ability of separation. More preciser results is obtained (Figure. 5.9 (c)) . Moreover, it can be seen on Figure. 5.9 (c) and Figure. 5.9 (b) that the proposed processing produces less artifact than conventional beamforming.

5.3.4 Robustness against noise

Based on the discussion before, in the noiseless case, smoothing-MUSICAL identifies raypaths more preciser than conventional beamforming with less artifacts. In this part, its robustness to noise will be evaluated when the signal to noise ratio decreases. Since the signal occupies a possible portion of the frequency band, we added white Gaussian noise only in this band. We define the SNR as follows: power ratio between the signal and the noise in the frequency band of signal. The results are presented for two different SNR: 0 dB to -15 dB.

SNR= 0 dB: Figure. 5.10 (b) shows the results obtained by beamforming of the signals recorded on the antenna. In this case, it is possible to separate the different raypaths. The corresponding spots are visible and separated in the DOA-temporal domain. At the same time, the separated results of Smoothing-MUSICAL is shown by Figure. 5.10 (c). However, smoothing-MUSICAL is not essential for this case in the view of robustness against noise.

SNR=-15dB: Let us study the case of a strongly noisy environment. As in the previous case, beamforming and smoothing-MUSICAL are respectively applied to the received signals in the configuration of point-array. The separated results of beamforming (Fig. 5.11 (b)) illustrate that the different raypaths are no longer easily to recognize from the large number of artifact produced by noise and monitoring of the arrival times can

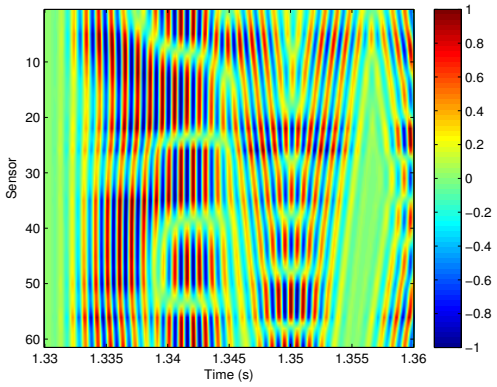

(a)

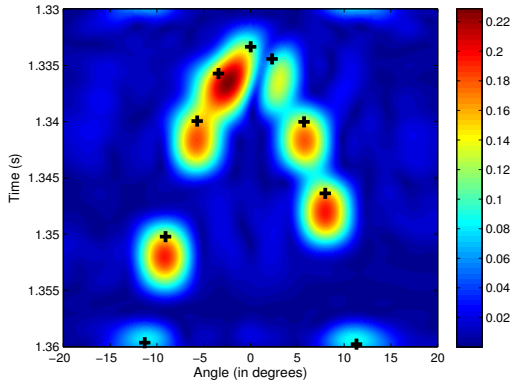

(b)

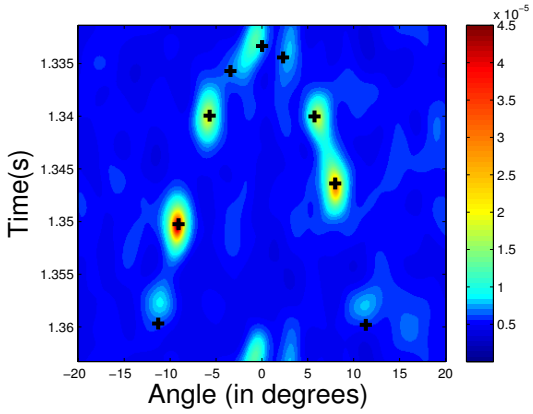

(c)

Figure 5.9: An experimental example of Recorded Signal (Small time-window and without noise) (a) Recorded Signal (without noise). (b) Separation results with Beamforming. (c) Separation results with Smoothing-MUSICAL.

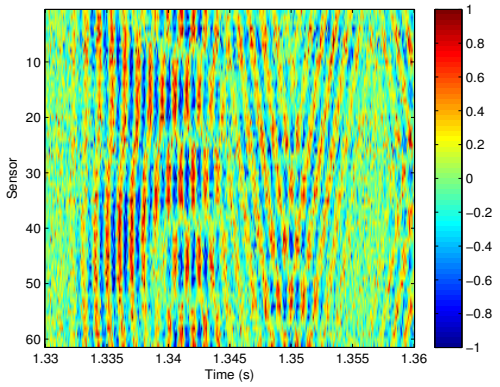

(a)

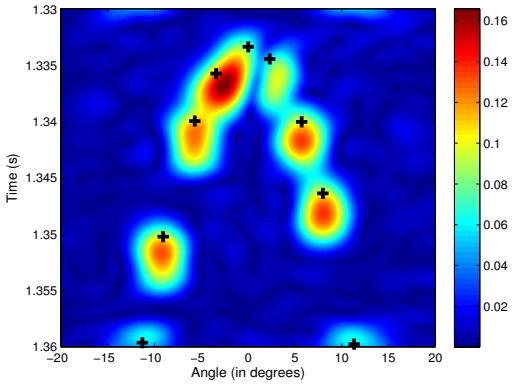

(b)

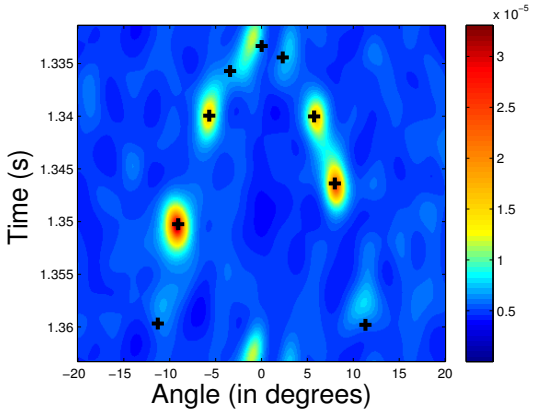

(c)

Figure 5.10: An experimental example of Recorded Signal (SNR=0dB) (a) Recorded Signal (SNR=0dB). (b) Separation results with Beamforming (SNR=0dB). (c) Separation results with Smoothing MUSICAL (SNR=0dB).

not be achieved. For smoothing-MUSICAL (Fig. 5.11(c)), the spots corresponding to different raypaths are still visible. It can therefore effectively limit the influence of noise in the data.

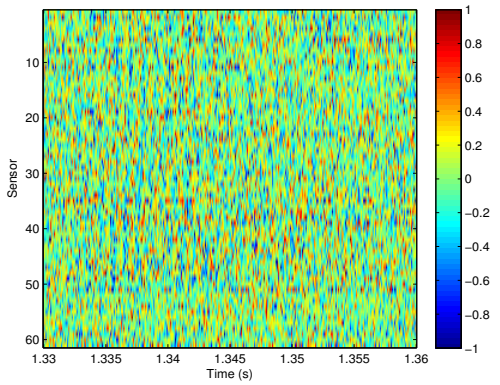

(a)

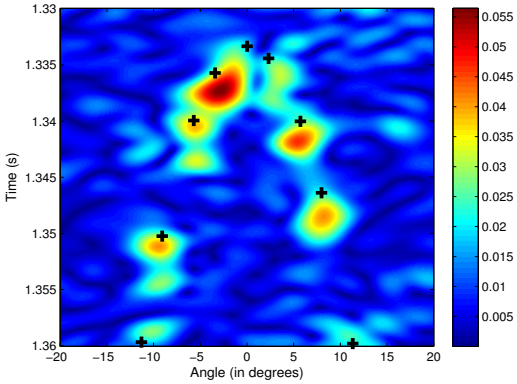

(b)

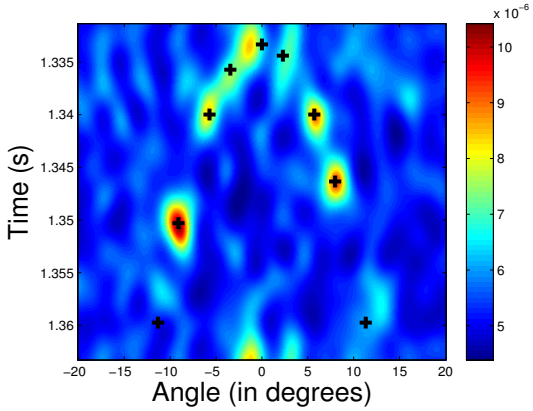

(c)

Figure 5.11: An experimental example of Recorded Signal (SNR=-15dB) (a) Recorded Signal (SNR=-15dB). (b) Separation results with Beamforming (SNR=-15dB). (c) Separation results with Smoothing MUSICAL (SNR=-15dB).

5.4 Application on real data

5.4.1 Configuration

A small-scale experiment is discussed in this part, so that we can further illustrate the performance of our methods. The principle on which these experiments are based is as follow: if the frequency of signals is multiplied by a factor and the spatial distances are divided by the same factor, the physical phenomena occurring in the environment remains the same. It achieves a reduced cost and a totally controlled experiment. The experiment presented here were performed at the ISTerre (Institut des Sciences de la Terre) lab in the ultrasonic tank which is developed by P. Roux. In this tank, a waveguide of 5-10 cm in depth and 1-1.5 m in length is constructed. A steel bar acts as the bottom, which is very reflective and perfectly flat. Particularly, a sensor is set at 0.0263m as an emitter. A vertical array composed of 64 sensors is taken as a reception. The depth of the first receiver is $3.55 \times 10^{-3}m$. The interval of two adjacent receivers is 0.75×10^{-3}m. The distance between the emitter and reference receiver is about 1.15 m and the source signal with a 1 MHz frequency bandwidth has a central frequency of 1.2 MHz. The first 760 samples in time domain of received signal with sampling frequency $F_e = 50MHz$ are used in this experiment.

5.4.2 Results

Separating results obtained by conventional beamforming is shown in Figure. 5.12 (b). Theoretical arrival positions noted by black crosses are computed from ray theory. Beamforming detects six raypaths successfully in accordance with the theoretical position, but it fails in separating the first two raypaths. For the same data, Smoothing-MUSICAL (Fig. 5.12 (c)) still holds the better separation performance for providing precise physical position in the plan of DOA and arrival time.

In particular, it can be seen on Figure. 5.12 (b) and Figure. 5.12 (c), the proposed processing manages to separate the first two raypaths, with the value of arrival time and the angle of reception respectively $(t^{'}, \theta) = (7.701 \times 10^{-4}, -0.2^{\circ})$ and $(t', \theta) = (7.716 \times 10^{-4}, -2.8^{\circ})$. But in that case, beamforming presents us only one mixed spot.

5.5 Conclusion

We propose a smoothing-MUSICAL method to separate highly correlated or coherent raypaths in shallow-water wave guide. The point-array configuration is considered to

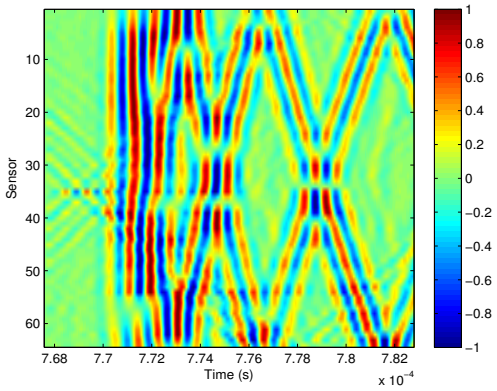

(a)

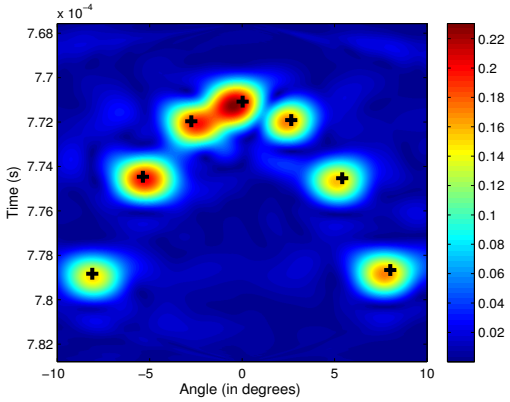

(b)

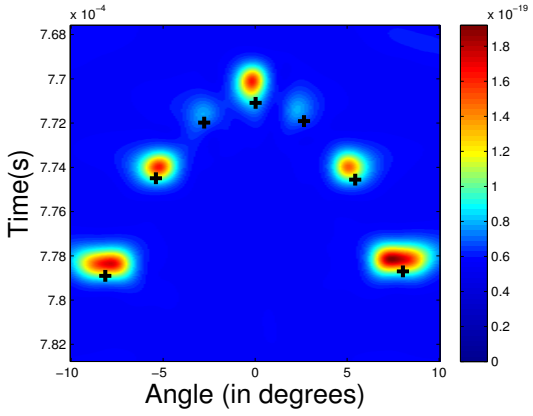

(c)

Figure 5.12: An experimental example of Recorded Signal for real data obtained at small scale (a) Recorded Signal for real data obtained at small scale. (b) Separation results with Beamforming for real data obtained at small scale. (c) Separation results with Smoothing MUSICAL for real data obtained at small scale.

separate more raypaths by providing arrival angle as a discriminating parameter. Compared with beamforming, the proposed processing gets a better separation of raypaths with less noise artifacts and accurate physical position, in particular for the close raypaths. Next, it will be applied to 2D configuration composed by an array in emission and an array in reception with real acoustic signal.

Chapter 6

Automatic Detection of the Number of Raypaths in a Shallow-Water Waveguide

Contents

6.1 Introduction . . . 105

6.2 Demonstration on Importance of Detection of the Number of Raypaths 107

6.3 Problem of Detection of Number of Raypaths . . . 109

6.4 Techniques for detection of the number of Raypaths . . . 110

6.4.1 Information Theoretic Criteria . . . 110

6.4.1.1 AIC . . . 110

6.4.1.2 MDL . . . 111

6.4.2 EFT . . . 111

6.4.2.1 Eigenvalue Profile Under Noise Only Assumption . . . 111

6.4.2.2 Principle of the Recursive EFT . . . 115

6.5 Simulations . . . 116

6.5.1 Performance in various SNR . . . 117

6.5.2 Performance for close raypaths . . . 120

6.6 Small-Scale Experiment . . . 120

6.6.1 Noise-whitening process . . . 120

6.6.2 Small-Scale Experiment . . . 123

6.7 Conclusion . . . 124

6.1 Introduction

As a first step of improvement, a smoothing-MUSICAL method (MUSIC Active Large-band), which is based on one realization in frequency domain and by a combination of MUSICAL and spatial-frequency smoothing, is developed for extracting the observation in the context of ocean acoustic tomography [JALT*11]. It gets more precise separation than beamforming under condition of prior knowledge of number of rayspaths. Like the general case of array processing, the smoothing-MUSICAL method also requires correct selection of model order. If the model order is poorly selected, the separation may be hampered. As far as the model-order selection problem is concerned, two commonly suggested approaches are Akaike information criterion (AIC) and Minimum description length (MDL) [WK85b]. They consist of minimizing the Kullback-Leibler (KL) discrepancy between the probability density function (PDF) of the data and the PDF of the model. With ideal assumptions of ergodic Gaussian random processes, the MDL criterion is shown to be asymptotically consistent, whereas AIC tends to overestimate the order of model. In contrast, these ideal assumptions may not be fulfilled in practice and several factors could result in the smallest eigenvalues being dispersed (for example: reduction number of samples or low SNR). Both AIC and MDL tend to overestimate or underestimate the order of model. For analyzing the performance and evaluating the probability of over or under estimation of AIC and MDL, theoretical results are presented in [XK95] [LR01]. Moreover, two variations of AIC and MDL are introduced: an order statistics approach is employed in the existing solution by Fishler and Messer [FM00]. In [MP05], a novel method for estimation of time delays and amplitudes of arrivals with maximum a posteriori MAP estimation is presented. And bypassing computationally demanding, gibbs sampling is proposed as an efficient means for estimating necessary posterior probability distributions. In the context of source localization, a Gibbs sampling-maximum a posteriori estimator [MM05] is used to extract arrival times of ray paths from time series received at vertical line arrays. In order to perform inversion of seabed reflection data to resolve sediment structure at a spatial scale below the pulse length of the acoustic source, a practical approach to model selection is used [DDH09], employing the Bayesian information criterion to decide on the number of sediment layers needed to sufficiently fit the data while satisfying parsimony to avoid overparametrization.

A new processor with uniformly improved performance is constructed at the cost of greater complexity; Valaee and Kabal [VK04] define the predictive description length (PDL) criterion as the length of a predictive code for the set of observations. It is com-

puted for the candidate models and is minimized over all models to select the best model and to determine the number of signals. Another group of methods is likelihood ratio test [Bar54] [Law56] [Gu98], which is performed by direct minimized KL of PDF of the model. It has been proved that a natural implementation of the information criterion is a more direct way of implementing the generalized likelihood ratio test with a specific threshold [SSL04]. Besides, an alternative Bayesian method is proposed by Djuric [Dju94] [Dju96].

By first considering the observation limitations, a test of determination the dimension of a signal subspace from short data records is explored by Shah and Tufts [ST94]. It is consisted of the interpretation of sum of squares of singular values as energy in a particular subspace. The constant false alarm rate thresholds are set up based on distributions derived from matrix perturbation ideas.

It is worth noting that a criterion based on eigenvalue ratios can be used to look for an eigenvalue gap between the noise and the signal eigenvalues [LR01]. As a following method, a test exploiting the exponential profile of the ordered noise eigenvalue, which is first introduced in [GLC96], is developed to estimate of the number of significant targets in time reversal imaging [QBL06]. Besides, for estimating the number of high-dimensional signals, a sample-eigenvalue-based procedure using relatively few samples is presented [NE08]. It could consistently detect the number of signals in white noise when the number of sensors is less than the number of signals.

Since a long duration of the received signal in the context of ocean acoustic tomography is unavailable, an exponential fitting test (EFT) using short-length samples is proposed to determine the number of raypaths in the following part, which would be considered robust and applicable. We define short-length samples as a concept that the number of samples equals the number of sensors. Most of parts presented in this chapter is based on our works in [JM11a] [JM11c] [JM11b]

This chapter is organized as follow: in Section A.7.1, the problem of detecting the number of raypaths is stated. Then, two information theoretic criteria are introduced as comparative methods in the Part A of Section 6.4. In the Part B of Section 6.4, the exponential fitting test is specifically developed. In order to illustrate its performance, the results of simulation are shown in Section A.7.3. Furthermore, the proposed test is applied to real data in Section 6.6, which is obtained in small scale environment. Considering the existence of colored noise, a whitening noise process is used as a preprocessing step. Section 6.7 provides the conclusion and future direction of research.

6.2 Demonstration on Importance of Detection of the Number of Raypaths

As shown by the experiment results we obtained in Chapter 5, smoothing-MUSICAL gets high resolution based on the prior knowledge of the number of raypaths. The survey of high-resolution methods also indicates that the model-order is necessary for subspace-based methods to acquire correct separation results. Before trying to find a theoretical solution, we give an example (Fig. 6.1. a, b, c) to show how the number of raypaths directly influences the separation results in smoothing-MUSICAL. In this sense, our study gives contributions to improve the environmental estimates in acoustic tomography. Besides, the correct knowledge of the number of raypaths is also helpful for all the separation algorithms to know whether there exist raypaths which are still not separated.

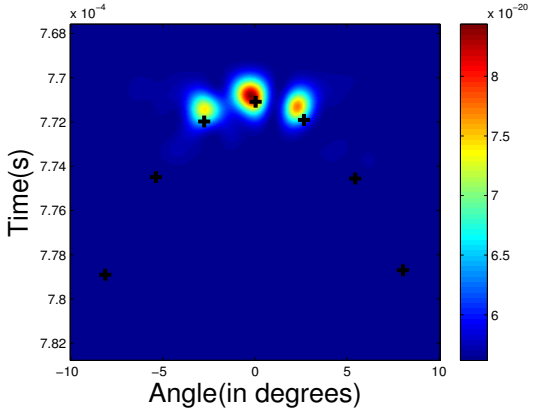

(a) $p = 3$

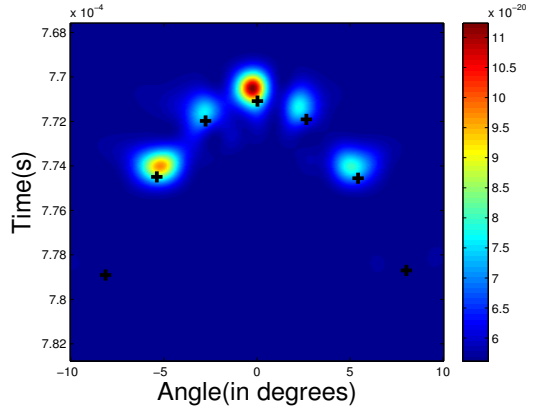

(b) $p = 5$

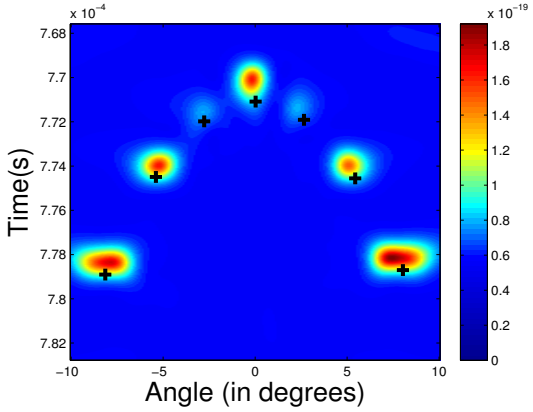

(c) $p = 7$

Figure 6.1: An experimental example of which the real number of raypaths equals 7 (a) Separation results using smoothing-MUSICAL with $P = 3$. (b) Separation results using smoothing-MUSICAL with $P = 5$. (c) Separation results using smoothing-MUSICAL with $P = 7$.

6.3 Problem of Detection of Number of Raypaths

To analyze the problem of detection of number of raypaths efficiently, the suitable model should be built first. In this chapter, the model is built on an acoustic field composed of P raypaths on a vertical array of M sensors ($P < M$). The temporal signal received on sensors is modeled as:

$$\mathbf{x}(t) = \mathbf{y}(t) + \mathbf{n}(t) = \mathbf{A}s(t) + \mathbf{n}(t) = \sum_{j=1}^{P} \mathbf{a}(\theta_j)s(t) + \mathbf{n}(t) \tag{6.1}$$

With:

- $\mathbf{x}(t)$: a $M \times 1$ observation vector. The ith component is the received signal on the ith sensor.
- $\mathbf{n}(t)$: additive white Gaussian noise of size $M \times 1$ with distribution $\mathcal{N}(0, \sigma_n^2\mathbf{I})$, which is assumed to be uncorrelated with the signals.
- $\mathbf{y}(t)$: the noiseless observation vector of size $M \times 1$, which spans the signal space generated by the steering vectors.
- $\mathbf{A}$: the matrix of the P steering vectors. Each steering vector $\mathbf{a}(\theta_j)$ for the j th raypath is generally characterized by the parameters of arrival angles θ_j.
- $s(t)$: the emitted signal.

Based on equation (A.17), the observation covariance matrix $\mathbf{R}$ is written as:

$$\mathbf{R} = E[\mathbf{x}(t)\mathbf{x}^*(t)] = \mathbf{R}_y + \mathbf{R}_n = \mathbf{A}\mathbf{\Lambda}_s\mathbf{A}^* + \sigma_n^2\mathbf{I} \tag{6.2}$$

With

- $\mathbf{R}_y$ is the covariance matrix of $\mathbf{y}(t)$.
- $\mathbf{R}_n$ is the noise covariance matrix.
- $\mathbf{\Lambda}_s$ is the covariance matrix of $s(t)$ and $*$ denotes the conjugate transpose.

The matrix $\mathbf{A}$ is assumed that it is of full column rank and $\mathbf{\Lambda}_s$ is nonsingular. The rank of $\mathbf{R}_y$ equals to the number of raypaths P. That is, there exists P nonzero eigenvalues corresponding to raypaths. Equivalently, the smallest $M - P$ eigenvalues of $\mathbf{R}_y$ are

equal to zero. Therefore, if the eigenvalues of $\mathbf{R}$ is arranged in a descending order as $\lambda_1 \geq \lambda_2 \cdots \geq \lambda_P$, the value of the smallest $M - P$ eigenvalues corresponding to noise is:

$$\lambda_{P+1} = \lambda_{P+2} = \cdots = \lambda_M = \sigma_n^2 \tag{6.3}$$

Hence, it is not difficult to determine P from the multiplicity of the smallest eigenvalue of $\mathbf{R}$. But in practice $\mathbf{R}$ is unknown. It is generally estimated by sample covariance matrix:

$$\hat{\mathbf{R}} = \frac{1}{N} \sum_{t=1}^{N} \mathbf{x}(t)\mathbf{x}^*(t) \tag{6.4}$$

Where N is the number of samples. Because $\hat{\mathbf{R}}$ is computed from a finite number of samples, the smallest $M - P$ eigenvalue is no longer equal to each other and σ_n^2 with probability one. Thus, in most cases the number of raypaths can't be determined directly by the above method.

6.4 Techniques for detection of the number of Raypaths

6.4.1 Information Theoretic Criteria

As noted in Section 6.1, several methods are studied for correct detection of the number of signals. It is known that two commonly suggested methods, an information theoretic criterion suggested by Akaike (AIC) [Aka73] [Aka74], and the minimum description length (MDL) proposed by Schwartz [Sch78] and Rissanen [Ris78], can be used for model selection. Wax and Kailath [WK85b] take the detection problem as a model selection problem and propose the following formulas for the detection of the number of signals received by a sensor array:

6.4.1.1 AIC

$$\begin{aligned} \hat{p} = arg \ \ & min_{k \in 0,1,\ldots,M-1} \\ & \left\{ -log(\tfrac{g(k)}{a(k)})^{N(M-k)} + k(2M-k) \right\} \end{aligned} \tag{6.5}$$

The first term in the bracket is computed from the log-likelihood of the maximum likelihood estimator of the parameters of the model. The second term is a bias correction term to make AIC be an unbiased estimate of the mean Kulback-liebler distance between the modeled density and the estimated density. $a(k)$ and $g(k)$ are respectively the geometric mean and arithmetic mean of the smallest $M - k$ eigenvalues, which are

denoted by (6.6) and (6.7). k is the number of free parameters that specifies a family of probability density functions, and $(\widehat{\lambda}_1 \geq \widehat{\lambda}_2 \cdots \geq \widehat{\lambda}_M)$ are eigenvalues generated by sample covariance matrix $\hat{\mathbf{R}}$ in (A.20). The number of raypaths $\widehat{p}$ can be estimated as the value of $k \in 0, 1, ..., p-1$ for which AIC is minimized.

$$a(k) = \frac{1}{M-k} \sum_{i=k+1}^{M} \widehat{\lambda}_i \tag{6.6}$$

$$g(k) = (\prod_{i=k+1}^{M} \widehat{\lambda}_i)^{\frac{1}{M-k}} \tag{6.7}$$

6.4.1.2 MDL

Although Schwartz [Sch78] and Rissanen [Ris78] solve the order selection problem respectively based on Bayesian and information theoretic arguments, it is highlighted that in the large-sample limit both methods get the same formulation. (6.8) is quite similar to the formulation of AIC except that the correction term is multiplied by $\frac{1}{2}logN$. MDL is also performed by a recursive process for $k \in 0, 1, ..., p-1$. The k which leads to the minimum MDL value is taken as the estimated number of raypaths p.

$$\begin{aligned} \widehat{p} = arg \ \ & min_{k \in 0,1,...,M-1} \\ & \left\{ -log(\tfrac{g(k)}{a(k)})^{N(M-k)} + \tfrac{1}{2}k(2M-k)logN \right\} \end{aligned} \tag{6.8}$$

With regard to the performance of these two methods, the MDL criterion is asymptotically consistent, whereas the AIC tends to overestimate [WK85b]. Actually, they have the same problem as we estimate the sample covariance matrix $\hat{\mathbf{R}}$ directly: the number of samples is finite in practice.

6.4.2 EFT

It is necessary to propose a method which considers the limitation of number of samples in view of practical limitations. For this reason, a test using an analytic expression of the ordered noise eigenvalues profile is introduced in this section.

6.4.2.1 Eigenvalue Profile Under Noise Only Assumption

To establish the mean profile of the decreasing noise eigenvalues, we need to calculate the expectation of each eigenvalue. For the zero-mean white Gaussian noise with power

σ_n^2, the sample covariance matrix has a Wishart distribution with N degrees of freedom. It is a multivariate generalization of χ^2 distribution and depends on M, N, σ_n^2. In this case, the joint probability of the ordered eigenvalues and the distribution of each eigenvalue can be obtained [Joh] [KS74]. The joint probability of the ordered eigenvalues is shown by (6.9). The distributions of each eigenvalue is given as zonal polynomial, which is a multivariate symmetric homogeneous polynomial and a fundamental tool in statistics and multivariate analysis [Jam60] [Jam61] as well as in the random matrix theory [Mui82]. However, calculating the expectation of each eigenvalue from the joint probability shown by (6.9) and the distribution of each eigenvalue using zonal polynomials are computationally unwieldy and gives intractable results for the moment.

$$\rho(\lambda_1, \ldots, \lambda_M) = \alpha \; exp\left(-\frac{1}{2\sigma^2}\sum_{i=1}^{M}\lambda_i\right)\left(\prod_{i=1}^{M}\lambda_i\right)^{\frac{1}{2}(N-M-1)}\prod_{i>j}(\lambda_j - \lambda_i) \tag{6.9}$$

As a result, we use an alternative approach to approximate the mean profile of ordered noise eigenvalue with the help of first and second order moments of the eigenvalues.

From simulation results, it turns out that an exponential law could be a good approximation to the mean profile of ordered noise eigenvalues. One result as an illustration for $M = 15$ is shown in Fig. 6.2. Fig. 6.2 (a) and Fig. 6.2. (b) show eight realizations respectively for the cases of $N = 15$ and $N = 1025$. Mathematically, the exponential law can be defined as (6.10) with two unknown parameters λ_1 and r.

$$\lambda_i = \lambda_1 r_e^{i-1}, \quad i \in 2, \ldots M \tag{6.10}$$

To determine λ_1 and r_e, we consider the first and second moments of the trace of the error of the noise covariance matrix $\mathbf{\Psi}$, where $\mathbf{\Psi}$ is defined by (6.11).

$$\mathbf{\Psi} = \hat{\mathbf{R}}_n - \mathbf{R}_n = \hat{\mathbf{R}}_n - \sigma_n^2\mathbf{I} \tag{6.11}$$

Given that $E(tr[\mathbf{\Psi}_{ij}]) = 0$, (6.12) is obtained:

$$M\sigma^2 = \sum_{i=1}^{M}\lambda_i \tag{6.12}$$

According to the definition of the error covariance matrix, the element Ψ_{ij} of $\mathbf{\Psi}$ is

expressed as:

$$\Psi_{ij} = \frac{1}{N}\sum_{t=1}^{N} n_i(t)n_j^*(t) - \sigma_n^2\delta_{ij} \tag{6.13}$$

Consequently, $E[\|\Psi_{ij}\|^2]$ can be computed as follows:

$$\begin{aligned} E\left[\|\Psi_{ij}\|^2\right] &= E\left[\left\|\frac{1}{N}\sum_{t=1}^{N} n_i(t)n_j^*(t) - \sigma_n^2\delta_{ij}\right\|^2\right] \\ &= E\left[\left\|\frac{1}{N}\sum_{t=1}^{N} n_i(t)n_j^*(t)\right\|^2\right] + E\left[\|\sigma_n^2\delta_{ij}\|^2\right] \\ &\quad + E\left[-2\Re\left\{\sigma_n^2\delta_{ij}\frac{1}{N}\sum_{t=1}^{N} n_i(t)n_j^*(t)\right\}\right] \end{aligned} \tag{6.14}$$

Where $\Re$ represents the real part of a complex value. Each term in (6.14) can be computed respectively:

$$\begin{aligned} E\left[\left\|\frac{1}{N}\sum_{t=1}^{N} n_i(t)n_j^*(t)\right\|^2\right] &= \frac{1}{N^2}N\sigma^4 = \frac{1}{N}\sigma_n^4 \\ E\left[\|\sigma_n^2\delta_{ij}\|^2\right] &= \sigma_n^4\delta_{ij} \\ E\left[-2\Re\left\{\sigma_n^2\delta_{ij}\frac{1}{N}\sum_{t=1}^{N} n_i(t)n_j^*(t)\right\}\right] & \\ = -\frac{2\sigma_n^2\delta_{ij}}{N}E\left[\Re\left\{\sum_{t=1}^{N} n_i(t)n_j^*(t)\right\}\right] & \\ = -\frac{2\sigma_n^2\delta_{ij}}{N}\left(\frac{N\sigma_n^2}{2}\right) = -\sigma_n^4\delta_{ij} & \end{aligned} \tag{6.15}$$

Finally,

$$E\left[\|\Psi_{ij}\|^2\right] = \frac{1}{N}\sigma_n^4 + \sigma_n^4\delta_{ij} - \sigma_n^4\delta_{ij} = \frac{1}{N}\sigma^4 \tag{6.16}$$

Since the trace of a matrix remains unchanged when the base changes, it follows that:

$$\sum_{i,j} E\left\{\|\Psi_{ij}\|^2\right\} = E(tr[\hat{\mathbf{R}}_n - \mathbf{R}_n]^2) = M^2\frac{\sigma_n^4}{N} \tag{6.17}$$

and using an approximation,

$$M^2\frac{\sigma_n^4}{N} = \sum_{i=1}^{M}(\lambda_i - \sigma_n^2)^2 \tag{6.18}$$

By combining of (6.10) and (6.12), we obtain:

$$M\sigma_n^2 = \sum_{i=1}^{M} \lambda_1 r_e^{i-1} \tag{6.19}$$

$$\lambda_1 = MJ_M\sigma_n^2 \tag{6.20}$$

where:

$$J_M = \frac{1 - r_e}{1 - r_e^M} \tag{6.21}$$

and it can obtain that:

$$(\lambda_i - \sigma_n^2) = (MJr_e^{i-1} - 1)\sigma_n^2 \tag{6.22}$$

By combining (A.34) with (6.18), the decay rate r_e is obtained from the following equation:

$$\frac{M+N}{MN} = \frac{(1-r_e)(1+r_e^M)}{(1-r_e^M)(1+r_e)} \tag{6.23}$$

In (6.10), r should be an exponential function. In this work, we assume that it is equal to $e^{-2a_{id}}$ based on two reasons. One reason is that the shape of $e^{-2a_{id}}$ is similar to the profile of ordered noise of assumption of short length (Fig. 1. (a)). The other reason is that it is easier to acquire the value of a_{id} through (21) thanks to even index. By substituting $r_e = e^{-2a_{id}}$, (6.23) becomes:

$$\frac{Mtanh(a_{id}) - tanh(a_{id})}{Mtanh(Ma_{id})} = \frac{1}{N} \tag{6.24}$$

where tanh is the hyperbolic tangent function, given by:

$$tanh(a_{id}) = \frac{\sinh(a_{id})}{\cosh(a_{id})} = \frac{e^{2a_{id}} - 1}{e^{2a_{id}} + 1} \tag{6.25}$$

The 4th order Taylor series expression of tanh(a) is written as follow,

$$tanh(a_{id}) = a_{id} - \frac{a_{id}^3}{3} + \frac{2a_{id}^5}{15} \tag{6.26}$$

Inserting (6.26) to (6.24), the following biquadratic equation is produced as:

$$\sigma^4 - \frac{15}{M^2+2}a_{id}^2 + \frac{45M^2}{N(M^2+1)(M^2+2)} = 0 \tag{6.27}$$

The positive solution of (6.27) is given by:

$$a_{id}(M,N) = \sqrt{\frac{15}{2(M^2+2)}\left[1 - \sqrt{\frac{4M(M^2+2)}{5N(M^2-1)}}\right]} \tag{6.28}$$

6.4.2.2 Principle of the Recursive EFT

With the assumption of P decorrelated or partly correlated raypaths, the recursive EFT is mainly based on the comparison between the profile of ordered eigenvalues of the observation covariance matrix and the theoretical profile of the ordered noise eigenvalues. A break point occurs when signal eigenvalue appears. The general test strategy is demonstrated by Fig. 6.3. In Fig. 6.3. , two eigenvalues corresponding to raypaths are contained in the profile of observable eigenvalues. When the eigenvalue corresponding to raypath appears, a gap makes the profile of recorded eigenvalue break from the EFT profile.

The recursive test is started from $P_t = 1$. Assuming the P_t smallest eigenvalues are noise eigenvalues, the previous eigenvalue λ_{M-P_t} is tested to determine if it corresponds to noise or a raypath. For each value of P_t, the test is performed by two steps:

In the first step, we predict the value of λ_{M-P_t} according to exponential model ((6.20)):

$$\hat{\lambda}_{M-P_t} = (P_t + 1) J_{P_t+1} \hat{\sigma_n}^2 \tag{6.29}$$

where:

$$J_{P_t+1} = \frac{1 - r_{P_t+1}}{1 - r_{P_t+1}^{P_t+1}} \tag{6.30}$$

$$\hat{\sigma}_n^2 = \frac{1}{P_t + 1} \sum_{i=0}^{P_t} \lambda_i \tag{6.31}$$

The prediction equation is obtained by combination of (6.29), (6.30) and (6.31):

$$\hat{\lambda}_{M-P_t} = J_{P_t+1} \sum_{i=0}^{P_t} \lambda_{M-i} \tag{6.32}$$

r_{P+1} is calculated by first getting a using (6.28) and then using the relationship $r = e^{-2a_{in}}$, where $(P_t + 1)$ should be used instead of M.

In the second step, two hypotheses are defined as follows:

- H_{P_t+1}: λ_{M-P_t} is an eigenvalue corresponding to noise.
- $\overline{H}_{P_t+1}$: λ_{M-P_t} is an eigenvalue corresponding to a raypath.

To decide between these hypotheses, the absolute error of λ_{M-P_t} and $\hat{\lambda}_{M-P_t}$ is calculated and then be compared with a threshold η_{P_t}. That is:

$$H_{P_t+1} : \left| \lambda_{M-P_t} - \hat{\lambda}_{M-P_t} \right| \leq \eta_{P_t} \tag{6.33}$$

$$\overline{H}_{P_t+1} : \left|\lambda_{M-P_t} - \hat{\lambda}_{M-P_t}\right| > \eta_{P_t} \tag{6.34}$$

If the absolute error of a certain value P is smaller than the related threshold, reset $P_t = P_t + 1$ and the test is repeated until $P_t = M - 1$; Otherwise, the recursive process is stopped with the detection result of $P = M - P_t$. Finally, we use the empirical distribution of the noise-only eigenvalue profile to find a suitable threshold. For instance, 10000 realizations are generated for $N = 15$ samples as well as an array of $M = 15$ sensors. The mean profile of ordered noise eigenvalue is computed, which is represented by the middle curve in Fig. 6.2. (a). Only eight realizations are displayed for clarity explanation. For each eigen index, there exists upper and lower noise eigenvalues. Half of the distance between them for eigen index P_t could be taken as the threshold η_{P_t}.

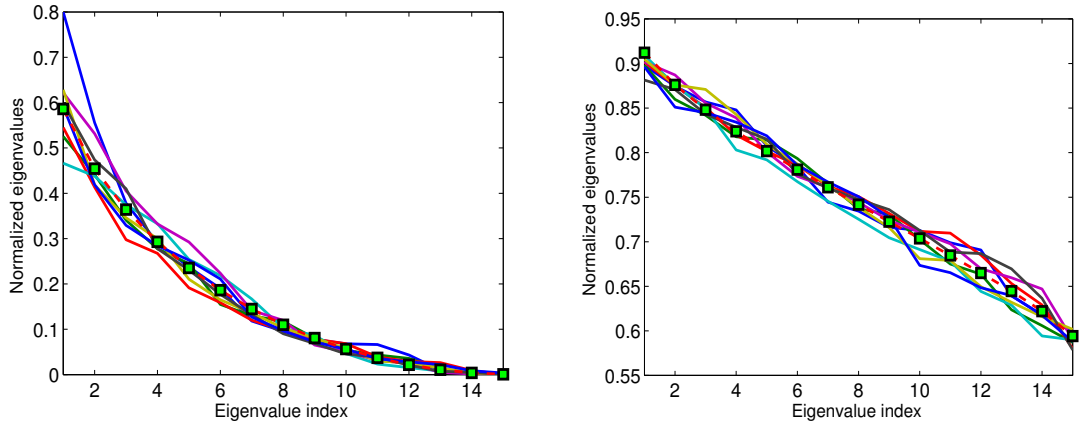

(a) (b)

Figure 6.2: Profile of ordered noise eigenvalues for eight realizations (a) Profile of ordered noise eigenvalues estimated by 15 samples. (b) Profile of ordered noise eigenvalues estimated by 1025 samples.

6.5 Simulations

In this section, we illustrate the performance of EFT with simulation data. The simulation is composed by two groups of experiments. In the first group, we test the general performance of EFT in various SNR. In the second group, the performance of EFT is addressed when the raypaths arrive very closely.

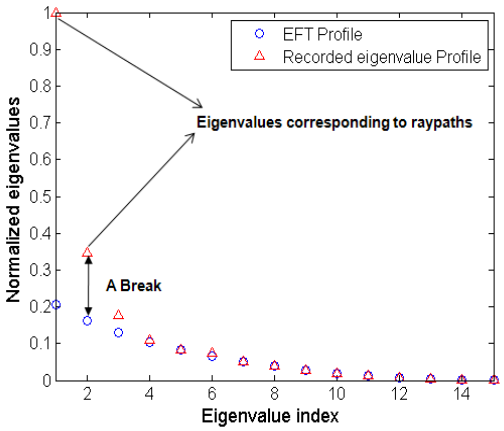

Figure 6.3: Profiles of eigenvalue with two eigenvalues corresponding to raypaths. When the eigenvalue corresponding to raypath appears, a break exists between the profile of EFT and the profile of recorded eigenvalues.

6.5.1 Performance in various SNR

For various SNR and different number of samples, six experiments are realized in the first group of experiments. In these experiments, five coherent raypaths arrive on 15 sensors. As the noise is added to raypaths, they could be considered as being partly correlated. As an illustration, two figures (Fig. 6.4 and Fig. 6.5) respectively plot the received raypaths and ordered eigenvalues profile for a specific SNR and number of samples. These eigenvalues are normalized by the largest one in each case. As comparative methods, AIC and MDL are also applied to these experiments. Considering the asymptotically consistent property of AIC and MDL, we chose $N = 1025$, which is much larger than the number of sensors. In this case, AIC and MDL still overestimate the number of rayspaths. The possibility of overestimation or underestimation mainly depends on the distribution of dispersed eigenvalues. It obeys the qualitative results in [LR01]. For fixed number of samples, over-modeling becomes more likely for increasing the noise eigenvalue dispersion. For fixed dispersion, over-modeling becomes more likely for increasing the number of data samples. Under-modeling may happen in cases where the signal eigenvalues are not well separated from the noise eigenvalues and the noise eigenvalues are clustered sufficiently closely. The results are shown in Table 6.5.1. The detection results for the case of $N = 15$ imply that EFT could detect relatively correctly for moderate or high SNR. For the example of SNR= 5dB, because of the correlation between raypaths and noise, EFT tends to overestimate. Obviously, AIC and MDL can not correctly detect the number of raypaths for short-length samples on account of asymptotically consistent performance.

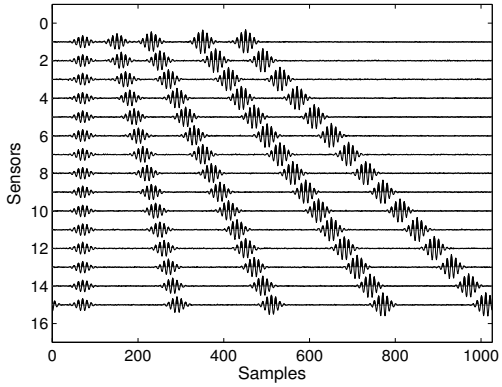

(a)

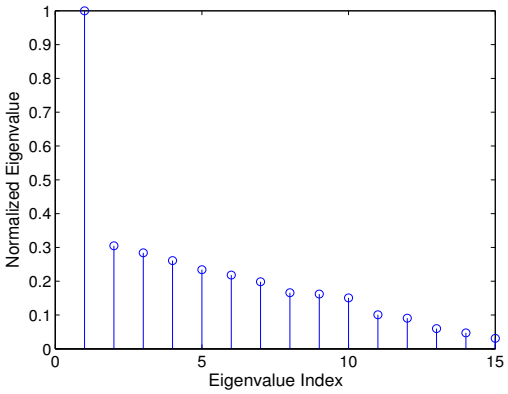

(b)

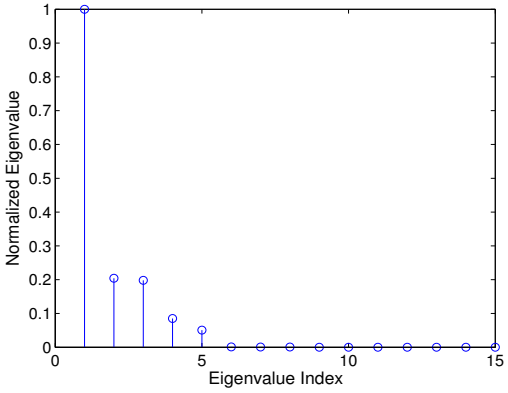

(c)

Figure 6.4: Profile of ordered eigenvalues in the first group of experiments when SNR = 20dB (a) the received signals on 15 sensors. (b) Profile of ordered eigenvalues estimated by 1025 samples. (c) Profile of ordered eigenvalues estimated by 15 samples.

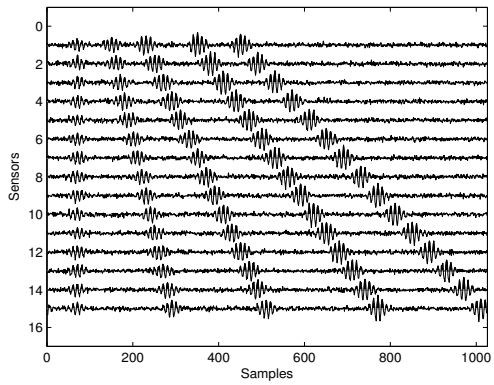

(a)

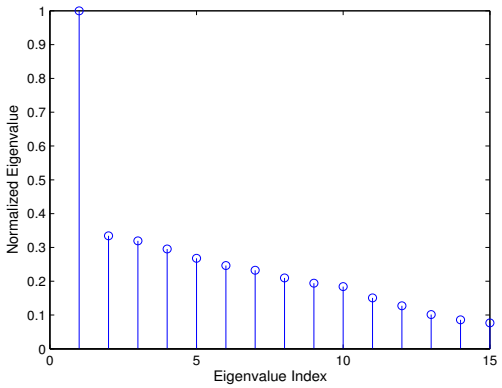

(b)

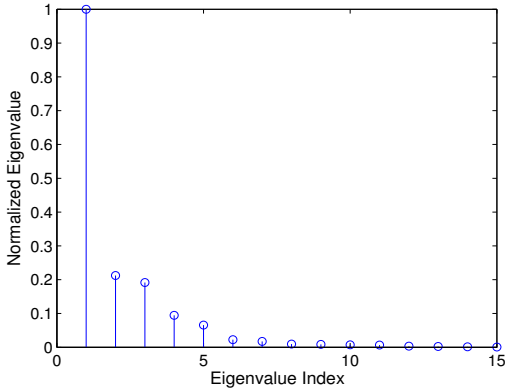

(c)

Figure 6.5: Profile of ordered eigenvalues in the first group of experiments when SNR = 5 dB (a) the received signals on 15 sensors. (b) Profile of ordered eigenvalues estimated by 1025 samples. (c) Profile of ordered eigenvalues estimated by 15 samples.

	SNR (dB)	AIC	MDL	EFT
$N = 1025$	20	14	14	—
	10	14	14	—
	5	14	12	—
$N = 15$	20	—	—	5
	10	—	—	5
	5	—	—	11

Table 6.1: Number of raypaths detected by AIC, MDL and EFT in the first group of experiments (the real number of raypaths $P = 5$)

6.5.2 Performance for close raypaths

To deeply illustrate the performance of our algorithm when raypaths arrive more closely, two experiments (SNR= 20dB) for $N = 1025$ and $N = 15$ are performed. In these experiments, the difference is not only the first two raypaths are more closer than the examples in the first group of experiments but also the third raypath crosses the first two because of the negative arrival angle (shown in Fig. 6.6 (a).). The detection results are shown in Table 6.5.2. EFT still detects correctly while AIC and MDL overestimate caused by the same reason in the discussion in Section 6.5.1. Fig. 6.6 (b) and Fig. 6.6 (c) illustrate the profiles of ordered eigenvalue for respectively $N = 1025$ and $N = 15$.

	SNR (dB)	AIC	MDL	EFT
$N = 1025$	20	14	14	—
$N = 15$	20	—	—	5

Table 6.2: Number of raypaths detected by AIC, MDL and EFT in the second group of experiments (the real number of raypaths $P = 5$)

6.6 Small-Scale Experiment

6.6.1 Noise-whitening process

As noted before, EFT is based on the assumption of white Gaussian noise. Conversely, in practical environment there exists colored noise. The interference of colored noise could be reduced if a noise-whitening process is included. Several methods can be used to estimate the noise covariance matrix. Here, we only discuss the residual analysis method proposed by Roger [Rog96]. The noise estimation is made simply through the inverse of its covariance matrix, which is first used to modify principal components transform with noise adjustment [Rog96] [RA96]. Then, Noise Subspace Projection (NSP) based on the residual method is developed respectively to estimate number of hidden nodes for

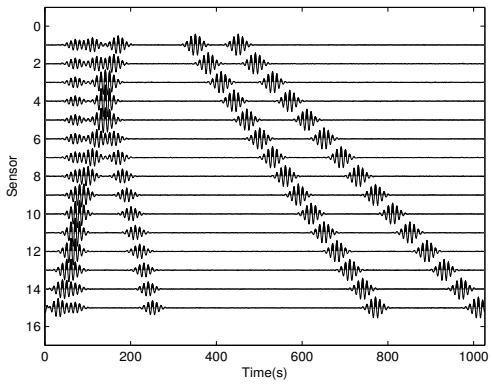

(a)

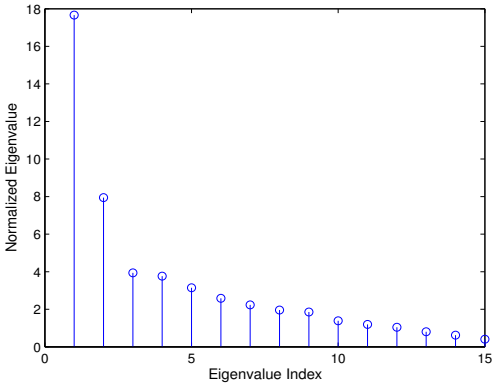

(b)

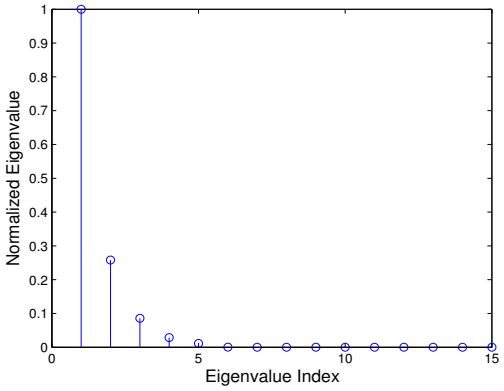

(c)

Figure 6.6: Profile of ordered eigenvalues in the second group of experiments when SNR = 20dB (a) the received signals on 15 sensors. (b) Profile of ordered eigenvalues estimated by 1025 samples. (c) Profile of ordered eigenvalues estimated by 15 samples.

a radial basis function neural network [DC99] and to determinate the intrinsic dimensionality of hyperspectral imagery [CD04].

Exploiting the signal model in Section 6.3, the observation covariance matrix $\mathbf{R}$ is decomposed as:

$$\mathbf{R} = \mathbf{D}_R \mathbf{E}_R \mathbf{D}_R \tag{6.35}$$

where $\mathbf{D}_R$ is a diagonal matrix of standard deviations and is given by $\mathbf{D}_R = diag\{\sigma_1, \sigma_2, \ldots, \sigma_M\}$ with $\{\sigma_l^2\}_{m=l}^{M}$ being diagonal elements of $\mathbf{R}$, and $\mathbf{E}_R$, which is represented by (6.36), has 1 on its principal diagonal and its other terms are the correlation coefficients between sensors.

$$\mathbf{E}_R = \begin{pmatrix} 1 & \rho_{12} & \rho_{13} & \cdots & \rho_{1M} \\ \rho_{21} & 1 & \rho_{23} & \cdots & \rho_{2M} \\ \rho_{31} & \rho_{32} & \ddots & \ddots & \vdots \\ \vdots & \vdots & \ddots & \ddots & \rho_{(M-1)M} \\ \rho_{M1} & \rho_{M2} & \cdots & \rho_{M(M-1)} & 1 \end{pmatrix} \tag{6.36}$$

Specifically, $\rho_{p,q}$ being the correlation coefficient at the (p,q)th entry of $\mathbf{R}$ and $p \neq q$.

In analogy with (6.35), the similar decomposition of inverse matrix of $\mathbf{R}$ can be obtained as follows:

$$\mathbf{R}^{-1} = \mathbf{D}_{R^{-1}} \mathbf{E}_{R^{-1}} \mathbf{D}_{R^{-1}} \tag{6.37}$$

where $\mathbf{D}_{R^{-1}}$ is a diagonal matrix given by $\mathbf{D}_{R^{-1}} = diag\{\varsigma_1, \varsigma_2, \cdots, \varsigma_M\}$ with $\{\varsigma_l^2\}_{m=1}^{M}$ being the values in the diagonal of $\mathbf{R}^{-1}$ and

$$\mathbf{E}_{R^{-1}} = \begin{pmatrix} 1 & \xi_{12} & \xi_{13} & \cdots & \xi_{1M} \\ \xi_{21} & 1 & \xi_{23} & \cdots & \xi_{2M} \\ \xi_{31} & \xi_{32} & \ddots & \ddots & \vdots \\ \vdots & \vdots & \ddots & \ddots & \xi_{(M-1)M} \\ \xi_{M1} & \xi_{M2} & \cdots & \xi_{M(M-1)} & 1 \end{pmatrix} \tag{6.38}$$

with $\xi_{p,q}$ being the correlation coefficient at the (p,q)th entry of $\mathbf{R}^{-1}$ and $p \neq q$. Referring to statistic theory and multiple linear regression [Ksh72] [Har01], the degree of correlation of received signal of the mth sensor on the other $M-1$ sensor can be described by the multiple correlation coefficient r_{M-m}^2. This linear relation explains the r_{M-m}^2 proportion of received signal is the variance corresponding to raypaths. The residual variance equals $\sigma_m^2(1 - r_{M-m}^2)$. Further, it turns out that [Ksh72] [Har01] the ς_m is

the reciprocal of the residual standard deviation. Thus, (6.39) is obtained:

$$\varsigma_m = \sigma_m^{-1}(1 - r_{M-m}^2)^{-\frac{1}{2}} = \frac{1}{\sqrt{\sigma_m^2(1 - r_{M-m}^2)}} \tag{6.39}$$

The major advantage of using ς_m over σ_m is that ς_m removes its correlation on other ς_k for $k \neq m$. Therefore, the noise covariance matrix $\mathbf{R}_n$ can be estimated by: $\mathbf{R}_n = diag\left\{1/\varsigma_1^2, 1/\varsigma_2^2, \ldots, 1/\varsigma_M^2\right\}$.

Based on the above discussion, the sample covariance matrix $\mathbf{R}$ can be whitened using the estimated noise covariance $\mathbf{R}_n$:

$$\mathbf{R}_w = \mathbf{R}_n^{-1/2}\mathbf{R}\mathbf{R}_n^{-1/2} \tag{6.40}$$

6.6.2 Small-Scale Experiment

A small-scale experiment is discussed in this part, so that we can further illustrate the performance of our methods. The experimental setup is diagramed as in Fig. 6.7. The principle on which these experiments are based is as follows: if the frequency of signals is multiplied by a factor and the spatial distances are divided by the same factor, the physical phenomena occurring in the environment remains the same. Namely, the small-scale experiment reproduces the actual physical phenomena occurring in nature in a smaller scale inside the laboratory. It achieves a reduced cost and a totally controlled experiment. The experiment presented here were performed at the ISTerre (Institut des Sciences de la Terre) in the ultrasonic tank which is developed by P. Roux. In this tank, a waveguide of 5-10 cm in depth and 1-1.5 m in length is constructed. A steel bar acts as the bottom, which is very reflective and perfectly flat. Particularly, a sensor is set at 0.0263m in depth range as the source. A vertical array composed of 64 sensors is used as a receiver. The depth of the first receiver is $3.55 \times 10^{-3}m$. The interval of two adjacent receivers is 0.75×10^{-3}m. The distance between the source and reference receiver is about 1.15 m and the source signal has 1 MHz frequency bandwidth a with central frequency of 1.2 MHz. Fig. 6.8 (a) shows that the first 5000 points in time domain of received signal with sampling frequency $F_e = 50MHz$.

In order to satisfy the criterion of short-length samples, 64 samples of recorded signal are chosen for analysis. In order to evaluate the effectiveness of EFT and NWEFT, the separation result of beamforming is provided in Fig. 6.8 (b). It matches by the theoretical locations denoted in the form of the crosses. The eigenvalue profile is shown by Fig. 6.8 (c). EFT detects 5 raypaths while the detection result of NWEFT is 6. Compared to the

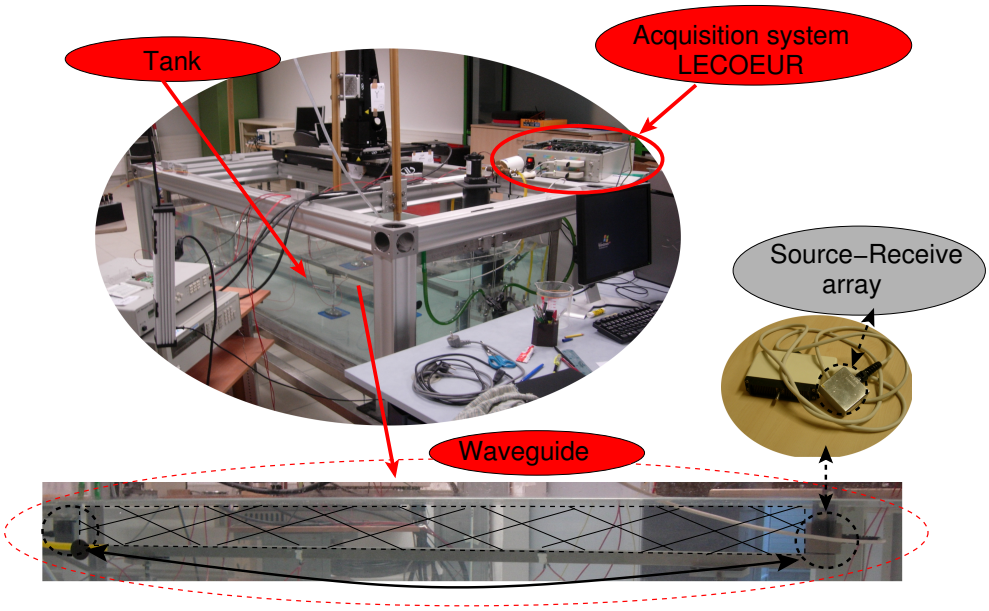

Figure 6.7: Experimental Setup of Small-scale Experiment in ISTerre

reference value 7 in Fig. 6.8 (b), these methods can be taken as being accepted. Based on the experiments, we can see that the overestimation caused by the correlation between the raypaths and noise, especially when the SNR is relatively low. Underestimation is caused by the correlation between raypaths.

6.7 Conclusion

In this chapter, a NWEFT method is proposed to automatically detect the number of raypaths in shallow-water waveguide. As AIC and MDL are confined by the duration of received signal, they fail in correctly detecting the number of raypaths. In contrast, the proposed method can determine the number of raypaths using short-length samples. Owing to the noise whitening process, it can be applied to the real application environment. In future, the detection method to consider the influence of correlation between raypaths as well as correlation between raypath and noise should be studied. Besides, this method can be extended to medium-length samples.

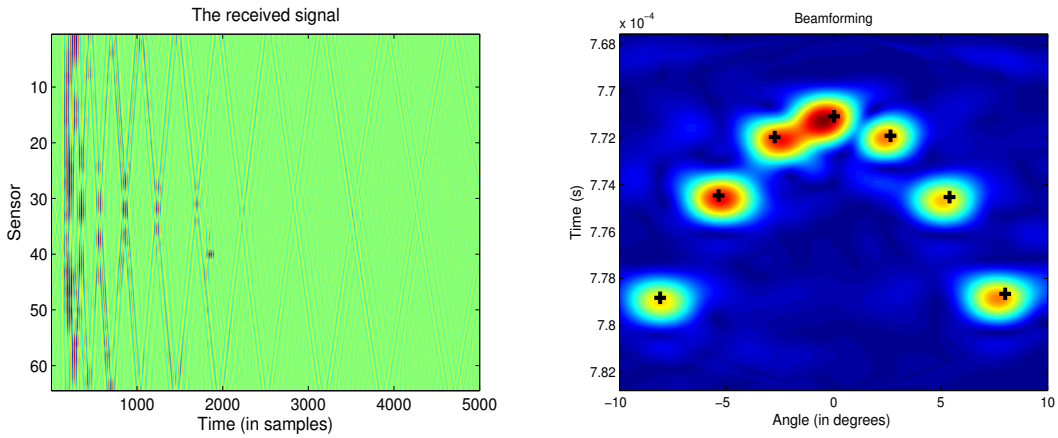

(a) (b)

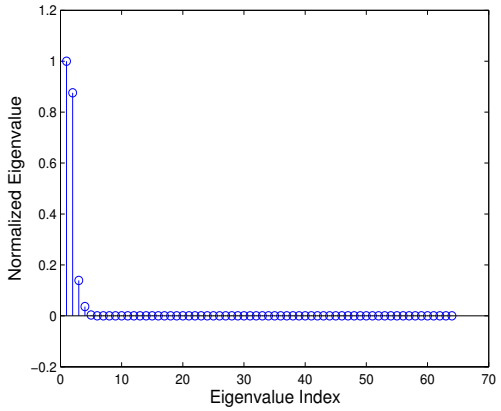

(c)

Figure 6.8: (a) The received signals on 64 sensors for 5000 samples. (b) Separation result of beamforming with theoretical location for 64 samples. It provides a reference value for checking the separation result of the proposed method. (c) Profile of ordered eigenvalues of 64 samples.

Chapter 7

Conclusion

Contents

7.1 **Summary of Contributions** 129

7.2 **Perspectives** 132

In this dissertation, we have presented our studies on the problem of source separation and detection (or source localization) in underwater acoustics, especially in the context of shallow-water OAT. Our main objective is to propose high-resolution processing method for raypath separation and detection in a more practical perspective, which means some practical limitations have been considered. In accordance with the investigation on the existing separation or localization methods in underwater acoustic and the survey on the high-resolution algorithms, we infer that subspace-based methods would be appropriately extended and applied to our application background. However, the coherent signals caused by multiple-paths propagation make subspace-based algorithms hardly possible to accurately separate them due to the rank deficiency of covariance matrix estimated from the received signals. Consequently, we accomplished the goal of separating coherent raypaths by presenting a smoothing-MUSICAL algorithm for high-resolution separation of coherent raypaths in Chapter 5. Additionally, its performance is illustrated by several simulations and an real experiment in a shallow-water waveguide. The correct detection of the number of raypaths is our secondary objective. Our attention for this problem was drawn from both the survey on existing high-resolution methods and the real difficulty we faced to in the process of studying on smoothing-MUSICAL algorithm. It turns out that selection of the model order is a common problem to all the subspace-based methods. The solution is achieved by proposing a noise-whitening fitting exponential test. Then, Its efficiency is tested on simulation data and real data.

All of contributions are summarized one by one as follows:

7.1 Summary of Contributions

Investigation on source separation (or localization) techniques in underwater acoustics

On the basis of briefly reviewing the well-known source separation (or localization) techniques in underwater acoustics, such as beamforming, matched-field processing, the time reversal mirror, etc, but also the novel and most interesting methods in recent publications, such as double-beamforming, a Gibbs sampler approach, etc, we divide these methods into two categories depending on whether they are under the assumption of the sound propagates in a homogenous space. Excepting the Gibbs sampler source-localization method, they are all beamforming-like methods and are connected by four key words: plane-wave, non-plane wave, point-array configuration and array-array configuration. For instance, matched-field processing is an extension of beaming for non-plane wave; double-beamforming is developed by using beamforming in a array-array

configuration to improve algorithm performance, which is in accord with the same theoretical basis – reciprocity property as time reversal mirror; If the ocean itself is used to construct the recipica field, the process of phase configuration is an implement ion of matched-field processing while the matched-field processing is a special case of time reversal morror in the configuration of point-array. Mathematically, they all use the 2-order statistic moments of the recorded signals. Resolution limitation still exists in these algorithms and the improvement of resolution is still a promising perspective for these methods. We hope that our attempt of global analysis on these methods can provide a brief guide for a first time exposure to an interested reader.

Survey on high-resolution methods

On the other hand, in signal processing domain high-resolution methods are introduced to improve the performance of classical beamforming-like method. In particular, the introduction of subspace-based methods gave a very important influence on not only theoretical study but also applications in corresponding to array processing. We first generally presented the existing techniques and noted them as an important represent for each technique type. The limitations and advantages of each method are discussed and compared. As a result of this survey, we found that there are several techniques which would be made adaptable to the context of shallow-water OAT so as to achieve the improvement of resolution. By combining the conclusion drawn from this survey and our application context, we finally specify our specific study topic of this dissertation. In a word, this global study, particularly on MUSIC-like method demonstrate us the encountered difficulties and the possible future study directions. We also hope that this work would be helpful to get an global acquaintance to the researcher in corresponding domain.

Proposal of a high-resolution processing for separating raypaths in a shallow-water waveguide

The coherent signals exists also in the context of shallow-water OAT as the multiple raypaths are produced by the same emitted signal through multiple-paths propagation. To deal with this difficulty as well as introduce a high-resolution processing, we combined spatial-frequency smoothing with MUSICAL algorithm and propose smoothing-MUSICAL algorithm for shallow water OAT. Particularly, we addressed the spatial smoothing, frequency-smoothing and spatial-frequency smoothing in the background of shallow-water OAT. Meanwhile MUSICAL was not only improved to be adaptable to the coherent raypaths by combing these smoothing methods as a preprocessing step but also was applied to the instance of shallow-water OAT. Through the results of simulations and real experiment in a tank, the proposed algorithm was examined. It displays

a better separation performance in terms of accuracy and the robust against noise. It accomplishes the separation with the instance of closely arrival raypaths whereas beamforming encounters difficulties. Besides, this is an important and initial attempt to ameliorate the separation performance by high-resolution techniques.

Presentation of a noise-whitening fitting exponential test for automatic detection the number of raypaths

As one of subspace-based methods, smoothing-MUSIAL successfully separates the raypaths on the basis of prior knowledge of raypath number. Besides, the correct information of raypath number itself can give a reference to check the separation performance of beamforming or other algorithms which can direct separate raypaths without such information. To overcome the shortcomings of classical information theory criteria, like the assumption of white-noise circumstance, asymptotically consistent, an EFT technique was developed only exploiting small-length sample. Moreover, we made it to be adaptable to color noise environment. We tested its performance with experiments. Although it performs well just in a high SNR instance, this is an effective attempt to find solution for this kind of problem.

7.2 Perspectives

Concerning perspectives, we would like to carry out them in terms of two aspects: 1) the improvement, extension or variation of the proposed algorithms in Chapter 5 and Chapter 6; 2) potential utilization of high-resolution methods in relevant applications of underwater acoustics.

Improvement of smoothing-MUSICAL according to error analysis

Indeed, in Chapter 5, we has drawn the conclusion from the experiments that smoothing-MUSICAL has largely improved the separation performance. However, As it is also shown by the experiment results, smoothing-MUSICAL still has some separation errors compared with theoretical location values. The reasons which cause these errors should be uncovered and analyzed. Several algorithms, like the method in [VS94] should be developed concerning these possible causes.

Multiple-dimensional smoothing-MUSICAL methods for shallow-water OAT

Inspired by the double-beamforming in [IRN*09], double-smoothing-MUSICAL type method would be extended to the array-array configuration in order to further improve resolution. The resolution should be also due to the novel discrimination term – emitted angle. Actrually, we has seen attempts on this in [LTNM*11]. They conclude that double-MUSICAL shows a better separation performance with more accurate values of the relevant parameters.

Higher-order high-resolution methods for applications in a waveguide

MUSICAL-4 type methods have been developed for non-gaussion signal process [Car89]. They have been applied in sonar, radar, seismic signal processing to overcome the drawbacks of algorithms based on 2-order statistic, such as a weak robustness to both modeling errors and the presence of a strong colored background noise whose spatial coherence is unknown, poor performance in the presence of several poorly angularly separated sources from a limited duration observation and the maximum of number of signals to be processed equal or larger than the number of sensors on an array. Deserved to be mentioned, MUSIC algorithm is recently extended to a $2-q$ order statistic [CFA06]. In this sense, the appropriate higher-order high-resolution algorithms should be considered and developed to the applications in a waveguide.

Travel time tomographic inversion employing high-resolution methods

We have addressed on analyzing and finding high-resolution of shallow-water OAT, so one of the following study direction is to combine these high-resolution methods with specific inversion methods like Bayesian approach should be explored and applied on experiment datas .

Improvement and extension of the proposed detection method

As we presented in Chapter 6, the proposed detection algorithm is still confined by the robustness to the noise and also the correlations existing between signals and noise. Thus, we ought to do some attempts concerning overcoming these drawbacks. Besides, the detection algorithm has the possibility to be extended to successfully detect the number of raypaths based on medium-length samples.

Source localization or geoacoustic using high-resolution methods

As we pointed out at the beginning of this dissertation, except tomography, numerous approaches to source localization, geoacoustic inversion rely on accurate raypath extraction with an array configuration [PC01] [PC01] [JCG08]. We can probably think about implementing this type of high-resolution methods on these applications as a result of the exsting connections.

Appendix A

Résumé en Français

A.1 Introduction

La tomographie acoustique océanique (TAO) consiste à utiliser les variations temporelles de la propagation du son dans l'océan pour en estimer les propriétés physiques telles que la température, la salinité ..... etc. Cette technique a d'abord été utilisée comme méthode de télédétection de l'océan à grande échelle et donc souvent sur des grandes profondeurs. Après la guerre froide, les études relatives aux eaux peu profondes sont devenues très attrayantes et primordiales pour les acousticiens, les océanographes..... etc. La tomographie acoustique océanique dans un guide d'onde en eau peu profonde donc à petite échelle, suit globalement le même processus que celui dédié aux eaux profondes. C'est à dire qu'il peut être décomposé en un problème direct et un problème inverse.

Comment définit-on le problème direct ? Mettons nous dans une configuration fréquentielle proche de la théorie des rayons. Le son va se propager dans l'océan par de multiples chemins ou trajets. Cette propriété va fournir un ensemble d'informations car chaque trajet va couvrir des parties différentes de l'océan. Toutefois, lorsque deux trajet sont proches, les paramètres, comme le temps de d'arrivée et/ou sa direction, ne peuvent pas être extraites directement et facilement à partir des signaux reçus. Pour cette raison, des techniques de traitement du signal sont explorées afin de séparer les trajets proches et ainsi d'extraire le plus d'information possible. Ceci sera identifié comme la résolution du probléme direct. L'efficacité du problème inverse est liée à la résolution du problème direct. Ainsi, l'amélioration de la performance du problème direct aura une grande importance pour obtenir un résultat d'inversion efficace pour la tomographie acoustique océanique. Il existe de nombreuses techniques en acoustique sous-marine,

dépendantes de la configuration de l'acquisition, pour extraire des trajets et localiser des sources. Même si la technique dite de la formation de voie est largement utilisé, il est encore tout à fait nécessaire de présenter des méthodes dite haute résolution pour extraire le plus efficacement possible des trajets. Bien que notre travail dans cette thèse se concentre principalement sur le problème direct de tomographie acoustique en eau peu profonde, il est possible d'étendre les méthodes haute résolution proposées même à d'autres applications similaires.

A.1.1 Objectifs

Sur la base de ce qui précède, nous voulons atteindre trois objectifs principaux dans cette thèse. Premièrement, nous présenterons une étude sur les techniques de traitement du signal existantes en acoustique sous-marine, en particulier pour les case de propagation en eaux peu profondes. Ensuite, un groupe de méthodes à haute résolution, sera proposé pour surmonter la limitation de la résolution spectrale des algorithmes classiquement utilisés et pour séparer les rayons cohérents dans un guide d'onde en eaux peu profondes. Par la suite, nous prêtons attention à l'une des limitations de la technique de sous-espace basée sur l'hypothèse de la connaissance au préalable de l'ordre du modèle. En conséquence, dans une troisièment partie, nous proposerons un test exponentiel d'estimation automatique du nombre de rayons fonctionnant sur un petit nombre d'échantillons. Une étape de traitement par blanchiment sera ajouté pour tenter de résoudre ce problème d'estimation de manière pratique en environnement peu profond.

A.1.2 Organisation du résumé

La section A.2 introduit d'abord les concepts de la tomographie acoustique océanique (TAO). Ensuite, l'environnement en eau peu profonde sera définie et nous présentons les principales caractéristiques d'un processus général de la TAO dans ce contexte. Un état de l'art sur des études récentes de l' TAO en eau peu profonde sera fourni.

En raison de la relation essentielle entre les méthodes existantes de traitement du signal acoustique en moins d'eau et le problème avant de l' TAO en eau peu profonde, une enquête sur ces méthodes est présentée dans la section A. 3.

Par conséquent, un examen complet de la méthode de résolution est décrite dans la section A. 4. Il est supposé que l'on peut trouver ou d'étendre certaines méthodes à haute résolution pour s'adapter à donner des solutions satisfaits dans le cadre du guide d'onde en eau peu profonde.

La section A. 5 présente un traitement à haute résolution appelée smoothing-MUSICAL pour tragets cohérentes.

Dans la section A. 6, nous proposons un noise-whitening exponential fitting test de détecter correctement le nombre des trajets dans un guide d'onde en eau peu profonde.

La section A. 7 résume la contribution des algorithmes proposés et tire des conclusions de ce manuscrit. Quelques travaux supplémentaires sont indiquées.

A.2 Connaissances de base sur la TAO

L'étude et l'analyse des propriétés physiques de l'océan se font essentiellement à l'aide de deux types de techniques. Premièrement, les mesures directes (in situ) des propriétés physiques telles que la conductivité, la température ou la densité de la colonne d'eau sont disponibles par l'intermèdiare de sondeurs. Ces instruments permettent de disposer d'informations directes sur les milieux, mais ils présentent d'importantes limitations d'utilisation en raison d'un échantillonnage spatial très limité par rapport à la taille des phénomènes physiques qui doivent être étudiés. Par ailleurs, il existe des techniques d'investigation qui consistent à propager une onde dans le milieu marin, pour approcher les propriétés physiques de l'interaction entre le milieu et cette onde. Ces techniques auront un meilleur espace d'échantillonnage, mais leur fiabilité est souvent plus faibles comparée aux mesures directes. En conséquence et lié à cette technique d'investigation, le concept de tomographie acoustique océanique (OAT en anglais pour Ocean Acoustic Tomography) a été proposé en 1979 par W. Munk et C. Wunsch [MW79] [MWW95] comme l'une des techniques indirectes importantes pour l'étude des propriétés physiques des océans. Elle est analogue à la tomographie par rayons X mais pour des océans.

A.2.1 Fondamentaux de l'acoustique océanique

Très tot, il a été souligné que l'océan pouvait être considéré comme un guide d'onde acoustique, c'est à dire limité en haut par la surface de la mer et en bas par le plancher océanique. La vitesse du son est une donnée importante pour l'ètude des océans. Globalement elle est proche de 1500 m/s et augmente avec la profondeur. Mais en dètail, on peut exprimer la dépendance de la vitesse du son en fonction de trois variables indépendantes [Bae81] (équation A.1) :

$$c = 1449.2 + 4.6T - 0.055T^2 + 0.00029T^3 + (1.34 - 0.01T)(S - 35) + 0.016z \qquad \text{(A.1)}$$

- c est la vitesse du son en mètres par seconde.
- T représente la température en degrés centigrades.
- S exprime la salinité en partie par millier.
- z est la profondeur en mètres.

A.2.2 Modèles de propagation du son

Pour pourvoir exprimer et faire des simulations, il est utile d'aborder le problème de la résolution de l'équation d'ondes. Cette équation d'onde permet de décrire la propagation du son dans l'eau. Concrètement, elle est obtenue à partir des équations de l'hydrodynamique, de ses coefficients et des conditions aux limites. Les solutions informatiques proposées [JKP*95] sont appelés modèles de propagation du son. Elles sont élaborées pour décrire la propagation du son dans la mer par une simulation informatique. Normalement, il y a quatre types de modèles de propagation du son : la théorie des rayons, la théorie par méthode spectrale (FFP), la théorie des modes normaux (NM) et la théorie par équation parabolique (PE). Le choix d'un modèles de propagation du son est dépendante de la valeur des fréquences propagées dans le milieu. Si les fréquences sont de l'ordre de quelques kHz et au-dessus, la théorie des rayons est principalement utilisée. Les trois autres types de modèles sont plus applicables et utilisables dans les cas ou les fréquences sont inférieures à 1 kHz.

A.2.3 Étapes Techniques générales de la TAO

Dans la conception originale de TAO, la mesure des temps de parcours des impulsions sonores est la première étape. Classiquement, le son est émis par une source et enregistré soit par un récepteur, soit par un réseau vertical ou horizontal constitué de plusieurs récepteurs. Nous appelons ces deux configurations, respectivement point à point et point à antenne. Dans l'idéal, l'impulsion temporelle correspondante à chaque rayon devrait être séparé à la réception. Quand ce n'est pas le cas, des processus de traitement doivent être mise en oeuvre. C'est le processus d'extraction de l'observation à partir des données enregistrées (montré dans la partie gauche de la figure A.1). Dans le mode point à point, les impulsions sonores ne peuvent être généralement séparés que par le paramètre temps d'arrivée alors que dans la configuration point à antenne, les angles de réception sont également disponibles comme un paramètre de discrimination. Pour décrire pleinement le concept de la TAO, les temps d'arrivées des impulsions correspondants à chaque rayon peuvent être calculés à partir des paramètres physiques

connus d'un modèle de propagation fixe (comme montré dans la partie droite de la figure A.1). Une fois, cette étape réalisée (problème direct), nous obtenons des mesures de la variation de température issues des observables et des mesures de la variation de température issues du modèle. Cette dernière sera lié à la valeur de la variation de célérité. Ensuite, un processus d'inversion sera nécessaire pour estimer les variations de vitesses du milieu.

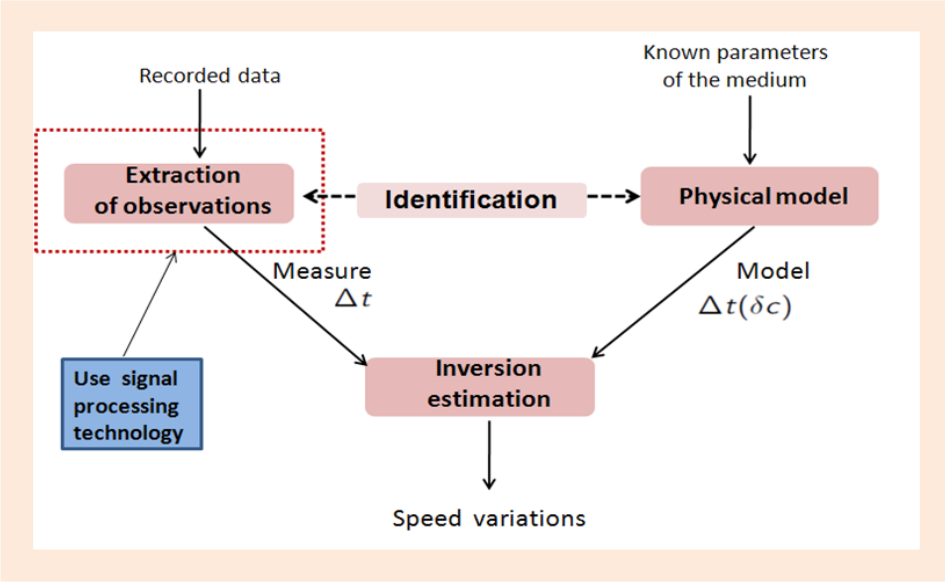

FIGURE A.1 – Deux principales étapes d'OAT

A.3 La TAO en eaux peu profondes

A.3.1 Eau peu profonde

Concentrons nous sur la définition de notre domaine d'acquisition caractérisé par un guide d'onde en eau peu profonde. Cette région est délimitée entre l'extrémité de la zone de surface et le rebord du plateau continental. En pratique, cela correspond à des environnements se trouvant à des profondeurs d'eau allant jusqu'à 200m. La motivation importante de la recherche sur l'acoustique d'eau peu profonde est fortement liée aux questions de défense naval (connaissance de l'environnement rapide REA), aux questions économiques et industrielles (installations portuaires, impact du traffic, exploration pétrolière...etc.), des questionnement en biologie (connaissance sur les mammifères marins et les poissons), en géologie (propriétés du fond marin et de la cartographie), en océanographie physique (température de l'eau, mesures des courants, état de surface).. etc. Cette zone cotière est un environnement différent des zones pélagiques. Tout

d'abord, il s'agit d'un milieu acoustique beaucoup plus compliqué car tous les facteurs importants, tels que la surface, la colonne d'eau, les propriétés du fond, sont spatialement et temporellement très variables. De plus, la caractéristique principale de la propagation en zone cotière est que l'onde sonore est réfractèe ou réfléchie par la surface et/ou le fond de facon importante. Il convient également de noter les plus forts effets 3D (à la fois aléatoire et les déterministes) que dans l'eau peu profonde.

A.3.2 Études récentes sur la TAO en zone cotière

Depuis une vingtaine d'années, la TAO est devenue un enjeux important et suscite un engouement. Les quatre théories classiquement utilisées ont été améliorées et affinées dans le contexte dse zones cotières [Pie65] [Mil69] [TW80] [MW83]. Par exemple, dans le prolongement de la théorie Mode Normal, est apparu la théorie mode normal couplée [Pie65] [Mil69] pour faire face à la dépendance du milieu entre la source et le récepteur, et pour appréhender les effets 3D dans la propagation. D'autre part, les efforts expérimentaux faites par des chercheurs dans le contexte des eaux peu profondes ont été réalisés. Par exemple, en océanographie, plusieurs expériences (de 1992 en mer de Barents [LJP*96], la campagne SWARM [ABC*97], l'expériences PRIMER [GPL*97][GBB*04], la campagne 2000-2001 ASIAEX [DZM*04], la récente campagne SW06 [TML*07]) sont concentrées sur l'étude des façades côtiéres. Pour éviter les limitations techniques de ces expériences à grande échelle très couteuses, une série d'expériences à petite échelle (de 1 à 8 km dans un guide d'onde de profondeur 50-120 m) en utilisant un signal acoustique à large bande [RCKH08] [RKH*04] [RJF*01] [KEK*01] [KKH*03] [EAH*02] [KHS*98] [HSK*99] a été effectuée. Inspiré par la configuration á deux dimensions (deux antennes), une formation de voies est effectuée simultanément sur les deux antennes (source et reception) pour séparer les rayons dans le cadre de la tomographie d'eau peu profonde [RCKH08]. Ce système sera validé en simulation et en données de cuve [IRNM08] [IRN*09] [RIN*11] pour extraire efficacement les trajets à partir des temps d'arrivées, des angles à l'émission et à la réception.

A.3.3 Propagation Multiple Targets

Dans la Fig. A.2, un exemple de propagation par rayons est représenté dans la configuration d'une source et d'un ensemble vertical de recepteurs. Un ensemble de rayons émis par une source sera réfractée ou réfléchie par la surface et / ou par le fond (le plateau continental). Ainsi, les rayons vont suivre des chemins différents et fournir des informations couvrant tout le milieu. Toutefois, cette propagation multiple va produire

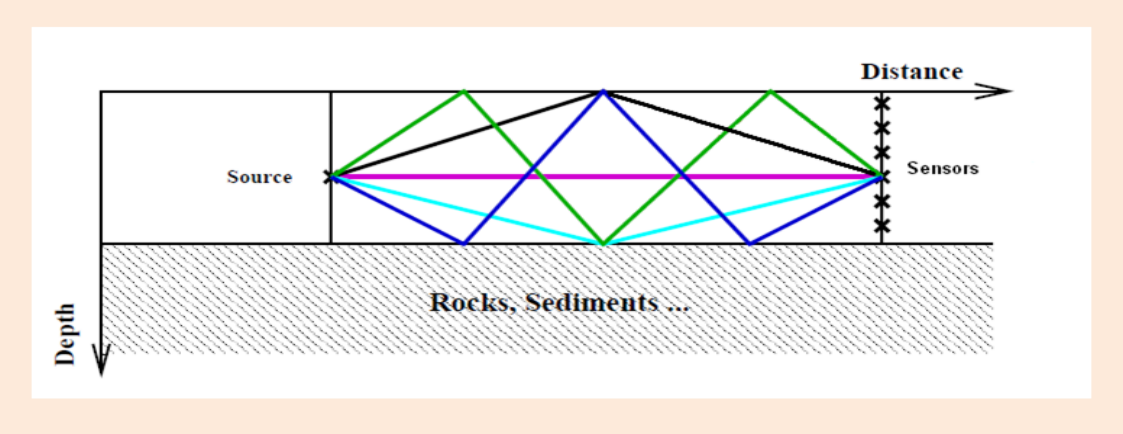

FIGURE A.2 – Propagation Multiple Targets

des interférences entre rayons. C'est pourquoi nous avons besoin de la technologie de traitement du signal pour séparer et identifier les trajectoires des rayons (figure A.1).

A.4 Traitement vectoriel en acoustique sous-marine

A la suite du chapitre 2, nous avons conclu que la TAO en eau peu profonde est un sujet de recherche actif et que la résolution du problème de séparation et de localisation des rayons par méthode de traitement du signal est toujours nécessaire. Dans ce chapitre, nous allons présenter un bref êtat de l'art sur ces techniques afin de résoudre notre problème dans un persperctive plus large.

Dans la partie suivante, nous allons donner un aperçu non seulement des techniques bien connues et classiques, comme la formation de voies, mais aussi quelques techniques importantes présentées plus récemment, comme le double-formation de voies et de la technique d'échantillonnage de Gibbs. Avant de commencer à discuter et comparer les algorithmes ci-dessus, nous tenons d'abord à répondre à plusieurs hypothéses importantes :

- *Onde plane* —- Dans la physique de la propagation des ondes, une onde plane est une onde à fréquence constante dont les fronts d'onde (surfaces de phase constante) sont des plans parallèles infinis normal au vecteur vitesse de phase. Ces ondes sont solution pour de l' équation d'onde scalaire dans un milieu homogène.

- *Milieu homogène* —- Un support de transmission ou une substance matérielle (solide, liquide, gaz ou plasma) qui peut propager des ondes d'énergie ;

- *Propriété de réciprocité*—- Parce que l'équation d'onde standard ne contient que des

dérivées, même si on donne une solution à l'équation des ondes, en utilisant un temps négatif, cette solution est aussi une solution.

Sur la base des méthode de séparation de source bien connues (ou localisation) et utilisées en acoustique sous-marine, tels que la formation de voies, le match field processing, la technique à retournement temporel, etc, mais aussi les nouvelles méthodes dans les publications récentes, telles comme la double formation de voies, l' échantillonneur de Gibbs, etc.. nous divisons ces méthodes en deux catégories, selon qu'elles sont sous l'hypothèse du son se propageant dans un espace homogène. Excepté l'échantillonneur de Gibbs, elles sont toutes des méthodes de types formation de faisceaux et mathématiquement, utilisent tous les moments statistiques d'ordre 2 des signaux enregistrés. Ces comparaisons sont illustrés dans le Tableau 3.1 et le Tableau 3.2. La limitation de résolution existe encore dans ces algorithmes et l'amélioration de la résolution est encore une perspective prometteuse pour ces méthodes. Nous espérons que notre tentative d'analyse globale sur ces méthodes puisse fournir un bref guide pour une exposition à un lecteur intéressé.

Method	Plane-wave	Experiment configuration
Beamforming	Yes	Point to array
Adaptive-beamformer	Yes	Point to array
MFP	No	Point to array
Time reversal mirror	No	Array to array
Double-beamforming	Yes	Array to array
Gibbs sampling approach	Yes	Point to array

TABLE A.1 – Comparaison des différentes méthodes de traitement d'antenne basée sur plusieurs crités (Onde place and configuration de l'expérimentation)-I

A.5 Les méthodes à haute résolution

De la revue des méthodes existantes pour résoudre le problème posé, nous avons constaté que l'amélioration de la résolution est toujours d'un grand intérêt, étant donné leur importance dans diverses applications de l'acoustique sous-marine. Plusieurs catégories

Method	Statistical order	Computations
Beamforming	2-order	1-D Search
Adaptive-beamformer	2-order	1-D Search
MFP	2-order	1-D Search
Time reversal mirror	2-order	—
Double-beamforming	2-order	2-D Search
Gibbs sampling approach	–	Iteration process

TABLE A.2 – Comparaison des différentes méthodes de traitement d'antenne basée sur plusieurs crités (Statistique et temsp de calcul)-II

de méthodes haute résolution sont proposées. Le mot "résolution" dans les thèmes de recherche de ce manuscrit est définie comme la capacité de distinguer les sources de signaux rapprochés. Bien que le sonar est l'un des domaines d'application classiques [Ows85] [Lig73] [Böh95], les méthodes haute résolution ont encore un grand potentiel pour d'autres applications acoustique, tels que la TAO, la localisation de source. Par conséquent, dans ce chapitre, nous avons sélectionné plusieurs méthodes représentatives pour donner une compréhension globale et mettre en valeur les plus récentes relativement à la formation de voies. Dans le même temps, nous précisons les problèmes concernant le tomographie acoustique en eau peu profonde qui nous voulons résoudre dans ce manuscrit.

Dans cette section, nous allons discuter et comparer ces algorithmes après la définition de plusieurs concepts importants.

- *Consistance* —- Dans cette discussion, la consistance se réfère à la propriété d'un estimateur, considéré comme une variable aléatoire indexé par le nombre d'éléments dans l'ensemble de données, à converger vers la valeur d'estimation conçue.

- *performance statistique* —- Nous utilisons le concept de bonne performance statistique pour désigner un estimateur qui atteint asymptotiquement la borne de Cramer-Rao (borne inférieure sur la matrice de covariance de tout estimateur sans biais).

- *Polarisation* —- Il s'agit d'une propriété de certains types d'ondes qui décrivent l'orientation de leurs oscillations, telles que les ondes électromagnétiques. Cependant, les ondes en acoustique sous marine ne sont pas polarisées.

Selon ces concepts et les différences entre ces méthodes à haute résolution, les techniques introduites sont comparées dans les quatre tableaux suivants. D'abord, ils ont presque tous une bonne performance statistique. La plupart des méthodes de sous-espaces sont basés sur les moments d'ordre 2 des signaux reçus, excepté l'algorithme

MUSIC-4. Le principal inconvénient des méthodes à sous-espace est lié d'une part à la sensibilité aux signaux cohérents et d'autre part au fait que la détection demande la connaissance au préalable du nombre de sources présent. Néanmoins, DML, SML et MAP-NSF évitent ces deux problèmes au détriment de la résolution relativement faible et du coût de calcul important. À notre avis, l'application à des signaux à multiple dimension avec des moments d'ordre élevé à des applications spécifiques sera probablement une tendance à l'avenir. A la fin de cette section, nous nous attendons à ce que la brève étude sur la méthode à haute résolution dans le chapitre 4 soit utile pour les lecteurs intéressés à sélectionner et à étendre des algorithmes adaptés à leurs domaines d'application.

Methode	Consistance	Cohérence	Statistique
Formation de voies	L=1	-	2-ordre
MUSIC	OUI	Non	2-ordre
DML	OUI		2-ordre
SML	OUI	OUI	2-ordre
MAP-NSF	OUI	OUI	2-ordre
Esprit	OUI	Non	2-ordre
Root-MUSIC	OUI	Non	2-ordre
MUSIC-4	OUI	Non	4-ordre
Q-MUSIC	OUI	Non	2-ordre
2D-MUSIC	OUI	Non	2-ordre

TABLE A.3 – Comparaison des méthodes à haute résolution à partir de different critéres (Consistance, Cohérence, Statistique)-I

Methode	Calcul	Dimension	Type de capteurs
Formations de voies	1-D	1-D	Scalaire
MUSIC	EVD, 1-D	1-D	Scalaire
DML	M-D	1-D	Scalaire
SML	M-D	1-D	Scalaire
MAP-NSF	M-D	1-D	Scalaire
Esprit	EVD	1-D	Scalaire
Root-MUSIC	EVD, polynomial	1-D	Scalaire
MUSIC-4	EVD, 1-D	1-D	Scalaire
Q-MUSIC	EVD, 1-D	M-D	Vector
2D-MUSIC	EVD, 1-D search	M-D	Scalaire

TABLE A.4 – Comparaison des méthodes à haute résolution à partir de different critéres (Calcul, imension, Type de capteurs)-II

Methode	Performance statistique	Polarisation
Formation de voies	-	OUI
MUSIC	Bonne	OUI
DML	Bonne	OUI
SML	Bonne	OUI
MAP-NSF	Bonne	OUI
Esprit	Bonne	–
Root-MUSIC	Bonne	–
MUSIC-4	Bonne	OUI
Q-MUSIC	Bonne	Non
2D-MUSIC	Bonne	OUI

TABLE A.5 – Comparaison des méthodes à haute résolution à partir de different critéres (Performance statistique, Polarisation)-III

Methode	Connaissance de l'ordre	Hypothéses signal	Géométrie de l'antenne
Formation de voies	Non	Gaussien	Arbitraire
MUSIC	OUI	Gaussien	Arbitraire
DML	Non	-	Arbitraire
SML	Non	-	Arbitraire
MAP-NSF	Non	-	Arbitraire
Esprit	OUI	Gaussien	ULA
Root-MUSIC	OUI	Gaussien	ULA
MUSIC-4	OUI	Non	Arbitraire
Q-MUSIC	OUI	Gaussian	Arbitraire
2D-MUSIC	OUI	Gaussien	Arbitraire

TABLE A.6 – Comparaison des méthodes à haute résolution à partir de different critéres (Connaissance de l'ordre, Hypothéses signal, Géométrie de l'antenne)-IIII

A.6 Séparation des trajets par méthodes haute résolution dans un guide d'onde en eau peu profonde

A.6.1 Introduction

Une autre caractéristique importante de propagation par trajets multiples dans le cas des TAO est que les rayons multiples sont souvent corrélés. En particulier, si le retard entre deux rayons est assez petit, les rayons seront cohérents. Sur la base de ce qui précède, il est essentiel de présenter un traitement à haute définition s'adaptant au cas des rayons cohérents ou très corrélées.

Afin de continuer à utiliser les méthodes de localisation en présence de sources fortement corrélées, des tecniques utilisant un lissage spatial efficace a été développé pour des sources à bande étroite, et largement étudiés par [EJS81] et [ESJ82]. Une analyse

complète est présentée sur des résultats de simulation par [SWK85], [RH93], [Red87], [Cho02].

Le problème de la détection de sources multiple, large bande et de l'estimation des DOA à partir des signaux reçus sur un réseau vertical s'adresse, en particulier, lorsque les sources sont totalement corrélées [WK87].

Malgré qu'il a l'avantage de localiser plusieurs sources cohérentes sans aucune technique de pré-traitement, il n'est pas encore tout à fait adaptée au contexte de la TAO. Récemment, [PM06] à présenter un nouveau champ d'onde du filtre pour les données sismiques multicomposantes en proposant des méthodes de lissage dans le domaine spatial e fréquenciel pour estimer correctement la matrice multi-composantes à large bande.

Dans ce chapitre, inspiré par [PM06], nous proposons un traitement à haute définition [JALT*11] [JM12] nommé par Smoothing-MUSICAL dans une configuration point à antenne. Cet algorithme combine l'algorithme MUSICAL [GB95] et la technique de lissage spatio-fréquenciel. Ses performances en résolution seront comparés à celle du traitement de formation de voies classique.

A.6.2 Smoothing-MUSICAL

En général, les méthodes à haute résolution nécessitent une modélisation précise des signaux reçus sur l'antenne (ondes planes, des sources non corrélées, ...). Ces méthodes ont été conçues pour les antennes passives avec l'hypothèse selon laquelle il n'existe aucune information sur la forme temporelle du signal reçu. Le signal est supposé être aléatoire et stationnaire (l'un des cas le plus simple est d'analyser des signaux à bande étroite). Par la suite, les méthodes à bande étroite ont été étendus aux signaux large bande. En tirant parti des caractéristiques fréquencielles, [GB95] nous proposons un algorithme MUSIC actif large bande utilisant des réalisations multiples dans l'hypothèse de sources décorrélées. Cependant, ces hypothèse sont difficiles à réaliser dans un environnement de Tomographie acoustique océanique. Ainsi, nous proposons l'algorithme smoothing-MUSICAL, qui est basé sur une réalisation unique et permet de séparer les rayons totalement corréélés. L'algorithme est décrit dans les sections suivantes :

A.6.2.1 Modéle de signal

Le modèle de signal est construit sur un champ acoustique composé de P rayons qui arrivent sur une antenne verticale de M capteurs. Le signal temporel reçu sur le capteur

m^{eme} est modélisé comme :

$$x_m(t) = \sum_{p=1}^{P} a_p s(t - \tau_{m,p}) + n_m(t) \tag{A.2}$$

Avec :

- $x_m(t)$: signal reçu sur le capteur $m^{ième}$.
- $s(t)$: signal émis par la source.
- a_p : amplitude de la $p^{ième}$ rayons reçu sur le capteur $m^{ième}$.
- $n_m(t)$: bruit additif reçu sur le $m^{ième}$ capteur.

Dans le domaine fréquentiel, l'équation A.2 s'écrit :

$$x_m(\nu) = \sum_{p=1}^{P} a_p s(\nu) \exp(-j2\pi\nu\tau_{m,p}) + n_m(\nu) \tag{A.3}$$

Le retard $\tau_{m,p}$ peut être exprimée comme suit :

$$\tau_{m,p} = t_p^{'} + t_m(\theta_p) \tag{A.4}$$

Où $t_p^{'}$ représente le temps d'arrivée du $p^{ième}$ rayons sur le capteur de référence, $t_m, (\theta_p)$ est le délai entre le capteur de référence et le $m^{ième}$ capteur. $t_m(\theta_p)$ est une fonction de θ_p, qui est la direction d'arrivée du rayon sur l'antenne.

L'équation A.3 peut être réécrite en utilisant A.4 comme suit :

$$x_m(\nu) = \sum_{p=1}^{P} a_p s(\nu) \exp(-j\nu(\Psi_p + (m-1)\Phi_p)) + n_m(\nu) \tag{A.5}$$

avec : $\Psi_p = 2\pi T_p$, $\Phi_p = 2\pi t_m(\theta_p)$.

Dans l'équation A.3, le terme $s(\nu)$ est l'amplitude déterministe du signal émis à la fréquence ν. L'amplitude de chaque rayons, a_p, est considérée comme aléatoires et non corrélées. De manière à séparer les termes déterministes des termes aléatoires, l'équation. A.3 peut s'écrire sous forme matricielle en utilisant les F bins de fréquence du signal :

$$\mathbf{x}_g = \mathbf{H}.\mathbf{c} + \mathbf{n}_g \tag{A.6}$$

Avec :

- $\mathbf{x}_g = [\mathbf{x}^T(\nu_1), \mathbf{x}^T(\nu_2), \ldots, \mathbf{x}^T(\nu_F)]^T$, un vecteur de dimension $M \times F$ obtenue par concaténation des vecteurs d'observation à chaque fréquence.
- $\mathbf{x}(\nu_i) = [x_1(\nu_i), x_2(\nu_i), \ldots, x_M(\nu_i)]^T$
- F : le nombre de bin de fréquence du signal.
- $\mathbf{n}_g = [\mathbf{n}^T(\nu_1), \mathbf{n}^T(\nu_2), \ldots, \mathbf{n}^T(\nu_F)]^T$, un vecteur de dimension $M \times F$ obtenue par concaténation de l'observation de vecteurs de bruit à chaque fréquence.
- $\mathbf{n}(\nu_i) = [n_1(\nu_i), n_2(\nu_i), \ldots, n_M(\nu_i)]^T$
- $\mathbf{c} = [a_1, a_2, \ldots, a_P]^T$ est un vecteur de dimension P.
- $\mathbf{H} = [\mathbf{h}_1, \mathbf{h}_2, \ldots, \mathbf{h}_P]^T$ rassemble les termes $e^{-2i\pi\nu_1\tau_{mp}}$ pour caractériser les fonctions de transfert entre les sources et les capteurs.
- $\mathbf{h}_p = [s(\nu_i)e^{-2i\pi\nu_1\tau_{1p}}, \ldots, s(\nu_F)e^{-2i\pi\nu_F\tau_{Mp}}]^T$ le terme $s(\nu_i)$ caractérisant le signal émis.
- T signifie transposé

Après l'étape de modélisation, nous allons présenter le principe de l'algorithme pour détecter et séparer les rayons à partir de l'estimation de la matrice interspectrale.

A.6.2.2 Estimation de la matrice interspectrale

Sur la base de l'équation. A.6, la matrice interspectrale des données reçues est obtenu sous la forme :

$$\mathbf{\Gamma} = E\{\mathbf{x}_g\mathbf{x}_g^*\} = \mathbf{H}\,\mathbf{\Gamma_C}\,\mathbf{H}^* + \mathbf{\Gamma_N} = \mathbf{\Gamma_Y} + \mathbf{\Gamma_N} \tag{A.7}$$

Où $*$ signifie transposé conjugué. $\mathbf{\Gamma_C}$ est la matrice de corrélation des sources de $P \times P$ de dimension. $\mathbf{\Gamma_Y}$ est la matrice interspectrale à large bande des sources. $\mathbf{\Gamma_N}$ est la matrice interspectrale du bruit large bande.

L'hypothèse des rayons non corrélées implique que $\mathbf{\Gamma}$ est diagonale et que son rang doit être au moins égal au nombre de rayons P. MUSICAL pourrait obtenir une séparation efficace avec cette hypothèse. Cependant, dans une expérience pratique, une réalisation unique et des rayons corrélés permet de classer la mèthide comme dèficiente. Lorsque les rayons sont parfaitement corrélés (ou cohérents), le rang de la matrice interspectrale est 1 (matrice singulière) et la séparation est impossible. Afin d'augmenter ce rang et permettent d'obtenir toutes les valeurs propres correspondant à l'espace signal, les techniques de lissage spatial et fréquenciel peuvent être utilisés. Bien qu'il existe des

techniques de lissage spatial et fréquenciel, l'extension des méthodes à bande étroite au cas large bande n'est pas directe car la nature et la structure des matrices interspectrales sont vraiment différents.

Lissage spatiale large bande

L'idée de base de la méthode de lissage spatial pour des signaux bande large est le même que celui utilisé dans la bande étroite. Il s'agit de diviser l'antenne principale composée de M capteurs dans $2K_s + 1$ sous-antenne qui se chevauchent partiellement (chaque sous-antenne avec $M - 2K_s$ capteurs successifs). L'antenne indicée k_s comprend les capteurs $[k_s, k_s + 1, \ldots, k_s + M - 2K_s]$. Tous ces $2K_s + 1$ sous-antennes sont utilisées pour estimer les $2K_s + 1$ matrices spectrales à large bande.

$$\hat{\mathbf{\Gamma}} = (2K_s + 1)^{-1} \sum_{k_s=1}^{2K_s+1} \underline{\mathbf{x}}_{g,k_s} \underline{\mathbf{x}}_{g,k_s}^{*} \tag{A.8}$$

Ces sous-réseaux sont censés être linéaire et uniforme. Il s'est avéré que si le nombre de sous-réseaux est supérieur ou égal au nombre de sources, la matrice spectrale est non singulière. A titre d'exemple, dans la Fig. A.3 un réseau uniforme linéaire avec $M = 7$ capteurs identiques (1, ..., 7) est divisé en sous-réseaux qui se chevauchent de taille $M - 2K_s = 5$, avec des capteurs (1, ..., 5) formant le premier sous-groupe, capteurs (2, ..., 6) formant le second sous-groupe, etc.

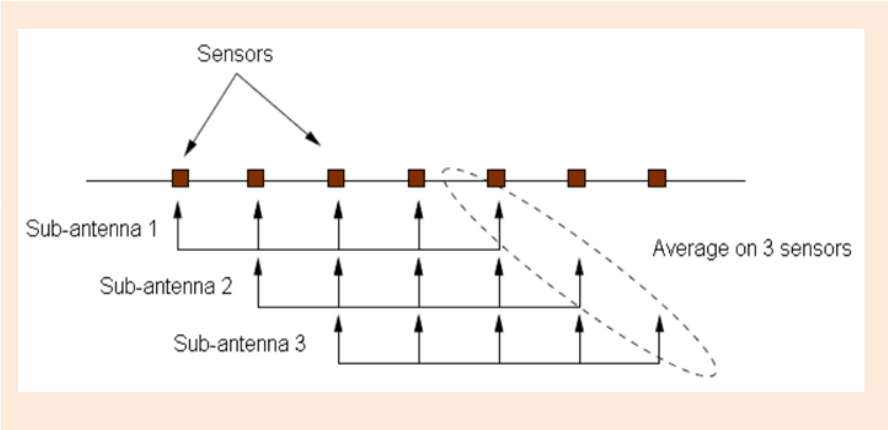

FIGURE A.3 – Structure d'antenne sous lissage spatial

Lissage en fréquence

Un processus de lissage est similaire à celui utilisée dans le paragraphe précédent peut être appliqué dans le domaine fréquentiel. Ceci est largement dû à la structure particulière des vecteurs d'observation large bande utilisés par MUSICAL, ou il est possible

d'introduire un lissage en fréquence si les deux hypothèses suivantes sont remplies :

1. Blanchiment préalable des signaux reçus ;
2. Canaux de fréquence régulierement espacés sur la bande d'analyse.

Pour cela, le lissage de fréquence est effectuée en divisant le groupe composé de F canaux de fréquence dans $2K_f + 1$ sous-bandes se recouvrant partiellement de canaux $F - 2K_f$. Ainsi, la sous-bande de l'index k_f est composée de canaux $[k_f, k_f + 1, \ldots, k_f + F - 2K_f]$. La matrice spectrale de l'observation est alors définie comme la moyenne de la matrice $2K_f + 1$ correspondant à la $2K_f + 1$ sous-bandes observées dans l'équation. A.9.

$$\hat{\mathbf{\Gamma}} = (2K_f + 1)^{-1} \sum_{k_f=1}^{2K_f+1} \underline{\mathbf{x}}_{g,k_f} \underline{\mathbf{x}}_{g,k_f}^{*} \tag{A.9}$$

Fig. A.4 montre un exemple de la division sous-bandes pour $F = 10$ et $K_f = 2$.

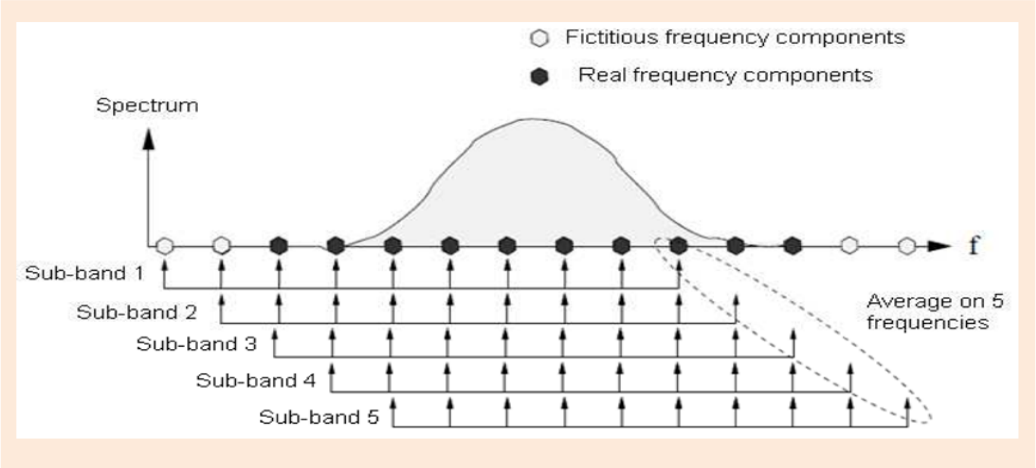

FIGURE A.4 – Structure de sous-bande pour le lissage fréquentiel

Lissage spacio-fréquenciel

Les deux méthodes décrites ci-dessus peuvent bien évidemment être utilisés séparément pour faire un lissage fort soit à distance ou en fréquence. Cela introduira un biais important dans l'estimation de la matrice. Pour résoudre ce problème, la combinaison des deux types de lissage offre plus de souplesse dans le traitement, en particulier pour l'antenne qui sont composés d'un nombre limité de capteurs et pour lesquels les méthodes de lissage spatial ne sont pas applicables [PM06]. (K_S, K_f respectivement désigne le facteur de lissage spatial et fréquentiel). De la seule observation disponible $\underline{\mathbf{x}}$, en utilisant conjointement les deux formes de lissage, il est possible de générer un ensemble de $(2K_s + 1)$ spatialement récidives $\underline{\mathbf{x}}_{g,k_s}$. Ces $1 + 2K_s$ récidives sont ensuite déplacé fréquentiellement

pour obtenir $K = (2K_s + 1)(2K_f + 1)$ récidives $\underline{\mathbf{x}}_{g,k_s,k_f}$. Enfin, on peut estimer la matrice interspectrale à large bande par la formule suivante :

$$\hat{\mathbf{\Gamma}} = (2K_s + 1)(2K_f + 1)^{-1} \sum_{k_s=1}^{2K_s+1} \sum_{k_f=1}^{2K_f+1} \underline{\mathbf{x}}_{g,k_s,k_f} \underline{\mathbf{x}}^*_{g,k_s,k_f} \tag{A.10}$$

Le rang de la matrice interspectrale ainsi estimée est égale à K. Pour parvenir à une séparation effective des rayons et le bruit, il est nécessaire de sélectionner K supérieur à P.

Estimation du sous-espace signal

En raison des hypothèses que les sources et le bruit ne sont pas corrélés, $\hat{\mathbf{\Gamma}}$ se dècompose en :

$$\hat{\mathbf{\Gamma}} = \hat{\mathbf{\Gamma}}_s + \hat{\mathbf{\Gamma}}_n \tag{A.11}$$

Parce que la matrice spectrale présente une symétrie hermitienne :

$$\hat{\mathbf{\Gamma}} = \hat{\mathbf{\Gamma}}^* \tag{A.12}$$

Elle peut être décomposé de façon unique à l'aide d'une EVD comme :

$$\hat{\mathbf{\Gamma}} = \mathbf{U}\mathbf{\Lambda}\mathbf{U}^* = \sum_{k=1}^{MF} \lambda_k \mathbf{u_k} \mathbf{u_k}^* = \sum_{k=1}^{P} \lambda_k \mathbf{u_k} \mathbf{u_k}^* + \sum_{k=P+1}^{MF} \lambda_k \mathbf{u_k} \mathbf{u_k}^* \tag{A.13}$$

ou $\mathbf{\Lambda} = diag(\lambda_1, \ldots, \lambda_M)$ sont les valeurs propres et $\mathbf{U}$ est un élément unitaire ($M \times F$) par ($M \times F$) matrice dont les colonnes sont les vecteurs-propres orthonormés $\mathbf{u}_1, \ldots,$ $\mathbf{u}_M$ de $\hat{\mathbf{\Gamma}}$. les valeurs propres λ_i correspond à l'énergie des données associées à la valeur propre u_i. Ils sont disposés comme suit : $\lambda_1 \geq \lambda_2 \geq \cdots \geq \lambda_M \geq 0$.

A.6.2.3 Projection sur le sous-espace bruit

Basé sur la décomposition en éléments propres, le sous-espace signal est engendré par les premiers vecteurs propres P de $\hat{\mathbf{\Gamma}}$. Le sous-espace bruit est engendré par les $MF - P$ vecteurs propres derniers. La projection orthogonale sur le sous-espace de bruit est estimée comme suit :

$$\hat{\mathbf{\Gamma}}_n = \sum_{k=P+1}^{MF} \mathbf{u_k} \mathbf{u_k}^* \tag{A.14}$$

Enfin, l'algorithme haute résolution consiste à maximiser la fonction suivante :

$$F_{s_{MUSIC}}(\theta, t^{'}) = \frac{1}{\mathbf{a}(\theta, t')^{*}\ \hat{\mathbf{\Gamma}}_n\ \mathbf{a}(\theta, t')} \tag{A.15}$$

avec : le vecteur de direction à large bande $\mathbf{a}(\theta, t^{'})$ qui est la concaténation des vecteurs $\mathbf{d}(\nu_i, \theta)$, qui est le vecteur de direction classique utilisé dans l'analyse de bande étroite. Il est écrit comme suit :

$$\mathbf{a}(\theta, t^{'}) = \begin{bmatrix} s(\nu_1)e^{-2i\pi\nu_1 t^{'}}\mathbf{d}^T(\nu_1, \theta) \\ \dots \\ s(\nu_F)e^{-2i\pi\nu_F t^{'}}\mathbf{d}^T(\nu_F, \theta) \end{bmatrix} \tag{A.16}$$

Où $\mathbf{d}(\nu_i, \theta) = [1, e^{-2i\pi\nu_i\tau_{1,2}(\theta)}, \dots, e^{-2i\pi\nu_i\tau_{1,M-1}(\theta)}]^T$. $\mathbf{d}(\nu_i, \theta)$ contient des informations relatives aux déphasages entre les capteurs à une fréquence donnée et pour un trajet de rayons d'angle d'arrivée θ.

A.6.3 Simulations

A.6.3.1 Configuration

Nous illustrons la méthode présentée précédemment sur deux ensembles de données synthétiques obtenus avec un algorithme équation parabolique. Nous allons utiliser ces deux ensembles de données synthétiques pour mettre en oeuvre plusieurs expériences en fonction des essais des propriétés différentes. Dans ces expériences, nous utilisons une source et une antenne verticale de 61 récepteurs. Dans le premier groupe d'expériences synthétique, la source est fixée à 40 m sous la mer et les récepteurs 61 sont régulièrement espacées dans la colonne d'eau comprise entre 25 m et 55 m. Nous choisissons les capteurs 31 que celui de référence. La distance entre la source et le capteur de référence est égal à 2 km. La configuration est représentée par Fig. A.5. La position de la source de la configuration expérience qui est exploré afin d'obtenir le second groupe de données synthètiques est fixé à 40.5 m.

La fréquence d'échantillonnage et la fréquence centrale du signal émis sont respectivement 10400 Hz et 1000 Hz. Les rayons sont propagés entre la source et un récepteur de l'antenne de réception. Tous les rayons sont enregistrées sur l'antenne de réception pour une source donnée.

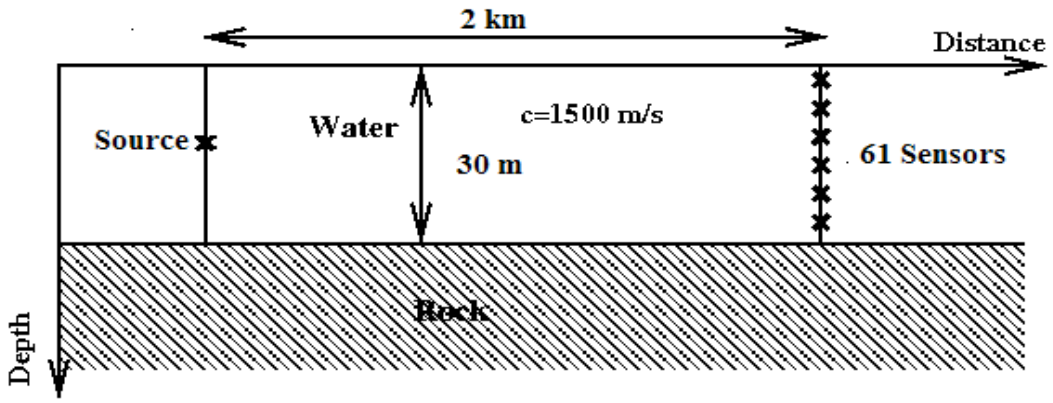

FIGURE A.5 – Configuration Point-Antenne permettant d'obtenir les données synthètiques

A.6.3.2 Grandes fenêtres temporelles de données

Dans le premier groupe de données synthétiques, on choisit un rapport grand fenêtre de temps (1560 échantillons dans le domaine temporel) pour tester les performances de séparation de l'algorithme proposé. Afin d'illustrer les performances de l'amélioration de smoothing-MUSICAL, nous prenons la formation de voies classique [DWM01] comme une méthode comparative. Les résultats de séparation pour le signal enregistré sont illustrés Figure A.6. Chaque point dans ces chiffres désigne un trajet de rayon avec le temps d'arrivée et de direction d'arrivée. En général, smoothing-MUSICAL donne une séparation plus précise avec une plus petite tache correspondant à chaque trajet par rapport aux algorithmes de formation de voies.

A.6.3.3 Robustesse en fonction du bruit

Dans cette section, la discussion sur la résolution de la méthode proposée sera effectuée sur une petite fenêtre temporelle de données (312 échantillons temporels). Sur la base de la discussion précédente, dans le cas sans bruit, smoothing-MUSICAL identifie les rayons plus precisément que le Formation de voie et ceux avec moins d'artefacts. Dans cette partie, la robustesse au bruit sera évalué en fonction du rapport signal à bruit. Comme le signal occupe une portion possible de la bande de fréquence, nous avons ajouté un bruit blanc gaussien uniquement dans cette bande. On définit le SNR comme suit : rapport de puissance entre le signal et le bruit dans la bande de fréquence de signal. Les résultats sont présentés pour deux différents SNR : 0 dB et -15 dB.

RSB = 0 dB : la Figure. A.7 (a) montre les résultats obtenus par formation de voies des signaux enregistrés sur l'antenne. Dans ce cas, il est possible de séparer les différents

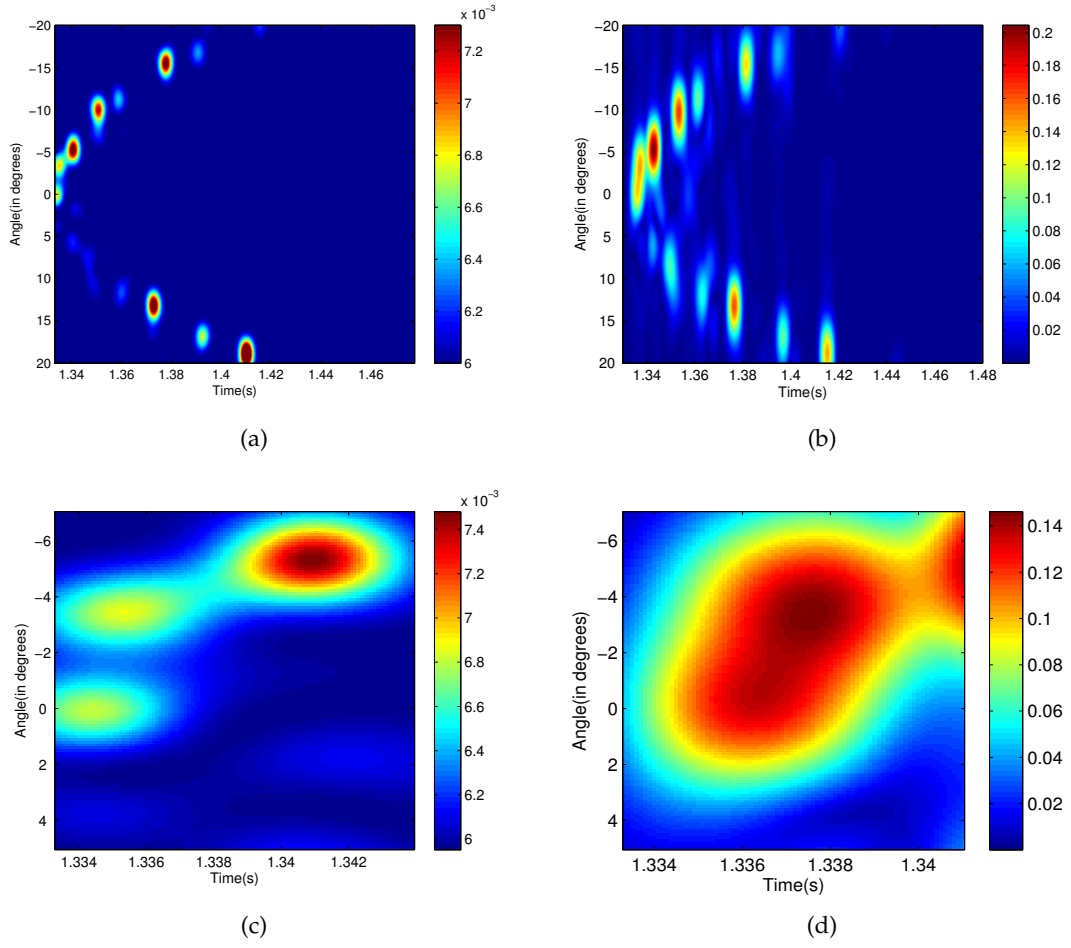

FIGURE A.6 – Résultat de séparation sur un signal enregistré (grande fenêtre de temps et sans bruit). (a) Avec smoothing-MUSICAL. (b) Avec Formation de voie. (c) Résultats de la séparation d'une partie du signal enregistré avec smoothing-MUSICAL. (d) Résultats de la séparation d'une partie du signal enregistré avec Formation de voies.

rayons. Les points correspondants sont visibles et séparés dans le domaine temps-DOA. Les résultats issus de smoothing-MUSICAL sont représentés Figure. A.7 (b). Cependant, smoothing-MUSICAL n'est pas indispensable dans ce cas dans la vue de la robustesse contre le bruit.

RSB = -15dB : Etudions le cas d'un environnement fortement bruité. Comme dans le cas précédent, la formation de voies et le lsmoothing-MUSICAL sont respectivement appliqués au signal reçu dans la configuration du point-antenne. Les résultats issus de la formation de voies sont (Fig. A.7 (c)) montrent que les différents rayons ne sont plus facilement reconnus en raison du grand nombre d'artefact produit par le bruit et le suivi des temps d'arrivée ne peut pas être atteint. Pour smoothing-MUSICAL (Fig. A.7(d)), les taches correspondantes aux différents rayons sont encore visibles.

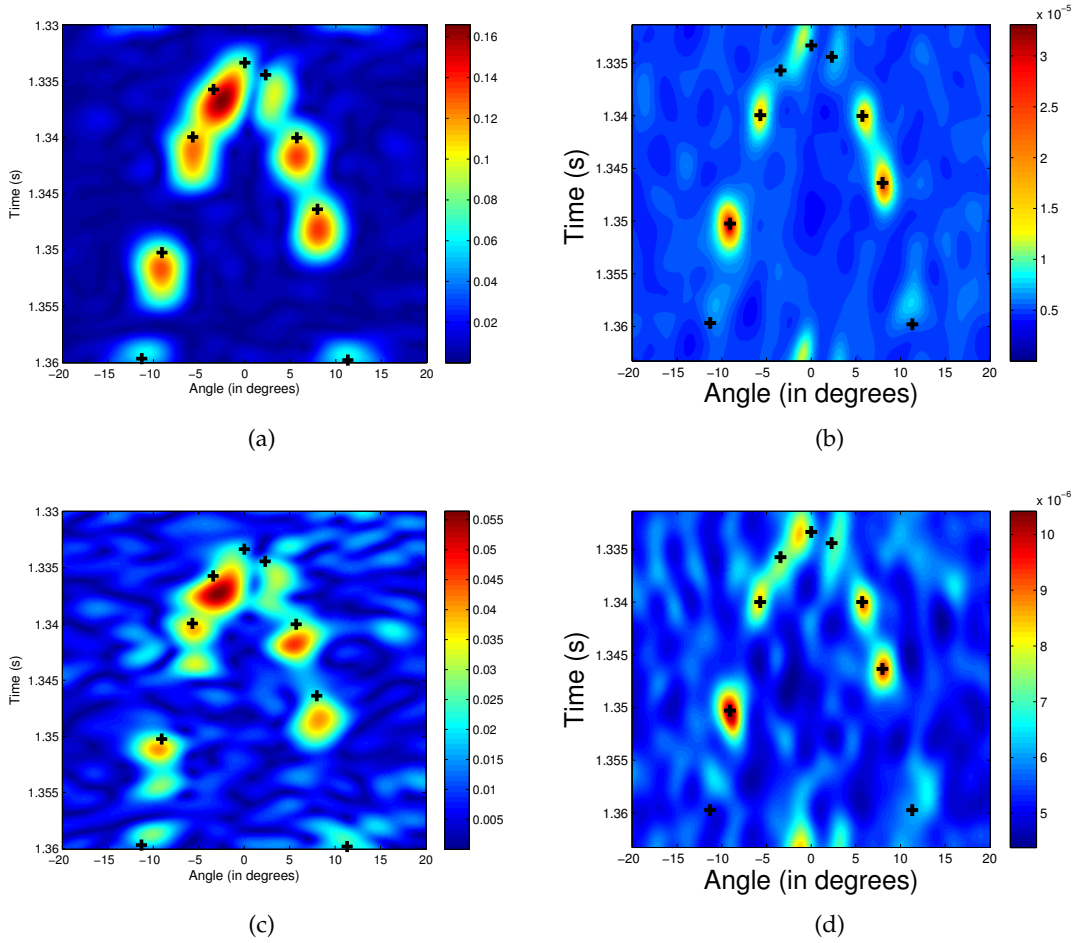

FIGURE A.7 – Un exemple expérimental de signal enregistré (RSB = 0 dB) (a) les résultats de séparation avec Formation de voie (RSB = 0 dB). (b)Les résultats de séparation avec smoothing-MUSICAL (RSB = 0 dB). (c) les résultats de séparation avec Formation de voie (RSB = -15 dB). (d)Les r'esultats de séparation avec smoothing-MUSICAL (RSB = -15dB).

A.6.4 Application sur des données réelles

A.6.4.1 Configuration

Une expérience à petite échelle est abordée dans cette partie, afin que nous puissions mieux illustrer la performance de nos méthodes. Le principe sur lequel se fondent ces expériences est le suivant : si la fréquence des signaux est multipliée par un facteur et les distances spatiales sont divisées par le même facteur, les phénomènes physiques se déroulant dans l'environnement reste le même. Il réalise un coût réduit et une expérience totalement contrôlés. L'expérience présentée ici a été réalisée à l'ISTerre (Institut des Sciences de la Terre) de laboratoire dans le bac à ultrasons qui est développé par P. Roux. Dans ce réservoir, un guide d'onde de 5-10 m de profondeur et de longueur 1-1.5 m est construit. Une barre d'acier sert de fond, ce qui est très réfléchissante et parfaitement plat. En particulier, un capteur est fixé à 0.0263m comme un émetteur. Un réseau vertical constitué de 64 capteurs est prise comme une réception. La profondeur du premier récepteur est de $3.55 \times 10^{-3}m$. L'intervalle de deux récepteurs adjacents est de 0.75×10^{-3}m. La distance entre l'émetteur et le récepteur de référence est 1,1437 m et le signal de source avec une largeur de bande de 1 MHz de fréquence a une fréquence centrale de 1,2 MHz. Les premiers points 760 dans le domaine temporel du signal reçu avec une fréquence d'échantillonnage $F_e = 50MHz$ sont utilisées dans cette expérience.

A.6.4.2 Résultats

La séparation des résultats obtenus par formation de voies classique est représentée dans la figure.5.12 (b). Les positions d'arrivée théorique sont notées par des croix noires et calculées à partir de la théorie des rayons. La formation de voie détecte six rayons avec succès en fonction de la position théorique, mais il ne peut pas séparer les deux premières rayons. Pour les mêmes données, smoothing-MUSICAL (Fig. 5.12 (c)) détient toujours la meilleure performance de séparation pour la position physique dans le plan de DOA et heure d'arrivée.

A.7 Détection automatique du nombre de trajets dans un guide d'onde en eau peu profonde

Dans une première étape d'amélioration, l'algorithme smoothing-MUSICAL (MUSIC actif à grande bande), est mis au point pour extraire l'observation dans le cadre de tomographie acoustique océanique [JALT*11]. On obtient une séparation plus précise

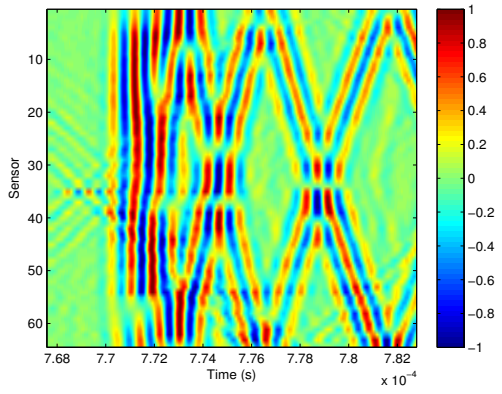

(a)

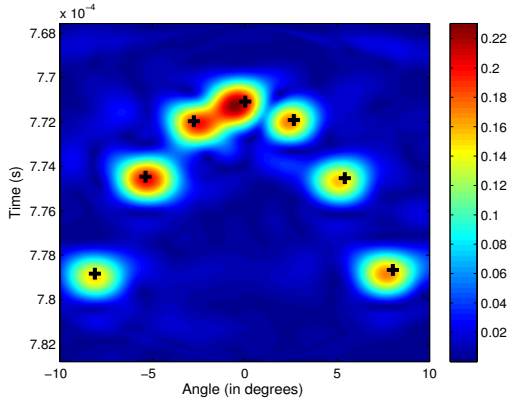

(b)

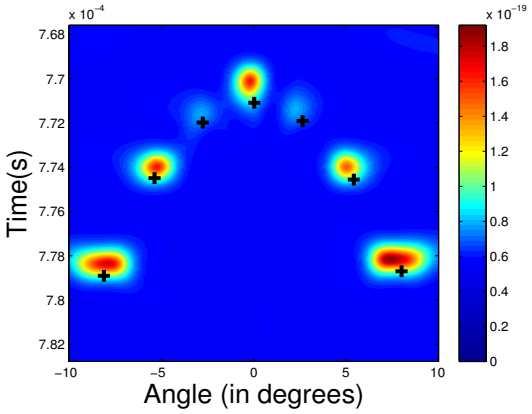

(c)

FIGURE A.8 – Un exemple expérimental de signal enregistré pour les données réelles obtenues à petite échelle (a) Signal enregistré pour les données réelles obtenues à petite échelle. (b) Résultats de séparation avec formation de voies pour les données réelles obtenues à petite échelle. (c) Résultats de séparation avec smoothing-MUSICAL pour les données réelles obtenues à petite échelle.

que la formation de voies sous condition de la connaissance préalable du nombre de rayons. Comme dans le cas général de traitement d'antenne, la méthode smoothing-MUSICAL exige une sélection correcte de l'ordre du modèle. Si l'ordre du modèle est mal choisi, la séparation peut être fausse.

En ce qui concerne le problème de sélection de modèle d'ordre, deux approches proposées sont généralement proposées : le critère d'information d'Akaike (AIC) et longueur de description minimale (MDL) [WK85b]. Ils se proposent de minimiser la divergence de Kullback-Leibler (KL) écart entre la fonction de densité de probabilité (PDF) des données et la PDF du modèle. Avec des hypothèses idéales de processus gaussiens aléatoires ergodiques, le critère MDL est montré pour être asymptotiquement consistant, alors que l'AIC a tendance à surestimer l'ordre du modèle. En revanche, ces hypothèses idéales ne peuvent pas être remplies dans la pratique et plusieurs facteurs pourraient entraîner une dispersion des plus petites valeurs propres (par exemple : nombre d'échantillons).

Les deux critères AIC et MDL ont tendance à surestimer ou sous-estimer l'ordre du modèle. Pour l'analyse de la performance et de l'évaluation de la probabilité de sur-ou sous-estimation de l'AIC et MDL, des résultats théoriques sont présentés dans [XK95] [LR01].

Deux variantes de l'AIC et MDL sont introduites : une approche pour les statistiques est employé dans la solution existante par Fischler et Messer [FM00]. Dans [MP05], une nouvelle méthode d'estimation des retards et amplitudes des arrivées avec un maximum d'une estimation MAP a posteriori est présenté. Dans le contexte de la localisation de la source, un échantillonnage de Gibbs-maximum a posteriori [MM05] est utilisé pour extraire les temps d'arrivée des trajets des rayons de séries chronologiques reçu.

Un groupe de méthodes proposé est le test du rapport de vraisemblance [Bar54] [Law56] [Gu98] Une méthode bayésienne alternative est proposée par Djuric [Dju94] [Dju96].

En considérant d'abord les limites d'observation, un test de la détermination de la dimension d'un sous-espace signal à partir des enregistrements de données courtes est explorée par Shah et Tufts [ST94]. Il est composé de l'interprétation de la somme des carrés des valeurs singulières dans un sous-espace particulier. Les seuils de taux constants fausses alarmes sont mises en place en fonction des distributions dérivées des perturbations de la matrice.

Il est à noter que le critère fondé sur les ratios de valeurs propres peuvent être utilisés pour rechercher une valeur propre écart entre le bruit et les valeurs propres de signaux [LR01]. En tant que méthode suivante, un test de l'exploitation du profil exponentiel

du bruit est d'abord introduit dans [GLC96], et développé pour estimer le nombre de cibles importantes en imagerie par renversement du temps [QBL06]. Par ailleurs, pour estimer le nombre de signaux de grande dimension, un exemple de procédure de valeur propre basée sur des échantillons relativement peu est pr'esent'e [NE08]. Il peut toujours détecter le nombre de signaux de bruit blanc lorsque le nombre de capteurs est inférieur au nombre de signaux.

Un test d'ajustement exponentiel (EFT) à l'aide de courte longueur des échantillons est proposé pour déterminer le nombre de rayons dans la partie suivante, qui serait considéré comme robuste et applicable . On définit de courte longueur d'échantillons en tant que concept que le nombre d'échantillons est égal au nombre de capteurs. La plupart des résultat présentés dans ce chapitre est basé sur nos travaux [JM11a] [JM11c] [JM11b].

A.7.1 Déetection du n ombre de rayons

Afin d'analyser le problème de la détection du nombre de raypaths efficacement, le modèle approprié devrait être construit en premier. Dans ce chapitre, le modèle est construit sur un champ acoustique composée de P rayons sur un réseau vertical de M capteurs ($P < M$). Le signal temporel reçu des capteurs est modélisé comme :

$$\mathbf{x}(t) = \mathbf{y}(t) + \mathbf{n}(t) = \mathbf{A}s(t) + \mathbf{n}(t) = \sum_{j=1}^{P} \mathbf{a}(\theta_j)s(t) + \mathbf{n}(t) \tag{A.17}$$

Avec :

- $\mathbf{x}(t)$: une $M \times 1$ vecteur d'observation. Le composant i ème est le signal reçu sur le capteur i ème.
- $\mathbf{n}(t)$: bruit additif blanc gaussien de taille $M \times 1$ avec une distribution $\mathcal{N}(0, \sigma_n^2\mathbf{I})$, ce qui est supposé être corrélés avec les signaux.
- $\mathbf{y}(t)$: le vecteur d'observation de la taille $M \times 1$, qui s'étend sur l'espace signal engendré par les vecteurs de direction.
- $\mathbf{A}$: la matrice des vecteurs directeurs P. Chaque vecteur directeur $\mathbf{a}(\theta_j)$ pour le trajet de rayon j ème est généralement caractérisée par les paramètres d'angles d'arrivé θ_j.
- $s(t)$: le signal émis.

Sur la base de l'équation (A.17), l'observation matrice de covariance $\mathbf{R}$ s'écrit :

$$\mathbf{R} = E[\mathbf{x}(t)\mathbf{x}^*(t)] = \mathbf{R}_y + \mathbf{R}_n = \mathbf{A}\mathbf{\Lambda}_s\mathbf{A}^* + \sigma_n^2\mathbf{I} \tag{A.18}$$

With

- $\mathbf{R}_y$ est la matrice de covariance de $\mathbf{y}(t)$.
- $\mathbf{R}_n$ est la matrice de covariance du bruit.
- $\mathbf{\Lambda}_s$ est la matrice de covariance de $s(t)$ et $*$ désigne la transposée conjuguée.

La matrice $\mathbf{A}$ est assumé de plein rang et inversible. Le rang de $\mathbf{R}_y$ est égal au nombre de rayons P. Autrement dit, il existe P valeurs propres non nulles correspondant à raypaths. De manière équivalente, le plus petit $M - P$ valeurs propres de $\mathbf{R}_y$ sont égaux à zéro. Par conséquent, si les valeurs propres de $\mathbf{R}$ est disposé dans un ordre décroissant comme $\lambda_1 \geq \lambda_2 \cdots \geq \lambda_P$, la valeur de la plus petite des valeurs propres $M - P$ correspondant au bruit est :

$$\lambda_{P+1} = \lambda_{P+2} = \cdots = \lambda_M = \sigma_n^2 \tag{A.19}$$

Par conséquent, il n'est pas difficile de déterminer à partir de P la multiplicité de la plus petite valeur propre de $\mathbf{R}$. Mais dans la pratique, $\mathbf{R}$ est inconnue. Il est généralement estimé par matrice de covariance :

$$\hat{\mathbf{R}} = \frac{1}{N}\sum_{t=1}^{N}\mathbf{x}(t)\mathbf{x}^*(t) \tag{A.20}$$

Où N est le nombre d'échantillons. Parce que $\hat{\mathbf{R}}$ est calculé à partir d'un nombre fini d'échantillons, la plus petite valeur propre $M - P$ n'est plus égale à l'autre et σ_n^2 avec probabilité un. Ainsi, dans la plupart des cas, le nombre de raypaths ne peut pas être déterminée directement par la méthode ci-dessus.

A.7.2 Exponentiel Fitting Test

Il est nécessaire de proposer une méthode qui prend en compte la limitation du nombre d'échantillons en vue de limitations pratiques. Pour cette raison, un test utilisant une expression analytique du bruit valeurs propres est présenté dans cette section.

A.7.2.1 Profil des valeurs propres

Afin d'établir le profil moyen des valeurs propres de bruit, nous devons calculer l'espérance de chaque valeur propre. Pour la valeur moyenne nulle de bruit blanc gaussien de puissance σ_n^2, la matrice de covariance de l'échantillon a une distribution de Wishart avec N degrés de liberté. Il s'agit d'une généralisation multivariée de χ^2 la distribution et dépend M, N, σ_n^2. Dans ce cas, la probabilité conjointe des valeurs propres ordonnées et la distribution de chaque valeur propre peut être obtenu [Joh] [KS74]. La probabilité jointe des valeurs propres ordonnées est indiquée par (A.21). Les distributions de chaque valeur propre est donné comme polynôme zonale, qui est un polynôme symétrique multivariée homogène et un outil fondamental dans les statistiques et l'analyse multivariée [Jam60] [Jam61] ainsi que dans la théorie des matrices aléatoires [Mui82]. Cependant, le calcul de l'espérance de chaque valeur propre de la probabilité conjointe montré par (A.21) et la distribution de chaque valeur propre en utilisant des polynômes zonaux sont calcul compliqué et donne des résultats difficiles à résoudre pour le moment.

$$\rho(\lambda_1, \ldots, \lambda_M) = \alpha \; exp\left(-\frac{1}{2\sigma^2}\sum_{i=1}^{M}\lambda_i\right)\left(\prod_{i=1}^{M}\lambda_i\right)^{\frac{1}{2}(N-M-1)}\prod_{i>j}(\lambda_j - \lambda_i) \tag{A.21}$$

Par conséquent, nous utilisons une approche alternative pour se rapprocher du profil moyen des valeurs propres du bruit ordonnée avec l'aide de moments d'ordre premier et deuxième valeurs propres.

A partir des résultats de simulation, il s'avère que une loi exponentielle pourrait être une bonne approximation du profil moyen des valeurs propres de bruit commandés. Un résultat comme une illustration pour $M = 15$ est montré dans la Fig. A.9. Fig. A.9 (a) et Fig. A.9. (b) montrent huit réalisations, respectivement, pour les cas de $N = 15$ and $N = 1025$. Mathématiquement, la loi exponentielle peut être définie comme (A.22) avec deux paramètres inconnus λ_1 and r_e.

$$\lambda_i = \lambda_1 r_e^{i-1}{}_{M,N}, \quad i \in 2, \ldots M \tag{A.22}$$

Pour déterminer λ_1 et r_e, nous considérons que les premier et deuxième moments de la trace de l'erreur de la matrice de covariance du bruit de $\mathbf{\Psi}$, où $\mathbf{\Psi}$ est définie par (A.23).

$$\mathbf{\Psi} = \hat{\mathbf{R}}_n - \mathbf{R}_n = \hat{\mathbf{R}}_n - \sigma_n^2\mathbf{I} \tag{A.23}$$

Étant donné que $E(tr[\mathbf{\Psi}_{ij}]) = 0$, (A.24), on obtient :

$$M\sigma^2 = \sum_{i=1}^{M} \lambda_i \tag{A.24}$$

Selon la définition de la matrice de covariance d'erreur, l'élément Ψ_{ij} de $\mathbf{\Psi}$ est exprimée en tant que :

$$\Psi_{ij} = \frac{1}{N} \sum_{i=1}^{N} n_i(t) n_j^*(t) - \sigma_n^2 \delta_{ij} \tag{A.25}$$

Par conséquent, $E[\|\Psi_{ij}\|^2]$ peut être calculée comme suit :

$$\begin{aligned} E\left[\|\Psi_{ij}\|^2\right] &= E\left[\left\|\frac{1}{N}\sum_{i=1}^{N} n_i(t) n_j^*(t) - \sigma_n^2\delta_{ij}\right\|^2\right] \\ &= E\left[\left\|\frac{1}{N}\sum_{i=1}^{N} n_i(t) n_j^*(t)\right\|^2\right] + E\left[\|\sigma_n^2\delta_{ij}\|^2\right] \\ &\quad + E\left[-2\Re\left\{\sigma_n^2\delta_{ij}\frac{1}{N}\sum_{i=1}^{N} n_i(t) n_j^*(t)\right\}\right] \end{aligned} \tag{A.26}$$

Lorsque $\Re$ représente la partie réelle d'une valeur complexe. Chaque terme de (6.14) peuvent être calculés respectivement :

$$\begin{aligned} E\left[\left\|\frac{1}{N}\sum_{i=1}^{N} n_i(t) n_j^*(t) - \sigma_n^2\delta_{ij}\right\|^2\right] &= \frac{1}{N^2} N\sigma^4 = \frac{1}{N}\sigma_n^4 \\ E\left[\|\sigma_n^2\delta_{ij}\|^2\right] &= \sigma_n^4\delta_{ij} \\ E\left[-2\Re\left\{\sigma_n^2\delta_{ij}\frac{1}{N}\sum_{i=1}^{N} n_i(t) n_j^*(t)\right\}\right] & \\ = -\frac{2\sigma_n^2\delta_{ij}}{N} E\left[\Re\left\{\sum_{i=1}^{N} n_i(t) n_j^*(t)\right\}\right] & \\ = -\frac{2\sigma_n^2\delta_{ij}}{N}\left(\frac{N\sigma_n^2}{2}\right) = -\sigma_n^4\delta_{ij} & \end{aligned} \tag{A.27}$$

Enfin,

$$E\left[\|\Psi_{ij}\|^2\right] = \frac{1}{N}\sigma_n^4 + \sigma_n^4\delta_{ij} - \sigma_n^4\delta_{ij} = \frac{1}{N}\sigma^4 \tag{A.28}$$

Depuis la trace d'une matrice reste inchangée lorsque les changements de base, il

s'ensuit que :

$$\sum_{i,j} E\left\{\left\|\Psi_{ij}\right\|^2\right\} = E(tr[\hat{\mathbf{R}}_n - \mathbf{R}_n]^2) = M^2\frac{\sigma_n^4}{N} \tag{A.29}$$

et en utilisant une approximation,

$$M^2\frac{\sigma_n^4}{N} = \sum_{i=1}^{M}(\lambda_i - \sigma_n^2)^2 \tag{A.30}$$

En combinant de (A.22) et (A.24), on obtient :

$$M\sigma_n^2 = \sum_{i=1}^{M}\lambda_1 r_e^{i-1} \tag{A.31}$$

$$\lambda_1 = MJ_M\sigma_n^2 \tag{A.32}$$

oú :

$$J_M = \frac{1-r}{1-r^M} \tag{A.33}$$

et il peut obtenir que :

$$(\lambda_i - \sigma_n^2) = (MJr^{i-1} - 1)\sigma_n^2 \tag{A.34}$$

En combinant (**??**) with (A.30), le taux de décroissance r_e est obtenu à partir de l'équation suivante :

$$\frac{M+N}{MN} = \frac{(1-r_e)(1+r_e^M)}{(1-r_e^M)(1+r_e)} \tag{A.35}$$

Dans (A.22), r devrait être une fonction exponentielle. Dans ce travail, nous supposons qu'il est égal à $e^{-2a_{id}}$ sur deux raisons. Une des raisons est que la forme de $e^{-2a_{id}}$ est similaire au profil du bruit ordonnée de prise en charge de courte longueur (Fig. 1. (A)). L'autre raison est qu'il est plus facile d'acquérir la valeur de a_{id} dans le cadre (21) grâce à la même index. En substituant $r_e = e^{-2a_{id}}$, (A.35) devient :

$$\frac{Mtanh(a_{id}) - tanh(a_{id})}{Mtanh(Ma_{id})} = \frac{1}{N} \tag{A.36}$$

où tanh la fonction tangente hyperbolique, donnée par :

$$tanh(a_{id}) = \frac{\sinh(a_{id})}{\cosh(a_{id})} = \frac{e^{2a_{id}} - 1}{e^{2a_{id}} + 1} \tag{A.37}$$

L'expression du 4ème ordre série de Taylor de tanh (a) est écrit comme suit,

$$tanh(a_{id}) = a_{id} - \frac{a_{id}^3}{3} + \frac{2a_{id}^5}{15} \tag{A.38}$$

Insertion (A.38) to (A.36), l'équation suivante biquadratique est produit comme :

$$\sigma^4 - \frac{15}{M^2+2}a_{id}^2 + \frac{45M^2}{N(M^2+1)(M^2+2)} = 0 \tag{A.39}$$

La solution positive de(6.27) est donnée par :

$$a_{id}(M,N) = \sqrt{\frac{15}{2(M^2+2)}\left[1 - \sqrt{\frac{4M(M^2+2)}{5N(M^2-1)}}\right]} \tag{A.40}$$

A.7.2.2 Principe de l'EFT récursif

Avec l'hypothèse des P rayons décorrélée ou partiellement corrélés, l'EFT récursif est principalement basée sur la comparaison entre le profil des valeurs propres ordonnées de la matrice de covariance d'observation et le profil théorique des valeurs propres de bruit commandés. Un point d'arrêt se produit lorsque valeur propre du signal apparaît. La stratégie de test général est démontré par la figure. A.10. Dans la Fig. A.10, deux valeurs propres correspondantes à des rayons sont contenues dans le profil de valeurs propres observables.

Le test récursif est démarré à partir de $P_t = 1$. En supposant que la P_t plus petites valeurs propres sont les valeurs propres de bruit, la précédente valeur propre λ_{M-P_t} est testée pour déterminer si elle correspond à un bruit ou un rayon. Pour chaque valeur de P_t, le test est effectué en deux étapes :

Dans la première étape, nous prévoyons la valeur de λ_{M-P_t} selon le modèle exponentiel ((A.32)) :

$$\hat{\lambda}_{M-P_t} = (P_t+1)J_{P_t+1}\hat{\sigma_n}^2 \tag{A.41}$$

où :

$$J_{P_t+1} = \frac{1 - r_{P_t+1}}{1 - r_{P_t+1}^{P_t+1}} \tag{A.42}$$

$$\hat{\sigma}_n^2 = \frac{1}{P_t+1}\sum_{i=0}^{P_t}\lambda_i \tag{A.43}$$

L'équation de prédiction est obtenue par la combinaison de (A.41), (A.42) et (A.43) :

$$\hat{\lambda}_{M-P_t} = J_{P_t+1} \sum_{i=0}^{P_t} \lambda_{M-i} \tag{A.44}$$

r_{P+1} est calculé en obtenant d'abord a utilisant (A.40) , puis en utilisant la relation $r = e^{-2a_{in}}$, ou $(P_t + 1)$ doit être utilisé à la place de M.

Dans la seconde étape, deux hypothèses sont définies comme suit :

- H_{P_t+1} : λ_{M-P_t} est une valeur propre correspondant au bruit.
- $\overline{H}_{P_t+1}$: λ_{M-P_t} est une valeur propre correspondant à un trajet de rayon.

Pour trancher entre ces hypothèses, l'erreur absolue de λ_{M-P_t} et $\hat{\lambda}_{M-P_t}$ est calculée et ensuite être comparée à un seuil η_{P_t}. C'est à dire :

$$H_{P_t+1} : \left|\lambda_{M-P_t} - \hat{\lambda}_{M-P_t}\right| \leq \eta_{P_t} \tag{A.45}$$

$$\overline{H}_{P_t+1} : \left|\lambda_{M-P_t} - \hat{\lambda}_{M-P_t}\right| > \eta_{P_t} \tag{A.46}$$

Si l'erreur absolue d'une certaine valeur P est inférieur au seuil, réinitialisez $P_t = P_t + 1$ et le test est répété jusquà $P_t = M - 1$; Sinon , le processus récursif est arrêté avec le résultat de la détection de $P = M - P_t$.

Enfin, nous utilisons la distribution empirique du profil de bruit uniquement des valeurs propres de trouver un seuil approprié. Par exemple, 10000 réalisations sont générés pour $N = 15$ ainsi que des échantillons d'un tableau de $M = 15$ capteurs. Le profil moyen de la valeur propre du bruit commandé est calculé, qui est représenté par la courbe du milieu de la figure. A.9. (a). Seuls huit réalisations sont affichées pour expliquer.

A.7.3 Simulations

Dans cette section, nous illustrons les performances de l'EFT sur des données de simulation. La simulation est composée de deux groupes d'expériences. Dans le premier groupe, nous testons la performance générale de l'EFT avec différents SNR. Dans le second groupe, la performance de l'EFT est calculée pour des rayons proches.

A.7.4 Performances pour divers RSB

Pour différents RSB et pour différent nombre d'échantillons sur six expériences, un premier groupe d'expériences est réalisé. Dans ces expériences, cinq rayons cohérentes ar-

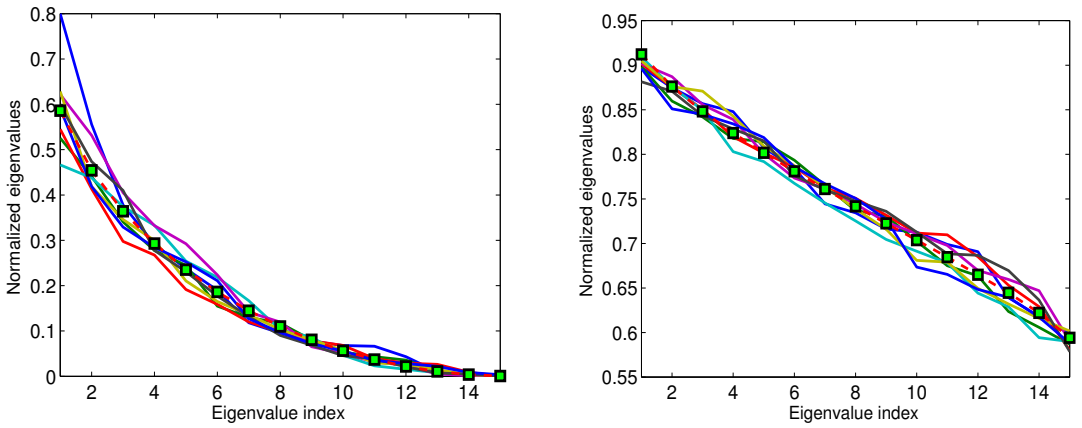

(a) (b)

FIGURE A.9 – Profil des valeurs propres ordonnées de bruit sur huit réalisations (a) Profil des valeurs propres ordonnées de bruit estimés par 15 échantillons. (b) Profil des valeurs propres ordonnées de bruit estimée par 1025 échantillons.

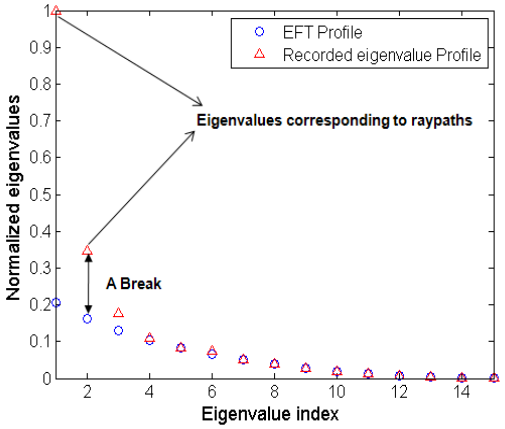

FIGURE A.10 – Profils des valeurs propres avec deux valeurs propres correspondant aux rayons. Lorsque la valeur propre correspond au rayons apparaît, une rupture existe entre le profil de l'EFT et le profil des valeurs propres enregistrées.

rivent sur 15 capteurs.

	RSB (dB)	AIC	MDL	EFT
$N = 1025$	20	14	14	—
	10	14	14	—
	5	14	12	—
$N = 15$	20	—	—	5
	10	—	—	5
	5	—	—	11

TABLE A.7 – Nombre de raypaths détectés par l'AIC, MDL et l'EFT dans le premier groupe d'expériences (le nombre réel de trajets $P = 5$)

A.7.4.1 Performance pour trajets proches

Pour illustrer les performances de notre algorithme lorsque les trajets arrivent de plus près, deux expériences (RSB = 20dB) pour $N = 1025$ et $N = 15$ sont effectuées. Dans ces expériences, la différence n'est pas seulement les deux premiers rayons qui sont plus proches que les exemples dans le premier groupe d'expériences, mais aussi le trajet du troisième rayon traverse les deux premiers en raison de l'angle d'arrivée négatif (indiqué sur la figure 6.6 (a).). Les résultats de détection sont présentés dans le tableau A.8

	RSB (dB)	AIC	MDL	EFT
$N = 1025$	20	14	14	—
$N = 15$	20	—	—	5

TABLE A.8 – Nombre de raypaths détectés par l'AIC, MDL et l'EFT dans le deuxième groupe d'expériences (le nombre réel de raypaths $P = 5$)

A.7.4.2 Expérience à petite échelle

Une expérience à petite échelle est abordée dans cette partie, afin que nous puissions mieux illustrer la performance de nos méthodes. Le dispositif expérimental est schématisé comme dans la Fig. **??**. Le principe sur lequel se fondent ces expériences est la suivante : si la fréquence des signaux est multipliée par un facteur et les distances spatiales sont divisées par le même facteur, les phénomènes physiques se déroulant dans l'environnement reste le même. À savoir, l'expérience à petite échelle reproduit les phénomènes physiques réels qui se produisent dans la nature à une plus petite échelle à l'intérieur du laboratoire. Il réalise un coût réduit et une expérience totalement contrôlés. L'expérience présentée ici a été réalisée à l'ISTerre (Institut des Sciences de la Terre) dans la cuve à ultrasons qui est développé par P. Roux. Dans ce réservoir, un guide d'onde de 5-10 m de profondeur et de longueur 1-1.5 m est construit. Une barre d'acier sert de fond, ce qui est

très réfléchissante et parfaitement plat. En particulier, un capteur est fixé à 0.0263m en profondeur comme source. Un réseau vertical constituéde 64 capteurs est utilisé comme récepteur. La profondeur du premier récepteur est de $3.55 \times 10^{-3}m$. L'intervalle de deux récepteurs adjacents est de 0.75×10^{-3}m. La distance entre la source et le récepteur de référence est 1,1437 m et le signal de source est 1 MHz de bande passante de fréquence avec une fréquence centrale de 1,2 MHz.

Dans ce chapitre, une méthode NWEFT est proposé pour détecter automatiquement le nombre de raypaths en guide d'onde en eau peu profonde. Comme AIC et MDL sont contraints par la durée du signal reçu, ils ne parviennent pas à détecter correctement le nombre de rayons. En revanche, la méthode proposée permet de déterminer le nombre de raypaths en utilisant des échantillons de courte longueur. Grace au processus de blanchiment du bruit, elle peut être appliquée à l'environnement d'application réelle. À l'avenir, l'influence de la corrélation entre raypaths ainsi que la corrélation entre le bruit et le trajet des rayons doivent être étudiés. En outre, cette méthode peut être étendue à des échantillons mi-longueur (entre 15 et 1025).

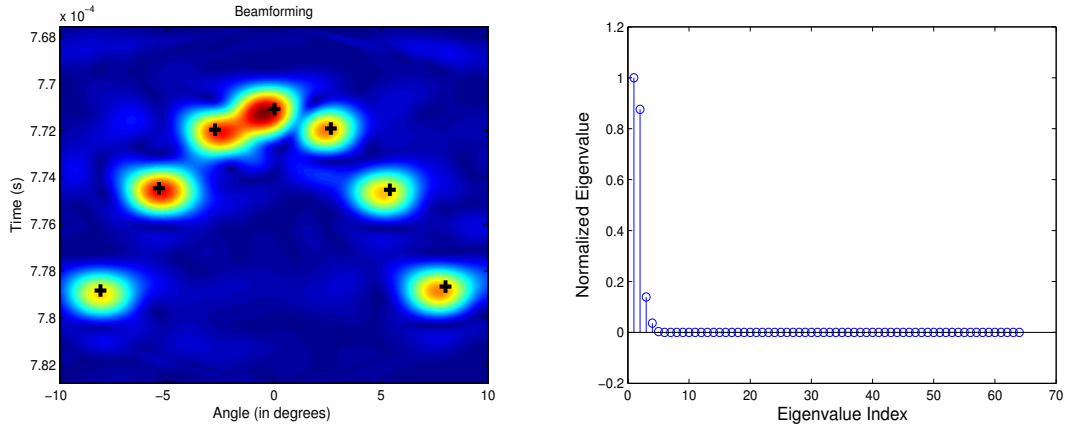

(a) (b)

FIGURE A.11 – (a) Résultat de la formation de voies avec emplacement théorique de 64 échantillons. Il fournit une valeur de référence pour vérifier le résultat de séparation de la méthode proposée. (b) Profil des valeurs propres ordonnées de 64 échantillons.

A.8 Conclusion

Dans cette thèse, nous avons présenté nos études sur le problème de la séparation de source et la détection (ou la localisation de source) en acoustique sous-marine, en particulier dans le contexte des eaux peu profondes. Notre objectif principal est de proposer une méthode de traitement à haute résolution pour la séparation et la détection des

rayons dans une perspective plus pratique, ce qui signifie que certaines limitations pratiques ont été pris en compte.

A.8.1 Sommaire des contributions

Techniques d'enquête sur la séparation de sources (ou localisation) en acoustique sous-marine

Sur la base des des techniques de séparation source bien connue (ou localisation) en acoustique sous-marine, tels que la formation de voies, les tecniques de Matchfield processing, les techniques à retournement temporel, etc, mais aussi les nouvelles méthodes telles que la double formation de voies, l' échantillonneur de Gibbs, etc, nous divisons ces méthodes en deux catégories, selon qu'ils sont sous l'hypothèse de propagation dans un espace homogène. Excepté l'échantillonneur de Gibbs, elles sont toutes des méthodes du type de la formation de voies. la Limitation de résolution existe encore dans ces algorithmes et à l'amélioration de la résolution est encore une perspective prometteuse pour ces méthodes. Nous espérons que notre tentative d'analyse globale sur ces méthodes peuvent fournir un guide pour un lecteur intéressé.

Enquête sur les méthodes à haute résolution

Dans le domaine de traitement de signaux, des méthodes haute résolution sont introduites pour améliorer la performance des méthode classique comme la formation de voies. Les limites et les avantages de chaque méthode sont discutées et comparées.

Proposition d'un traitement à haute résolution pour séparer les rayons

Les signaux cohérents existent également dans le cadre de l'eau peu profonde car les rayons multiples sont produites par le même signal émis à travers de multiples chemins de propagation. Pour faire face à cette difficulté, et mettre en place un traitement à haute résolution, nous avons combiné l'algorithme de lissage en fréquence avec l'algorithme MUSICAL pour proposer l'algorithme dit du smoothing-MUSICAL pour la TAO en eau peu profonde.

Présentation du test EFT pour la détection automatique du nombre de raypaths

L'algorithme smoothing-MUSICAL sépare avec succès les rayons sur la base de la connaissance au préalable du nombre de rayons. Pour pallier les lacunes des critères classiques de la théorie de l'information (AIC et MDL), une technique EFT a été développé permettant l'exploitation à petite longueur de l'échantillon. De plus, nous avons fait une adaptation pour un environnement du bruit coloré.

A.8.2 Perspectives

En ce qui concerne les perspectives, nous tenons à les réaliser en fonction de deux aspects : 1) la variation de l'amélioration, l'extension ou des algorithmes proposés, 2) l'utilisation potentielle des méthodes à haute résolution dans les applications pertinentes de l'acoustique sous-marine.

Amélioration de lissage MUSICAL selon l'analyse d'erreur

En effet, nous avons tiré comme la conclusion de ces expériences que le lmoothing-MUSICAL a largement amélioré la performance de séparation. Cependant, le moothing-MUSICAL a encore quelques erreurs de séparation par rapport aux valeurs théoriques des emplacements des rayons. Plusieurs algorithmes, comme la méthode de référence. [VS94] devraient être développées.

Multiples dimensions de lissage MUSICAL méthodes d'eau peu profonde OAT

Inspiré par la double formation de voies en Réf. [IRN*09], la méthode de type double lissage moothing-MUSICAL serait étendue à la configuration de réseau à réseau afin de continuer à améliorer la résolution.

méthodes haute résolution d'ordre supérieur pour des applications dans un guide d'onde

Les méthodes de type MUSICAL-4 ont été développés pour les processus non-gaussien de signal de [Car89]. Elles ont été appliquées en sonar, radar, traitement du signal sismique pour pallier les inconvénients des algorithmes basés sur les statistique d'ordre 2. Les algorithmes d'ordre supérieur devraient être considérés et mis au point pour les applications dans un guide d'onde.

Inversion tomographique utilisant des méthodes à haute résolution

Une possible poursuite serait de combiner ces méthodes à haute résolution avec des méthodes d'inversion apour l'analyse et la recherche en tomographoe des eaux peu profondes. Cette approchie doit être explorées et appliquées sur données expérimentales.

Amélioration et extension de la méthode de détection proposée

Comme nous l'avons présenté, l'algorithme de détection proposé est encore limité par la robustesse au bruit, ainsi que les corrélations existant entre les signaux et le bruit. Ainsi, nous devons faire quelques tentatives relatives à remédier à ces inconvénients. Par ailleurs, l'algorithme de détection a la possibilité d'être étendu à détecter avec succès le nombre de rayons basées sur des échantillons de longueur moyenne.

Bibliography

[AASAM04] Al-Ardi E., Shubair R., Al-Mualla M.: Computationally efficient high-resolution doa estimation in multipath environment. *Electronics Letters 40*, 14 (2004), 908–910. 81

[ABC*97] Apel J., Badiey M., Chiu C., Finette S., Headrick R., Kemp J., Lynch J., Newhall A., Orr M., Pasewark B., et al.: An overview of the 1995 swarm shallow-water internal wave acoustic scattering experiment. *Oceanic Engineering, IEEE Journal of 22*, 3 (1997), 465–500. 21, 140

[Aka73] Akaike H.: Information theory and an extension of the maximum likelihood principle. In *Second international symposium on information theory* (1973), vol. 1, Springer Verlag, pp. 267–281. 110

[Aka74] Akaike H.: A new look at the statistical model identification. *Automatic Control, IEEE Transactions on 19*, 6 (1974), 716–723. 110

[Bae81] Baer R.: Propagation through a three-dimensional eddy including effects on an array. *The Journal of the Acoustical Society of America 69* (1981), 70. 11, 137

[Bar54] Bartlett M.: A note on the multiplying factors for various χ 2 approximations. *Journal of the Royal Statistical Society. Series B (Methodological)* (1954), 296–298. 106, 158

[Bar83] Barabell A.: Improving the resolution performance of eigenstructure-based direction-finding algorithms. In *Acoustics, Speech, and Signal Processing, IEEE International Conference on ICASSP'83.* (1983), vol. 8, IEEE, pp. 336–339. 61

[BB02] Bourennane S., Bendjama A.: Locating wide band acoustic sources using higher order statistics. *Applied Acoustics 63*, 3 (2002), 235–251. 54

[BBB*82] Behringer D., Birdsall T., Brown M., Cornuelle B., Heinmiller R., Knox R., Metzger K., Munk W., Spiesberger J., Spindel R., et al.: A demonstration of ocean acoustic tomography. 18

[BBR*96] Booth N., Baxley P., Rice J., Schey P., Hodgkiss W., D'Spain G., Murray J.: Source localization with broad-band matched-field processing in shallow water. *Oceanic Engineering, IEEE Journal of 21*, 4 (1996), 402–412. 16, 43

[BBS02] Bourennane S., Bendjama A., Sessarego J.: Propagator methods for finding wideband source parameters. *Applied acoustics 63*, 3 (2002), 253–281. 54

[Ber85] Berger J.: *Statistical decision theory and Bayesian analysis*. Springer, 1985. 34

[BG88] Buckley K., Griffiths L.: Broad-band signal-subspace spatial-spectrum (bass-ale) estimation. *Acoustics, Speech and Signal Processing, IEEE Transactions on 36*, 7 (1988), 953–964. 80, 82

[BHF09] Bourennane S., Han D., Fossati C.: Fast coherent signal subspace-based method for bearing and range of buried objects estimation in the presence of colored noise. *Selected Topics in Applied Earth Observations and Remote Sensing, IEEE Journal of 2*, 4 (2009), 329–338. 54

[BK79] Borgiotti G., Kaplan L.: Superresolution of uncorrelated interference sources by using adaptive array techniques. *Antennas and Propagation, IEEE Transactions on 27*, 6 (1979), 842–845. 41

[BK80] Bienvenu G., Kopp L.: Adaptivity to background noise spatial coherence for high resolution passive methods. In *Acoustics, Speech, and Signal Processing, IEEE International Conference on ICASSP'80.* (1980), vol. 5, IEEE, pp. 307–310. 53

[Boh84] Bohme J.: Estimation of source parameters by maximum likelihood and nonlinear regression. In *Acoustics, Speech, and Signal Processing, IEEE International Conference on ICASSP'84.* (1984), vol. 9, IEEE, pp. 271–274. 56, 57

[Boh85] Bohme J.: Source-parameter estimation by approximate maximum likelihood and nonlinear regression. *Oceanic Engineering, IEEE Journal of 10*, 3 (1985), 206–212. 56

[Boh86] Bohme J.: Estimation of spectral parameters of correlated signals in wavefields. *Signal Processing 11*, 4 (1986), 329–337. 58

[Böh95] Böhme J.: Statistical array signal processing of measured sonar and seismic data. In *Proceedings of SPIE* (1995), vol. 2563, p. 2. 53, 143

[BX90] Buckley K., Xu X.: Spatial-spectrum estimation in a location sector. *Acoustics, Speech and Signal Processing, IEEE Transactions on 38*, 11 (1990), 1842–1852. 54

[Cap69] Capon J.: High-resolution frequency-wavenumber spectrum analysis. *Proceedings of the IEEE 57*, 8 (1969), 1408–1418. 41

[Car89] Cardoso J.: Source separation using higher order moments. In *Acoustics, Speech, and Signal Processing, 1989. ICASSP-89., 1989 International Conference on* (1989), IEEE, pp. 2109–2112. 132, 170

[CD04] Chang C., Du Q.: Estimation of number of spectrally distinct signal sources in hyperspectral imagery. *Geoscience and Remote Sensing, IEEE Transactions on 42*, 3 (2004), 608–619. 122

[CFA06] Chevalier P., Ferréol A., Albera L.: High-resolution direction finding from higher order statistics: The-music algorithm. *Signal Processing, IEEE Transactions on 54*, 8 (2006), 2986–2997. 132

[Cho02] Choi Y.: Subspace-based coherent source localisation with forward/backward covariance matrices. In *Radar, Sonar and Navigation, IEE Proceedings-* (2002), vol. 149, IET, pp. 145–151. 81, 146

[CKS92] Collins M., Kuperman W., Schmidt H.: Nonlinear inversion for ocean-bottom properties. *The Journal of the Acoustical Society of America 92*, 5 (1992), 2770–2783. 21

[CM94] Cardoso J., Moulines É.: How much more doa information in higher-order statistics? In *Proc. IEEE Workshop on Statistical Signal and Array Processing* (1994), Citeseer. 66

[CN89] Chiang H., Nikias C.: The esprit algorithm with higher-order statistics. In *Higher-Order Spectral Analysis, 1989. Workshop on* (1989), IEEE, pp. 163–168. 65

[Col93a] Collins M.: A split-step padé solution for the parabolic equation method. *The Journal of the Acoustical Society of America 93* (1993), 1736. 17

[Col93b] Collins M.: A two-way parabolic equation for elastic media. *The Journal of the Acoustical Society of America 93* (1993), 1815. 17

[Cox73] Cox H.: Resolving power and sensitivity to mismatch of optimum array processors. *The Journal of the acoustical society of America 54* (1973), 771. 41

[CZO87] Cox H., Zeskind R., Owen M.: Robust adaptive beamforming. *Acoustics, Speech and Signal Processing, IEEE Transactions on 35*, 10 (1987), 1365–1376. 28, 41

[DC99] Du Q., Chang C.: An interference rejection-based radial basis function neural network for hyperspectral image classification. In *Neural Networks, 1999. IJCNN'99. International Joint Conference on* (1999), vol. 4, IEEE, pp. 2698–2703. 122

[DDH09] Dettmer J., Dosso S., Holland C.: Model selection and bayesian inference for high-resolution seabed reflection inversion. *The Journal of the Acoustical Society of America 125* (2009), 706. 105

[DJ92] Dowling D., Jackson D.: Narrow-band performance of phase-conjugate arrays in dynamic random media. *The Journal of the Acoustical Society of America 91* (1992), 3257. 42

[Dju94] Djuric P.: Model selection based on asymptotic bayes theory. In *Statistical Signal and Array Processing, 1994., IEEE Seventh SP Workshop on* (1994), IEEE, pp. 7–10. 106, 158

[Dju96] Djuric P.: A model selection rule for sinusoids in white gaussian noise. *Signal Processing, IEEE Transactions on 44*, 7 (1996), 1744–1751. 106, 158

[DL90] Daugherty J., Lynch J.: Surface wave, internal wave, and source motion effects on matched field processing in a shallow water waveguide. *The Journal of the Acoustical Society of America 87* (1990), 2503. 41

[Dow93] Dowling D.: Phase-conjugate array focusing in a moving medium. *The Journal of the Acoustical Society of America 94* (1993), 1716. 42

[Dow94] Dowling D.: Acoustic pulse compression using passive phase-conjugate processing. *The Journal of the Acoustical Society of America 95* (1994), 1450. 42

[Dud06] Duda T.: *Initial results from a Cartesian three-dimensional parabolic equation acoustical propagation code*. Tech. rep., DTIC Document, 2006. 17

[DWM01] Dzieciuch M., Worcester P., Munk W.: Turning point filters: Analysis of sound propagation on a gyre-scale. *The Journal of the Acoustical Society of America 110* (2001), 135. 30, 90, 95, 153

[DZM*04] Dahl P., Zhang R., Miller J., Bartek L., Peng Z., Ramp S., Zhou J., Chiu C., Lynch J., Simmen J., et al.: Overview of results from the asian seas international acoustics experiment in the east china sea. *Oceanic Engineering, IEEE Journal of 29*, 4 (2004), 920–928. 21, 140

[EAH*02] Edelmann G., Akal T., Hodgkiss W., Kim S., Kuperman W., Song H.: An initial demonstration of underwater acoustic communication using time reversal. *Oceanic Engineering, IEEE Journal of 27*, 3 (2002), 602–609. 21, 140

[EC83] Er M., Cantoni A.: Derivative constraints for broad-band element space antenna array processors. *Acoustics, Speech and Signal Processing, IEEE Transactions on 31*, 6 (1983), 1378–1393. 41

[EEM78] Ehrenberg J., Ewart T., Morris R.: Signal-processing techniques for resolving individual pulses in a multipath signal. *The Journal of the Acoustical Society of America 63* (1978), 1861. 31, 33

[EJS81] Evans J., Johnson J., Sun D.: High resolution angular spectrum estimation techniques for terrain scattering analysis and angle of arrival estimation. In *Proc. 1st ASSP Workshop Spectral Estimation* (1981), pp. 134–139. 80, 145

[ESJ82] Evans J., Sun D., Johnson J.: *Application of advanced signal processing techniques to angle of arrival estimation in ATC navigation and surveillance systems*. Tech. rep., DTIC Document, 1982. 80, 145

[FCD*00] Fink M., Cassereau D., Derode A., Prada C., Roux P., Tanter M., Thomas J., Wu F.: Time-reversed acoustics. *Reports on progress in Physics 63* (2000), 1933. 21

[Fin93] Fink M.: Time-reversal mirrors. *Journal of Physics D: Applied Physics 26* (1993), 1333. 42

[Fin97] Fink M.: Time reversed acoustics. *Physics Today 50* (1997), 34. 21

[Fin99] Fink M.: Time-reversed acoustics. *Scientific American 281*, 5 (1999), 91–97. 21

[FM00] Fishler E., Messer H.: On the use of order statistics for improved detection of signals by the mdl criterion. *Signal Processing, IEEE Transactions on 48*, 8 (2000), 2242–2247. 105, 158

[Foc65] Fock V.: *Electromagnetic diffraction and propagation problems*, vol. 1. Pergamon Press London, 1965. 16

[FPWC89] Fink M., Prada C., Wu F., Cassereau D.: Self focusing in inhomogeneous media with time reversal acoustic mirrors. In *Ultrasonics Symposium, 1989. Proceedings., IEEE 1989* (1989), IEEE, pp. 681–686. 42

[GB95] Gounon P., Bozinoski S.: High resolution spatio-temporal analysis by an active array. In *Acoustics, Speech, and Signal Processing, 1995. ICASSP-95., 1995 International Conference on* (1995), vol. 5, IEEE, pp. 3575–3578. 80, 82, 146

[GBB*04] Gawarkiewicz G., Brink K., Bahr F., Beardsley R., Caruso M., Lynch J., Chiu C.: A large-amplitude meander of the shelfbreak front during summer south of new england: Observations from the shelfbreak primer experiment. 21, 140

[GDM94] Gonen E., Dogan M., Mendel J.: Applications of cumulants to array processing: direction-finding in coherent signal environment. In *Signals, Systems and Computers, 1994. 1994 Conference Record of the Twenty-Eighth Asilomar Conference on* (1994), vol. 1, IEEE, pp. 633–637. 81

[GG84] Geman S., Geman D.: Stochastic relaxation, gibbs distributions, and the bayesian restoration of images. *Pattern Analysis and Machine Intelligence, IEEE Transactions on*, 6 (1984), 721–741. 35

[GJ82] Griffiths L., Jim C.: An alternative approach to linearly constrained adaptive beamforming. *Antennas and Propagation, IEEE Transactions on 30*, 1 (1982), 27–34. 28

[GLC96] Grouffaud J., Larzabal P., Clergeot H.: Some properties of ordered eigenvalues of a wishart matrix: application in detection test and model order selection. In *Acoustics, Speech, and Signal Processing, 1996. ICASSP-96. Conference Proceedings., 1996 IEEE International Conference on* (1996), vol. 5, IEEE, pp. 2463–2466. 106, 159

[GPL*97] Gawarkiewicz G., Pickart R., Lynch J., Chiu C., Smith K., Miller J.: The shelfbreak front primer experiment. *The Journal of the Acoustical Society of America 101* (1997), 3016. 21, 140

[GRS96] Gilks W., Richardson S., Spiegelhalter D.: *Markov chain Monte Carlo in practice*. Chapman & Hall/CRC, 1996. 35

[GS90] Gelfand A., Smith A.: Sampling-based approaches to calculating marginal densities. *Journal of the American statistical association* (1990), 398–409. 35

[Gu98] Gu H.: Estimating the number of signals and signal resolution. *Signal Processing, IEEE Transactions on 46*, 8 (1998), 2267–2270. 106, 158

[GVL80] Golub G., Van Loan C.: An analysis of the total least squares problem. *SIAM Journal on Numerical Analysis* (1980), 883–893. 63

[GVL96] Golub G., Van Loan C.: *Matrix computations*, vol. 3. Johns Hopkins Univ Pr, 1996. 63

[Har01] Harris R.: *A primer of multivariate statistics*. Lawrence Erlbaum, 2001. 122

[HFB*10] Han D., Fossati C., Bourennane S., et al.: Localization of buried objects in presence of phase errors and unkown noise. *In proceeding of 18th European Signal Processing Conference.* (2010), 1354–1358. 54

[HN99] Hawkes M., Nehorai A.: Effects of sensor placement on acoustic vector-sensor array performance. *Oceanic Engineering, IEEE Journal of 24*, 1 (1999), 33–40. 67

[HN03] Hawkes M., Nehorai A.: Wideband source localization using a distributed acoustic vector-sensor array. *Signal Processing, IEEE Transactions on 51*, 6 (2003), 1479–1491. 67

[Hot33] Hotelling H.: Analysis of a complex of statistical variables into principal components. *Journal of educational psychology 24*, 6 (1933), 417. 53

[HSK*99] Hodgkiss W., Song H., Kuperman W., Akal T., Ferla C., Jackson D.: A long-range and variable focus phase-conjugation experiment in shallow water. *The Journal of the Acoustical Society of America 105* (1999), 1597. 21, 140

[IRN*09] Iturbe I., Roux P., Nicolas B., Virieux J., Mars J.: Shallow-water acoustic tomography performed from a double-beamforming algorithm: simulation results. *Oceanic Engineering, IEEE Journal of 34*, 2 (2009), 140–149. 15, 21, 29, 32, 63, 79, 80, 132, 140, 170

[IRNM08] Iturbe I., Roux P., Nicolas B., Mars J.: Ocean acoustic tomography using a double-beamforming algorithm. *The Journal of the Acoustical Society of America 123*, 5 (2008), 3912–3912. 3, 21, 63, 140

[Jaf88] Jaffer A.: Maximum likelihood direction finding of stochastic sources: A separable solution. In *Acoustics, Speech, and Signal Processing, 1988. ICASSP-88., 1988 International Conference on* (1988), IEEE, pp. 2893–2896. 58

[JALT*11] Jiang L., Aulanier F., Le Touzé G., Nicolas B., Mars J.: Raypath separation with high resolution processing. In *proceedings of OCEANS, 2011 IEEE-Spain* (2011), IEEE, pp. 1–5. 82, 105, 146, 156

[Jam60] James A.: The distribution of the latent roots of the covariance matrix. *The Annals of Mathematical Statistics* (1960), 151–158. 112, 161

[Jam61] James A.: Zonal polynomials of the real positive definite symmetric matrices. *The Annals of Mathematics 74*, 3 (1961), 456–469. 112, 161

[JCG08] Jiang Y., Chapman N., Gerstoft P.: Short range travel time geoacoustic inversion with vertical line array. 133

[JD91] Jackson D., Dowling D.: Phase conjugation in underwater acoustics. *The Journal of the Acoustical Society of America 89* (1991), 171. 42

[JD92] Johnson D., Dudgeon D.: *Array signal processing: concepts and techniques*. Simon & Schuster, 1992. 28

[JKP*95] Jensen F., Kuperman W., Porter M., Schmidt H., Bartram J.: Computational ocean acoustics. *Quarterly Journal of the Royal Meteorological Society 121*, 525 (1995), 1177. 14, 138

[JM11a] Jiang L., Mars J.: Automatic detection of the number of raypaths. In *proceedings of OCEANS 2011* (2011), IEEE, pp. 1–4. 106, 159

[JM11b] Jiang L., Mars J.: Automatic detection of the number of raypaths in colored noise using short-length samples. *The Journal of the Acoustical Society of America 130*, 4 (2011), 2392. 106, 159

[JM11c] Jiang L., Mars. J. I.: Automatic detection of the number of raypaths in a shallow-water waveguide. *revised and submit to IEEE Journal of Ocean Engineering* (2011). 106, 159

[JM12] Jiang L., Mars. J. I.: Raypath separation with high resolution processing in a shallow-water waveguide. *Submit to The Journal of the Acoustical Society of America* (2012). 82, 146

[Joh] Johnson N.: Kotz. s.(1972): Distributions in statistics: Continuous multivariate distributions. 112, 161

[KB90] Kaveh M., Bassias A.: Threshold extension based on a new paradigm for music-type estimation. In *Acoustics, Speech, and Signal Processing, 1990. ICASSP-90., 1990 International Conference on* (1990), IEEE, pp. 2535–2538. 54

[KEK*01] Kim S., Edelmann G., Kuperman W., Hodgkiss W., Song H., Akal T.: Spatial resolution of time-reversal arrays in shallow water. *The Journal of the Acoustical Society of America 110* (2001), 820. 21, 140

[KFP92] Krim H., Forster P., Proakis J.: Operator approach to performance analysis of root-music and root-min-norm. *Signal Processing, IEEE Transactions on 40*, 7 (1992), 1687–1696. 54

[KHS*98] Kuperman W., Hodgkiss W., Song H., Akal T., Ferla C., Jackson D.: Phase conjugation in the ocean: Experimental demonstration of an acoustic time-reversal mirror. *The journal of the Acoustical Society of America 103* (1998), 25. 21, 44, 140

[KI80] Kuperman W., Ingenito F.: Spatial correlation of surface generated noise in a stratified ocean. *The Journal of the Acoustical Society of America 67* (1980), 1988. 38

[KKH*03] Kim S., Kuperman W., Hodgkiss W., Song H., Edelmann G., Akal T.: Robust time reversal focusing in the ocean. *The Journal of the Acoustical Society of America 114* (2003), 145. 16, 21, 47, 140

[KL04] Kuperman W., Lynch J.: Shallow-water acoustics. *Physics Today 57*, 10 (2004), 55–61. 16, 43

[Koo37] Koopmans T.: *Linear regression analysis of economic time series*. No. 20. De erven F. Bohn nv, 1937. 53

[KS74] Krishnaiah P., Schuurmann F.: On the evaluation of some distributions that arise in simultaneous tests for the equality of the latent roots of the covariance matrix. *Journal of multivariate analysis 4*, 3 (1974), 265–282. 112, 161

[Ksh72] Kshirsagar A.: *Multivariate analysis*, vol. 2. M. Dekker, 1972. 122

[Law56] Lawley D.: Tests of significance for the latent roots of covariance and correlation matrices. *Biometrika 43*, 1/2 (1956), 128–136. 106, 158

[LD12] Lin Y., Duda T.: A higher-order split-step fourier parabolic-equation sound propagation solution scheme. 17

[Lee48] Lee H.: Eigenvalues and canonical forms of matrices with quaternion coefficients. In *Proceedings of the Royal Irish Academy. Section A: Mathematical and Physical Sciences* (1948), vol. 52, JSTOR, pp. 253–260. 71

[LF46] Leontovich M., Fock V.: Solution of the problem of propagation of electromagnetic waves along the earthÂs surface by the method of parabolic equation. *Acad. Sci. USSR. J. Phys 10* (1946), 13–24. 16

[Lig73] Liggett W.: Passive sonar: fitting models to multiple time series. *Signal Processing* (1973), 327–345. 53, 143

[LJP*96] Lynch J., Jin G., Pawlowicz R., Ray D., Plueddemann A., Chiu C., Miller J., Bourke R., Parsons A., Muench R.: Acoustic travel-time perturbations due to shallow-water internal waves and internal tides in the barents sea polar front: Theory and experiment. *The Journal of the Acoustical Society of America 99*, 2 (1996), 803–821. 20, 140

[LL93] Lo Y., Lee S.: *Antenna Handbook: Applications*, vol. 3. Springer, 1993. 30

[LR01] Liavas A., Regalia P.: On the behavior of information theoretic criteria for model order selection. *Signal Processing, IEEE Transactions on 49*, 8 (2001), 1689–1695. 105, 106, 117, 158

[LTNM*11] Le Touzé G., Nicolas B., Mars J., et al.: Double music actif large bande pour la tomographie sous-marine. 132

[McC82] McClellan J.: Multidimensional spectral estimation. *Proceedings of the IEEE 70*, 9 (1982), 1029–1039. 63

[Men91] Mensa D.: High resolution radar cross-section imaging. *Boston, MA, Artech House, 1991, 280 p. 1* (1991). 64

[MF53] Morse P., Feshbach H.: Methods of theoretical physics. *International Series in Pure and Applied Physics, New York: McGraw-Hill, 1953 1* (1953). 29

[Mic00] Michalopoulou Z.: A gibbs sampling approach to matched-field source localization and deconvolution. *The Journal of the Acoustical Society of America 108* (2000), 2646. 15, 35, 36

[Mil69] Milder D.: Ray and wave invariants for sofar channel propagation. *The Journal of the Acoustical Society of America 46* (1969), 1259. 20, 140

[MLBM05] Miron S., Le Bihan N., Mars J.: Vector-sensor music for polarized seismic sources localization. *EURASIP Journal on Applied Signal Processing 2005* (2005), 74–84. 16, 67, 71, 72

[MLBM06] Miron S., Le Bihan N., Mars J.: Quaternion-music for vector-sensor array processing. *Signal Processing, IEEE Transactions on 54*, 4 (2006), 1218–1229. 16, 67, 71, 72

[MM05] Michalopoulou Z., Ma X.: Source localization in the haro strait primer experiment using arrival time estimation and linearization. *The Journal of the Acoustical Society of America 118* (2005), 2924. 105, 158

[MP05] Michalopoulou Z., Picarelli M.: Gibbs sampling for time-delay-and amplitude estimation in underwater acoustics. *The Journal of the Acoustical Society of America 117* (2005), 799. 33, 35, 105, 158

[Mui82] Muirhead R.: *Aspects of multivariate statistical theory*, vol. 42. Wiley Online Library, 1982. 112, 161

[MW79] Munk W., Wunsch C.: Ocean acoustic tomography: A scheme for large scale monitoring. *Deep Sea Research Part A. Oceanographic Research Papers 26*, 2 (1979), 123–161. 10, 18, 137

[MW83] Munk W., Wunsch C.: Ocean acoustic tomography: Rays and modes. *Reviews of Geophysics 21*, 4 (1983), 777–793. 20, 140

[MWW95] Munk W., Worcester P., Wunsch C.: *Ocean acoustic tomography*. Cambridge Univ Pr, 1995. 3, 10, 18, 79, 137

[NE08] Nadakuditi R., Edelman A.: Sample eigenvalue based detection of high-dimensional signals in white noise using relatively few samples. *Signal Processing, IEEE Transactions on 56*, 7 (2008), 2625–2638. 106, 159

[NP94a] Nehorai A., Paldi E.: Acoustic vector-sensor array processing. *Signal Processing, IEEE Transactions on 42*, 9 (1994), 2481–2491. 67

[NP94b] Nehorai A., Paldi E.: Vector-sensor array processing for electromagnetic source localization. *Signal Processing, IEEE Transactions on 42*, 2 (1994), 376–398. 67

[OBP94] Odendaal J., Barnard E., Pistorius C.: Two-dimensional superresolution radar imaging using the music algorithm. *Antennas and Propagation, IEEE Transactions on 42*, 10 (1994), 1386–1391. 63

[Ows85] Owsley N.: Sonar array processing. *Array Signal Processing* (1985), 115–193. 53, 143

[PC01] Pignot P., Chapman N.: Tomographic inversion of geoacoustic properties in a range-dependent shallow-water environment. *The Journal of the Acoustical Society of America 110* (2001), 1338. 133

[PF91] Porat B., Friedlander B.: Direction finding algorithms based on high-order statistics. *Signal Processing, IEEE Transactions on 39*, 9 (1991), 2016–2024. 65

[Pie65] Pierce A.: Extension of the method of normal modes to sound propagation in an almost-stratified medium. *The Journal of the Acoustical Society of America 37* (1965), 19. 20, 140

[PM06] Paulus C., Mars J.: New multicomponent filters for geophysical data processing. *Geoscience and Remote Sensing, IEEE Transactions on 44*, 8 (2006), 2260–2270. 81, 82, 88, 146, 150

[PRK86] Paulraj A., Roy R., Kailath T.: A subspace rotation approach to signal parameter estimation. *Proceedings of the IEEE 74*, 7 (1986), 1044–1046. 62

[QBL06] Quinlan A., Barbot J., Larzabal P.: Automatic determination of the number of targets present when using the time reversal operator. *The Journal of the Acoustical Society of America 119* (2006), 2220. 106, 159

[QWZH05] Qi C., Wang Y., Zhang Y., Han Y.: Spatial difference smoothing for doa estimation of coherent signals. *Signal Processing Letters, IEEE 12*, 11 (2005), 800–802. 81

[RA96] Roger R., Arnold J.: Reliably estimating the noise in aviris hyperspectral images. *International Journal of Remote Sensing 17*, 10 (1996), 1951–1962. 120

[RCKH08] Roux P., Cornuelle B., Kuperman W., Hodgkiss W.: The structure of raylike arrivals in a shallow-water waveguide. *The Journal of the Acoustical Society of America 124* (2008), 3430. 3, 21, 29, 140

[Red87] Reddi S.: On a spatial smoothing technique for multiple source location. *Acoustics, Speech and Signal Processing, IEEE Transactions on 35*, 5 (1987), 709–709. 81, 146

[RH93] Rao B., Hari K.: Weighted subspace methods and spatial smoothing: Analysis and comparison. *Signal Processing, IEEE Transactions on 41*, 2 (1993), 788–803. 80, 146

[RIN*11] Roux P., Iturbe I., Nicolas B., Virieux J., Mars J.: Travel-time tomography in shallow water: Experimental demonstration at an ultrasonic scale. *The Journal of the Acoustical Society of America 130* (2011), 1232. 3, 21, 79, 140

[Ris78] Rissanen J.: Modeling by shortest data description. *Automatica 14*, 5 (1978), 465–471. 110, 111

[RJF*01] Rouseff D., Jackson D., Fox W., Jones C., Ritcey J., Dowling D.: Underwater acoustic communication by passive-phase conjugation: Theory and experimental results. *Oceanic Engineering, IEEE Journal of 26*, 4 (2001), 821–831. 21, 140

[RK89] Roy R., Kailath T.: Esprit-estimation of signal parameters via rotational invariance techniques. *Acoustics, Speech and Signal Processing, IEEE Transactions on 37*, 7 (1989), 984–995. 62

[RKH*04] Roux P., Kuperman W., Hodgkiss W., Song H., Akal T., Stevenson M.: A nonreciprocal implementation of time reversal in the ocean. *J. Acoust. Soc. Am 116*, 2 (2004), 1009–1015. 15, 21, 31, 32, 79, 140

[Rog96] Roger R.: Principal components transform with simple, automatic noise adjustment. *International journal of remote sensing 17*, 14 (1996), 2719–2727. 120

[RPK86] Roy R., Paulraj A., Kailath T.: Esprit–a subspace rotation approach to estimation of parameters of cisoids in noise. *Acoustics, Speech and Signal Processing, IEEE Transactions on 34*, 5 (1986), 1340–1342. 62

[RR93] Rajagopal R., Rao P.: Generalised algorithm for doa estimation in a passive sonar. In *Radar and Signal Processing, IEE Proceedings F* (1993), vol. 140, IET, pp. 12–20. 81

[SA89] Stoica P., Arye N.: Music, maximum likelihood, and cramer-rao bound. *Acoustics, Speech and Signal Processing, IEEE Transactions on 37*, 5 (1989), 720–741. 95

[Sch78] Schwarz G.: Estimating the dimension of a model. *The annals of statistics 6*, 2 (1978), 461–464. 110, 111

[Sch86] Schmidt R.: Multiple emitter location and signal parameter estimation. *Antennas and Propagation, IEEE Transactions on 34*, 3 (1986), 276–280. 53, 64, 80

[SN90] Stoica P., Nehorai A.: Music, maximum likelihood, and cramer-rao bound: further results and comparisons. *Acoustics, Speech and Signal Processing, IEEE Transactions on 38*, 12 (1990), 2140–2150. 95

[SRD*07] Schroeder M., Rossing T., Dunn F., Hartmann W., Campbell D., Fletcher N.: Springer handbook of acoustics. 15, 12, 13

[SS90] Stoica P., Sharman K.: Maximum likelihood methods for direction-of-arrival estimation. *Acoustics, Speech and Signal Processing, IEEE Transactions on 38*, 7 (1990), 1132–1143. 58

[SSL04] Stoica P., Selen Y., Li J.: On information criteria and the generalized likelihood ratio test of model order selection. *Signal Processing Letters, IEEE 11*, 10 (2004), 794–797. 106

[ST94] Shah A., Tufts D.: Determination of the dimension of a signal subspace from short data records. *Signal Processing, IEEE Transactions on 42*, 9 (1994), 2531–2535. 106, 158

[ST98] Stutzman W., Thiele G.: *Antenna theory and design*, vol. 320. J. Wiley, 1998. 30

[Ste83] Steele A.: Comparison of directional and derivative constraints for beamformers subject to multiple linear constraints. *Communications, Radar and Signal Processing, IEE Proceedings F 130*, 1 (1983), 41–45. 41

[SWK85] Shan T., Wax M., Kailath T.: On spatial smoothing for direction-of-arrival estimation of coherent signals. *Acoustics, Speech and Signal Processing, IEEE Transactions on 33*, 4 (1985), 806–811. 80, 81, 146

[Tap77] Tappert F.: The parabolic approximation method. *Wave propagation and underwater acoustics* (1977), 224–287. 16, 17

[TCL87] Tremblay R., Carter G., Lytle D.: A practical approach to the estimation of amplitude and time-delay parameters of a composite signal. *Oceanic Engineering, IEEE Journal of 12*, 1 (1987), 273–278. 31, 33

[TDF91] Tolstoy A., Diachok O., Frazer L.: Acoustic tomography via matched field processing. *The Journal of the Acoustical Society of America 89* (1991), 1119. 16, 42, 43

[TML*07] Tang D., Moum J., Lynch J., Abbot P., Chapman R., Dahl P., Duda T., Gawarkiewicz G., Glenn S., Goff J., et al.: Shallow water'06: A joint acoustic propagation/nonlinear internal wave physics experiment. 20, 21, 140

[TO97] Tan K., Oh G.: Estimating directions-of-arrival of coherent signals in unknown correlated noise via spatial smoothing. *Signal Processing, IEEE Transactions on 45*, 4 (1997), 1087–1091. 81

[TW80] Tindle C., Weston D.: Connection of acoustic beam displacement, cycle distances, and attenuations for rays and normal modes. *The Journal of the Acoustical Society of America 67*, 5 (1980), 1614–1622. 20, 140

[VHV91] Van Huffel S., Vandewalle J.: *The total least squares problem: computational aspects and analysis*, vol. 9. Society for Industrial Mathematics, 1991. 63

[VK04] Valaee S., Kabal P.: An information theoretic approach to source enumeration in array signal processing. *Signal Processing, IEEE Transactions on 52*, 5 (2004), 1171–1178. 105

[VS94] Viberg M., Swindlehurst A.: A bayesian approach to auto-calibration for parametric array signal processing. *Signal Processing, IEEE Transactions on 42*, 12 (1994), 3495–3507. 58, 59, 132, 170

[Vur79] Vural A.: Effects of perturbations on the performance of optimum/adaptive arrays. *Aerospace and Electronic Systems, IEEE Transactions on*, 1 (1979), 76–87. 41

[VVB88] Van Veen B., Buckley K.: Beamforming: A versatile approach to spatial filtering. *ASSP Magazine, IEEE 5*, 2 (1988), 4–24. 28

[Wax92] Wax M.: Detection and localization of multiple sources in noise with unknown covariance. *Signal Processing, IEEE Transactions on 40*, 1 (1992), 245–249. 56, 57

[WJ90] Walton E., Jouny I.: Bispectrum of radar signatures and application to target classification. *Radio Science 25*, 2 (1990), 101–113. 64

[WK85a] Wang H., Kaveh M.: Coherent signal-subspace processing for the detection and estimation of angles of arrival of multiple wide-band sources. *Acoustics, Speech and Signal Processing, IEEE Transactions on 33*, 4 (1985), 823–831. 80, 81, 82

[WK85b] Wax M., Kailath T.: Detection of signals by information theoretic criteria. *Acoustics, Speech and Signal Processing, IEEE Transactions on 33*, 2 (1985), 387–392. 105, 110, 111, 158

[WK87] Wang H., Kaveh M.: On the performance of signal-subspace processing–part ii: Coherent wide-band systems. *Acoustics, Speech and Signal Processing, IEEE Transactions on 35*, 11 (1987), 1583–1591. 81, 146

[Woo85] Wood R.: Quaternionic eigenvalues. *Bulletin of the London Mathematical Society 17*, 2 (1985), 137–138. 71

[WOV91] Wahlberg B., Ottersten B., Viberg M.: Robust signal parameter estimation in the presence of array perturbations. In *Acoustics, Speech, and Signal Processing, 1991. ICASSP-91., 1991 International Conference on* (1991), IEEE, pp. 3277–3280. 58, 59

[XB93] Xu X., Buckley K.: An analysis of beam-space source localization. *Signal Processing, IEEE Transactions on 41*, 1 (1993), 501. 54

[XK95] Xu W., Kaveh M.: Analysis of the performance and sensitivity of eigendecomposition-based detectors. *Signal Processing, IEEE Transactions on 43*, 6 (1995), 1413–1426. 105, 158

[Yan87] Yang T.: A method of range and depth estimation by modal decomposition. *The Journal of the Acoustical Society of America 82* (1987), 1736. 41

[YF97] Yuen N., Friedlander B.: Doa estimation in multipath: an approach using fourth-order cumulants. *Signal Processing, IEEE Transactions on 45*, 5 (1997), 1253–1263. 81

[ZPS85] Zeldovich B., Pilipetskii N., Shkunov V.: Principles of phase conjugation. In *Berlin and New York, Springer-Verlag (Springer Series in Optical Sciences. Volume 42), 1985, 262 p.* (1985), vol. 42. 42

Author's Publications

1. **L. Jiang**, F. Aulanier, G. Le Touzé, B. Nicolas, and J.I. Mars. Raypath separation with high resolution processing. In *OCEANS, 2011 IEEE-Spain*, pages 1–5. IEEE, 2011.

2. **L. Jiang** and J. I. Mars. Automatic detection of the number of raypaths. In *OCEANS 2011*, pages 1–4. IEEE, 2011.

3. **L. Jiang** and J. I. Mars. Automatic detection of the number of raypaths in colored noise using short-length samples. *The Journal of the Acoustical Society of America*, 130(4) : 2392, 2011.

4. **L. Jiang** and J. I. Mars. Automatic detection of the number of raypaths in a shallow-water waveguide. *revised and submit to IEEE Journal of Ocean Engineering*, 2011.

5. **L. Jiang** and J. I. Mars. Raypath separation with high resolution processing in a shallow-water waveguide. *Submit to The Journal of the Acoustical Society of America*, 2012.

6. **L. Jiang** and J. I. Mars. Automatic detection of the number of raypaths in colored noise using short-length samples. *Journées d' étude "Acoustique et Applications Navales" (JAAN 2011)*, France, 2011.

Title : Separation and detection of raypaths in a shallow-water waveguide

Abstract : As the studies on shallow-water acoustics became an active field again, this dissertation focuses on studying the separation and detection of raypaths in the context of shallow-water ocean acoustic tomography. As a first step of our work, we have given a brief review on the existing array processing techniques in underwater acoustics so as to find the difficulty still faced by this type of methods. Consequently, we made a conclusion that it is still necessary to improve the separation resolution in order to provide more useful information for the inverse step of ocean acoustic tomography. Thus, a survey on high-resolution method are provided to discover the technique which can be extended to separate the raypaths in our application background. Finally, we proposed a high-resolution method called smoothing-MUSICAL (MUSIC Active Large), which combines the spatial-frequency smoothing with MUSICAL algorithm, for efficient separation of coherent or fully correlated raypaths. However, this method is based on the prior knowledge of the number of raypaths. Thus, we introduce an exponential fitting test (EFT) using short-length samples to determine the number of raypaths. These two methods are both applied to synthetic data and real data acquired in a tank at small scale. Their performances are compared with the relevant conventional methods respectively.

Keywords : array processing, shallow water, source separation, ocean acoustic tomography, smoothing-MUSICAL, exponential fitting test.

Titre : Séparation et détection de trajet dans un guide d'onde en eau peu profonde

Résumé : En acoustique sous marine, les études sur les zones en eau peu profondes sont redevenues stratégiques. Cette thèse porte sur l' étude de la séparation et la détection de trajet dans le cadre des eaux peu profondes tomographie acoustique océanique. Dans une premiére étape de notre travail, nous avons donné un bref aperçu sur les techniques existantes de traitement acoustique sous-marine afin de trouver la difficulté toujours confrontés à ce type de méthodes. Par conséquent, nous avons fait une conclusion qu'il est encore né cessaire d'améliorer la résolution de séparation afin de fournir des informations plus utiles pour l' étape inverse de la tomographie acoustique océanique. Ainsi, une enquête sur les mthodes haute résolution est effecutée. Enfin, nous avons proposé une méthode à haute résolution appelée lissage MUSICAL (MUSIC Active large band), qui combine le lissage de fréquence spatiale avec l'algorithme MUSICAL, pour une séparation efficace de trajet cohérentes ou totalement corrélés. Cependant, cette méthode est basée sur la connaissance a priori du nombre de trajet. Ainsi, nous introduisons un test (exponential fitting test) (EFT) à l'aide de courte longueur des échantillons pour déterminer le nombre de trajets. Ces deux méthodes sont appliquées à la fois des données synthétiques et les données réelles acquises dans un réservoir à petite échelle. Leurs performances sont comparées avec les méthodes conventionnelles pertinentes.

Mots clés : traitement d'antenne, séparation de sources, eau peu profonde, tomographie acoustique océanique, smoothing-MUSICAL, exponential fitting test.